Controlled Co-Delivery of Chemotherapeutic Drugs using Stimuli-Responsive Nano-formulations for Pancreatic Cancer

Mandana Emamzadeh

Department of Pharmaceutics

School of Pharmacy

University College London

PhD Thesis

2018

This thesis is dedicated to my wonderful parents

Mr. Seyed Masoud Emamzadeh and Ms. Mehri Hamidi

For their endless love, support and encouragement

Declaration

I, Mandana Emamzadeh confirm that the work presented in this thesis is my own. Where information has been derived from other sources, I confirm that this has been indicated in the thesis.

Publications

- Mandana Emamzadeh, Didier Desmaële, Patrick Couvreur, and George Pasparakis (2018). Dual Controlled Delivery of Squalenoyl-Gemcitabine and Paclitaxel using Thermo-Responsive Polymeric Micelles for Pancreatic Cancer. Journal of materials chemistry B, 2018,6, 2230-2239.

- Mandana Emamzadeh, Mina Emamzadeh and George Pasparakis (2018). Dual Controlled Delivery of Gemcitabine and Cisplatin using Polymer Modified Thermo-sensitive Liposome for Pancreatic Cancer. International Journal of Nanomedicine (in progress).

Presentations

- European University Consortium for Pharmaceutical Sciences in Paris-Sud University. (4-11 July 2015)
- PhD research day in UCL School of Pharmacy. (18 September 2015)
- Liposome Advances: Progress in Drug and Vaccine Delivery conference. London, UK. (19-11 December 2015)
- Doctoral School Research Day. (1-2 March 2016)
- UCL Small Molecule Dragons' Den. (7 July 2016)
- 4th Symposium on Innovative Polymers for Controlled Delivery (SIPCD 2016) in Suzhou, China. (23–26 September 2016)
- PhD research day in UCL School of Pharmacy. (7 April 2017)
- International Conference and Exhibition on Nanomedicine and Drug Delivery in Osaka, Japan. (29-31 May 2017)

Impact

Pancreatic cancer, in spite of the low incident, is the fourth most lethal cancer in the world. Statistics reveal that since 1971 the ten-year survival rates improved in most of cancers except in pancreatic cancer which remained at a shocking low of 1%. Therefore, the development of more potent therapeutic modalities for pancreatic cancer is of paramount importance.

This research focused on the development of nano-formulations carrying chemotherapeutic drugs for the treatment of pancreatic cancer based on novel polymeric responsive nano-carriers with multiple drug co-encapsulation properties. The nano-formulations improve the delivery of clinically used chemotherapeutic drugs as front line treatments. As a result, they can reduce the systemic toxicity that occurs due to their non-specific distribution in healthy tissue and organs by targeting the tumor sites only. This, in effect, will reduce the side effects, increase the overall survival rates and patient compliance.

In the longer term, the potential impact of this research beyond academia could encompass towards the improvement of cancer therapies for patients with pancreatic cancer, by improving the quality of their life via the development of more potent, albeit less systemically toxic therapies. In addition, this research delivers new knowledge on the development of responsive nano-formulations for precision medicine and targeting which could impact a range of other diseases and not just pancreatic cancer.

Moreover, the completion of the project established several collaborations, and networks with academic researchers across and within the nanotechnology field. The research was appreciated by both academics and industrial delegates in internationally recognised scientific meetings such as the European University Consortium for Pharmaceutical Sciences, Paris, France; Liposome Advances: Progress in Drug and Vaccine Delivery'

conference, London, UK; 4th Symposium on Innovative Polymers for Controlled Delivery (SIPCD 2016), Suzhou, China; International Conference and Exhibition on Nanomedicine and Drug Delivery, Osaka, Japan 2017. The knowledge exchanged with other academics and industrial researchers developed good understanding which reflected on the research, design and process, formulation development and overall progress in the field of precision medicine.

Acknowledgments

I would like to take this opportunity to express my deepest appreciation to my parents for funding this project and having faith in me. I am thankful to my siblings Mehrnoush, Mina and Kianoosh for their invaluable support, encouragement, concern and love over the years and always being by my side.

My special thanks to Professor Patrick Couvreur and Dr. Didier Desmaële for their contribution in this project. My sincere gratitude to my supervisor Dr. George Pasparakis for his help and guidance.

Table of Contents

List of Figures 13

List of Tables 22

List of Abbreviations 24

Chapter 1 27

Dual Controlled Delivery of Squalenoyl-Gemcitabine and Paclitaxel using Thermo-Responsive Polymeric Micelles for Pancreatic Cancer 27

1.1 Abstract 28

1.2 Introduction 30

1.2.1 Types of pancreatic cancer 30

1.2.2 Tumor vasculature and blood flow 30

1.2.3 Tumor Hypoxia and Acidity 32

1.2.4 Enhanced permeability and retention effect of tumor vasculature 33

1.2.5 Rationale for using nanoparticles in cancer therapy 37

1.2.6 Polymers in nanomedicine 40

1.2.6.1 Free radical polymerisation 40

1.2.6.2 Reversible Addition/Fragmentation Chain Transfer Polymerisation 42

1.2.7 Stimuli-responsive polymers 44

1.2.8 Polymeric micelles 47

1.2.9 Thermotherapy 48

1.2.10 Chemotherapeutic drugs for pancreatic cancer 51

1.2.10.1 Gemcitabine 51

1.2.10.2 Squalenoyl-Gemcitabine 54

1.2.10.3 Paclitaxel 55

1.2.10.4 Synergistic antitumor activity of nanoparticle albumin-bound (nab)-paclitaxel and Gemcitabine 58

1. 3 Aim 61

1. 4 Materials 62

1. 5 Methods 62

1.5.1 One pot synthesis of Poly (DiEGMA-co-OEGMA$_{300}$)-b-EHMA by RAFT polymerisation 62
1.5.2 Nuclear magnetic resonance (NMR) spectroscopy 63
1.5.3 Gel permeation chromatography (GPC) 65
1.5.4 Determination of the polymers' LCST 67
1.5.5 Critical micelle concentration (CMC) of Poly (DiEGMA-co-OEGMA$_{300}$)-b-EHMA 67
1.5.6 Preparation of drug loaded thermo-responsive polymeric micelles ... 68
1.5.7 Dynamic light scattering (DLS) 68
1.5.8 Stability studies 70
1.5.9 Transmission electron microscopy (TEM) 71
1.5.10 HPLC analysis for drug encapsulation and release determination .. 72
1.5.11 Drug encapsulation efficiency 73
1.5.12 Determination of in vitro drug release 74
1.5.13 In vitro cytotoxicity assay 74
1.5.14 Calculation of the combination index 76
1.5.15 Synthesis of a fluorescent polymer for cellular uptake assessment 77
1.5.16 Thermo-dependent cellular uptake of fluorescent polymer 77
1.5.17 Flow Cytometry analysis 78
1.5.18 Colonogenic cell survival assay 79

1. 6 Results and Discussion 81
1.6.1 One pot synthesis of Poly (DiEGMA-co-OEGMA$_{300}$)-b-EHMA by RAFT polymerisation 81
1.6.2 Nuclear magnetic resonance spectroscopy 86
1.6.3 Gel permeation chromatography 87
1.6.4 LCST Determination 88
1.6.5 CMC of Poly (DiEGMA-co-OEGMA$_{300}$)-b-EHMA 89
1.6.6 Dynamic light scattering 90
1.6.7 Stability studies 93
1.6.8 TEM characterisation 93
1.6.9 Drug encapsulation efficiency 97
1.6.10 Determination of in vitro drug release 98
1.6.11 In vitro cytotoxicity assay 101

1.6.12 The combination index calculation 108
1.6.13 Thermo-dependent cellular uptake of fluorescent thermo-responsive polymer 109
1.6.14 Flow Cytometry 113
1.6.15 Clonogenic cell survival assay.....115
1. 7 Conclusion 118
Chapter 2 119
Dual Controlled Delivery of Gemcitabine and Cisplatin using Polymer Modified Thermo-sensitive Liposome for Pancreatic Cancer 119
2.1 Abstract.....120
2.2 Introduction 122
2.2.1 Traditional thermosensitive liposomes (TTL).....123
2.2.2 Lysolipid-containing thermosensitive liposomes (LTL) 127
2.2.3 Polymer modified thermosensitive liposomes (PMTL).....129
2.2.4 Cisplatin.....132
2.2.5 Optimisation of chemotherapy by combination drug therapy.....134
2.3 Aim.....136
2.4 Materials 137
2.5 Methods 137
2.5.1 One pot synthesis of Poly (DiEGMA-co-OEGMA$_{300}$)-b-EHMA by RAFT polymerisation 137
2.5.2 Nuclear magnetic resonance spectroscopy.....137
2.5.3 Gel permeation chromatography 138
2.5.4 Determination of the polymers' LCST.....138
2.5.5 Preparation of polymer modified thermo-sensitive liposomes (PMTL) 138
2.5.6 Synthesis of a fluorescent polymer for cellular uptake assessment 139
2.5.7 Amount of polymer bound on the surface of PMTL 139
2.5.8 Dynamic light scattering 139
2.5.9 Transmission electron microscopy 139
2.5.10 HPLC analysis for drug encapsulation and release determination 139

2.5.11 Drug encapsulation efficiency.....140
2.5.12 Determination of in vitro drug release.....140
2.5.13 In vitro cytotoxicity assay.....141
2.5.14 The combination index calculation 142
2.5.15 Thermo-dependent cellular uptake of fluorescent liposome 142
2.5.16 Flow Cytometry analysis.....142
2.5.17 Clonogenic cell survival assay.....143
2.6 Results and discussion 144
2.6.1 Amount of polymer bound on the surface of PMTL 144
2.6.2 Dynamic light scattering 144
2.6.3 Transmission electron microscopy 147
2.6.4 HPLC analysis for drug encapsulation and release determination ..150
2.6.5 Determination of in vitro drug release.....151
2.6.6 In vitro cytotoxicity assay.....153
2.6.7 The combination index analysis 164
2.6.8 Thermo-dependent cellular uptake of fluorescent liposome 166
2.6.9 Flow Cytometry 172
2.6.10 Clonogenic cell survival assay.....176
2.7 Conclusion 183
3. Thesis conclusion 184
4. Future work.....186
5. References 188

List of Figures

Figure 1. Vascular system in A) Normal tissue B) Solid tumor. Red represents well-oxygenated arterial blood, blue represents poorly oxygenated venous blood, and green represents lymphatic vessels. Adapted from Trédan, O. et al. 2007. 31
Figure 2. The tumor microenvironment including tumor cells and the extracellular matrix (ECM) surrounding a blood vessel. Adapted from Trédan, O. et al. 2007. 32
Figure 3. The diagram shows pH gradients in normal tissue, blood, tumor tissue and endosome-lysosome. Adapted from Liu, Y. et al. 2013. 33
Figure 4. Differences between normal and tumor tissues vasculature. A. Normal tissues contain linear endothelial cells wrapped by pericytes to sustain blood vessel barrier. The extracellular matrix contains collagen fibres, fibroblast and macrophages. Moreover, the lymphatic drainage operates effectively due to the presence of lymph vessels. B. Tumor tissues contain defective blood vessels due to the presence of gaps between endothelial cells and fewer adherent pericytes. The extracellular matrix of tumors contains more collagen fibres, fibroblasts and macrophages than in normal tissue. The interstitial fluids and soluble proteins are inefficiently removed due to absence of lymph vessels. Adapted from Heldin, C. H. et al. 2004. 34
Figure 5. Nanomedicines' accumulation in different tumors demonstrated as normalised average T/N ratios. The number in parentheses indicates the total number of patients included in the study, and the number above parentheses represents the number of clinical studies of an individual tumor. * Indicates that in one study, the nanomedicine was not detected because the concentration was lower than the limit of detection. In those studies, the presence of nanomedicine in normal tissues was arbitrarily set at the limit of detection (i.e., the lowest number of nanomedicine that could be detected). The red line denotes T/N ratio of 1 (i.e., columns above the red lines had a degree of preferential accumulation in the tumor). Adapted from (Natfji, A. A. et al 2017). 36

Figure 6. Schematic diagrams of PEGylated nanoparticle. A. A low surface coverage of PEG chains B. A high surface coverage of PEG chains on nanoparticles. Adapted from (Owens D. E. III et al. 2006). 38
Figure 7. Nanomedicines in drug delivery. (a) Types of nanocarriers currently described in preclinical and clinical studies. (b) Schematic representation of PEGylation and ligand grafting. (Adapted from Danhier, F. et al. 2010). 39
Figure 8. Monomer arrangement in variety of ways to form polymer. 40
Figure 9. The mechanism of FRP. Adapted from Colombani, D.1997. 41
Figure 10. General comparison of polymers made with FRP against those made using RAFT polymerisation. Adapted from Controlled Radical Polymerization Guide Aldrich® Materials Science. 43
Figure 11. Four classes of RAFT agents: A) Dithiobenzoates, B) Trithiocarbonates, C) Dithiocarbamates, and D) Xanthates. Adapted from Controlled Radical Polymerisation Guide Aldrich® Materials Science. 43
Figure 12. The mechanism of RAFT polymerisation. Adapted from Moad, G. et al. 2005, 2006, 2009, 2012. 44
Figure 13. Stimuli-responsive release of a drug from a nanocarrier.....45
Figure 14. Thermo-responsive polymer responds to temperature and shows sharp coil to globule transition from soluble to insoluble. Adapted from De las Heras Alarcon, C. et al. 2005. 45
Figure 15. Chemical structures of commonly used thermo-responsive polymers. 46
Figure 16. The amphiphilic block copolymers self-assemble to form a TR polymeric micelle having hydrophobic core and hydrophilic shell. By application of heat at LCST, the hydrophilic shell turns hydrophobic and leads to micelle dissociation. 47
Figure 17. Adjunction of mild hyperthermia with chemotherapy. The green dots represent the chemotherapeutic drug released locally from the nano-carrier after application of US (Husseini, G. A. et al. 2014).....50
Figure 18. Gemcitabine structure. 52
Figure 19. Gemcitabine is continuously phosphorylated to its active metabolites by deoxycytidine kinase intracellularly. 52
Figure 20. The chemical structure of Squalenoyl-gemcitabine. 54
Figure 21. The chemical structure of squalene. 55

Figure 22. Paclitaxel structure. 56
Figure 23. Three generations of branded paclitaxel formulations (Adapted from sorrentotherapeutics.com Accessed April 2016).....58
Figure 24. Cell cycle (Adapted from www.le.ac.uk).....59
Figure 25. TR polymeric micelles encapsulate Sq-Gem and PTX at body temperature. After application of heat the micelles disintegrate and release the drugs.....61
Figure 26. TR polymeric micelles accumulate within the tumor site by the EPR effect. After application of heat at the tumor site, the micelles are disrupted and release the drugs and induce cancer cell apoptosis. 61
Figure 27. After application of an external magnetic field (blue arrow), the nuclear magnetic moments (red arrow) align with or against the field. Adapted from (chem.libretexts.org) 64
Figure 28. The mechanism of an NMR spectrometer (Adapted from Rice university website). 64
Figure 29. The nucleus feels weaker magnetic field due to electron density shielding the nucleus resulting in less chemical shift and moving upfields. Conversely, the nucleus feels stronger magnetic field due to deshielding due to the decreased electron density around the nucleus resulting in increasing chemical shift and moving downfields.....65
Figure 30. Cross section of porous beads in the stationary phase of the column (adapted from http://www.waters.com last accessed Oct. 2017).....66
Figure 31. The porous beads inside the column elute the molecules of various sizes at different retention time (adapted from http://www.waters.com last accessed January 2018).....67
Figure 32. Schematic of a DLS instrument (Adapted from LSinstruments)....69
Figure 33. Analysis procedure of typical intensity vs time plot for three differently sized particles diffusing in solution (Adapted from www.otsukael.com).....70
Figure 34. TEM layout describing the path of electron beam (Adapted from JEOL 2000FX Handbook).....72
Figure 35. HPLC system set up (Adapted from www.Waters.co.uk).....73
Figure 36. Demonstration of the drug release studies A. below LCST B. at LCST using the dialysis cassette. 74

Figure 37. MTT assay plate setup.....76
Figure 38. schematic of a flow cytometer. The cells flowing in a single file stream of fluid passes through an argon-ion laser. Emitted light is collected by forward angle light scatter detector, side-scatter detector (1), and multiple fluorescence emission detectors (2–4). The signals are amplified and converted to digital form for analysis (A) and display (D) on a computer screen (Brown, M. et al. 2000).....79
Figure 39. A. Lauryl methacrylate (LMA) B. 2-Ethylhexyl methacrylate (EHMA) C. n-Butyl methacrylaye (BMA).....82
Figure 40. Synthesis of Poly (DiEGMA-co-$OEGMA_{300}$)-b-EHMA by RAFT polymerisation.....84
Figure 41. ^{1}H NMR spectrum of Poly (DiEGMA-co-$OEGMA_{300}$)-b-EHMA in $CDCl_3$.....86
Figure 42. GPC traces of Poly (DiEGMA-co-$OEGMA_{300}$)-b-EHMA block co-polymer (red curve) and Poly (DiEGMA-co-$OEGMA_{300}$) polymer (blue curve) determined by GPC using DMF as mobile phase. 87
Figure 43. Thermo-responsive polymer soluble in water below the LCST but insoluble at the LCST.....89
Figure 44. The CMC was measured by plotting pyrene intensity ratio (I330/I310) versus logarithm of polymer concentration. 90
Figure 45. Size and distribution of polymeric micelles measured by DLS in triplicate. 90
Figure 46. Size and size distribution of A. Sq-Gem B. PTX C. Sq-Gem and PTX loaded polymeric micelles measured by DLS in triplicate. 92
Figure 47. Demonstrate disassembly of polymeric micelles by time. 93
Figure 48. TEM images of A. Blank B. Sq-Gem C. PTX D. Co-loaded TR polymeric micelles. The scale bars show the size of A. 100 nm B-D. and 200 nm.....95
Figure 49. The histogram of size distribution of A. Blank B. Sq-Gem C. PTX D. Co-loaded TR polymeric micelles obtained from TEM images. 97
Figure 50. HPLC chromatogram of A. PTX B. Sq-Gem C. PTX and Sq-Gem. 98
Figure 51. Sq-Gem drug release from polymeric micelles below and at the LCST.....99

Figure 52. TX drug release from polymeric micelles below and at the LCST. 99
Figure 53. Combinational Sq-Gem and PTX drug release from polymeric micelles below and at LCST. 100
Figure 54. Show the characteristics of MiaPaCa-2 cells in low density. A. The microscope was adjusted on 4x lens. The scale bar is 1000μm. B. The microscope was adjusted on 10x lens. The scale bar is 400μm. 102
Figure 55. Show the characteristics of MiaPaCa-2 cells in high density. A. The microscope was adjusted on 4x lens. The scale bar is 1000μm. B. The microscope was adjusted on 10x lens. The scale bar is 400μm. 103
Figure 56. MiaPaCa-2 cells' viability was measured at a range of concentrations of 0.0001 to 10 μM of drug loaded micelles after 72 hr.....104
Figure 57. Cytotoxicity effect of blank TR micelles BL and AL after 72 hr....105
Figure 58. Cytotoxicity of Sq-Gem alone, Sq-Gem loaded micelles below LCST and Sq-Gem loaded micelles at LCST after 72 hr. 106
Figure 59. Cytotoxicity of PTX alone, PTX loaded micelles below LCST and PTX loaded micelles at LCST after 72 hr. 106
Figure 60. Cytotoxicity of Sq-Gem and PTX, Sq-Gem and PTX loaded micelles below LCST and Sq-Gem and PTX loaded micelles at LCST after 72 hr.....107
Figure 61. The cellular uptake of thermoresponsive polymers could be accurately controlled by temperature (Hiruta, Y. et al. 2014). 110
Figure 62. Thermo-responsive micelles enhance cellular uptake due to changes on the surface corona with thermal response (Abulateefeh, S. R. et al. 2013). 111
Figure 63. Cellular uptake of fluorescent TR polymer A. below and B. at LCST. The scale bars show the size of 400 μm.....112
Figure 64. The flow cytometry graph is plotted between number of cells along Y -axis and cell fluorescence intensity (in arbitrary units) along the X-axis. A. The graph shows standard curve of MiaPaCa-2 cells without fluorescent probing. B. The graph shows results obtained from below LCST (green curves) and at LCST (red curves). 114
Figure 65. Shows the standard colonies formed from MiaPaCa-2 cells without application of formulations after 14 days. The scale bar shows the size of 1000 μm. 115

Figure 66. The survival fraction of MiaPaCa-2 cells decreased as the concentration of drug increased. P value 0.0001 to 0.001 indicated with *** meaning extremely significant; P value 0.001 to 0.01 indicated with ** meaning very significant; P value 0.01 to 0.05 indicated with * meaning significant. 117
Figure 67. Liposome structure 122
Figure 68. Possible mechanisms involved in combination with hyperthermia and thermosensitive liposome therapy. (a) Non-thermosensitive liposomes extravasate inside the tumor by the EPR effect, (b) Mild hyperthermia further increases tumor vasculature pore size and enhances non-thermosensitive liposome extravasation, and (c) Combination of TTL and hyperthermia increases extravasation of TTL in the tumor interstitium. Adapted from (Landon, C. D. et al. 2011). 123
Figure 69. Presents the behavior of TTL around T_m (42-45 °C). DPPC (1,2-dipalmitoyl-sn-glycero-3-phosphocholine) is a lipid bilayer component. Below T_m, the lipid bilayer is solid and closely packed which ceases the drug permeability. However above T_m, there is formation of grain boundaries which appear due to the presence of both solid and liquid phases. The grain boundaries are able to increase the permeation to some extent. Adapted from (Al-Ahmady, Z.et al. 2016). 124
Figure 70. Shows the formation of grain boundaries between the solid and the liquid interface in TTL. Adapted from (Ta, T. et al. 2013). 125
Figure 71. DPPC structure. 125
Figure 72. HSPC structure. 125
Figure 73. DSPE-PEG2000 structure. 126
Figure 74. Shows A. unilamellar liposomes and B. PEGylated unilamellar liposomes. The liposomes coated by PEG in order to avoid opsonisation in the bloodstream. The blue sphere represents the encapsulated hydrophilic drug. Adapted from http://reflexions.ulg.ac.be (Last accessed: January 2017). 126
Figure 75. Cholesterol structure. 127
Figure 76. 1-palmitoyl-2-hydroxy-sn-glycero-3-phosphatidylcholine (MPPC) structure. 128

Figure 77. 1-stearoyl-2-hydroxy-sn-glycero-3-phosphocholine (MSPC) structure. 128
Figure 78. Shows accumulation of lysolipids at the grain boundaries and formation of stable defects which lead to increase of the content release. Adapted from (Ta, T. et al. 2013). 128
Figure 79. Presents the structure of LTL where the incorporation of lysolipids in the lipid membrane reduces the T_m. Below T_m, there is drug leakage through the grain boundaries produced by the lysolipids. Above T_m, there is ultrafast drug release due to formation of larger nanopores by the lysolipids. Adapted from (Al-Ahmady, Z. et al. 2016). 129
Figure 80. Shows the mechanism of drug release from PMTL. Below the LCST, the polymer chains are hydrophilic and soluble in the surrounding aqueous medium. However, at the LCST the polymer turns hydrophobic and undergoes coil to globule transition which destabilises the lipid bilayer and releases the drug. Adapted from (Al-Ahmady, Z. et al. 2016). 130
Figure 81. Schematic demonstration of the PMTL made by Kono et al. a. Its thermosensitive block copolymer consists of the hydrophilic block [poly(EOEOVE)] and a hydrophobic anchor for its fixation onto the liposome b. Membrane forming egg yolk phosphatidylcholine (EYPC) c. Membrane stabilising cholesterol d. Highly hydrophilic and non-toxic N-[methoxy (polyethylene glycol) 5000]-distearoyl phosphatidylethanolamine (PEG-PE). The red dots represent DOX. Adapted from (Kono, K. et al. 2010). 131
Figure 82. Cisplatin structure. 133
Figure 83. Mechanism of action of cisplatin. ‘G’ represents Guanine nucleobase. Adapted from (Reedijk, J. et al. 1984). 133
Figure 84. Schematic demonstration of proposed polymer modified thermo-sensitive liposome. After application of heat, the TR block undergoes coil to globule transition and leads to disruption of lipid membrane and content release. 136
Figure 85. The graphs show the size distribution of A. Blank PMTL and B, Gemcitabine C. Cisplatin D. GemCis loaded PMTL liposomes measured by DLS in triplicate 146

Figure 86. TEM images of PMTL encapsulated A. Gemcitabine only B. Cisplatin only C. GemCis in combination. The scale bars show the size of 500 nm. 148
Figure 87. The histograms show the size distribution of liposomes loaded with A. Gemcitabine only B. Cisplatin only C. GemCis in combination. 149
Figure 88. HPLC chromatogram showing the separation of Cis and Gem around 2 min and 10 min respectively. 150
Figure 89. Combinational loaded TTL liposomes revealed controlled release profile below (BL) and at LCST (AL). 152
Figure 90. Combinational loaded PMTL liposomes drug release profile below (BL) and at LCST (AL). 153
Figure 91. The characteristics of BxPC-3 cells in low density. A. The microscope was adjusted on 4x lens. The scale bar is 1000 μm. B. The microscope was adjusted on 10x lens. The scale bar is 400 μm. 154
Figure 92. The characteristics of BxPC-3 cells in high density. A. The microscope was adjusted on 4x lens. The scale bar is 1000 μm. B. The microscope was adjusted on 10x lens. The scale bar is 400 μm. 155
Figure 93. MiaPaCa-2 cells viability of loaded TTL (drug concentrations from 0.0001 to 100 μM) after 72hr. 156
Figure 94. MiaPaCa-2 cells' viability of loaded PMTL (drug concentrations from 0.0001 to 100 μM) after 72hr. 157
Figure 95. BxPC-3 cells viability was measured with wide range of concentrations (0.0001 to 100 μM) of loaded TTL after 72 hr. 158
Figure 96. BxPC-3 cells viability was measured with wide range of concentrations (0.0001 to 100 μM) of loaded PMTL after 72hr. 159
Figure 97. the structure of poly(APr-co-NIPAM)-2C_{12} (Kono, K. et al. 1999). 167
Figure 98. Liposome–cell interaction is affected by hydrophilicity and hydrophobicity properties of liposomes surface (Wang, J. et al. 2017). 168
Figure 99. Cellular uptake of PMTL-fl by MiaPaCa-2 cells(A) below and (B) at the LCST, the scale bar shows the size of 400 μm. 170
Figure 100. Cellular uptake of PMTL-fl by BxPC-3 cells (A) below and (B) at the LCST, the scale bar shows the size of 1000 μm. 171

Figure 101. A. The graph shows standard curve of MiaPaCa-2 cells without any fluorescent tag. B. MiaPaCa-2 cells were incubated for 30 min in the presence of O-fluorescein-tagged block co-polymer. The graph shows results obtained from below LCST (green curves) and at LCST (red lines).....173
Figure 102. The flow cytometry graph is plotted between number of cells along Y -axis and cell fluorescence, a.u. along X-axis. A. The graph shows standard curve of MiaPaCa-2 cells without a fluorescent tag. B. The graph shows fluorescent intensity obtained from below LCST (green curves) and at the LCST (red curves).....175
Figure 103. Standard colonies formed by A. MiaPaCa-2 cells B. BxPC3 cells without application of formulations after 14 days. The scale bar shows the size of 1000 μm.....179
Figure 104. The percentage survival fraction of MiaPaCa-2 cells post treatment with GemCis loaded TTL and PMTL after 14 days. P value 0.001 to 0.01 indicated with ** means very significant; P value 0.01 to 0.05 indicated with * means significant. The P values were calculated from comparison of the percentage survival fraction of the nano-formulations with the free GemCis. 180
Figure 105. The percentage survival fraction of BxPC-3 cells post treatment with GemCis loaded TTL and PMTL after 14 days. P value 0.0001 to 0.001 indicated with *** means extremely significant; P value 0.001 to 0.01 indicated with ** means very significant; P value 0.01 to 0.05 indicated with * means significant. P value was calculated from comparison of the percentage survival fraction of the nano-formulations with the free GemCis. 181

List of Tables

Table 1. Available clinical data about the variations of tumor perfusion according to tumor type, size, stage, and location. 37
Table 2. A total of 861 patients were randomly administered nab-paclitaxel plus gemcitabine (431 patients) or gemcitabine (430) (Van Hoff, D. D. et al. 2013).....57
Table 3. Recent studies on co-encapsulating and co-delivery of drugs for treatment of several diseases. 60
Table 4. Summary of block co-polymers synthesised by RAFT polymerisation. (-) represents insolubility of polymers and inability to form micelles.....85
Table 5. Average particle size of TR polymeric micelles.....91
Table 6. Stability of micelles was measured by DLS for a week. 93
Table 7. The IC_{50} values of native and encapsulated drugs measured by the MTT cytotoxicity assay.....108
Table 8. CI values of Sq-Gem and PTX loaded micelles on MiaPaCa-2. 109
Table 10. A brief summary of PMTLs with different thermoresponsive block copolymers. Some of these PMTLs progressed to preclinical investigation. Adapted from (Al-Ahmady, Z. et al. 2016).....132
Table 11. HPLC gradient method.....140
Table 12. Size and distribution of blank and loaded PMTL liposomes obtained by DLS. 145
Table 13. The average encapsulation efficiency of liposomes. 151
Table 14. Cytotoxicity profiles of native and encapsulated drugs in TTL and PMTL, on MiaPaCa-2 cells measured by MTT cytotoxicity assay after 72hr. 161
Table 15. The cytotoxicity curves of native and encapsulated drugs in TTL and PMTL, on BxPC-3 cells measured by MTT cytotoxicity assay after 72hr. 163
Table 16. The IC_{50} values of native and encapsulated drugs in TTL and PMTL, on two different pancreatic cancer cell lines MiaPaCa-2 and BxPC-3 incubated for 72hr. 164

Table 17. CI values of GemCis loaded liposomes on MiaPaCa-2 cells incubated for 72hr. 165
Table 18. CI values of GemCis loaded liposomes on BxPC-3 cells incubated for 72hr. 166
Table 19. Digital photographs of the clonogenic assay of MiaPaCa-2 cells performed with the combination of free GemCis or loaded in TTL and PMTL below and at the LCST for 14 consecutive days in 6-well plates (the diameter of each well is approx. 34.8 mm). 177
Table 20. Digital photographs of the clonogenic assay of BxPC-3 cells performed with the combination of free GemCis or loaded in TTL and PMTL below and at the LCST for 14 consecutive days in 6-well plates (the diameter of each well is approx. 34.8 mm). 178

List of Abbreviations

AIBN	2,2′-Azobis(2-methylpropionitrile)
AL	At LCST
ATRP	Atom transfer radical polymerisation
BL	Below LCST
BMA	Butyl methacrylate
$CDCl_3$	Deuterated chloroform
CDDP	Cisplatin
Chol	Cholesterol
CI	Combination index
CMC	Critical micelle concentrations
CRP	Controlled radical polymerisation
CTA	Chain transfer agent
DiEGMA	Di(ethylene glycol) methyl ether methacrylate
dFdCTP	Gemcitabine triphosphate
DLS	Dynamic light scattering
DOX	Doxorubicin
DPBS	Dulbecco's phosphate buffered saline
DPPC	1,2-dipalmitoyl-*sn*-glycero-3-phosphocholine
DSPE-PEG2000	1,2-distearoyl-*sn*-glycero-3-phosphoethanolamine-N-[amino(polyethylene glycol)-2000] (ammonium salt)
EE	Encapsulation efficiency
EHMA	2-Ethylhexyl methacrylate
EPR	Enhanced permeability and retention effect
FBS	Fetal bovine serum
FOMA	Fluorescein *O*-methacrylate
FRP	Free radical polymerisation
GEM	Gemcitabine
GemCis	Gemcitabine plus Cisplatin
GPC	Gel permeation chromatography

HIFU	High intensity focused ultrasound
HPLC	High-performance liquid chromatography
HSPC	L-α-phosphatidylcholine, hydrogenated (Soy)
HT	Hyperthermia
IC_{50}	Half maximal inhibitory concentration
LCST	Lower critical solution temperatures
LMA	Lauryl methacrylate
LRP	Living radical polymerisation
MPS	Mononuclear phagocyte system
MTT	Thiazolyl Blue Tetrazolium Bromide
NPs	Nanoparticles
OEGMA 300	Oligo (ethylene glycol) methyl ether methacrylate M_n 300
OD	Optical density
OX	Oxaliplatin
PBS	Phosphate-buffered saline
PDA	Pancreatic ductal adenocarcinoma
PDI	Polydispersity index
PE	Plating efficiency
PEG	Poly(ethylene glycol)
PEGMA	Poly(ethylene glycol) methacrylates
PEGMA360	Poly(ethylene glycol) methacrylate
PEGMA300	Poly(ethylene glycol) methyl ether methacrylate
PEO	Poly(ethylene oxide)
pH_e	Extracellular tumor pH
pH_i	Intracellular tumor pH
PIPDR	pH-induced drug resistance
PMTL	Polymer modified thermosensitive liposomes
PNIPAM	Poly(N-isopropylacrylamide)
PPO	Poly(propylene oxide)
PTX	Paclitaxel
RAFT	Reversible Addition/Fragmentation Chain Transfer Polymerisation
RAFT agent	2-Cyano-2-propyl benzodithioate

SF	Survival fraction
SQ-GEM	Squalenoyl-Gemcitabine
SR	Stimuli-responsive
TEM	Transmission electron microscopy
THF	Tetrahydrofuran
T_m	Transition temperature
TR	Thermo-responsive
TTL	Traditional thermosensitive

Chapter 1

Dual Controlled Delivery of Squalenoyl-Gemcitabine and Paclitaxel using Thermo-Responsive Polymeric Micelles for Pancreatic Cancer

1.1 Abstract

Pancreatic cancer is the fourth leading cause of cancer death in the world. It is an aggressive type of cancer in which about 80% of patients have locally advanced or metastatic pancreatic cancer at the time of diagnosis. Unfortunately, in spite of the low incident it has high mortality. Gemcitabine (GEM) is the most potent anti-cancer drug for the treatment of pancreatic cancer but it undergoes deamination in the bloodstream and becomes biologically inactive and therefore it should be protected and delivered to the site of action. Paclitaxel (PTX) is another anti-neoplastic drug with a strong cytotoxic effect on pancreatic cancer cells however its hydrophobic nature makes it insoluble in blood. Therefore to improve their delivery, nano-carriers such as thermo-responsive (TR) polymeric micelles were used to encapsulate these chemotherapeutic drugs. TR polymeric micelles comprise block copolymers with a hydrophilic thermo-responsive block and a hydrophobic block. These synthetic block copolymers self-assemble into micelles that carry anti-cancer drugs within their core. In addition, they exhibit a thermo-reversible hydrophilic-to-hydrophobic phase transition (or lower critical solution temperature, LCST) above body temperature by an external temperature stimulus (such as ultrasound) which in turn induces a sharp disruption of the micellar formulation leading to confined and precise drug release. The proposed nanomedicinal design reduces the systemic toxicity by increasing the bioavailability of the anticancer drugs inside the tumor without affecting the surrounding healthy tissue.

In this research, a poly [(di(ethylene glycol) methyl ether methacrylate –co-poly(ethylene glycol) methyl ether methacrylate$_{300}$) –b- (2-ethylhexyl methacrylate)] [poly (DiEGMA-co-OEGMA$_{300}$)-b-EHMA] block copolymer was synthesised by reversible addition fragmentation chain transfer (RAFT) polymerisation and self-assembled to nano-sized micelles encapsulating Squalenoyl-Gemcitabine (Sq-Gem) and PTX. These TR polymeric micelles exhibited a LCST at 40°C and showed good stability by achieving a low CMC value. They were capable of halting the drug release below the LCST but

increased the release significantly above the polymers' LCST by achieving a nearly burst release profile. In vitro cytotoxicity assays on MiaPaCa-2 pancreatic cancer cell line revealed that the combinational co-delivery of Sq-Gem and PTX with thermo-responsive micelles had a synergistic effect and considerably decreased cancer cell viability compared to each drug separately. In addition, the polymeric micelles reduced the IC_{50} (half maximal inhibitory concentration) of the native drugs by improving their cellular uptake.

1.2 Introduction

Pancreatic cancer is one of the most lethal malignancies with very low survival rate. Despite of having low incidence it ranks as the fourth most common cause of cancer mortality (Kim, V. M. et al. 2015; Raimondi, S. et al. 2009). Risk factors for this malignant disease include smoking, family history of chronic pancreatitis, advancing age, male gender, diabetes mellitus, obesity, and non-O blood group (Amundadottir, L. et al. 2009; Klein, A. P. et al. 2004; Wolpin, B. M. et al. 2009).

1.2.1 Types of pancreatic cancer

There are two types of pancreatic cancer according to the types of cells involved. Exocrine pancreatic cancer, also known as adenocarcinoma, which is a cancer that initiates from the glandular tissue or pancreatic ducts which are responsible for producing digestive fluids. The majority of pancreatic cancers are adenocarcinomas and since these tumors do not interfere with the secretion of hormones they do not cause signs or symptoms so the disease is usually in advanced stage when the tumor invades the surrounding tissues or metastasises to distant organs. Surgical resection remains the only possible solution for curative therapy. Endocrine pancreatic cancer is a disease in which cancerous cells initiate within the tissues of the pancreas that are responsible for secreting hormones such as insulin. This type of the pancreatic cancer is rare (Braganza, J. M. et al. 1982).

1.2.2 Tumor vasculature and blood flow

Pancreatic cancer tumours have abnormal and dysfunctional vasculature and supply irregular blood flow to cancer cells (Figure 1). Moreover, the dense stroma makes a significant diffusion barrier that impairs drug delivery compared with healthy tissues (Olive, K. P. et al. 2009). Studies performed by the Komar group also showed reduced blood flow, high ratio of glucose uptake and high metabolic activity in pancreatic cancer tumors which leads to

hypoxic tumor microenvironment (Komar, G. et al. 2009). In addition, the absence of lymph vessels induce an increase of the interstitial fluid pressure within tumor tissues which inhibits the distribution of larger molecules and compresses blood vessels such that blood is diverted away from the center of the tumor towards the periphery (Heldin, C. H. et al. 2004; Milosevic, M. F. et al. 1998; Stohrer, M. et al. 2000).

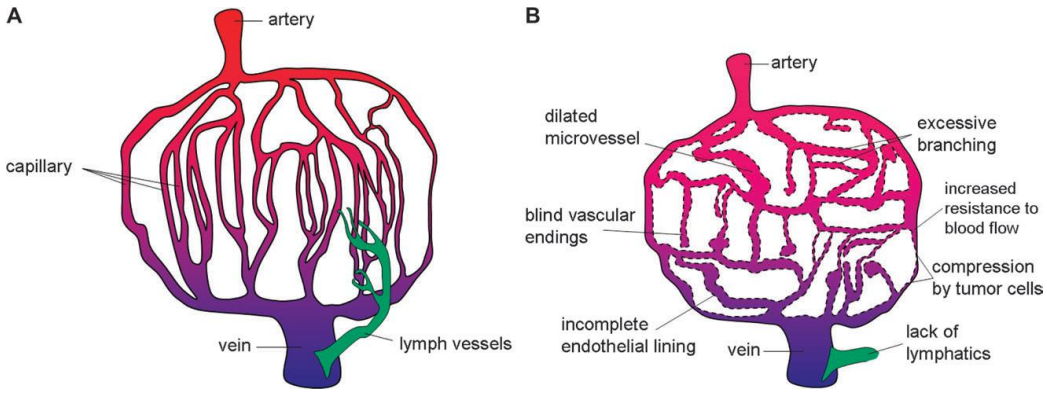

Figure 1. Vascular system in A) Normal tissue B) Solid tumor. Red represents well-oxygenated arterial blood, blue represents poorly oxygenated venous blood, and green represents lymphatic vessels. Adapted from Trédan, O. et al. 2007.

Anticancer drugs must be distributed throughout the tumor vasculature, cross vessel walls, and traverse the tumor tissue in high concentration in order to kill cancer cells therefore this process depends heavily on the vasculature because anticancer drugs accumulate to tumors via the blood. But since vasculature is heterogeneous in tumors, only part of tumor cells are exposed to the drugs and this influences the drug sensitivity of the tumor. On the other hand, the drug distribution and concentration within the tumor also depends on gradients in the rate of cell proliferation which decreases with increasing the distance from the tumor blood vessels (Figure 2). Consequently, slowly proliferating cells at increasing distances from tumor blood vessels are likely to be resistant to therapy due to low drug concentration (Michalski, C. W. et al. 2010; Grippo, P. J. et al. 2012; Trédan, O. et al. 2007).

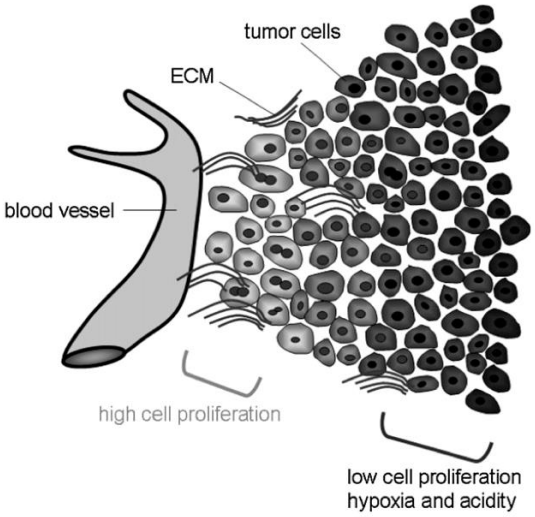

Figure 2. The tumor microenvironment including tumor cells and the extracellular matrix (ECM) surrounding a blood vessel. Adapted from Trédan, O. et al. 2007.

1.2.3 Tumor Hypoxia and Acidity

Due to the inhomogeneous vascular network leading to insufficient oxygen supply to tumor, the tumor uses the glycolytic pathway instead of respiration to produce the energy required to survive and proliferate. During glycolysis glucose is converted to lactic acid and other acidic metabolites resulting in the acidification of the extracellular environment of cancer cells. Hence, tumor tissues have extracellular tumor pH (pH_e) value of ≈ 6.5-7.2 and intracellular tumor pH (pH_i) value of ≈ 7.4 (Figure 3)(Song, C. W. et al. 2006; Trédan, O. et al. 2007). Furthermore, there are pH gradients inside tumor cells where the pH drops as low as 5.0-6.5 and 4.5-5.0 in endosomes and lysosomes respectively (Gao, G. H. et al. 2013; Li, R. et al. 2011; Liu, Y. et al. 2013; Zhu, S. et al. 2012).

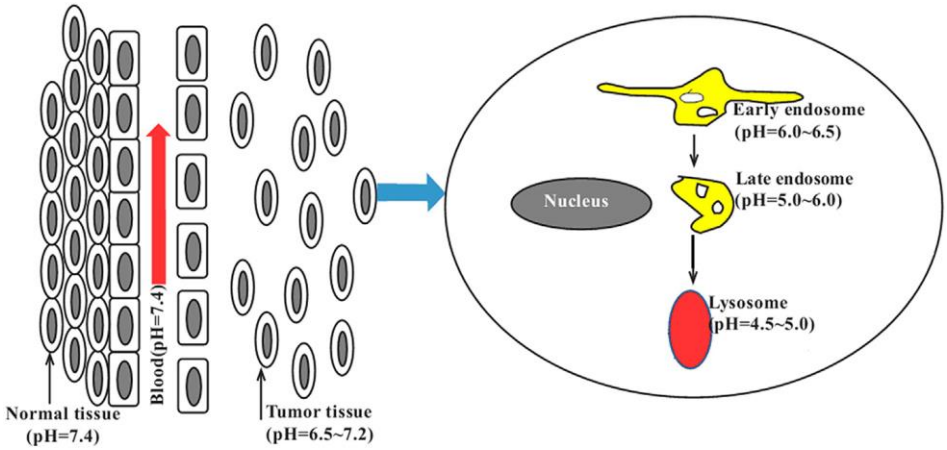

Figure 3. The diagram shows pH gradients in normal tissue, blood, tumor tissue and endosome-lysosome. Adapted from Liu, Y. et al. 2013.

1.2.4 Enhanced permeability and retention effect of tumor vasculature

Previously, it was thought that active targeting or receptor-mediated targeting was the only way of delivering nanocarriers to tumor sites. It was accomplished by using ligands on the surface of nanocarriers that could bind to overexpressed receptors found on cancer cells (Kataoka, K. et al. 2001; Torchillin, V. P. 2001). Conversely, Maeda identified the passive targeting of nanocarriers to solid tumors. He revealed the existence of passive accumulation into tumors in the absence of targeting ligands through the enhanced permeability and retention effect (EPR) (Maeda, H. 2001; Matsumura, Y. et al. 1986). In addition, Bae explained that active targeting process could only occur after passive accumulation in tumors (Bae, Y. H. 2009). The EPR occurs due to the high permeability of tumor vasculature compared to normal tissue (pore sizes 400–800 vs. 5–10 nm) which results from high proportion of proliferating endothelial cells, pericyte deficiency, and aberrant basement membrane formation (Figure 4). Furthermore, the absence of lymphatic vessels in the tumors leads to insufficient drainage from cancer tissues which allow nano-sized drug carriers to have longer retention times. Hence, the EPR effect helps nano-sized drug carriers to penetrate across the tumor vasculature while being unable to enter healthy tissue and consequently leads to lower administrated doses and reduced systemic toxicity (Abulateefeh, S. R. et al. 2011; Danhier, F. et al. 2010; Heldin, C. H. et al. 2004).

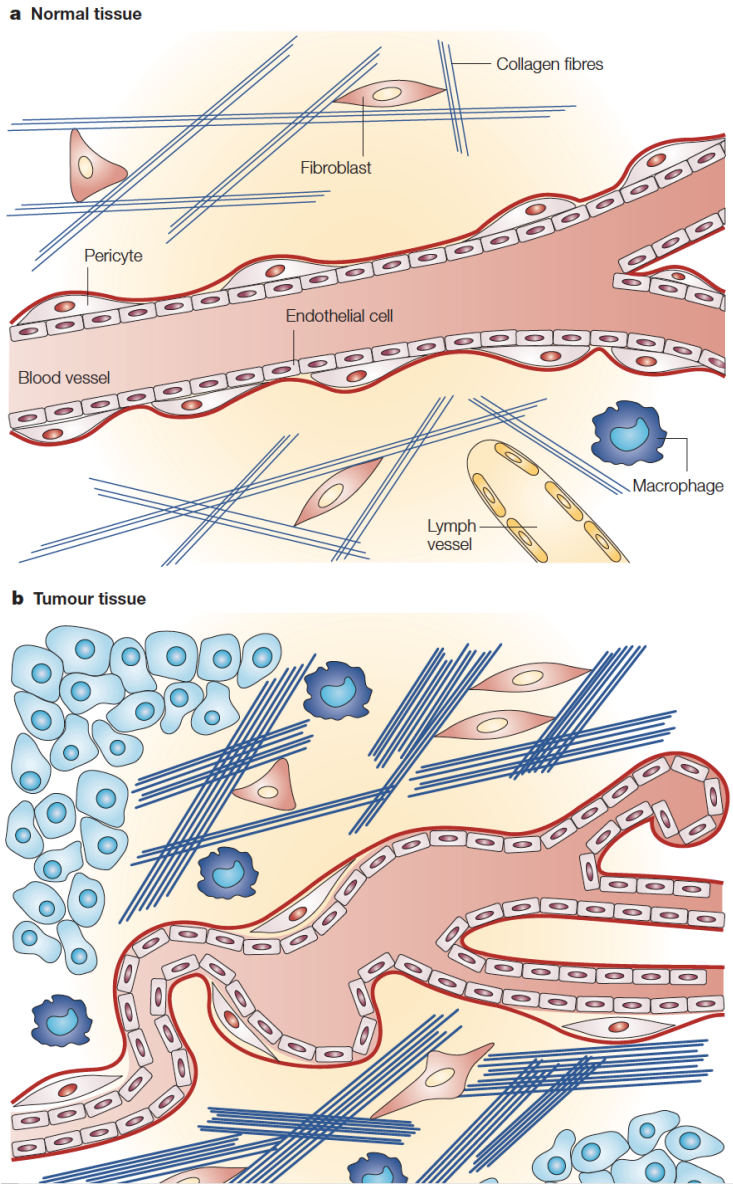

Figure 4. Differences between normal and tumor tissues vasculature. **A.** Normal tissues contain linear endothelial cells wrapped by pericytes to sustain blood vessel barrier. The extracellular matrix contains collagen fibres, fibroblast and macrophages. Moreover, the lymphatic drainage operates effectively due to the presence of lymph vessels. **B.** Tumor tissues contain defective blood vessels due to the presence of gaps between endothelial cells and fewer adherent pericytes. The extracellular matrix of tumors contains more collagen fibres, fibroblasts and macrophages than in normal tissue. The interstitial fluids and soluble proteins are inefficiently removed due to absence of lymph vessels. Adapted from Heldin, C. H. et al. 2004.

Since blood vessels in solid tumors have unique characteristics that are not observed in healthy blood vessels, the exploitation of these vascular abnormalities by macromolecular (nano-sized) drug carriers can be used as an excellent tumor-selective target (Danhier, F. et al. 2010). Many

chemotherapeutic drugs used today are molecules of low molecular weight. They cannot distinguish tumor tissue from healthy tissue and diffuse through most healthy tissues as well as tumor tissues leading to increased suboptimal treatment due to excessive side effects (Maeda, H. et al. 1989). Most of these drugs have plasma half-life of less than 20 min and therefore they must be encapsulated in nano-sized carries of larger molecular size for long time circulation to reach the tumor (Maeda, H. 2001). Ultimately, due to the EPR effect the macromolecules accumulate in tumor tissue at very high concentration (Matsumura, Y. et al. 1986; Noghuchi, Y. et al. 1998). Generally, this concentration is 5-10 times higher than in plasma 24 hr after intravenous injection and 10 times higher than that of healthy tissue (Maeda, H. et al. 1989). Moreover, the drug concentration increases 10-50 fold within 1-2 days of administration (Iyer, A. K. et al. 2006).

EPR has become a dogma in nanomedicinal drug delivery to tumors after intravenous injection. In addition, it has been considered as a universal anatomical property of all solid tumors which been used for passive targeting of nanomedicinal cancer therapy. However, the EPR effect is unlikely to be equivalent in all tumor types. The evaluation of the EPR effect in humans has only been reported to some tumor types and is poorly understood (Konno, T. et al. 1984; Maeda, H. 2015)

The EPR effect and its role in nanomedicinal formulations is dependent on several factors such as:

• Tumor: type, size, proliferation rate, necrosis, intra-tumoural volume, and anatomical location

• Vasculature: density, volume, permeability, distribution relative to stromal and tumour cells, and blood flow

• Stroma: architecture, density, composition, and matrix rigidity

• Macrophages: number and function

• Lymphatics: density, function, and location within and around the tumour

• Interstitial fluid pressure: local effects and cross-tumour pressure gradients (Hare, J. I. et al.2017).

Natfiji and coworkers summarised 24 studies to investigate the relationship between the magnitudes of EPR in different tumor types. They demonstrated the data as tumor/normal tissue content ratio (T/N ratio) (Figure 5). Among 14 tumor types examined, 6 tumor types showed the highest levels of normalised T/N ratios of accumulation of nanomedicine in the tumor site. These were (i) pancreatic adenocarcinoma, (ii) colon, colorectal, and rectal cancers, (iii) breast cancer, (iv) stomach cancer, (v) brain cancer and brain metastases, and (vi) ovarian cancer (Natfji, A. A. et al 2017).

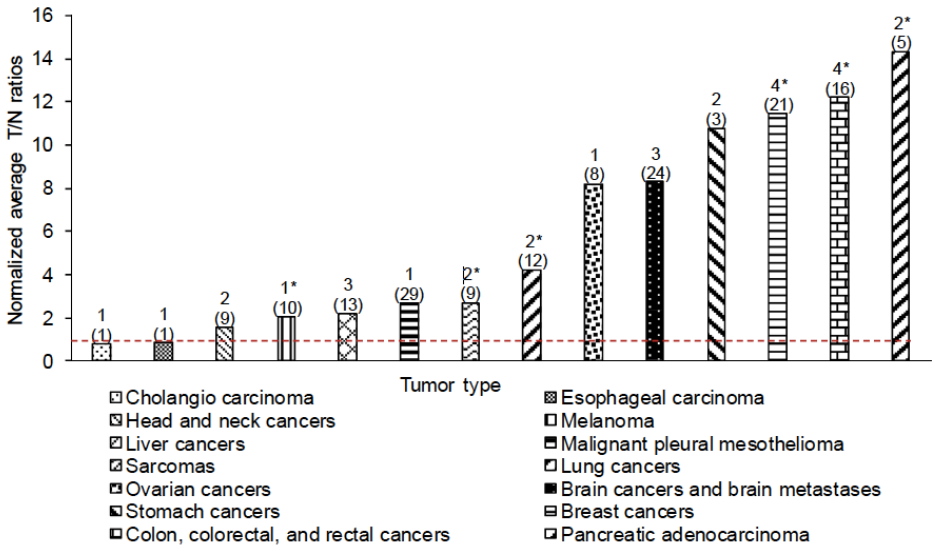

Figure 5. Nanomedicines' accumulation in different tumors demonstrated as normalised average T/N ratios. The number in parentheses indicates the total number of patients included in the study, and the number above parentheses represents the number of clinical studies of an individual tumor. * Indicates that in one study, the nanomedicine was not detected because the concentration was lower than the limit of detection. In those studies, the presence of nanomedicine in normal tissues was arbitrarily set at the limit of detection (i.e., the lowest number of nanomedicine that could be detected). The red line denotes T/N ratio of 1 (i.e., columns above the red lines had a degree of preferential accumulation in the tumor). Adapted from (Natfji, A. A. et al 2017).

Further studies performed by Wilhelm et al. focused on the accumulation of nanoparticles in animal models. The tumors with the highest accumulation of injected dose were skin, pancreas, brain, and liver tumors with percentage of 1.3, 0.8, 0.8, and 0.7 respectively, followed by breast, cervix, prostate, and colon at 0.6% (Wilhelm, S. et al. 2016).

Furthermore, Natfiji and coworkers investigated the effect of tumor perfusion (according to tumor type, size, stage, and location) on the magnitudes of EPR (Table 1). The result showed that the blood perfusion in most of the cases was higher in pancreatic tumor compared to normal tissue.

Table 1. Available clinical data about the variations of tumor perfusion according to tumor type, size, stage, and location.

Tumor Type	Tumor Stage, Size, or Location	Blood Flow in Tumor Tissue	Blood Flow in Normal Tissue
Pancreatic cancers	Tumor classification: WHO 1	284 mL/100 g/min	130.4 mL/100 g/min
	Tumor classification: WHO 2	229.1 mL/100 g/min	130.4 mL/100 g/min
	Tumor classification: WHO 3	153.5 mL/100 g/min	130.4 mL/100 g/min
	Tumor diameter <2 cm	292 mL/100 g/min	130.4 mL/100 g/min
	Tumor diameter ≥2 cm	159.8 mL/100 g/min	130.4 mL/100 g/min
	Tumors with lymph node metastases	141.6 mL/100 g/min	130.4 mL/100 g/min
	Tumors without lymph node metastases	264 mL/100 g/min	130.4 mL/100 g/min
	Tumors with liver metastases	122.8 mL/100 g/min	130.4 mL/100 g/min
	Tumors without liver metastases	236.5 mL/100 g/min	130.4 mL/100 g/min
	All tumors (stages ≥ IIB)	45.7 ± 18.2 mL/min/dL[a]	113.8 ± 48.2 mL/min/dL[a]
	Medium-size tumors[d]	51 ± 3.9 mL/min/dL[a]	113.8 ± 48.2 mL/min/dL[a]
	Large-size tumors[d]	21.1 ± 7.9 mL/min/dL[a]	113.8 ± 48.2 mL/min/dL[a]
	Very large–size tumors[d]	45.1 ± 7.4 mL/min/dL[a]	113.8 ± 48.2 mL/min/dL[a]

a Data presented as mean ± SD. Data calculated for tumors with identified stage. The size of tumors was considered as medium if tumors were on stage IIB or with low-grade neuroendocrine tumor, as large if tumors were on stage III, and as very large if tumors were on stage IV or with high-grade neuroendocrine tumor. Adapted from (Natfji, A. A. et al 2017).

1.2.5 Rationale for using nanoparticles in cancer therapy

The ideal goal of chemotherapy is to increase the survival time and the quality of patients' life by diminishing systemic toxicity. The latter occurs due to the distribution of the drugs non-specifically across the body affecting both normal and tumor cells. This goal can be achieved by protecting the anti-cancer drugs in systemic circulation and deliver them to the tumor site by using nanoparticles (Dand, N. 2013; Danhier, F. et al. 2010). The nanoparticles should have sizes larger than 10 nm to avoid filtration by the kidney and smaller than 100 nm to avoid liver clearance. Furthermore, they should be hidden from the Mononuclear phagocyte system (MPS) which recognises and removes foreign materials from the blood by opsonisation followed by phagocytosis (Dimou, A. et al 2012). The most common method to protect nanoparticles from the MPS is PEGylation (Figure 6) which comprises the coating of the nanoparticles' surface with polyethylene glycol (PEG). PEGylation has been shown to increase the blood circulation half-life by

several orders of magnitude. The PEGylated nanoparticles have a protective hydrophilic layer around them which hinder the adsorption of opsonin and prevent the opsonisation process (Blanco, E. et al. 2015; Owens D. E. III et al. 2006).

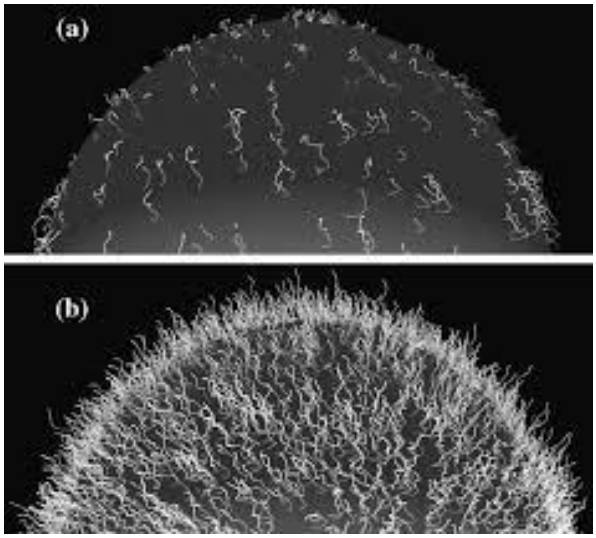

Figure 6. Schematic diagrams of PEGylated nanoparticle. A. A low surface coverage of PEG chains B. A high surface coverage of PEG chains on nanoparticles. Adapted from (Owens D. E. III et al. 2006).

Figure 7 shows the tumor targeting of nanomedicinal therapeutics to overcome the lack of specificity of anti-cancer drugs. Nanoparticles (Figure 7A) are solid and spherical structures ranging up to 200nm. Polymeric micelles (Figure 7A) consist of a hydrophobic core in which hydrophobic drugs can be encapsulated and a hydrophilic corona which prevents interaction of the core with the blood stream and also improves the circulation time of the drugs (Croy, S. R. 2006).

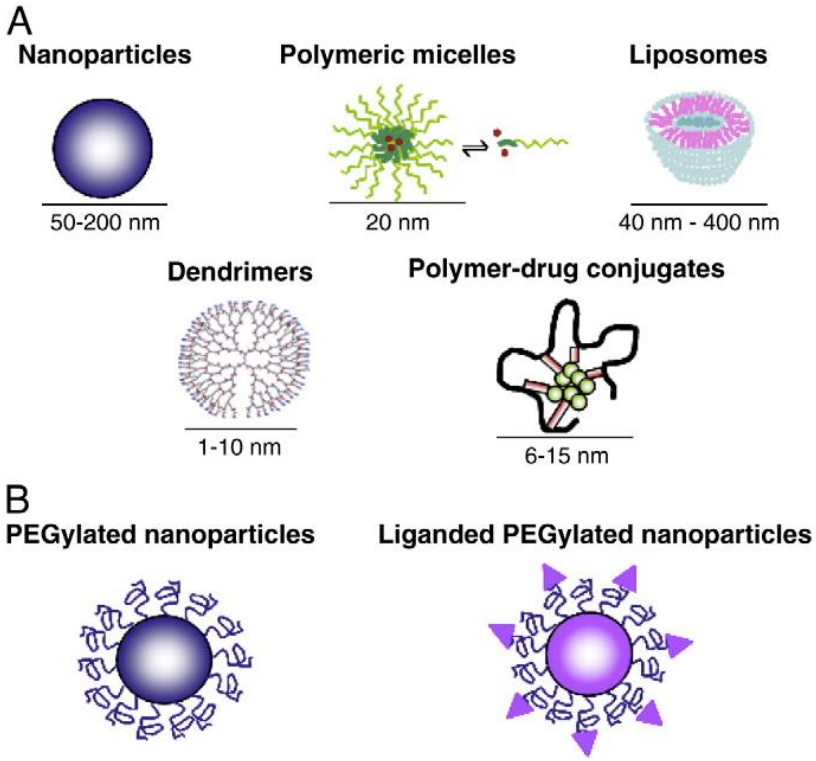

Figure 7. Nanomedicines in drug delivery. (a) Types of nanocarriers currently described in preclinical and clinical studies. (b) Schematic representation of PEGylation and ligand grafting. (Adapted from Danhier, F. et al. 2010).

Liposomes (Figure 7A) are sphere shaped vesicles produced from natural phospholipids which form a lipid bilayer surrounded by polar head groups in the interior core and the exterior shell. In addition, the amphipathic nature of phospholipids makes liposomes capable of entrapping hydrophobic drugs within the lipid bilayer, hydrophilic drugs in the aqueous compartment and drugs with intermediate log P partition between lipid and aqueous phases, i.e. both in the bilayer and in the aqueous core (Akbarzadeh, A. et al. 2013; Immordino, M. et al. 2006; Torchilin, V. P. 2005). Dendrimers (Figure 7A) are nano-sized highly branched perfectly symmetric polymers. Drug molecules can be either covalently attached to the surface groups or incorporated within their polymeric mesh compartments (Nanjwade, B. K. et al. 2009). Polymer-drug conjugates (Figure 7A) are polymeric nanoparticles which are synthesised by conjugating drug molecules to the polymer backbone using a suitable linker (Duncan, R. 2006).

1.2.6 Polymers in nanomedicine

Polymerisation is a process in which monomers repetitively attach covalently to form a polymer. Monomers within a polymer may be arranged along the backbone in a variety of ways and form different types of topologies (Figure 8)(Gregory, A. et al. 2012).

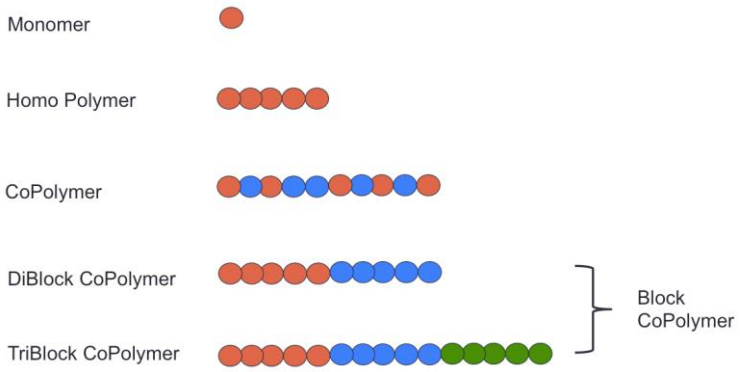

Figure 8. Monomer arrangement in variety of ways to form polymer.

1.2.6.1 Free radical polymerisation

There are different types of polymerisation techniques each having their own strengths and weaknesses. One of the most widely employed polymerisation techniques is free radical polymerisation (FRP) since it is adaptable to many types of monomers using convenient equipment, within a suitable temperature range (typically 0-100°C) and often shows adequate reproducibility (Mishra, V. et al. 2012).

Mechanism of FRP

FRP starts by the initiation step (1) which is the generation of radicals due to thermal decomposition of an initiator, followed by the propagation step (2) which is the growth of polymer chain by the successive additions of monomers to the highly reactive radicals; finally the termination step (3) in which the reaction of two radicals produce an inactive polymer (Figure 9)(Colombani, D. 1997).

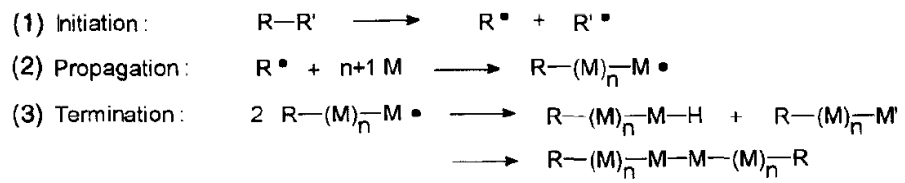

Figure 9. The mechanism of FRP. Adapted from Colombani, D.1997.

Polymers synthesised by FRP tend to have broad polydispersity because there is no control over their propagation and termination which consequently results in significant amounts of high and very low molar mass polymer chains. The lowest polydispersity that can be achieved is at least 1.5 and it usually reaches to 2-3 for poly vinyl monomers. This is because of the following limitations:

- The polymer chains do not initiate simultaneously due to the slow decomposition of the radical initiators.
- High reactivity or low stability of free radicals and their facile coupling and/or disproportionation reactions.
- Termination between two growing radicals or premature termination. (Colombani, D. 1997; Matyjaszewski, K. et al. 2005).

A negative feature of this polymerisation technique is its inability in synthesising block copolymers via the sequential addition of monomers. This is because after synthesising a homopolymer there are no living radicals present at the end of each polymer chain to reinitiate the copolymerisation of the second monomer. Therefore, in order to overcome these problems living radical polymerisation (LRP), also referred to as controlled radical polymerisation (CRP) was developed which provides polymers with narrow molar-mass distributions, block copolymers and polymers with various architectures (Matyjaszewski, K. et al. 2005; Mishra, V. et al. 2012). The most commonly used LRP techniques are:

- Reversible Addition/Fragmentation Chain Transfer Polymerisation (RAFT)

- Atom Transfer Radical Polymerisation (ATRP)
- Nitroxide-mediated Polymerisation (NMP)

LRP is a process in which there is an active site in each polymer chain where chain growth occurs indefinitely without termination. There are constant numbers of active sites in a batch which is equal to the number of initiator molecules applied at the onset of the reaction. As a result, the number-average degree of polymerisation is simply determined by the molar ratio of the molar mass of the monomer feed by the molar mass of the initiator used. Under such conditions, the molar mass distribution within the prepared polymer chains is expected to be narrow. Once the polymerisation reaction is completed, the active sites remain living, allowing either to functionalise the chain ends by induced deactivation or to re-initiate the polymerisation of a second monomer to yield a block copolymer (Vana, P. 2007).

1.2.6.2 Reversible Addition/Fragmentation Chain Transfer Polymerisation

RAFT is a living/controlled radical polymerisation method which allows for the polymerisation of many monomers including (meth)acrylates, (meth)acrylamides, acrylonitrile, styrenes, dienes, and vinyl monomers. In addition, this method is able to tolerate unprotected functionalities such as OH, NR2, COOH, CONR2 and SO3H either in the monomer or the solvent.

Unlike FRP, in RAFT all chains are initiated at the beginning of the reaction, grow at a similar rate, and complete the polymerisation as there is no irreversible chain transfer or termination (Figure 10). Since initiation happens quickly with respect to propagation, the molecular weight distribution is very narrow and leads to low polydispersity index (PDI). Moreover, chains can be extended by further addition of monomers into the reaction and form a block copolymer (Becer, C. R. et al. 2008).

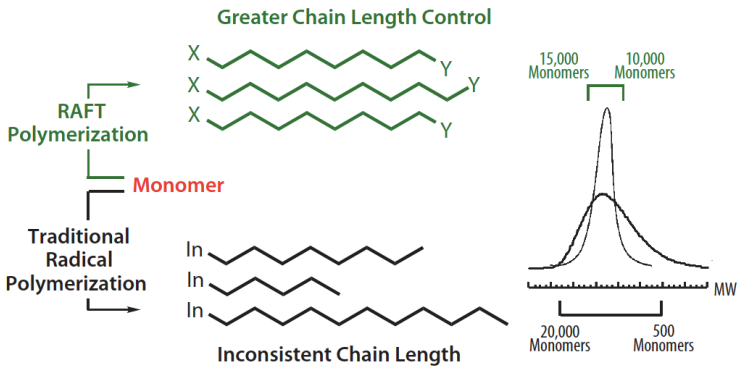

Figure 10. General comparison of polymers made with FRP against those made using RAFT polymerisation. Adapted from Controlled Radical Polymerization Guide Aldrich® Materials Science.

RAFT exhibits low PDI due to the addition of a chain transfer agent (CTA) (ZC(=S)SR), also known as RAFT agent. Commonly used RAFT agents include thiocarbonylthio compounds such as dithioesters, dithiocarbamates, trithiocarbonates and xanthates which mediate the polymerisation via a reversible chain-transfer process (Figure 11). (Moad, G. et al. 2005, 2006, 2009, 2012)

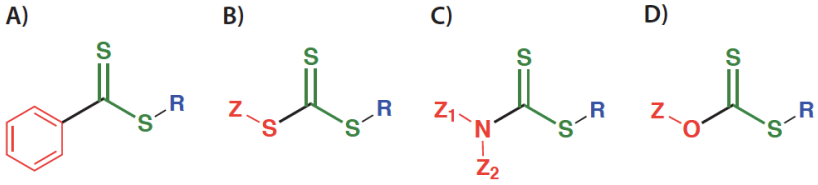

Figure 11. Four classes of RAFT agents: A) Dithiobenzoates, B) Trithiocarbonates, C) Dithiocarbamates, and D) Xanthates. Adapted from Controlled Radical Polymerisation Guide Aldrich® Materials Science.

Mechanism of RAFT polymerisation

Initiation and radical–radical termination that occur in free radical polymerisation can be eliminated by the addition of a propagating radical ($P^{\bullet}_{n}$) to the thiocarbonylthio compound [RSC(Z)=S (1)] (Figure 12). Fragmentation of the intermediate radical gives a polymeric thiocarbonylthio compound [PnS(Z)C=S (3)] and a new free radical (R•). This free radical (R•) reacts with the monomer to form a new propagating radical ($P^{\bullet}_{m}$). There will be rapid

equilibrium between the active propagating radicals ($P^{\bullet}_n$ and $P^{\bullet}_m$) and the dormant polymeric thiocarbonylthio compounds (3) that equalises the probability for all chains to grow simultaneously and produce narrowly dispersed polymers. Once the polymerisation is complete or stopped, most of the chains carry the thiocarbonylthio end-group and can be collected as stable materials (Moad, G. et al. 2005, 2006, 2009, 2012).

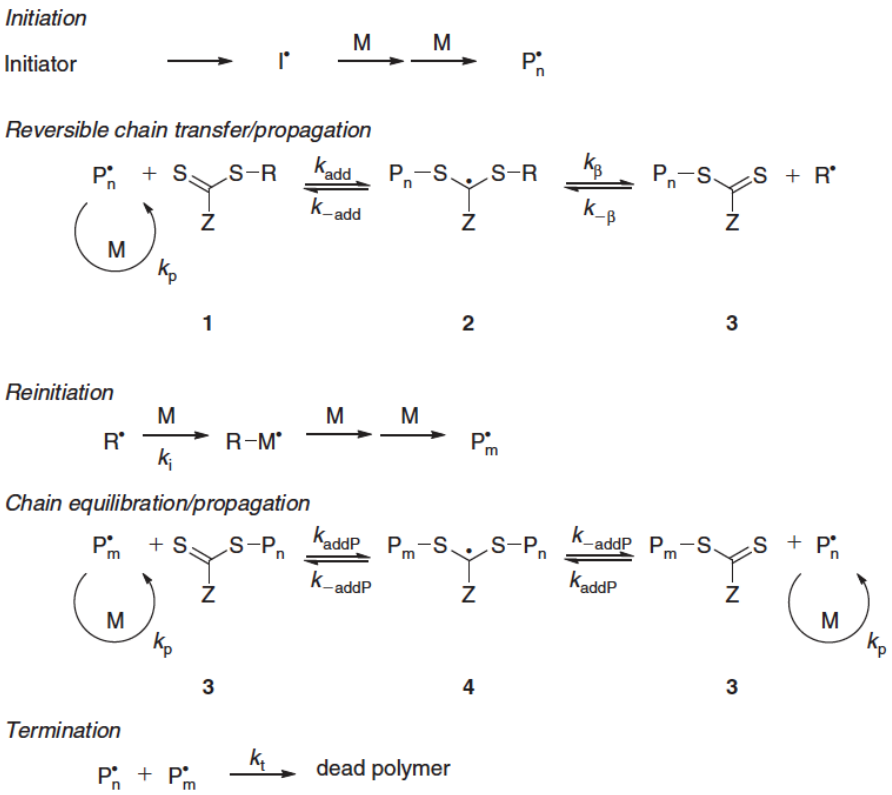

Figure 12. The mechanism of RAFT polymerisation. Adapted from Moad, G. et al. 2005, 2006, 2009, 2012.

1.2.7 Stimuli-responsive polymers

Stimuli-responsive polymers are also known as ‘smart’ polymers because of their behaviour in response to external stimuli such as temperature, pH or light (Figure 13).

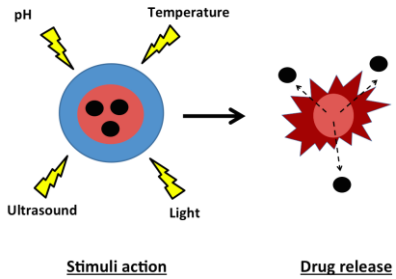

Figure 13. Stimuli-responsive release of a drug from a nanocarrier.

Stimuli-responsive polymers which exhibit a thermo-reversible hydrophilic-to-hydrophobic phase transition are called thermo-responsive (TR) polymers. TR polymers show sharp coil to globule transition from soluble to insoluble at a temperature which is known as lower critical solution temperature (LCST) (Figure14) (Bernstein, R. E. et al. 1977; Fleige, E. et al. 2012; Henderson, E. et al. 2009; Ougizawa, T. et al. 1986; Plate, N. A. et al. 1999; Zhang, Y. et al. 2007).

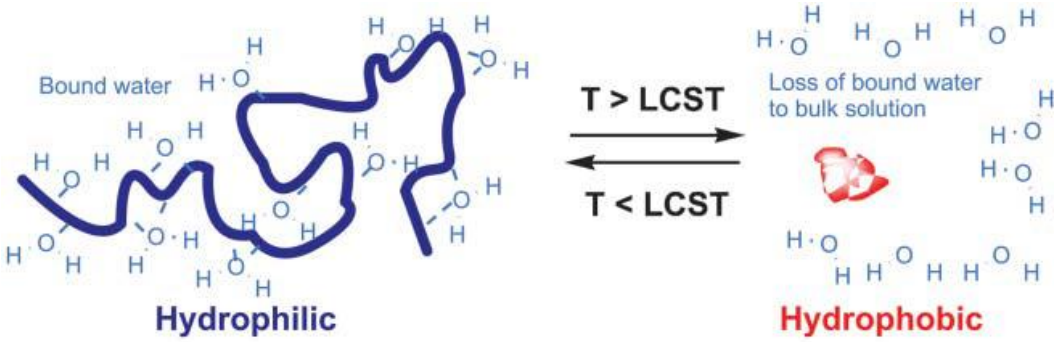

Figure 14. Thermo-responsive polymer responds to temperature and shows sharp coil to globule transition from soluble to insoluble. Adapted from De las Heras Alarcon, C. et al. 2005.

The LCST phenomenon is largely dependent on the hydrogen-bonding capabilities of the constituent monomer units. Furthermore, there must be a balance between polymer-water interaction and hydrophobic interaction to facilitate thermo-responsive properties. At the LCST, this balance is disrupted and polymer-polymer interaction is favored compared to polymer-water interaction which leads to insolubility of the polymer in water. In other words, the balance between the hydrophilic and the hydrophobic moieties of the molecular structure of the polymer regulates the thermo-responsive

properties. Two polymers showing this property are poly(N-isopropylacrylamide) (PNIPAM) and poly(ethylene glycol methacrylate) (PEGMA) (Figure 15)(Becer, C. R. 2008; De las Heras Alarcon, C. et al. 2005; Lutz, J. F. 2008).

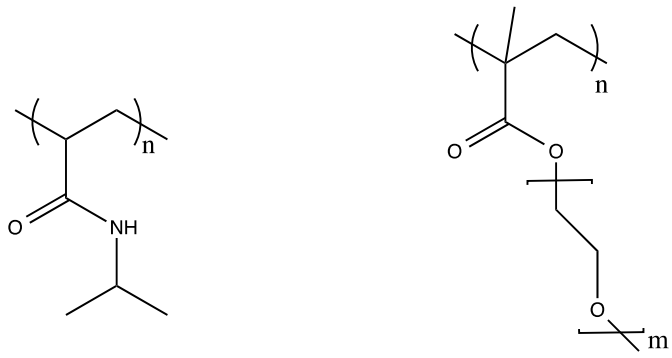

Poly(N-isopropylacrylamide) **Poly (ethylene glycol) methacrylates**

Figure 15. Chemical structures of commonly used thermo-responsive polymers.

The mechanism and nature of the LCST can be explained thermodynamically by the Gibbs energy of a system.

$$\Delta G = \Delta H - T\Delta S$$

ΔG	Change in free energy, indicating the direction of a chemical reaction
ΔH	Change in enthalpy
ΔS	Change in entropy
T	Temperature

When the polymer dissolves in water at low temperature there is formation of a large number of hydrogen bonds between the solvent and the solute which is favored by the enthalpy of dissolution. As the temperature increases the hydrogen bonds are disrupted resulting in a reduced enthalpic contribution and an increasing entropic contribution. Therefore, the entropic contribution dominates and phase separation is favored over dissolution (Abulateefeh, S. R. et al. 2011; De las Heras Alarcon, C. et al. 2005).

As hydrogen bonding plays an important role in LCST, altering the number of these bonds can shift the LCST onset to lower or higher temperatures by rational design. This can be achieved by co-polymerisation with other hydrophilic or hydrophobic monomers to increase or decrease the LCST respectively (Becer, C. R. 2008; Lutz, J. F. 2008).

1.2.8 Polymeric micelles

As described earlier, polymeric micelles consist of amphiphilic block copolymers having a hydrophilic and a hydrophobic block. After self-assembly, the hydrophilic block forms a shell, and the hydrophobic block forms a core, which encapsulates the hydrophobic drug and protects it from the surrounding medium (Figure 16) (Kataoka, K. et al. 2012). Moreover, these polymeric micelles can turn to stimuli-responsive micelles by incorporating thermo-responsive block segments in the outer shell (de Las Heras Alarcon, C. et al. 2005).

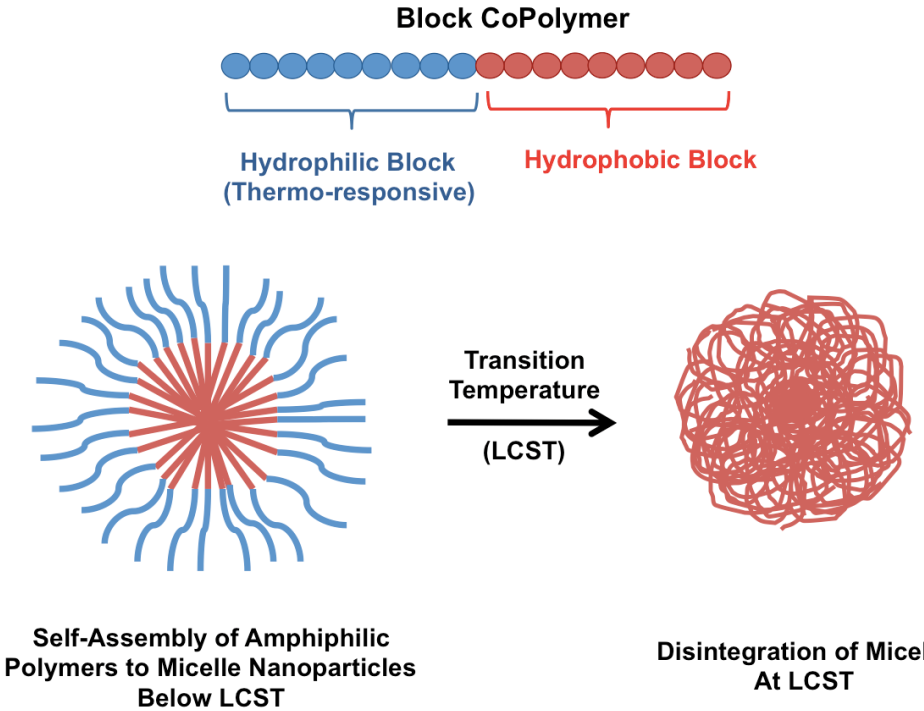

Figure 16. The amphiphilic block copolymers self-assemble to form a TR polymeric micelle having hydrophobic core and hydrophilic shell. By application of heat at LCST, the hydrophilic shell turns hydrophobic and leads to micelle dissociation.

The colloidal stability of thermo-responsive polymeric micelles is compromised at the LCST. The TR shell is transformed from hydrophilic to hydrophobic by application of local hyperthermia and releases the encapsulated hydrophobic contents at the tumor site (Chung, J. E. et al. 1999. Fleige, E. et al. 2012; Gil, E. S. et al. 2004; Smith, A. E. et al 2010; York, A. W. et al. 2008). The optimum size of the polymeric micelle for effective tumour penetration and distribution in poorly vascularised tumours as pancreatic adenocarcinoma is ca. 30-40 nm (Cabral, H. et al. 2011). The advantages of polymeric micelles over other types of nano carriers are:

- They are made up of high molecular weight polymers which enhance the stability and elongate their dissociation time upon dilution in the blood stream.

- Their shell consists of hydrophilic polymers that are able to circulate in the blood for longer periods of time without being recognised and cleared.

- Prolonged shelf life.

- They have appropriate size that enables them to escape renal excretion which allows for extravasation and accumulation at the tumor site.

- The physical entrapment of hydrophobic drugs is relatively easy and efficient (Husseini, G. A. et al. 2008).

1.2.9 Thermotherapy

Thermotherapy or the use of mild hyperthermia (HT) in adjunction with chemotherapy has recently received significant interest (Husseini, G. A. et al.

2014). This method involves raising the temperature of tumor tissues. There are several reasons for using HT to treat cancer:

- Mild HT enhances the therapeutic effectiveness by increasing the local blood flow at the exposed area (Kong, G. et al. 2000).

- By tuning the LCST of TR micelles, highly selective delivery to tumor tissues can be further enhanced without affecting healthy tissues (Howard, B. et al. 2006; Rapoport, N. Y. et al. 1999).

- Mild HT enhances the extravasation of tumor blood vessels and improves the transfer of drugs and nano-carriers. This is because heat disaggregates the endothelial cells of tumor vessels leading to morphological changes which in turn increase the pore size between cells (Kong, G. et al. 2000).

- Both human and rodent culture cells have been shown to grow and divide constantly at temperatures below 40–42 °C. Cell death can occur due to exposure to any temperature above the normal growth temperature (Lepock, J. R. et al. 2003).

- Cancer cells are not inherently more susceptible than normal cells to heat, but because of the low oxygen level, acid concentration and insufficient nutrients in the tumor microenvironment, these cells are less able to tolerate the added stress such as heat (Freeman, C. et al. 2008).

- High HT (43–46 °C) rapidly destroys cancer cells by damaging several cellular components such as membranes, the cytoskeleton (Velichko, A. K. et al. 2013) and induces direct DNA denaturation (Lepock, J. R. 1993).

- High HT induces cell death at different phases of the cell cycle. The mitotic phase shows the highest heat sensitivity by damaging of the

mitotic apparatus leading to inefficient mitosis followed by consecutive polyploidy. Furthermore, in the S-phase the cells undergo chromosomal damage. In both S- and M-phases, cell death occurs slowly compared to G1-phase which do not show any microscopic damage but the cell death occurs immediately after hyperthermia (Hildebrandt, B. et al. 2002).

Local hyperthermia can be supplied by high intensity focused ultrasound (HIFU) probes. Studies showed that mild hyperthermia induced by HIFU could be used as an effective treatment which may enhance cell apoptosis and reduce tumor growth in pancreatic carcinoma (Gasselhuber, A. et al. 2012; Kirui, D. K. et al. 2015; Lee, E. S. et al. 2013; Lee, J. Y. et al. 2011; Li, J. et al. 2008; Schroedera, A. et al. 2009; Staruchi, R. M. et al. 2012). Ultrasound (US) is finding a place in drug delivery because of its non-invasive nature, its ability to focus on targeted tissues, and by rendering cell membranes more permeable (Figure 17). US can be defined as pressure waves having frequencies of 20 kHz or greater. These waves are generated by piezoelectric transducers that are in contact with water, gel, or some other media that can efficiently transmit ultrasonic waves.

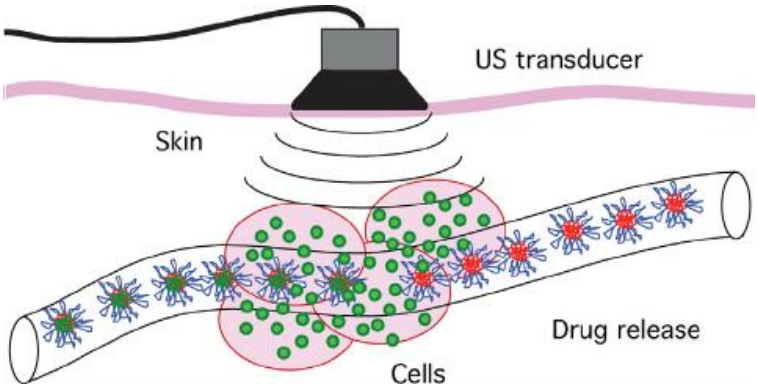

Figure 17. Adjunction of mild hyperthermia with chemotherapy. The green dots represent the chemotherapeutic drug released locally from the nano-carrier after application of US (Husseini, G. A. et al. 2014).

The transducers can transfer sound waves into the body tissue only and not into air. Hence, they are placed in direct contact with tissue or the skin without the presence of air in between by using fluids such as water or ultrasonic gels. US can penetrate deeply depending upon the wavelength and the tissue type;

therefore, it can be used for local tissue hyperthermia (Husseini, G. A. et al. 2008).

Pluronics® micelles gained special attention in ultrasonic drug delivery (Pitto-Barry, A. et al. 2014). They are triblock copolymers often denoted by PEO-PPO-PEO where PEO represent the hydrophilic block poly(ethylene oxide), and PPO the slightly hydrophobic middle block poly(propylene oxide). Rapoport et al. successfully entrapped anticancer drugs such as doxorubicin for ultrasonically triggered release. *In vitro* cell viability results showed that the micelles protected the cells from DOX induced cytotoxicity when US was not applied. Conversely, the cell death increased significantly even more than free DOX when US was applied (Rapoport, N. Y. et al. 1999).

Similarly, Howard el al. studied the effect of ultrasound on paclitaxel in micelles of methyl capped poly(ethylene oxide)-co-poly-(L-lactide)-tocopherol on a breast cancer drug-resistant cell line. They reported that paclitaxel accumulation inside the cells was reduced without ultrasonication when compared to free or non-encapsulated paclitaxel. This was due to cell protection from the chemotherapeutic drug by encapsulation using polymeric micelles. However, after applying ultrasound, the drug accumulation from the encapsulated paclitaxel drastically increased. The study showed that polymeric micelles in conjunction with ultrasound were effective in tumor regression and improving the drug uptake (Howard, B. et al. 2006).

1.2.10 Chemotherapeutic drugs for pancreatic cancer

1.2.10.1 Gemcitabine

Gemcitabine (GEM) (2',2' –difluorodeoxycytidine; dFdC) (Gemzar®) is a nucleoside analogue and is the front-line drug for treatment of pancreatic cancer (Figure 18)(Daman, Z. et al. 2014).

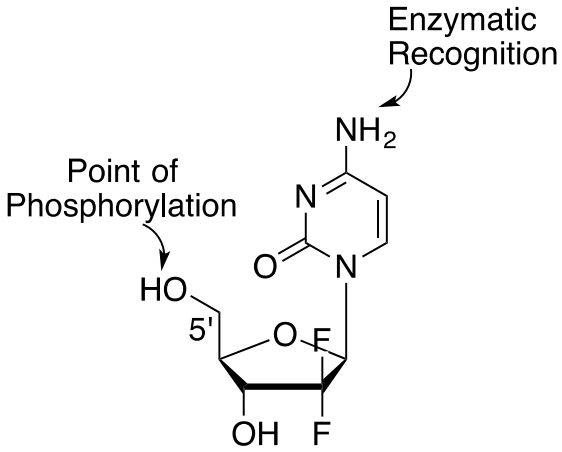

Figure 18. Gemcitabine structure.

GEM acts as an antineoplastic agent when it is converted to its active metabolite by deoxycytidine kinase in the cell cytoplasm (Figure 19). 5'-diphosphate and 5'-triphosphate derivatives are two active metabolites of GEM that after phosphorylations inhibit further cancer cell proliferation by disrupting DNA synthesis. Gemcitabine 5'-diphosphate prevents ribonucleotide reductase, an enzyme responsible for regulating total rate of DNA synthesis, whereas gemcitabine 5'-triphosphate integrates into the DNA and hinders nuclear replication (Weiss, J. T. et al. 2014; Wu, W. et al. 2007).

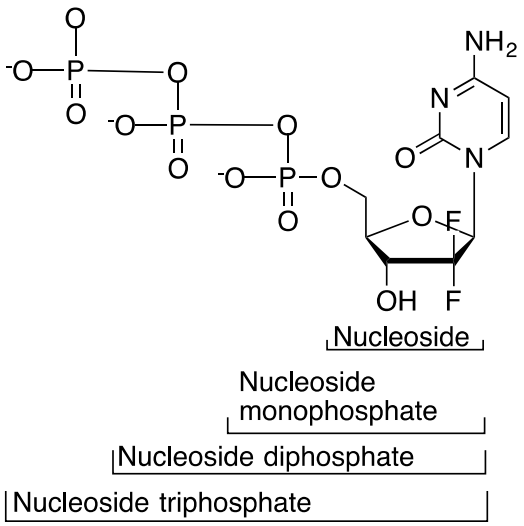

Figure 19. Gemcitabine is continuously phosphorylated to its active metabolites by deoxycytidine kinase intracellularly.

Pancreatic tumors develop GEM resistance over time. The resistance is related to the mechanism of action of GEM as it is a very hydrophilic drug (LogP: -1.4), it enters cells by using membrane proteins called nucleoside transporters. The main transporters are:

- Human equilibrative nucleoside transporter 1 and 2 (hENT1 and hENT2).
- Human concentrative nucleoside transporter 1 and 3 (hCNT1 and hCNT3).

There are low expressions of hENT1 on pancreatic tumors which block the cellular uptake of GEM and consequently decrease its toxicity towards cancer cells. In addition, this transporter is bidirectional in nature and as a result may cause drug efflux at higher concentrations. Similarly, the loss of hCNT1 cell surface expression and activity was found to correlate directly with high GEM chemoresistance. hENT2 is involved in the development of GEM chemoresistance by the loss of plasma membrane localisation and/or transport function which is one of the causes of the impaired uptake of the drug, resulting in a gain of chemoresistance. hCNT3 exhibits electrostatic interaction with the hydroxyl group of gemcitabine in order to transport the substrate (Chung, W. G. et al. 2012; Hung, S. W. et al. 2012; Nishio, R. et al. 2011; Reddy, H. et al. 2007).

Intravenous infusion of GEM (Trade name: Gemzar®) is prepared by reconstitution of GEM in a 0.9% sodium chloride injection. GEM's short plasma half-life (8–17 min) gives rise to administration of high dosing of 1000-1250 mg/m^2 as a 30 min intravenous infusion (once weekly for a 3 or 4 week cycle) in order to achieve the therapeutic drug level (Bender, D. M. et al. 2009; Cattel, L. et al. 2006; Immordino, M. L. 2004). After administration, GEM rapidly undergoes deamination by cytidine deaminase in the human plasma and the liver and hence becomes biologically inactive since it is not a substrate for further phosphorylation to monophosphate by deoxycytidine kinase (Bender, D. M. et al. 2009). Therefore, many different approaches have been tested to improve GEM stability and its protection against rapid metabolic inactivation either by modification of the amine group such as PEG-

gemcitabine (Vandana, M. et al. 2010; Chuang, K. H. et al. 2010), squalenoylation (Bui, D. T. et al. 2014; Desmaële, D. et al. 2012) or by protection of the amine group by encapsulating the drug in liposomes (Graeser, R. et al. 2009; Kirui, D. K. 2015; May, J. P. 2013; Paolino, D. et al. 2010; Zhou, Q. et al. 2012) or in polymeric micelles (Chitkara, D. et al. 2013; Daman, Z. et al. 2014).

1.2.10.2 Squalenoyl-Gemcitabine

In this research, in order to entrap hydrophilic GEM inside the hydrophobic micellar core the drug should be hydrophobised by synthesising its lipid derivative. Therefore, a lipophilic amino-protected GEM derivative, squalenoyl-Gemcitabine (Sq-Gem) (Figure 20) was used in which GEM ishydrophobised by attaching to squalene having 30 carbons chain.

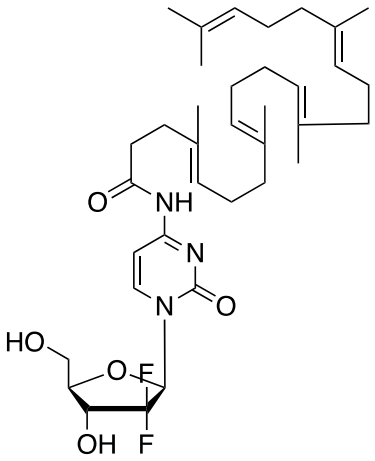

Figure 20. The chemical structure of Squalenoyl-gemcitabine.

Squalene (Figure 21) is an acyclic triterpene with the formula $C_{30}H_{50}$, an intermediate in the cholesterol biosynthesis pathway, which is widely distributed in nature with significant amounts found in olive oil and olive leaves. It contains two farnesol moieties joined in a tail-to-tail manner which cause symmetrical distribution of the 6 double bonds, 10 methylenes and 8 methyl groups in respect of the C12–C13 bonding (Desmaële, D. et al. 2012).

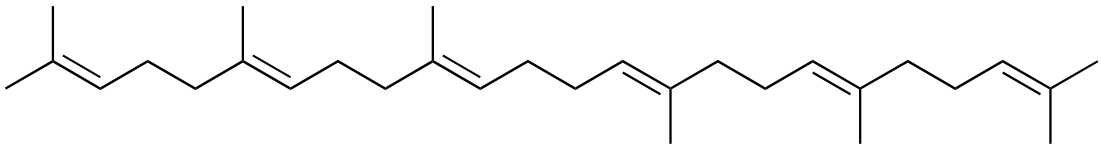

Figure 21. The chemical structure of squalene.

Couvreur et al. have synthesised bioconjugates of various drugs with squalene by covalent linkage through the method called as “squalenoylation”. These lipid–drug conjugates construct nanoassemblies of 100–300 nm in aqueous media which have improved the pharmacokinetics and increased the therapeutic index of the associated drugs (Desmaële, D. et al. 2012). The mechanism by which the Sq-Gem nanoparticles interacted with cells was investigated by using various endocytosis and active transport inhibitors. Unexpectedly, the cell entry of Sq-Gem occurred by a passive diffusion rather than by endocytosis or by an active transport through the nucleoside transporter hENT1 (Bildstein, L. et al. 2010). In addition, they found that Sq-Gem penetration accelerated due to the presence of cholesterol in the lipid monolayer. As a result, the penetration of Sq-Gem is enhanced due to the presence of cholesterol abundance in lipid rafts of cancer cells leading to increased cytotoxic activity (Pili, B. et al. 2010).

In short, the squalenoylation of Gem by Couvreur and coworkers revealed that Sq-Gem form nanoassemblies in the shape of spherical particles of 100-150 nm. Sq-Gem nanoassemblies showed higher anti-proliferative and cytotoxic effects compared to native GEM in BxPC-3, Capan-1 and Panc-1 human pancreatic cells. In addition, the conjugate helped to slow down the metabolism in plasma, decreased tumor growth, prevented further invasion of tumor cells and prolonged the survival time of RNK-16 LGL leukemia bearing rats (Couvreur, P. et al. 2006; Réjiba, S. et al. 2011).

1.2.10.3 Paclitaxel

Paclitaxel (PTX) is an antineoplastic agent used for the treatment of ovarian,

breast, lung and pancreatic cancers (Figure 22). PTX binds to beta-tubulin subunits and enhances the polymerisation and stabilisation of microtubules. The extraordinary stability of microtubule disrupts their normal dynamics required for cell division. As a result, microtubules assemble in the form of bundles leading to abnormal mitotic spindles after production and inhibit cell replication. (Adams J. D. et al 1993; Hamel, E. et al. 1981; Parness, J. et al. 1981; Rowinsky, E.K. et al 1990; Schiff, P.B. et al. 1979; Schiff, P.B. et al. 1981).

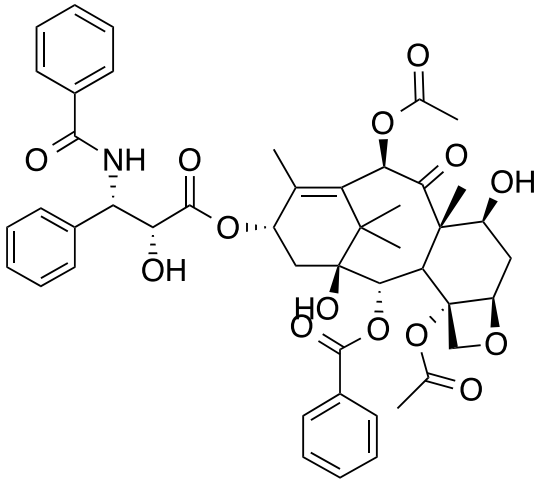

Figure 22. Paclitaxel structure.

PTX is poorly soluble in aqueous media (less than 0.03 mg/ml) which makes its delivery challenging. Hence formulations of Paclitaxel have been developed using carriers or solvents (Singla, A. K. et al. 2002; Suffness, M. 1995).

The first PTX formulation used was Taxol ® Injection which was a clear yellowish viscous solution that consists of 6 mg/mL of the active drug in 50% of polyethoxylated castor oil (Cremophor® EL) and 50% anhydrous ethanol (1:1 v/v mixture). The formulation is available in 30 mg (5 mL), 100 mg (16.7 mL), and 300 mg (50 mL) multidose vials. For administration, the drug is diluted 5-20 times in saline or 5% dextrose to final concentration of 0.3 to 1.2 mg/mL. (Suffness, M. 1995; http://www.accessdata.fda.gov accessed April 2016). However, Cremophor is not an inert vehicle and has many side effects

such as severe anaphylactic hypersensitivity reactions, lipoprotein patterns and hyperlipidaemia, neurotoxicity and reversal of the P-glycoprotein activity. Therefore alternative formulations were developed to allow for a better control of the toxicity and pharmacological interactions related to the use of Cremophor (Gelderblom, H. et al. 2001).

To overcome Cremophor related side effects, a new PTX formulation was developed using PTX in combination with albumin which is known as nab-paclitaxel, nanoparticle albumin–bound paclitaxel or protein-bound paclitaxel under the trade name Abraxane®. This formulation currently is used as first-line treatment, in combination with GEM, for the treatment of metastatic adenocarcinoma of the pancreas with fewer side effects. (http://www.cancerresearchuk.org; http://www.cancer.gov accessed April 2016). The mechanism of delivery of nab-paclitaxel has been mediated by active transport of albumin into the interstitial space via gp60-mediated transcytosis (Vogel S. M. et al. 2001). In an international randomised phase III trial, patients with metastatic pancreatic cancer who were treated with a combination of Abraxane® and Gemzar® lived longer than patients who were treated with GEM alone. Patients who received both drugs also lived longer without their disease getting worse (Table 2) (Van Hoff, D. D. et al. 2013).

Table 2. A total of 861 patients were randomly administered nab-paclitaxel plus gemcitabine (431 patients) or gemcitabine (430) (Van Hoff, D. D. et al. 2013).

	Gemcitabine group	**Nab-paclitaxel + Gemcitabine group**
The median overall survival	6.7 months	8.5 months
The survival rate	22%	35%
The median progression-free survival	3.7 months	5.5 months
The response rate	7%	23%

The next generation of branded PTX formulation branded as Cynviloq™ will be launched to the market by Sorrento therapeutics. Cynviloq™ (Genexol-

PM®) is a paclitaxel-loaded micellar diblock copolymer for the treatment of metastatic breast cancer, non-small cell lung cancer and pancreatic cancer. The polymeric micelles consist of a hydrophobic poly-lactide block and a hydrophilic poly(ethylene glycol) block which self-assemble and encapsulate PTX within their core. The new formulation is smaller in size and has more drug loading capacity compared to Taxol ® and Abraxane®(Figure 23)(Liggins, R. T. et al. 2002).

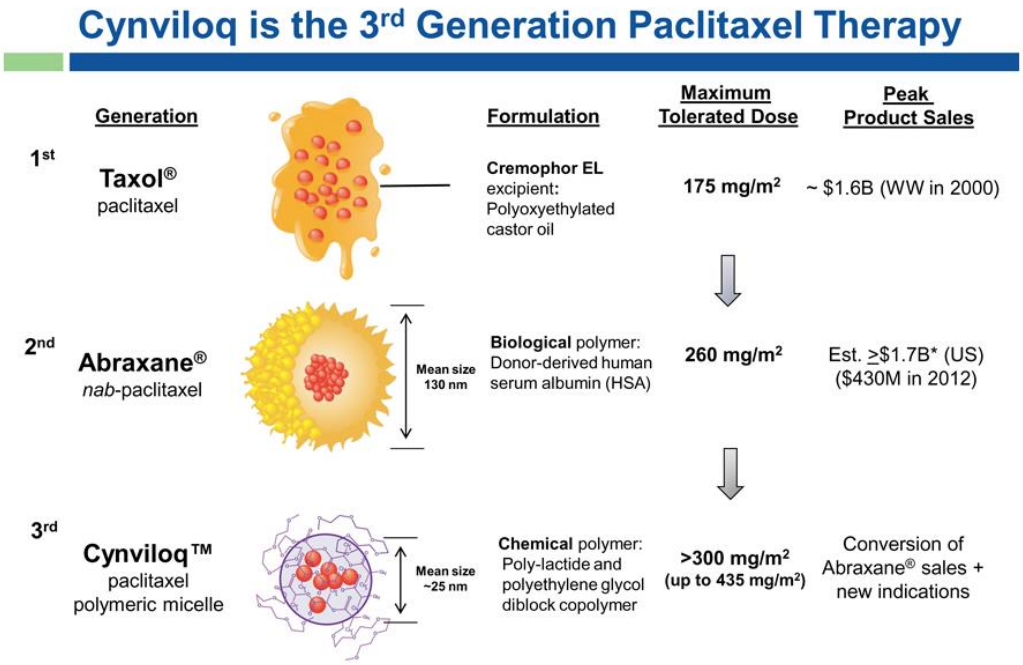

Figure 23. Three generations of branded paclitaxel formulations (Adapted from sorrentotherapeutics.com Accessed April 2016).

1.2.10.4 Synergistic antitumor activity of nanoparticle albumin-bound (nab)-paclitaxel and Gemcitabine

The Tuveson research group investigated synergistic antitumor activity of nab-paclitaxel when administered clinically in combination with GEM on patients with metastatic pancreatic ductal adenocarcinoma (PDA). The combination treatment exhibited synergistic antitumor activity and improved drug delivery. In addition, they also reported that administration of nab-paclitaxel and GEM caused tumor regression and reduced metastasis (Frese, K. K. et al. 2012). Furthermore, Von Hoff and co-workers reported that nab-

paclitaxel induced angiogenesis, resulting in increased perfusion and delivery of GEM (Von Hoff D.D. et al. 2011).

Another study was designed to assess the clinical efficacy of the combinational therapy of nab-paclitaxel and GEM. The results demonstrated an increase in the median survival of GEM monotherapy from 6.8 months to 12.2 months after combinational therapy in a phase III trial with comparable patients (Conroy, T. et al. 2011).

Gemcitabine and paclitaxel show their antitumoral effects through induction of apoptosis or a cell-cycle arrest in S and M phase, respectively (figure 24).

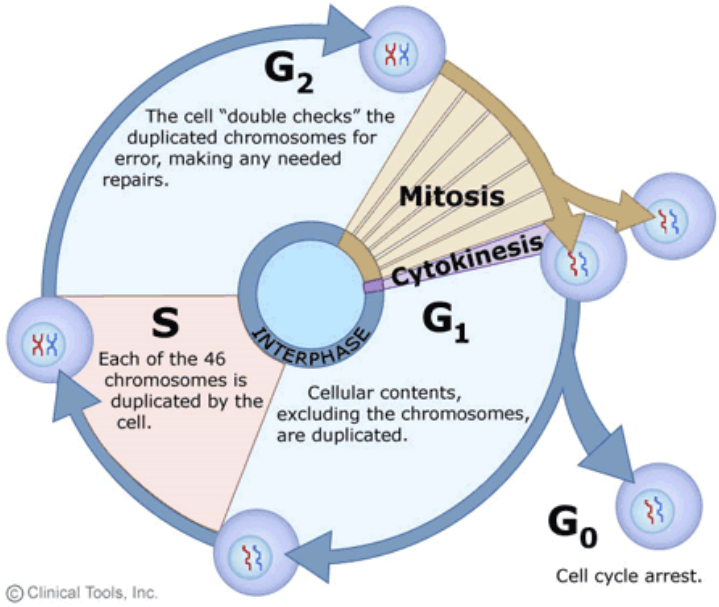

Figure 24. Cell cycle (Adapted from www.le.ac.uk).

Tuveson et al. have explained that the mechanism behind the improved delivery in combinational treatment was due to increase intratumoral GEM levels as a result of decrease in the primary GEM metabolising enzyme, cytidine deaminase. Nab-paclitaxel reduced the levels of cytidine deaminase protein through reactive oxygen species–mediated degradation, leading to increased stabilisation of GEM and increased the amount of its activated metabolite gemcitabine triphosphate (dFdCTP) in tumors (Frese, K. K. et al. 2012).

To the best of my knowledge, this is one of the very first reports on co-encapsulation and co-delivery of two potent chemotherapeutic drugs by thermoresponsive polymeric micelles. Also the present study constitutes the very first report on drug synergism augmentation by thermoresponsive polymeric micelles accompanied by simultaneous cell membrane interaction. Recent studies conducted on co-encapsulation and co-delivery of drugs using different types of polymeric micelles are shown in table 3.

Table 3. Recent studies on co-encapsulating and co-delivery of drugs for treatment of several diseases.

Co- delivery	Nano-carrier	Treatment	Reference
Gemcitabine and miR-205	cationic polymeric mixed micelles	advanced pancreatic cancer	(Mondal, G. et al. 2017)
Doxorubicin and *α*-tocopheryl succinate	pH sensitive polymeric micelle	colon cancer	(Debele, T. A. et al. 2017)
Paclitaxel and retinoic acid	mixed polymeric micelle	multidrug resistance	(Emami, J. et al. 2017)
Doxorubicin and P-glycoprotein siRNA	polymeric micelle	multidrug resistance	(Zhang, C-G. et al. 2016)
Paclitaxel and lapatinib	pluronic F127 polymeric micelle	metastatic breast cancer	(Dehghan Kelishady, P. et al. 2015).
Doxorubicin and paclitaxel	pluronic-based functional polymeric mixed micelles	multidrug resistance	(Chen, Y. 2015)
Doxorubicin and paclitaxel	polymeric micelles	non-small cell lung cancer	(Lv, S. et al. 2014)
Doxorubicin and thioridazine	polymeric micelles	breast cancer	(Ke, X.-Y. et al. 2014)

1. 3 Aim

The objective of this research was to synthesise thermo-responsive polymeric micelles which could be used as a nano-carrier to co-encapsulate two chemotherapeutic drugs, Sq-Gem and PTX, in order to improve their delivery (Figure 25) and exert their synergistic cytotoxic effect (Figure 26).

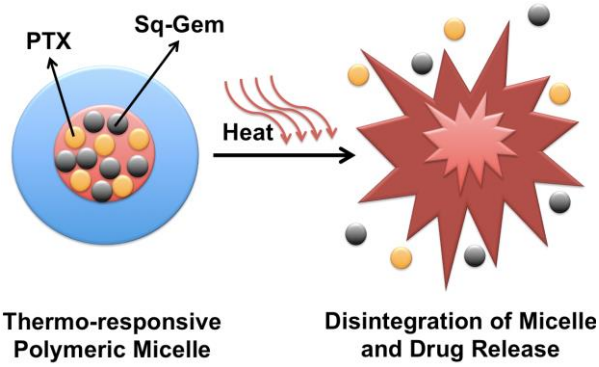

Figure 25. TR polymeric micelles encapsulate Sq-Gem and PTX at body temperature. After application of heat the micelles disintegrate and release the drugs.

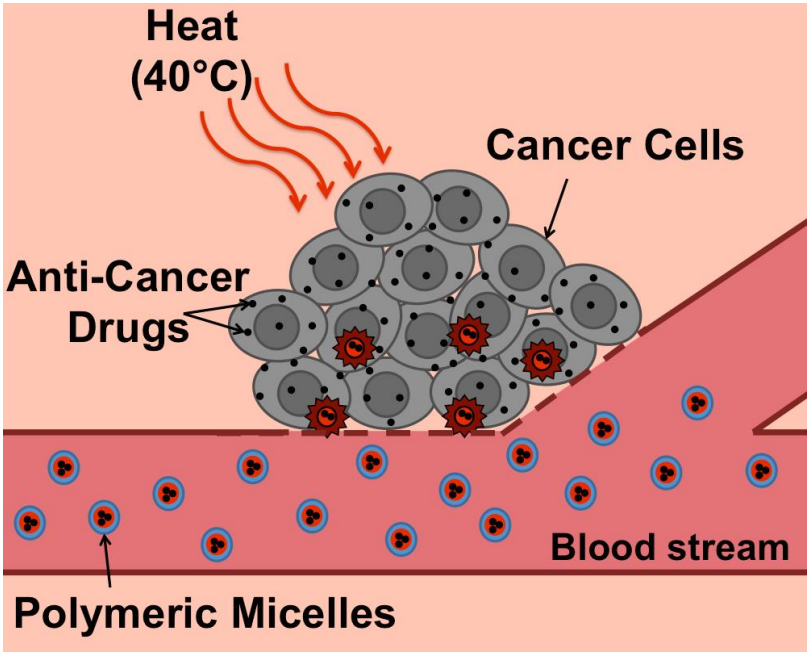

Figure 26. TR polymeric micelles accumulate within the tumor site by the EPR effect. After application of heat at the tumor site, the micelles are disrupted and release the drugs and induce cancer cell apoptosis.

1. 4 Materials

All solvents were of analytical or HPLC grade and were purchased from Sigma-Aldrich. Double distilled water was used throughout all the experiments. 2,2′-azobis(2-methylpropionitrile) (AIBN), 2-butanone, 2-cyano-2-propyl benzodithioate (CTA/RAFT agent), 2-ethylhexyl methacrylate (EHMA), 3% phosphotungstic acid reagent, deuterated chloroform ($CDCl_3$), diethyl ether, di(ethylene glycol) methyl ether methacrylate (DiEGMA), dimethyl sulfoxide (DMSO), dulbecco's modified eagle's medium- high glucose (DMEM), dulbecco's phosphate buffered saline (DPBS), fetal Bovine serum (FBS), fluorescein *O*-methacrylate, hexane, lauryl methacrylate, L-glutamine, oligo(ethylene glycol) methyl ether methacrylate ($OEGMA_{300}$), phosphate buffered saline (PBS) tablets, phosphotungstic Acid Reagent 3%, penicillin-Streptomycin, pyrene, dimethylformamide (DMF), thiazolyl blue tetrazolium bromide (MTT), paclitaxel (PTX), taxus brevifolia was purchased from Fluorochem Ltd. MiaPaCa-2 cell line was purchased from ATTC company. Squalenoyl-gemcitabine (Sq-Gem) was provided by Prof. Patrick Couvreur's research group at Paris-Sud University.

1. 5 Methods

1.5.1 One pot synthesis of Poly (DiEGMA-co-$OEGMA_{300}$)-b-EHMA by RAFT polymerisation

DiEGMA (6 mmol, 1.107 mL), $OEGMA_{300}$ (4 mmol, 1.143 mL), AIBN (0.02 mmol, 3.3 mg) and CTA (0.08 mmol, 18 mg) were dissolved in 2-butanone (8 mL) in a 25 mL round bottom flask. The reaction mixture was sealed with a rubber septum and purged with argon for 10 minutes. The polymerisation started by placing the vessel in an oil bath at 75°C and was left under magnetic stirring. After 24 hours, EHMA (4 mmol, 896 µl) was dissolved in 3 mL 2-butanone and purged with Ar, and introduced to the reaction via a fine

needle. The reaction was stopped after 24 hours by cooling it down and exposing it to air. The polymer was precipitated in excess hexane, dried under reduced pressure, and collected as a pink viscous fluid (yield: 78%). The targeted DP for hydrophilic block and hydrophobic block were 120 and 50 respectively.

1.5.2 Nuclear magnetic resonance (NMR) spectroscopy

Liquid state ^{1}H NMR spectra of the polymers were recorded on a Bruker NMR spectrometer (Ultrashield 400 MHz). The polymers were dissolved in deuterated chloroform ($CDCl_3$) for analysis.

^{1}H NMR is a nuclei specific spectroscopy method which uses intense magnetic fields to perform analytical experiments on the nuclei of atoms. The atom consists of subatomic particles such as electrons, protons and neutrons which contain an intrinsic physical property called spin. The net spin of a nucleus follows certain principles which are as follows:

- There is no spin in the nucleus when the number of neutrons and the number of protons are both even.
- The nucleus has an integer spin (i.e. 1, 2, 3) when the number of neutrons and the number of protons are both odd.
- The nucleus has a half-integer spin (i.e. 1/2, 3/2, 5/2) when addition of the number of neutrons and the number of protons is odd.

In quantum mechanics, the nucleus with spin I, has 2I + 1 possible orientations or energy levels (Figure 27). Therefore, a nucleus with spin ½ has 2 possible orientations, the low energy level in which spins align with the external magnetic field (B_0) and the high energy level in which the spins align against B_0.

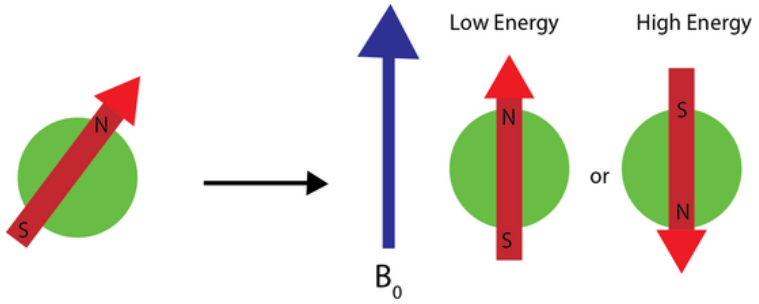

Figure 27. After application of an external magnetic field (blue arrow), the nuclear magnetic moments (red arrow) align with or against the field. Adapted from (chem.libretexts.org)

A nucleus is spinning on its axis in the lower energy level in the presence of a magnetic field. If the energy is absorbed by the nucleus the angle of precession will change. This change in the orientation of the rotational axis is known as the energy transition or spin flip at which the nucleus opposes the applied magnetic field at the higher energy level. The NMR measures the precession frequency which is identical to the transition frequency that caused a spin flip (Figure 28).

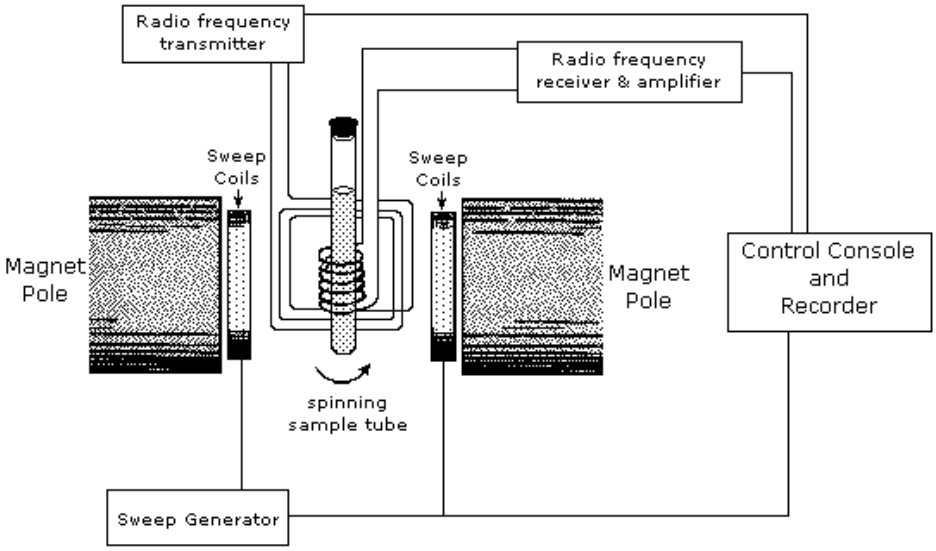

Figure 28. The mechanism of an NMR spectrometer (Adapted from Rice university website).

However, only a small proportion of the nuclei are in the lower energy state and can absorb energy. Hence by exciting these nuclei, the populations of the higher and lower energy levels will become equal and there will be no further absorption of radiation. The phenomenon at which the spin system is

saturated is called the relaxation process which returns the nuclei to their lower energy state.

Each nucleus is surrounded by orbiting electrons which create magnetic field. Thus, the nucleus experiences a local magnetic environment which shields the nucleus from the externally applied magnetic field. This means that different frequency is required to change the energy levels and excite the spin flip. This phenomenon is known as shielding (Figure 29). Conversely, the presence of an electronegative atom can decrease the electron density around the nucleus and help to resonate at lower field strengths.

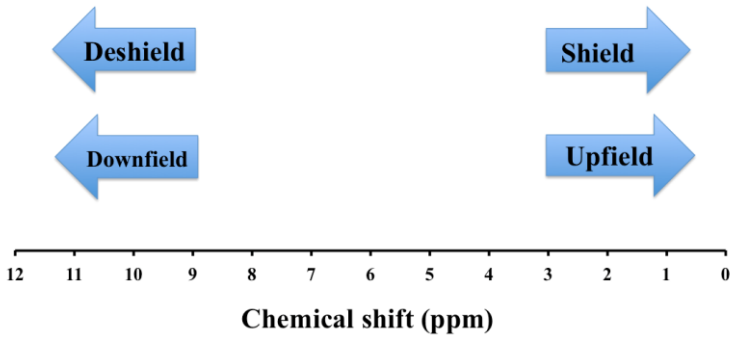

Figure 29. The nucleus feels weaker magnetic field due to electron density shielding the nucleus resulting in less chemical shift and moving upfields. Conversely, the nucleus feels stronger magnetic field due to deshielding due to the decreased electron density around the nucleus resulting in increasing chemical shift and moving downfields.

The chemical shift with unit of parts per million is the resonant frequency of a nucleus relative to a standard molecule (usually tetramethylsilane, $Si(CH_3)_4$) in a magnetic field. For example, a peak at a chemical shift of 9.0 ppm means that the nucleus needs a magnetic field nine millionths less than the field needed by tetramethylsilane to produce resonance (Becker, E. D. 1999).

1.5.3 Gel permeation chromatography (GPC)

GPC was conducted with DMF as the mobile phase containing 5 mM NH_4BF_4 additive at 70 ˚C at a flow rate of 1.00 mL/min. The GPC system was equipped with a solvent pump (Viscotek VE 1121), a degasser (Viscotek VE

7510), two Styragel columns (MGHHR-M E0057 and MGHHR-M E0058) and a refractive index detector (Viscotek VE 3580). The apparatus was calibrated prior to analysis by using linear poly(methyl methacrylate) polymers with narrow molecular weight distributions as standards. Then, 100 µL of polymer aliquots in DMF (40 mg/mL) was injected to the instrument to determine the average molecular weight (M_n) and index of polydispersity ($Đ_M$).

GPC also referred to as size exclusion chromatography (SEC) was used to characterise the polymer. GPC separates the molecules by using solid stationary and liquid mobile phases. The stationary phase in the column consists of tightly packed porous beads of controlled porosity and particle size (Figure 30).

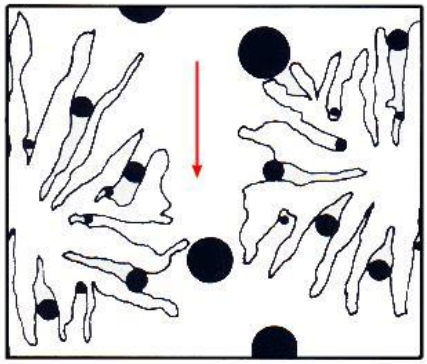

Figure 30. Cross section of porous beads in the stationary phase of the column (adapted from http://www.waters.com last accessed Oct. 2017).

The separation mechanism in the column is based on the hydrodynamic size of the molecule (Figure 31). The polymer sample is injected into the mobile phase and pumped through the GPC column. Small molecules take more time permeating across the porous matrix of the column, therefore their retention time increases. On the contrary, larger molecules' retention time is relatively shorter as they are unable to permeate through all of the pores, therefore they elute first. Detectors (refractive index, UV-Vis, light scattering and viscometer) monitor and record the separation. GPC software collects and collates the data and calculates the relative molecular weight values of polymer by

reference to their retention time using conventional calibration (Moore, 1964; Skoog, 2006).

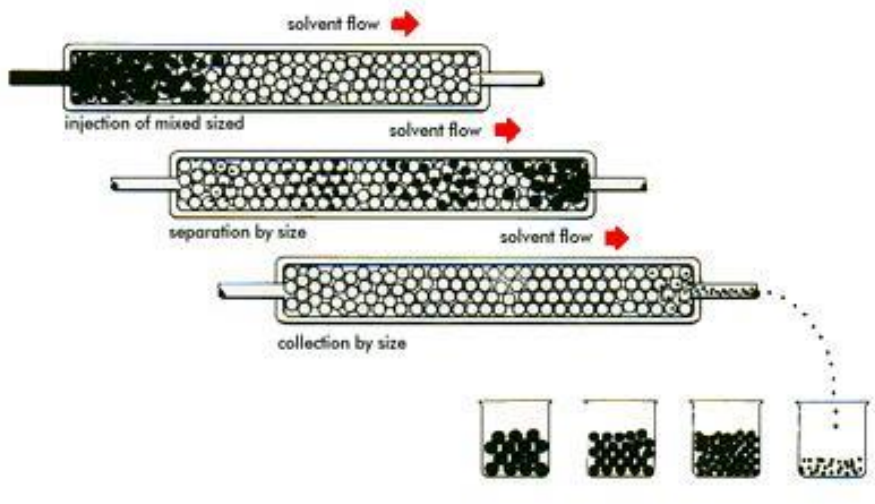

Figure 31. The porous beads inside the column elute the molecules of various sizes at different retention time (adapted from http://www.waters.com last accessed January 2018).

1.5.4 Determination of the polymers' LCST

The polymers (5 mg) were dissolved in 1 mL of PBS pH 7.4 and gradually heated by immersing the solution in a water bath of predetermined temperature and the LCST value was determined as the onset of optical turbidity for each sample by an Agilent Cary series UV-Vis spectrophotometer at 550 nm.

1.5.5 Critical micelle concentration (CMC) of Poly (DiEGMA-co-$OEGMA_{300}$)-b-EHMA

The formation of polymeric micelles by Poly (DiEGMA-co-$OEGMA_{300}$)-b-EHMA was studied using a standard pyrene procedure by florescence spectroscopy (Chung, J.E. et al. 1999; Jones, M.C. et al. 1999, Lee, S.C. et al. 2007). Briefly, 20 µl aliquots of pyrene in acetone (6.5×10^{-5} M) were added to a series of glass vials and the acetone was allowed to evaporate in open air. Subsequently, 1 mL of various concentrations of block copolymer samples

in water (ranging from 0.002 to 10 mg/mL) was added to each glass vial and left to equilibrate overnight under vigorous stirring. The fluorescence intensity of pyrene was measured using a spectrofluorometer (SpectraMax multi-mode microplate reader, Molecular device) where the excitation spectra were recorded from 280 to 350 nm and emission wavelength was fixed at 370 nm (Zhao, X. et al. 2012).

1.5.6 Preparation of drug loaded thermo-responsive polymeric micelles

The thin-film hydration method was used to load the drug molecules in the polymeric micelles. Polymer (5 mg/mL) and PTX/ Sq-Gem (500 µg/mL each) were dissolved in acetone (2 mL) and transferred in a 10 mL round bottom flask, followed by slow vacuum drying until a thin film was formed on the walls of the flask. Subsequently, hydration with 1 mL of PBS (pH 7.4) under vigorous stirring at room temperature for 5 min took place in order to form the micelles. The prepared micelles were further sonicated for 5 min before passing them through a 0.2 µm filter in order to isolate them as a nearly monodispersed suspension. The suspension was centrifuged (Sigma 3-16 KL) at 13300 rpm for 10 min at room temperature and the pellet was analysed by HPLC to measure the drug encapsulation efficiency.

1.5.7 Dynamic light scattering (DLS)

The particle size of the polymeric micelles were determined using a Zetasizer Nano ZS, Malvern Instruments Ltd., UK. The scattered laser beam (632.8 nm) was measured at an angle of 175°. The micelles were prepared by the thin-film hydration method as previously described (section 1.5.6). All samples were measured in a quartz cuvette at 25° C and the data were recorded by Malvern Zetasizer software 7.11.

DLS (Figure 32) operates on the principle of Brownian motion which is the random movement of particles in liquid due to the constant bombardment with molecules in their surrounding medium. The Brownian motion varies

depending upon the size of the particles: large particles have slow Brownian motion whereas smaller particles have rapid Brownian motion. This motion can be further influenced by temperature and viscosity and therefore monitoring of these factors is crucial for achieving the correct interpretation of size. DLS comprises a laser beam, a monochromatic light source, to illuminate the sample. After light strikes the particles in motion, the intensity of the scattered light is collected by a detector to determine the particle size distribution. The light scattering signal gives information about the particles' size and motion.

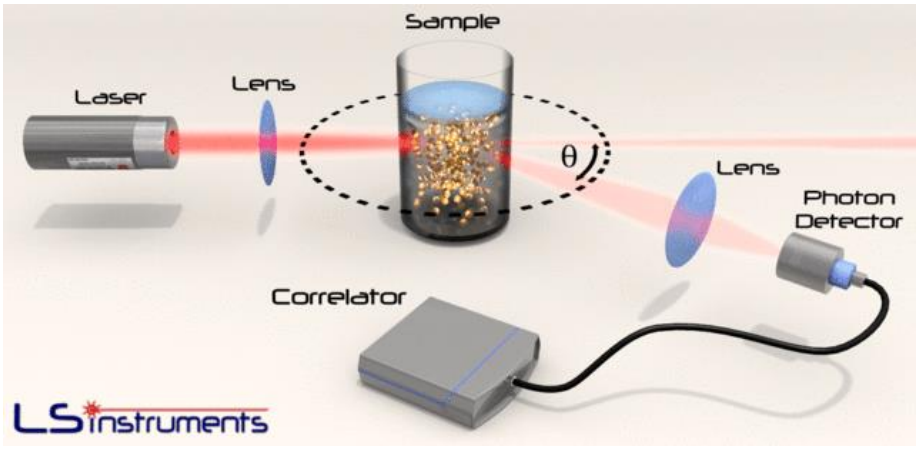

Figure 32. Schematic of a DLS instrument (Adapted from LSinstruments).

The random motions of the particles produce signals having different intensity due to the fluctuation of the scattered light (Figure 33). Then the correlator uses an auto correlation function (ACF) to determine the particle size by correlating the intensity to the diffusion coefficient of the particles.

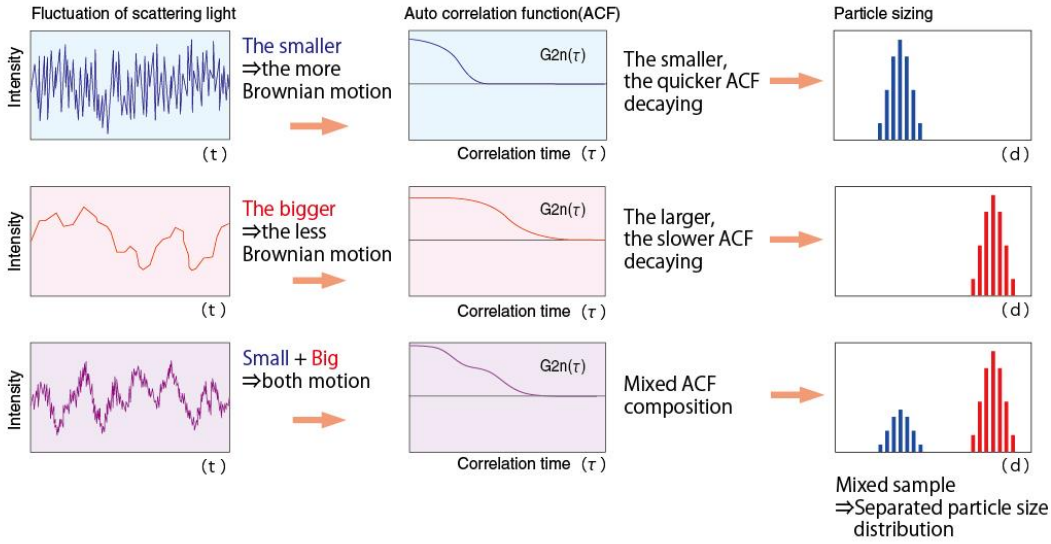

Figure 33. Analysis procedure of typical intensity vs time plot for three differently sized particles diffusing in solution (Adapted from www.otsukael.com)

The auto correlation function examines the changes in intensity of the scattered light over periods of time for a volume of particles. Once the diffusion coefficient is known the hydrodynamic radius can be determined using the Stokes-Einstein equation (Berne, B. J. et al.1976).

$$D=K_BT/6\pi\eta R$$

D = translational diffusion coefficient

K_B = Boltzmann's constant

T= Absolute temperature

η = Viscosity

R= hydrodynamic radius

1.5.8 Stability studies

The stability of the micelles was performed in order to elucidate their colloidal stability over time at static conditions. In colloidally stable micelles, the hydrophobic block of the polymers forms sufficient cohesion force in the hydrophobic core of micelles which in turn prevents dissociation of the

micelles over time. The micelles were prepared by the thin-film hydration method as previously described (section 1.5.6). The size of the synthesised polymeric micelles was measured using DLS for one week in order to monitor their stability in solution.

1.5.9 Transmission electron microscopy (TEM)

The morphology and size of the polymeric micelles was determined by TEM on a FEI/PHILIPS CM120 BioTwin microscope (Figure 34). A carbon coated copper grid was soaked by a drop of distilled water and after a few seconds it was removed by filter paper. Then a drop of the micellar suspension was placed on the grid and left to dry in open air. Before imaging, a drop of a staining solution (1% uranyl acetate reagent) was applied to enhance the contrast of the sample and a few seconds later it was also gently absorbed by filter paper. After drying, the grid was transferred to the sample holder ready to be introduced to the electron beam.

Electrons are emitted from a source that consists of a cathode and an anode. A ray of electrons is produced by heating up the cathode and are then collected by the anode and accelerate into a high energy beam towards the sample. TEM comprises high vacuum which helps keeping the electrons as a coherent beam since the electrons are negatively charged and repel each other as they travel through the air. The beam passes through an electromagnetic coil called condenser lenses to turn into more powerful and precise focus. The beam is then transmitted through the sample depending upon its electron transparency. The transmitted beam is focused by another electromagnetic coil, the objective lens, to form the image. Then, the image is enhanced by objective apertures which improve the contrast by blocking out high-angle diffracted electrons. The enhanced image is passed through the intermediate and projector lenses in order to be magnified on the fluorescent plate at the base of the instrument and is displayed on a screen (Williams D. B.et al. 2009).

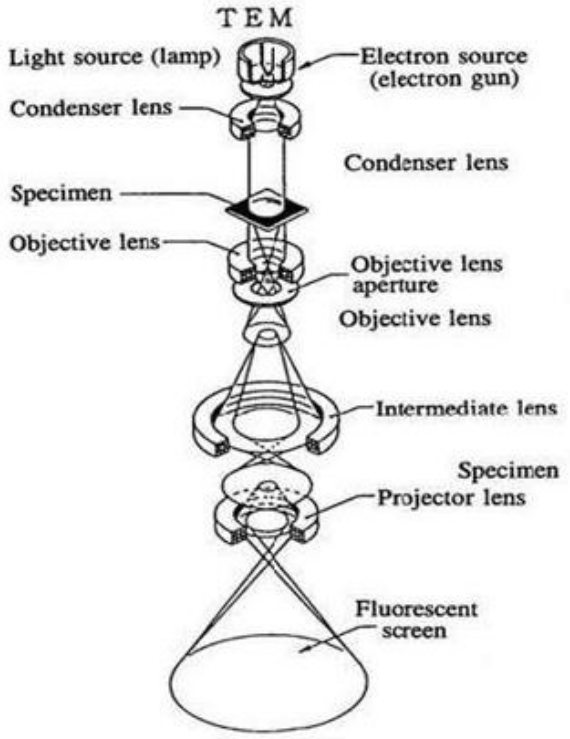

Figure 34. TEM layout describing the path of electron beam (Adapted from JEOL 2000FX Handbook).

1.5.10 HPLC analysis for drug encapsulation and release determination

An HPLC (High-performance liquid chromatography) assay for the quantification of both PTX and Sq-Gem was developed using an Agilent Technologies 1200 Series HPLC system. The chromatographic separation was achieved using a Phenomenex Synergi™ 4 µm Polar-RP 80 Å, LC Column 250 x 4.6 mm. Methanol and water (85:15) was introduced to the column as mobile phase under isocratic conditions. The mobile phase was pumped through the column at a flow rate of 1 mL/min. The UV detector was set at 250 nm and the injection volume was 20 µL. PTX and Gem-Sq standard solutions used for quantification were prepared by suitably diluting a 100 µg/mL working standard of each drug in a mixture of 80:20 methanol:water. The data was acquired and analysed using ChemStation for LC, software by Agilent Technologies, UK.

HPLC (Figure 35) is used to separate, identify and quantify each molecules. As all other chromatography techniques, it has a stationary phase that consists of a column packed with silica gel and a mobile phase comprising organic solvents and their mixtures. The pump helps to pressurise the mobile phase (methanol and water (85:15)) through the column and regulates the flow rate. The injector introduces the sample into the continuously flowing mobile phase stream that conveys the sample into the column filled with silica gel. Each component of the sample mixture interacts differently with silica at different lengths of the column as they flow through it. This is due to the dissimilar degree of polarity of the components. The UV detector measures the absorbance of the components at predetermined wavelength and monitors the chromatogram on a computer screen (Lough, W. J. et al. 1995).

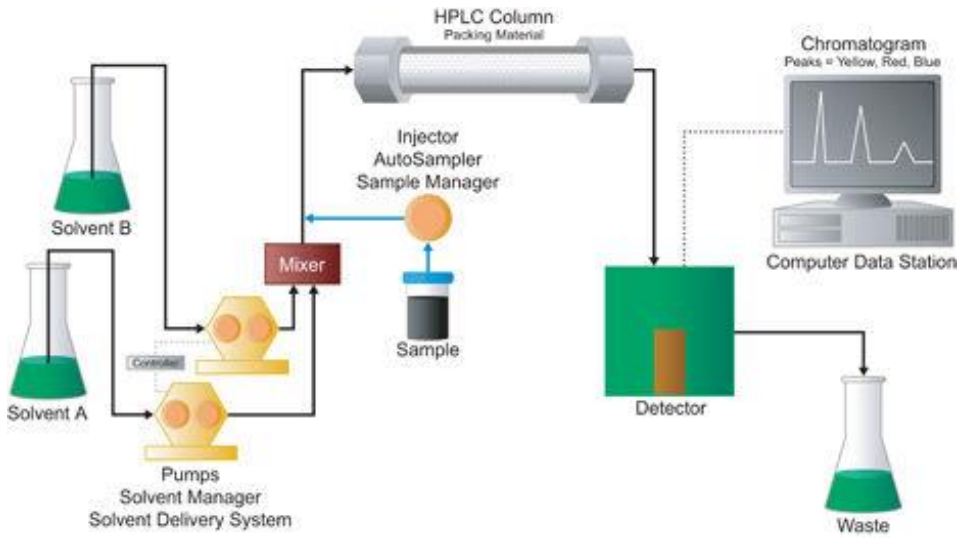

Figure 35. HPLC system set up (Adapted from www.Waters.co.uk).

1.5.11 Drug encapsulation efficiency

The drug encapsulation efficacy of PTX and Sq-Gem of the micelles was analysed by HPLC analysis in order to measure the amount of drug entrapped within the micelle's core. The encapsulation efficiency (EE) was calculated using formula:

$$EE(\%) = \frac{\text{Weight of initial drug} - \text{weight of unentrapped drug}}{\text{Weight of initial drug}} \times 100$$

1.5.12 Determination of in vitro drug release

The drug release profile from the micelles was evaluated using a Slide-A-Lyzer dialysis cassette (MWCO 7 kDa, Spectrum laboratories) (Figure 36). Drug loaded micelles (polymer 5 mg/mL, and PTX/Sq-Gem 500 µg/mL each) dispersed in 5 mL of PBS pH 7.4 (0.01 M) were transferred in the dialysis cassette by using a syringe, which was then immersed in 200 mL PBS pH 7.4 (0.01 M) containing 1% Tween 20. The drug release experiments were performed under mild stirring below and at LCST, 37°C and 40°C respectively, in order to compare the drug release profiles at different temperatures. At predetermined time intervals, aliquots (0.5 mL) were withdrawn from the cassette, which were replenished with fresh PBS pH 7.4 (0.01 M). The collected samples were centrifuged (Thermo Scientific Heraeus Fresco 17) at 13300 rpm for 10 min and analysed by HPLC to measure the drug concentration released at each time interval.

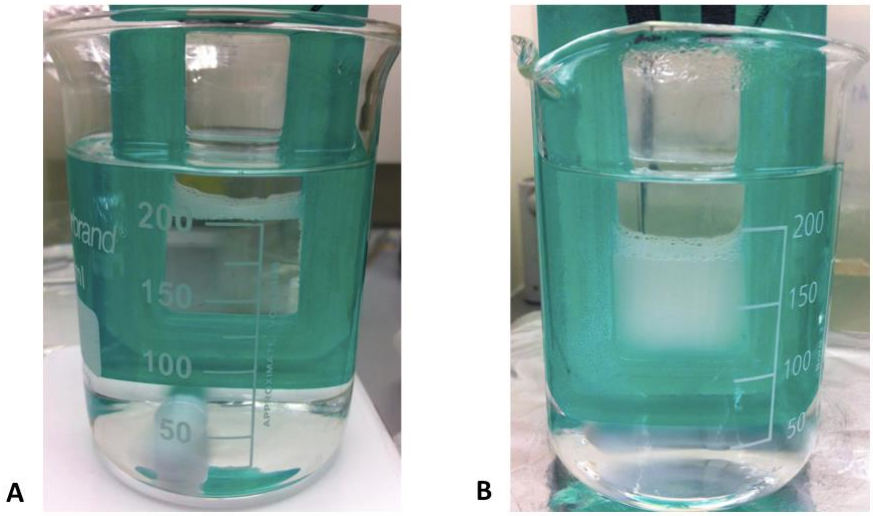

Figure 36. Demonstration of the drug release studies **A.** below LCST **B.** at LCST using the dialysis cassette.

1.5.13 In vitro cytotoxicity assay

The cytotoxicity studies were performed with the use of the MTT assay. MiaPaCa-2 cells were seeded in a 96-well plate at a density of 1×10^4 cells per

well. Cells were incubated in Dulbecco's modified eagle's medium- high glucose and supplemented with 10% fetal bovine serum, 1% penicillin-streptomycin and 1% L-glutamine. Incubation was performed either at 37°C (below) or 40°C (at LCST) in humidified atmosphere with 5% CO_2 for 24 h before the assay. Then, the medium was replaced with 200 µL medium containing block copolymer micelles loaded with 0.0001 - 10 µM of each drug. The free drugs were dissolved in DMSO and then diluted in the medium; briefly, concentrated stock solutions of Sq-Gem and PTX were prepared (1 mg/200 µL of DMSO). 3 µL of stock solution was diluted in 1997 µl of medium to achieve 10 µM for each drug. Further dilutions were carried out to obtain less concentrated samples. After incubation for 72 h, the medium was replaced by 100 µL of fresh medium and 25 µL of MTT stock solution (5 mg/mL in PBS) and incubated for an additional 4 h. Subsequently, the medium was removed and the formazan crystals were dissolved in 200 µL of DMSO. The plates were shaken for 2 min at room temperature before measuring the optical density (OD) at 570 nm on a SpectraMax® M2/M2e Multimode Microplate Reader, with SoftMax® Pro Software.

The MTT (3-(4,5-Dimethyl-2-thiazolyl)-2,5-diphenyl-2H-tetrazolium bromide) assay is one of the most reliable and consistent methods used to determine the cytotoxic effects of drugs on cell lines in vitro (Sylvester, P. W. 2011; Uludag, H. et al. 1990). The reason for the use of tetrazolium salts in cell biology is due to their unique characteristics, being both water soluble and lipophilic in nature. In addition, their most important feature is the presence of net positive charge that facilitates improved cellular uptake via the plasma membrane. In living cells the mitochondrial activity reduces tetrazolium salts to insoluble formazan crystals by the enzyme NAD(P)H-oxidoreductases. Thus, there is a linear relationship between cell viability, mitochondrial activity and reduction of salt to formazan. In turn, the formazan concentration can be measured by its optical density (OD) at 570 nm of treated cells and compared with the OD of cells not exposed to drugs (Berridge, M.V. et al. 2005; Mosmann, T. 1983; Van Meerloo, J. et al. 2011).

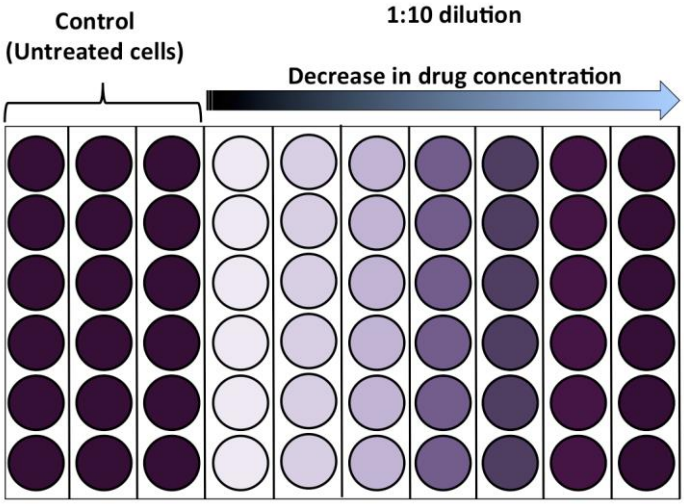

Figure 37. MTT assay plate setup.

Figure 37 shows the final stage of the MTT assay where the produced formazan crystals in each well are dissolved in DMSO in order to measure the OD. Control cells were not exposed to the drugs and appeared as dark purple representing high mitochondrial activity as a result of high cell viability. However, the wells having the highest drug concentration showed very pale purple color revealing the fact that there was less formation of formazan due to reduction of mitochondrial activity.

1.5.14 Calculation of the combination index

The combination index (CI) was investigated in order to measure the combinatorial therapeutic effect resulting from co-delivery of Sq-Gem and PTX. When CI > 1 implies antagonistic behavior, CI = 1 corresponds to additive behavior and CI < 1 represents synergistic behavior (Chou, T. C. 1984). CI was calculated based on the IC_{50} values obtained from MTT assay by using the following equation.

$$\mathrm{CI} = \frac{\mathrm{IC50\ (A+B)}}{\mathrm{IC50\ (A)}} + \frac{\mathrm{IC50\ (A+B)}}{\mathrm{IC50\ (B)}}$$

Where IC_{50} (A) and IC_{50} (B) are the IC_{50} values obtained from each drug separately. IC_{50} (A+B) is the IC_{50} value of both drugs in combination (Li, H.

2016).

1.5.15 Synthesis of a fluorescent polymer for cellular uptake assessment

A copolymer of DiEGMA and $OEGMA_{300}$ with molar ratio of 60:40 and degree of polymerization of 120 was synthesised. DiEGMA (6 mmol, 1.107 mL), $OEGMA_{300}$ (4 mmol, 1.143mL), AIBN (0.02 mmol, 3.3 mg) and CTA (0.08 mmol, 18mg) were dissolved in 2-butanone (8 mL) in a 25 mL round bottom flask. The reaction mixture was sealed with a rubber septum and purged with argon. The polymerisation started by placing the vessel in an oil bath at 75°C and was left under magnetic stirring. After 24 hours, the hydrophobic block with degree of polymerisation of 50 was synthesised by introducing an argon-purged solution (3 mL, 2-butanone) with EHMA (3.95 mmol, 885 µL) and fluorescein *O*-methacrylate (FOMA) (0.05 mmol, 20 mg) to the reaction via a fine needle. The reaction was stopped after 24 hours by cooling it down and exposing it to air. The polymers were washed twice in excess hexane in order to dissolve unreacted monomer and to precipitate the synthesised polymer. The precipitated polymer was dried under reduced pressure and collected as a pink-yellowish viscous fluid (yield: 73%).

1.5.16 Thermo-dependent cellular uptake of fluorescent polymer

The effect of temperature on the cellular uptake of the TR nanoparticles below and above their thermal transition temperatures was studied using Fluorescence microscopy. MiaPaCa-2 cells were seeded in 6-well plates at a concentration of $1x10^5$ cells/well and incubated at 37 °C and 5% CO_2 to allow the cells to attach and reach confluency. The media in each well was replaced with 2 mL of media containing 2 mg of fluorescent polymer and incubated at 37 °C (below LCST) or 40 °C (at LCST) for 30 min. The media was removed and the cells were rinsed with Dulbecco's phosphate buffered saline (DPBS) once, at room temperature. The washed cells were then fixed using 4% paraformaldehyde phosphate buffer solution for 20 min and rinsed twice with

DPBS. The cells were observed in 6-well plates using a EVOS® FL Imaging microscope microscope.

1.5.17 Flow Cytometry analysis

MiaPaCa-2 cells were plated in a 6-well plate at a density of $1x10^5$ cells per well. After the cells reached confluency, each well was treated with 2 mg of poly (DiEGMA-co-$OEGMA_{300}$)-b-(EHMA-co-FOMA) which was dissolved in 2 mL of culture medium. After 30 min, the cells were washed with cold PBS (4 °C) several times to stop the intake. 1 mL of cold PBS (4°C) was added, the cells were scraped and transferred into Nalgene® centrifuge tubes to be analysed by a MACSQuant Analyzer 10 Flow Cytometer.

Flow Cytometry is a process that measures multiple characteristics of individual cells flowing in a single file in a stream of fluid (Figure 38). This process is performed at rates of thousands of cells per second. A beam of laser light is directed at a hydrodynamically-focused stream of fluid that carries the cells. As the cells flow in front of an argon-ion laser, they absorb light, get excited and emit light at varying wavelengths. The light is emitted in all directions and is collected via optics which direct the light to a series of filters and dichroic mirrors that isolate particular wavelength bands. The detector in line with the light beam is used to measure forward scatter (FSC) while another one is placed perpendicularly to the stream and is used to measure side scatter (SSC). The detectors collect the combination of scattered and fluorescent light which is analysed by a computer connected to the flow cytometer (Bakke, A. 2001; Brown, M. et al. 2000).

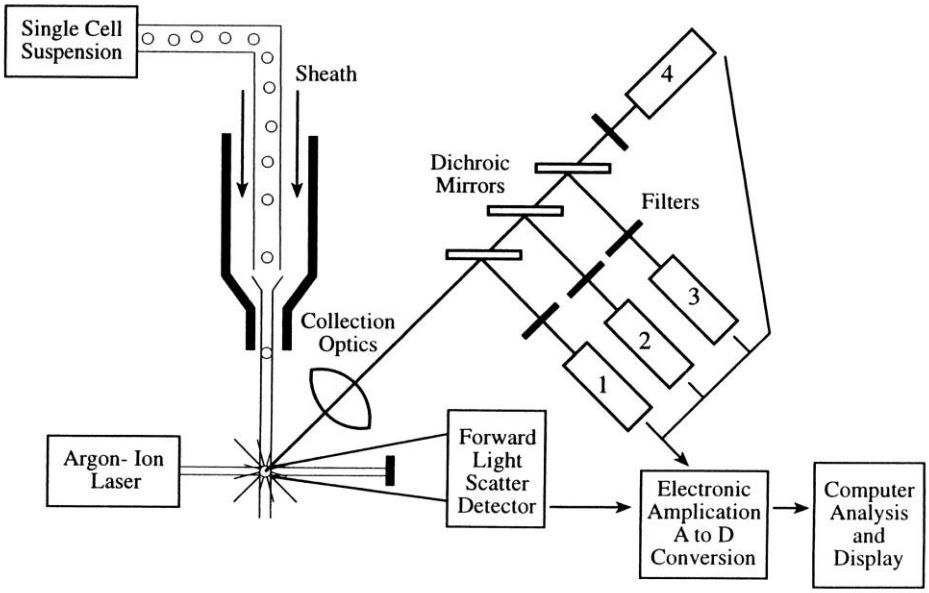

Figure 38. schematic of a flow cytometer. The cells flowing in a single file stream of fluid passes through an argon-ion laser. Emitted light is collected by forward angle light scatter detector, side-scatter detector (*1*), and multiple fluorescence emission detectors (*2–4*). The signals are amplified and converted to digital form for analysis (A) and display (D) on a computer screen (Brown, M. et al. 2000).

1.5.18 Colonogenic cell survival assay

The colonogenic cell survival assay measures the long term cytostatic effect of a cytotoxic agent, by measuring the proliferative ability of a single cell to form a viable colony. (Roper P.R.,1976). $2x10^5$ MiaPaCa-2 cells were seeded in 25 cm^2 T-flasks (using 5 mL of culture medium). Once the cells reached confluency, each flask was treated with different concentration of drugs in combination. One flask was left untreated to serve as a control. After 24 hours, the treated and untreated flasks were trypsinised, counted and subsequently 250 cells from each flask were seeded in the 6 well plate. After 14 days, the colonies were washed with PBS and then fixed using methanol and acetic acid at a ratio of 3:1. The colonies were stained with 0.5% crystal violet solution (diluted with methanol) for 5 min. The stained plates were rinsed in the tray full of distilled water and left in the fume hood over night to dry. Colonies appeared as clusters of violet stained cells visualised with the naked eye. The number of air-dried colonies for the average of three colony counts for each plate was recorded. A cluster of 50 or more cells were counted as one colony.

The plating efficiency (PE) was calculated by dividing the number of colonies counted by the number of cells plated and then multiplying by 100:

$$\%\ \text{Plating efficiency} = \frac{\text{No. of colonies counted}}{\text{No. of cells plated}} \text{x}100$$

The PE was used to investigate the percentage of single cells seeded in the plates that form a colony. The PE of the control was considered as 100%. By determining the PE, the survival fraction of single cells seeded in the plates was also calculated by dividing the PE of the treated cells by the PE of the control and then multiplying by 100:

$$\%\ \text{Survival fraction} = \frac{\text{PE of the treated cells}}{\text{PE of the control}} \text{x}100$$

The survival fraction was calculated to find out the fraction of surviving cells after the exposure to the different concentrations of drugs (Munshi et al. 2005).

All experiments were performed in triplicate.

1. 6 Results and Discussion

1.6.1 One pot synthesis of Poly (DiEGMA-co-OEGMA$_{300}$)-b-EHMA by RAFT polymerisation

Both hydrophilic and hydrophobic blocks of the polymer play important roles in micelles' stability. The hydrophilic block is responsible for the solubility of the carrier in the aqueous environment by exerting hydrogen bonding and dipole-dipole forces with water molecules. Furthermore, the hydrophobic block contributes more in the colloidal stability since it is responsible for the cohesion of the micelle's core and reduces the tendency of the micelles to dissociate. Yet for achieving optimum colloidal stability and preventing premature micelle dissociation there should be a balance between the chain lengths of the two blocks (Owen, S. C. et al. 2012). Therefore, several block copolymers with different hydrophilic and hydrophobic chain lengths were synthesised (Table 4) to optimise the ratio for achieving a balanced block copolymer with sharp thermo-responsive behavior.

DiEGMA-co-OEGMA$_{300}$ copolymer (60:40) with several degrees of polymerisation (DP) from range of 50-150 was used to synthesise hydrophilic blocks of different chain length. DP is defined by the number of monomers on each polymer block and can be calculated using the following formula,

$$\mathrm{DP} = \frac{\text{No. of moles of monomer}}{\text{No. of moles of RAFT chain transfer agent}}$$

Different structures of hydrophobic monomers (Figure 39) were initially tested in order to determine the foremost hydrophobic monomer that exhibits the highest cohesive force in the core in order to form colloidally stable TR micelles.

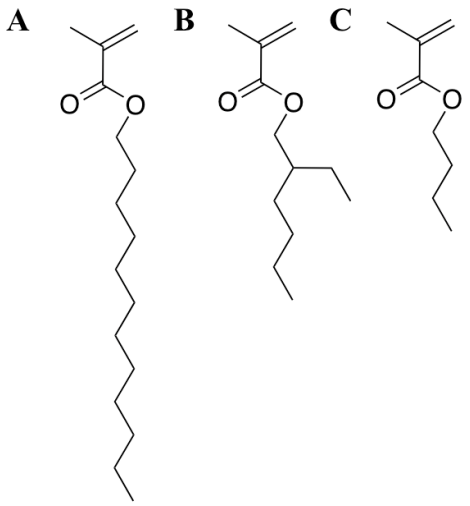

Figure 39. A. Lauryl methacrylate (LMA) **B.** 2-Ethylhexyl methacrylate (EHMA) **C.** n-Butyl methacrylaye (BMA).

The block co-polymers with BMA and LMA as hydrophobic block were synthesised by one pot polymerisation method as previously described (section 1.5.1). Furthermore, The LCST of the block co-polymers was determined as previously described in section 1.5.4. The average size of the micelles prepared from self-assembled block co-polymers was measured by DLS (refer to section 1.5.7).

The synthesis of the hydrophobic block started with the use of BMA which had a short carbon chain. In trial 1 (Table 4) the DP of the hydrophilic and hydrophobic block was 50 and 40 respectively, the polymer was soluble in water and showed thermo-responsive activity. In addition, the block copolymer assembled and formed micelles having average size of 18 nm. In contrast, in trials 2 and 3 the DP of the hydrophilic blocks were increased to 100 and 150 respectively and no micelles formation were observed. Polymeric micelles prepared by BMA were stable in water but not in PBS pH 7.4 (0.01 M) in which they precipitated after 2 hours incubation.

Therefore LMA with longer carbon chain was more hydrophobic and was selected to increase the cohesion in the micelle's core to enhance the colloidal stability. However, the monomer was too hydrophobic and the resulting block copolymers were not soluble in water even after reducing the

DP to 10. In trials 9 and 10 the DP for hydrophilic blocks increased to 150 and the hydrophobic blocks were reduced to DP of 30 and 20 respectively. In spite of being soluble in water, the polymers did not self-assemble to form stable micelles.

Finally, EHMA was used as a hydrophobic monomer with longer carbon chain than BMA and shorter than LMA. In trial 11, the DP ratio between the hydrophilic and the hydrophobic block was close which rendered the polymer hydrophobic and insoluble in water with no thermo-responsive activity. Trials 12 and 13 successfully produced polymers which were soluble in water, showed thermo-responsive behaviour and self-assembled to polymeric micelles having size of 36 nm. Finally, the block co-polymer synthesised in trial 13 was selected because it exhibited a LCST above body temperature in serum.

The block copolymers were synthesised by RAFT polymerisation (Figure 40) using DiEGMA:$OEGMA_{300}$ with ratio of 60:40 in order to achieve a LCST onset at 40°C. Then the TR block (Figure 40, 1) was used as a macro-RAFT agent to initiate the co-polymerisation of the hydrophobic block made by EHMA.

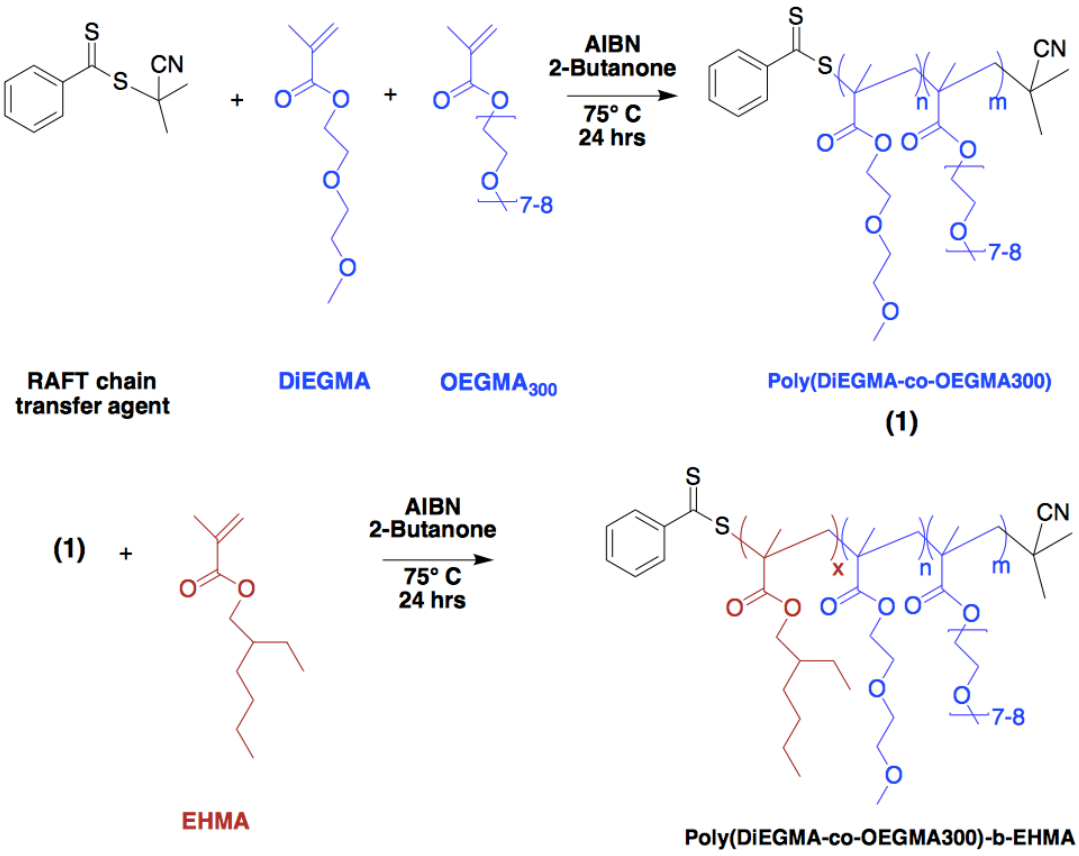

Figure 40. Synthesis of Poly (DiEGMA-co-OEGMA$_{300}$)-b-EHMA by RAFT polymerisation.

Table 4. Summary of block co-polymers synthesised by RAFT polymerisation. (-) represents insolubility of polymers and inability to form micelles.

Trial	Hydrophilic Monomers (60:40)	Hydrophobic Monomer	DP of Hydrophilic Block	DP of Hydrophobic Block	LCST in PBS (0.01 M) (°C)	LCST in Serum (°C)	Size (nm)
1	DiEGMA: $OEGMA_{300}$	BMA	50	40	42	38.5	18
2	DiEGMA: $OEGMA_{300}$	BMA	100	40	43	38	-
3	DiEGMA: $OEGMA_{300}$	BMA	150	40	43	40	-
4	DiEGMA: $OEGMA_{300}$	LMA	50	40	-	-	-
5	DiEGMA: $OEGMA_{300}$	LMA	100	50	-	-	-
6	DiEGMA: $OEGMA_{300}$	LMA	100	20	-	-	-
7	DiEGMA: $OEGMA_{300}$	LMA	100	10	-	-	-
8	DiEGMA: $OEGMA_{300}$	LMA	150	50	-	-	-
9	DiEGMA: $OEGMA_{300}$	LMA	150	30	42	41	-
10	DiEGMA: $OEGMA_{300}$	LMA	150	20	42	41	-
11	DiEGMA: $OEGMA_{300}$	EHMA	50	40	-	-	-
12	DiEGMA: $OEGMA_{300}$	EHMA	100	50	38	35	36
13	DiEGMA: $OEGMA_{300}$	EHMA	120	50	40	38	36

1.6.2 Nuclear magnetic resonance spectroscopy

The ^{1}H NMR spectrum of Poly (DiEGMA-co-$OEGMA_{300}$)-b-EHMA in $CDCl_3$ was obtained and all the proton peaks were assigned successfully (Figure 41). The appearance of the aromatic ring of the RAFT chain transfer agent at chemical shift of 7.40 ppm confirmed the successful RAFT polymerisation.

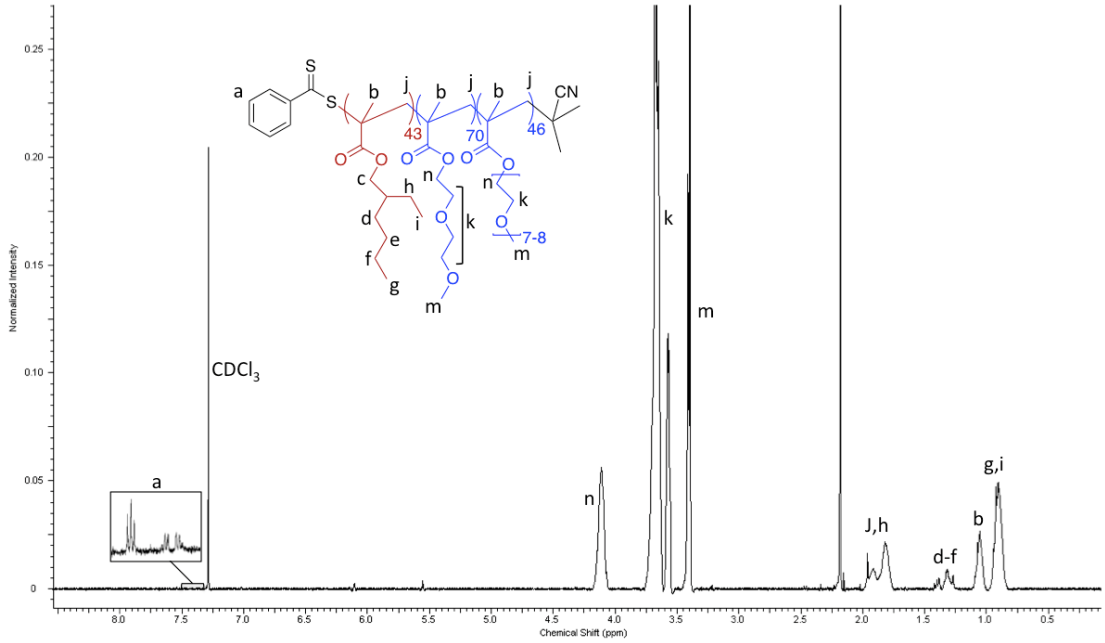

Figure 41. ^{1}H NMR spectrum of Poly (DiEGMA-co-$OEGMA_{300}$)-b-EHMA in $CDCl_3$.

The ^{1}H NMR spectra shows upfield signals attributed to the methyl groups in the polymer chain (peaks 'g,i') and the polymer backbone (peak 'b') at approximately 0.8 ppm and 1.0 ppm respectively. The methylene group (peaks 'd to f') appeared as a broader peak at 1.3 ppm. The signals of CH_2 groups (peak 'j' and ''h') appeared at 1.8 ppm. The methyl groups at the end of each $OEGMA_{300}$ segment (peak 'm') which are attached to the electronegative O group had a chemical shift at 3.4 ppm. The ^{1}H NMR spectra also showed chemical shifts at around 3.7 ppm and 4.1 ppm corresponding to methylene groups (peak 'k' and 'n' respectively) of the $OEGMA_{300}$ pendant units under the influence of the electronegative O groups which are deshielded downfields.

1.6.3 Gel permeation chromatography

The Number Average Molecular Weight (Mn) and polydispersity index (PDI) of the RAFT synthesised Poly (DiEGMA-co-$OEGMA_{300}$) and Poly (DiEGMA-co-$OEGMA_{300}$)-b-EHMA polymers were analysed by GPC (Figure 42). GPC data confirmed that the obtained products had a M_n of 31,600 Da and 39,500 Da for p(DiEGMA-$OEGMA_{300}$) and p(DiEGMA-co-$OEGMA_{300}$)-b-EHMA, respectively; the degree of polymerisation (DP) was close to the initial feed for both blocks (DP_{GPC} for p(EHMA) and p(DiEGMA-co-$OEGMA_{300}$) was 43 and 116, respectively); also the final polymer had a narrow polydispersity index of 1.3, $Đ_M$ indicated well-controlled polymerisation. Only a very minor tailing of the GPC trace was observed which was also persistent in the polymer chromatogram, but this was negligible given the relatively low $Đ_M$ value.

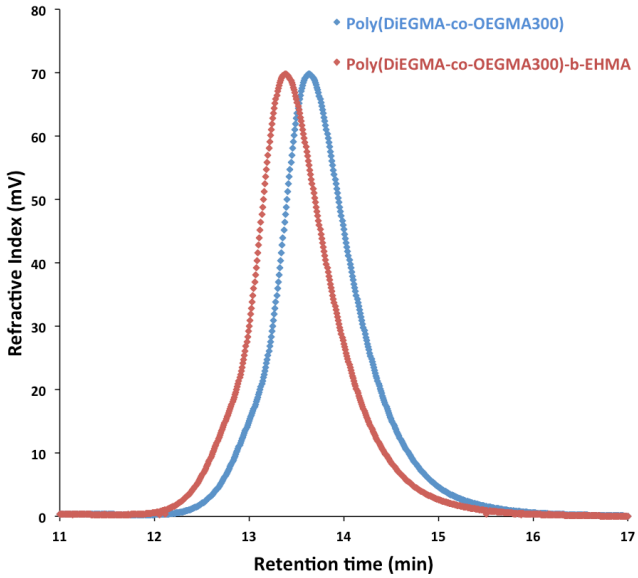

Figure 42. GPC traces of Poly (DiEGMA-co-$OEGMA_{300}$)-b-EHMA block co-polymer (red curve) and Poly (DiEGMA-co-$OEGMA_{300}$) polymer (blue curve) determined by GPC using DMF as mobile phase.

1.6.4 LCST Determination

Thermo-responsive Poly(DiEGMA-co-$OEGMA_{300}$) consists of two hydrophilic thermo-responsive monomers DiEGMA and $OEGMA_{300}$. The homopolymers of DiEGMA and $OEGMA_{300}$ have a LCST of 26°C and 64°C respectively (Lutz, J. F. 2008). Previous studies showed that copolymerisation of two or more thermo-responsive monomers will change the LCST and the rate of the phase transition of the polymer considerably (Dou, Y. N. et al. 2014; Saniei, N. 2009; Schild, H. G. et al. 1990; Schild, H. G. 1992; Roth, P. T. et al. 2010; Ward, M. A. et al. 2011). Therefore, DiEGMA and $OEGMA_{300}$ having different LCST were copolymerised in different molar ratios in order to achieve the desired LCST at 40°C.

The synthesised co-polymers with different monomer feed were dissolved in PBS pH 7.4 (0.01 M). The LCST is usually lower in PBS compared to water because of the presence of salt in these mediums (Du, H. et al. 2010; Liu, X. 2008). As described earlier, the LCST occurs due to the rapid elimination of the solvation hydration layer around the polymer leading to its precipitation (Horne, R.A. et al. 1971; Ataman, M. 1987). The LCST of thermo-responsive polymers is inversely proportional to the concentration of salts in the surrounding medium. The reason for the decrease of the LCST in salt solutions can be explained by the Hofmeister ion interaction effect which results from specific interactions between the salt ions and the polymer, as well as between the salt ions and the water molecules' orientation in the hydration shell surrounding the polymer (Eeckman, F. et al. 2001). These interactions result in an increase of the hydrophobicity of the polymer chains which consequently lowers the LCST onset (Zhang, Y. et al. 2006; Zhang, Y. et al. 2007).

The co-polymer of DiEGMA-co-$OEGMA_{300}$ with molar ratio of 60:40 showed a LCST at 40°C in PBS pH 7.4 (0.01 M) (Figure 43) and therefore this monomer ratio was used as the stimulus responsive block.

Figure 43. Thermo-responsive polymer soluble in water below the LCST but insoluble at the LCST.

1.6.5 CMC of Poly (DiEGMA-co-OEGMA$_{300}$)-b-EHMA

Polymer micellisation was studied by florescence spectroscopy using pyrene as fluorescence probe. Measuring the CMC value is important for determining the micelle's stability in aqueous media and in blood; the lower the CMC value, the higher the stability of the micelles will be (Owen, S. C. et al. 2012). Upon micellisation, the pyrene probe is partitioned into the less polar hydrophobic core which induces a change in the environment polarity and in turn increases the fluorescence intensity (Aguiar, J. et al. 2003; Kalyanasundaram, K. et al. 1997). As a result, the encapsulated pyrene exhibits a shift in the excitation band from 310 nm to 330 nm reflecting the fact that pyrene is partitioned into the micelle's hydrophobic core. Figure 44 represents a plot of the intensity ratio (I330/I310) of pyrene excitation spectra versus the logarithm of polymer concentration. The CMC value was determined from the point of X axis (logarithm of polymer concentration) at which the intensity ratio sharply increases. The critical micelle concentration of the polymer was found to be ca. 5 mg/L, which is in accord with similar studies (Zhao, X. et al. 2012) and also verifies the colloidal stability of the polymer in solution.

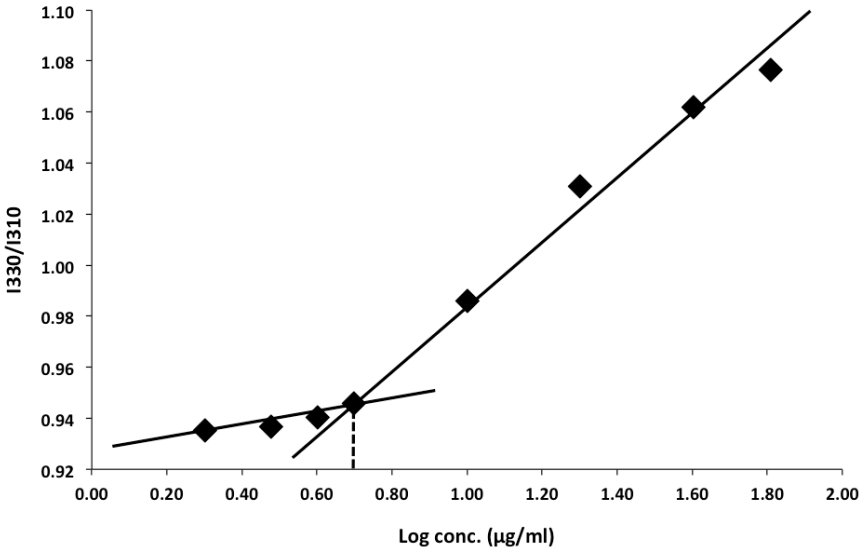

Figure 44. The CMC was measured by plotting pyrene intensity ratio (I330/I310) versus logarithm of polymer concentration.

1.6.6 Dynamic light scattering

DLS was used to determine the size distribution profile of the micelles (Figure 45). The micelles suspension had 35.9 nm size and very low PDI of 0.16 which revealed very uniform size distribution.

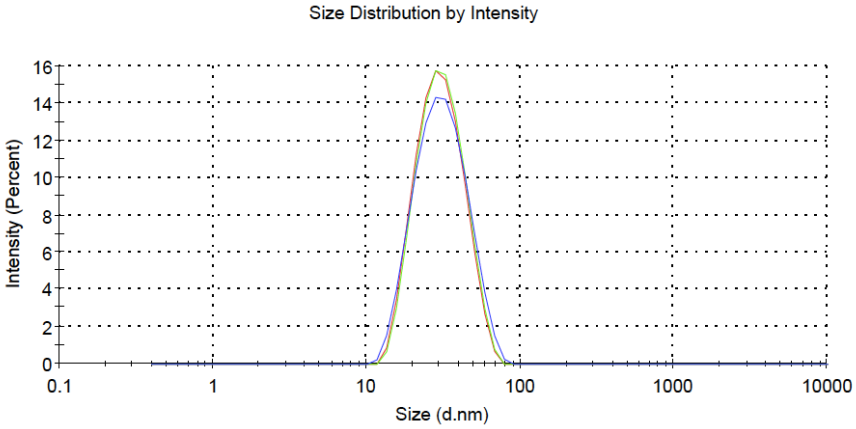

Figure 45. Size and distribution of polymeric micelles measured by DLS in triplicate.

Moreover, the micelles were loaded with Sq-Gem and PTX separately and in combination. The average particle size increased in the loaded micelles compared to drug-free ones. Further increase in average diameter was observed when Sq-Gem and PTX were co-loaded. Table 5 demonstrates blank and loaded-micelles size and distribution having narrow polydispersity index (PDI).

Table 5. Average particle size of TR polymeric micelles

	Average size (nm)	*PDI*
Blank micelles	35.90 ± 1.3	0.16 ± 0.01
Sq-Gem micelles	45.34 ± 1.3	0.38 ± 0.02
PTX micelles	47.85 ± 1.5	0.25 ± 0.01
Sq-Gem and PTX micelles	49.90 ± 1.2	0.24 ± 0.01

According to research performed by the Couvreur group, Sq-Gem could form nano-assemblies in the size of 130 ±8 nm with a PDI of 0.120 (Bekkara-Aounallah, F. et al. 2008; Couvreur, P. et al. 2006). However, the low average size and PDI in Sq-Gem loaded (Table 5) and co-loaded Sq-Gem and PTX micelles confirmed that there was no self-assembly of Sq-Gem in the formulation.

Figure 46 shows the graphs obtained by DLS to demonstrate the uniform size and distributions of loaded-micelles having narrow PDI.

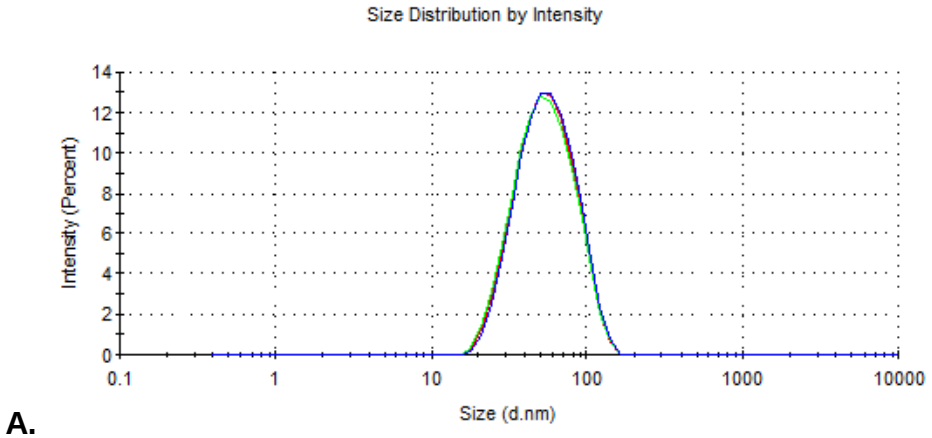

A.

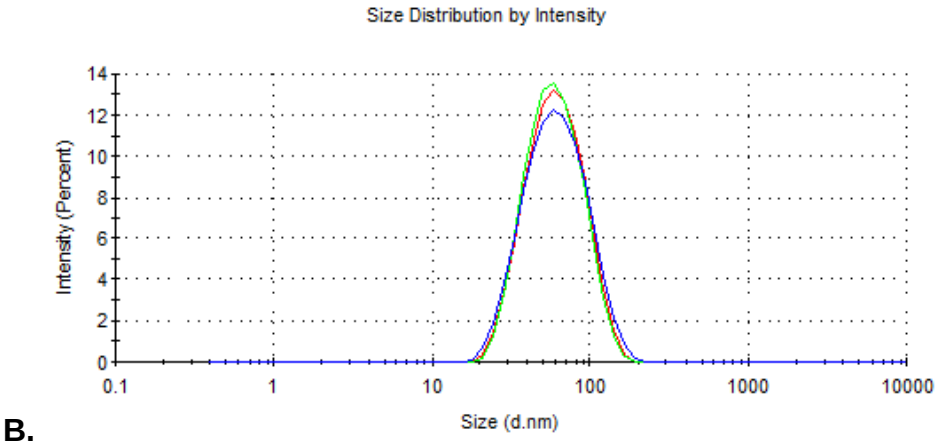

B.

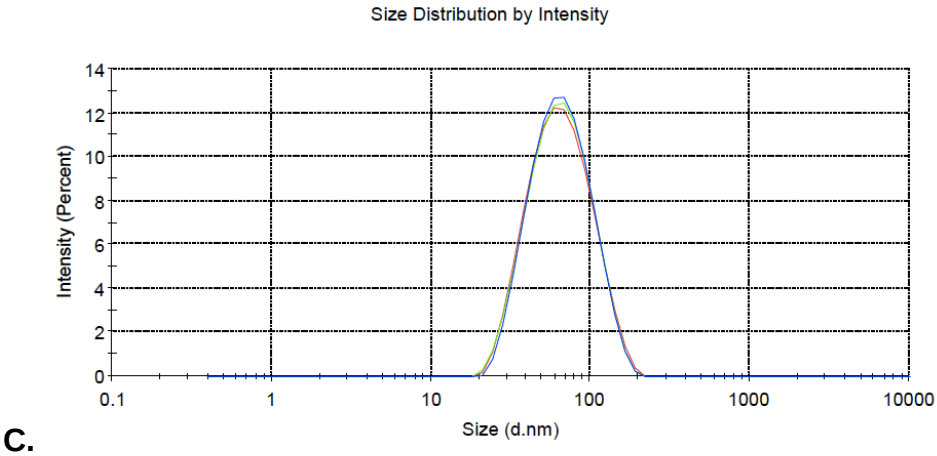

C.

Figure 46. Size and size distribution of **A.** Sq-Gem **B.** PTX **C.** Sq-Gem and PTX loaded polymeric micelles measured by DLS in triplicate.

1.6.7 Stability studies

The stability of the micelles was monitored by measuring their particle size with DLS. The stability studies were carried out in PBS (0.01M) at room temperature everyday for a week (Table 6). The size of the micelles remained constant for 7 days until precipitation of the polymers showed dissociation of the micelles over time (Figure 47).

Table 6. Stability of micelles was measured by DLS for a week.

Polymeric Micelles Average size								
Day	**0**	**1**	**2**	**3**	**4**	**5**	**6**	**7**
Size (nm)	35.89	36.26	36.23	34.24	35.57	34.43	33.39	-
PDI	0.34	0.44	0.48	0.45	0.41	0.45	0.36	-

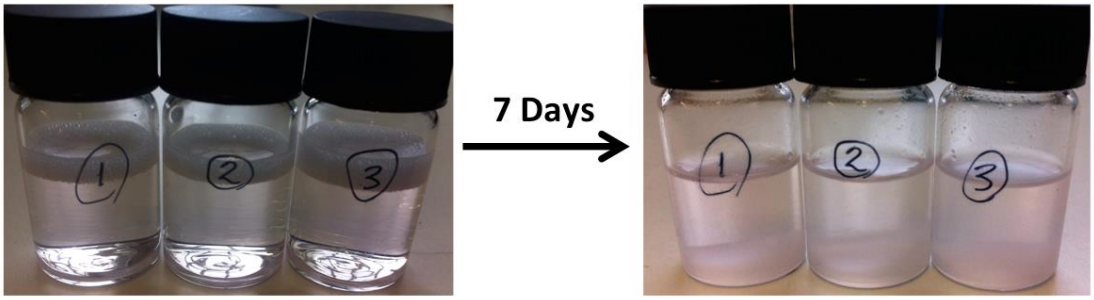

Figure 47. Demonstrate disassembly of polymeric micelles by time.

1.6.8 TEM characterisation

TEM was used to study the size and morphology of the micelles as a complementary method to DLS. The size and distribution of the micelles which was studied using DLS were further measured by TEM.

Figure 48 shows the TEM images of blank and co-loaded micelles. The TEM images confirmed the spherical shape of the micelles which were nearly mono-disperse without the presence of any large polymeric aggregates in the suspension. The monodispersity of the suspension is due to the sonication of

the micellar formulation for appropriate amount of time which breaks down any inter-micellar interaction (Zhao, J. et al. 2009). The blank micelles showed an average diameter of 36 nm. The micelles size increased in the loaded micelles which was in accordance of DLS studies.

A.

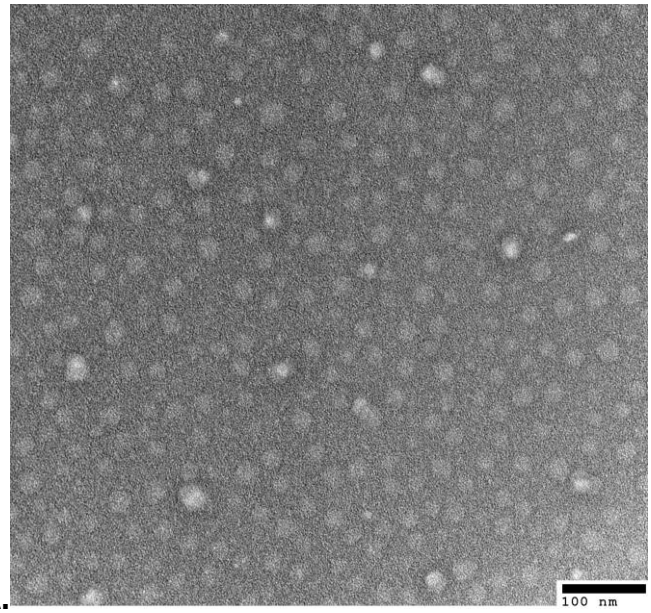

B.

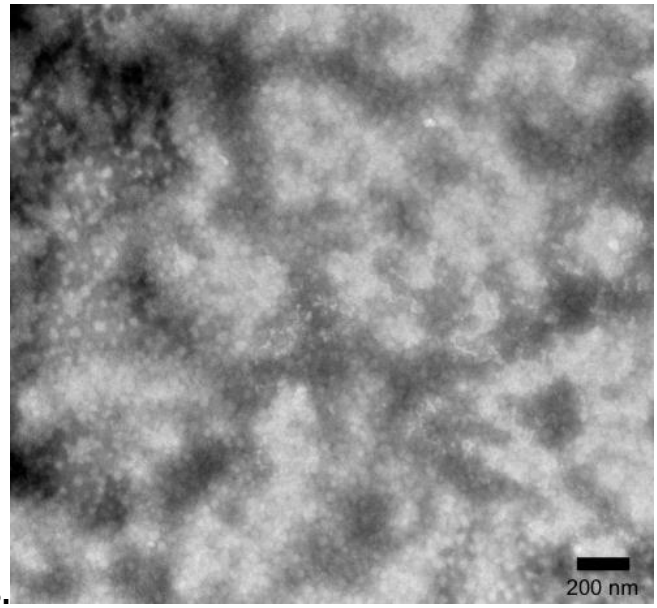

C.

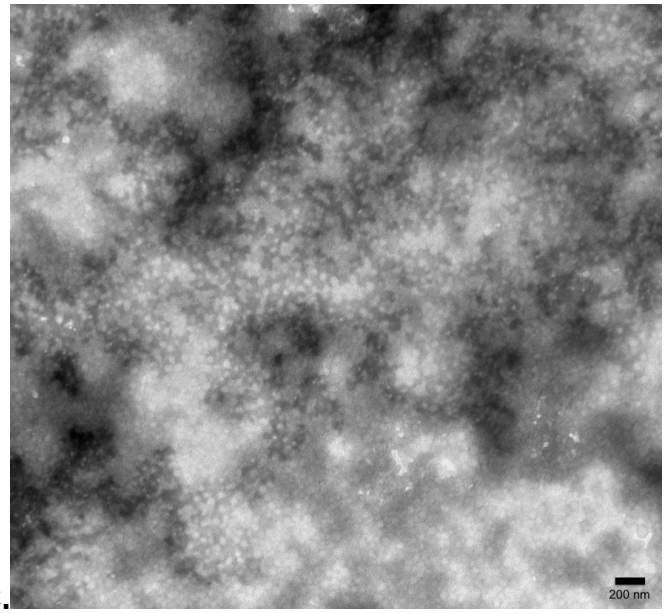

D.

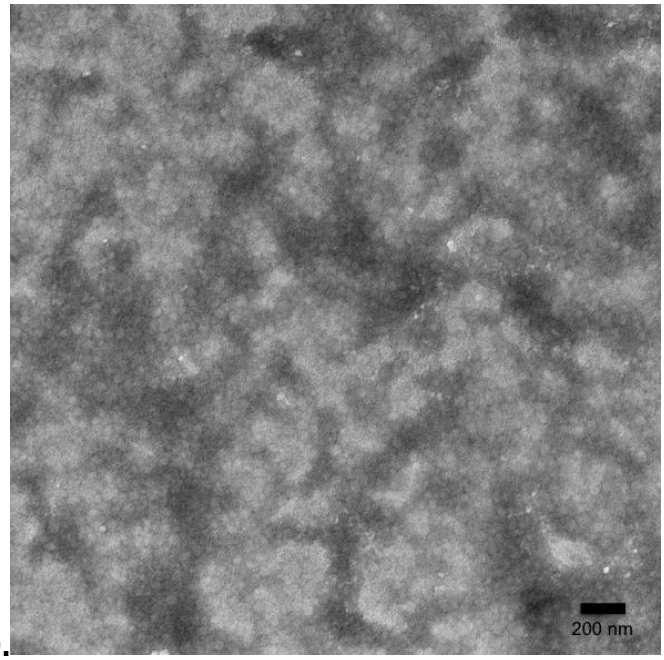

Figure 48. TEM images of **A.** Blank **B.** Sq-Gem **C.** PTX **D.** Co-loaded TR polymeric micelles. The scale bars show the size of **A.** 100 nm **B-D.** and 200 nm.

The size distribution of the micelles was measured from the TEM images using ImageJ software (Figure 49). The size of 100 micelles was measured to plot a histogram of diameter range distribution. The frequency distribution curve of the micelles showed Gaussian size distribution. The most frequent micelle size (mode) that appeared in data set was 36 nm and increased to 49 nm for blank and co-loaded micelles, respectively. In addition, the average micelle diameter size was measured to be 34.55 ± 2.93 nm and increased to

47.25 ± 2.58 nm for blank and co-loaded micelles, respectively. The values are in good agreement with the size and distribution obtained by DLS.

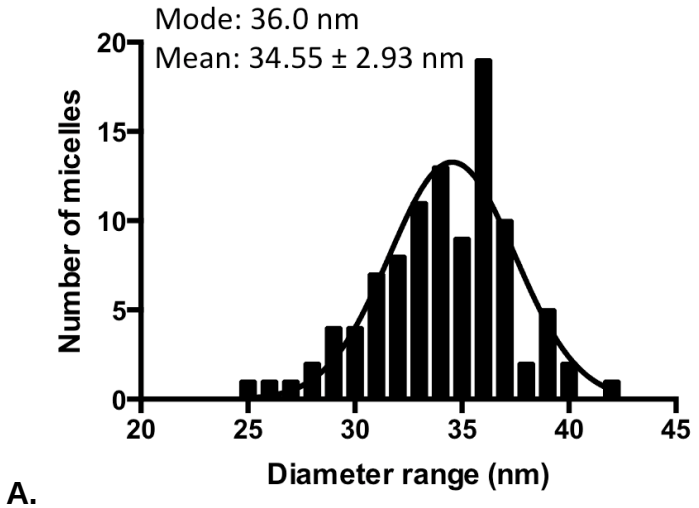

A.

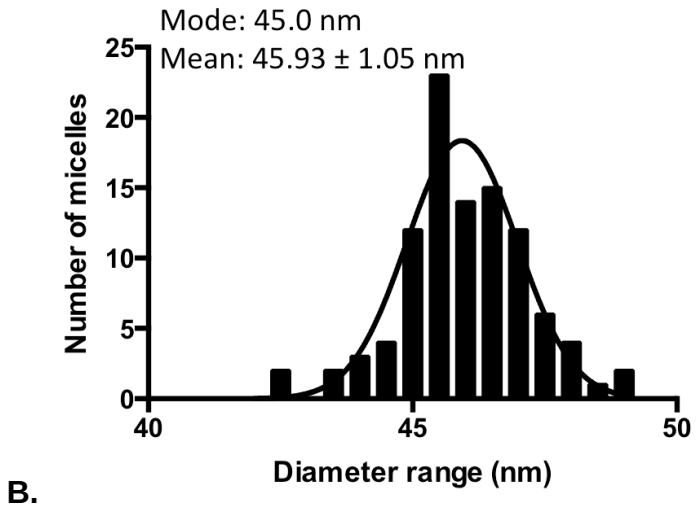

B.

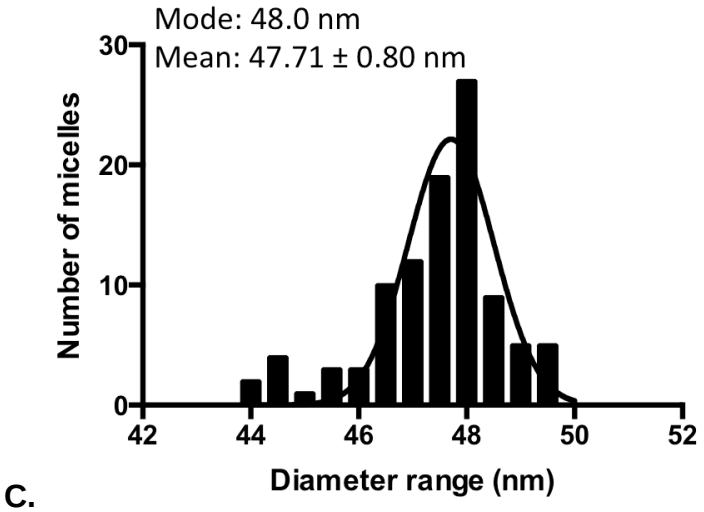

C.

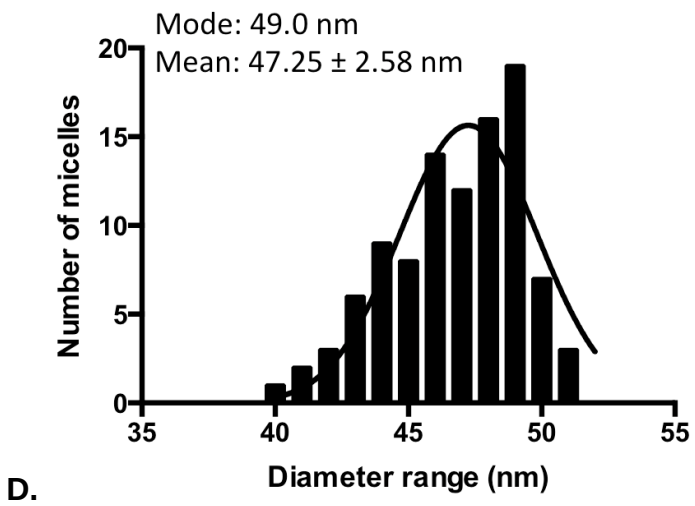

Figure 49. The histogram of size distribution of **A.** Blank **B.** Sq-Gem **C.** PTX **D.** Co-loaded TR polymeric micelles obtained from TEM images.

1.6.9 Drug encapsulation efficiency

Sq-Gem and PTX loaded polymeric micelles were analysed by HPLC in order to measure the amount of drug encapsulated within the micelles' core. The separations were achieved using water and methanol as the mobile phase; PTX and Sq-Gem peak appeared at around 4.5 min and 8 min respectively (Figure 50). The area under the curve was measured and the concentration of each drug was determined by using known concentrations of a previously prepared standard curve. Indeed, it was possible to load PTX, Sq-GEM, or both, in the micelles at a drug encapsulation efficiency of 10% per mass of polymer (i.e. 0.5 mg of each drug per 5 mg of polymer) without any measurable loss of drug during preparation.

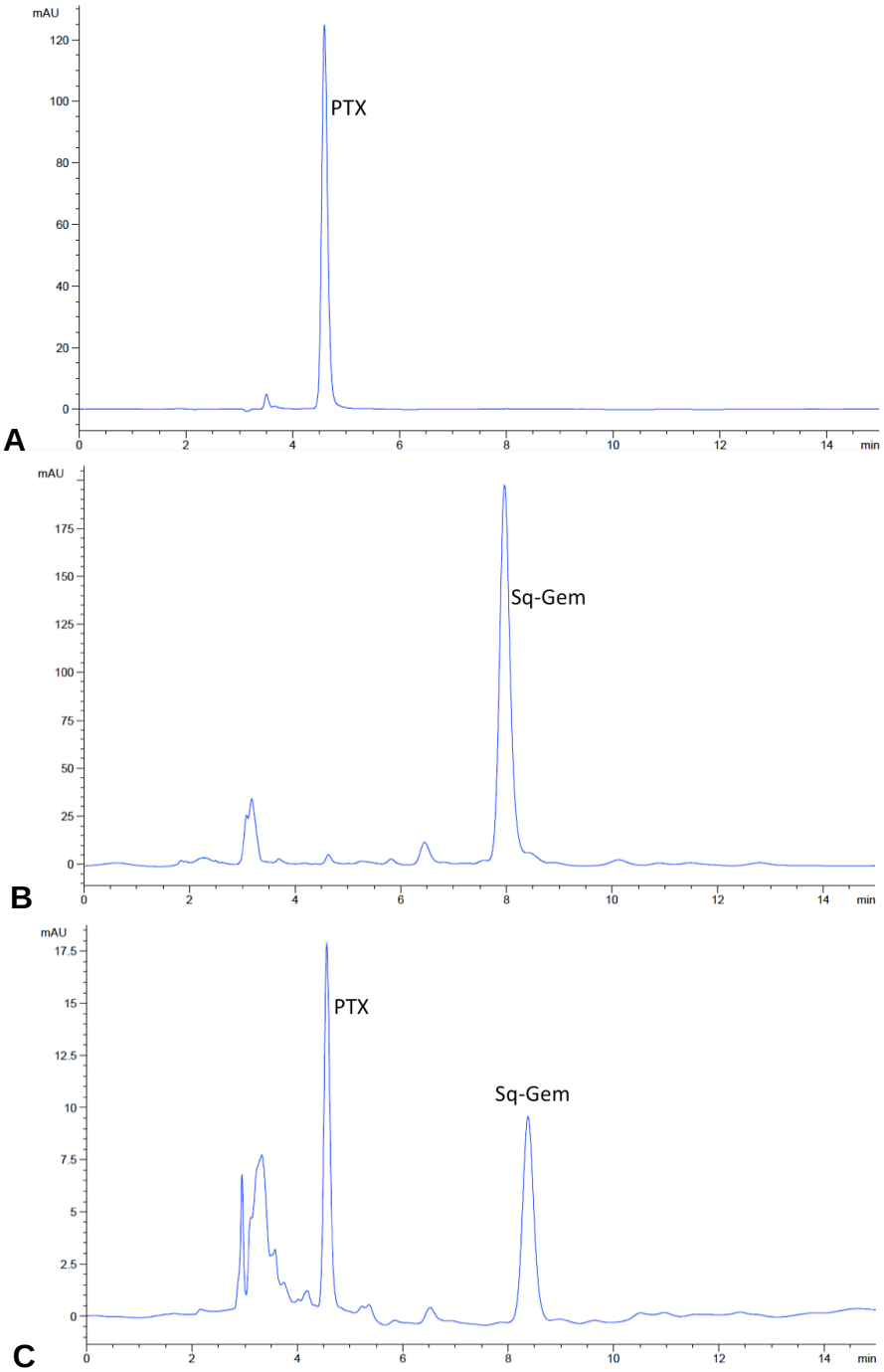

Figure 50. HPLC chromatogram of A. PTX B. Sq-Gem C. PTX and Sq-Gem.

1.6.10 Determination of in vitro drug release

The drug release profile of the two drugs separately loaded or co-loaded, below and above the polymers' LCST was measured. In the case of Sq-Gem (Figure 51), below the LCST the release rate followed a zero-order rate, reaching ca. 37% and 67% within 2 and 4 hours, respectively. At the LCST,

the release rapidly reached nearly 80% which plateaued at ca. 90% in 4 hours.

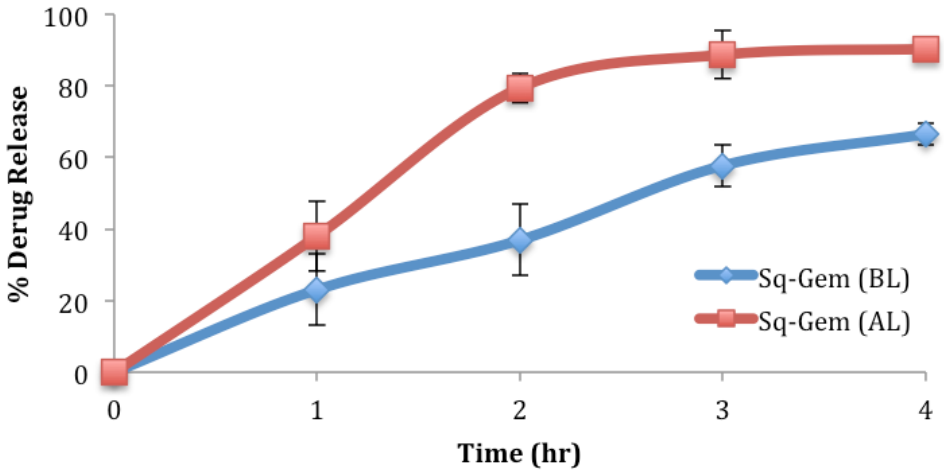

Figure 51. Sq-Gem drug release from polymeric micelles below and at the LCST.

For PTX (Figure 52), it was found that 50% of the drug was released in one hour followed by a slower release rate which eventually resulted in ca. 80% release in 4 hours, below the LCST. At the LCST, the PTX release was significantly more pronounced, reaching ca. 85% in 1 hour before plateauing to >90% release within 4 hours.

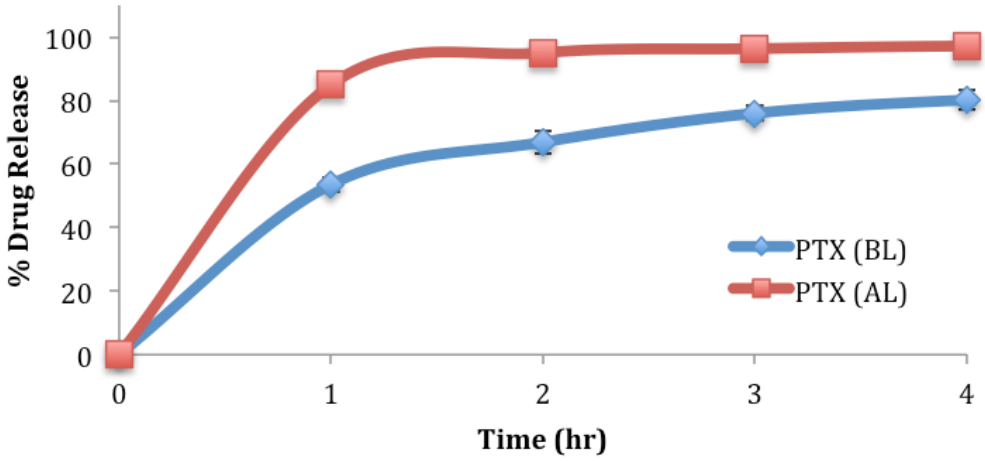

Figure 52. TX drug release from polymeric micelles below and at the LCST.

In the case of the Sq-Gem and PTX co-loaded micelles (Figure 53), it was observed that PTX exhibited a more linear release profile both below and at the LCST and the release reached ca. 57% and 40% at and below the LCST, respectively. The temperature effect was more pronounced in the release pattern of Sq-Gem where it was found that ca. 65% was released within 2 hours at the LCST (vs. 42% below the LCST) and reached >70% in 4 hours at the LCST compared to ca 57% below the LCST. Overall, it can be concluded that the effect of the micelle disruption due to the thermal collapsing of the p(DiEGMA-OEGMA$_{300}$) corona had a more pronounced impact on the formulations of singly loaded drugs and to lesser extent to the PTX/Sq-Gem co-loaded micelles; it may be assumed that in the co-loaded sample, hydrophobic intermolecular interactions between PTX, Sq-Gem and the p(EHMA) polymer segments may be stronger and hence somewhat stabilise the overall formulation against the thermal collapsing of the micellar corona. The possible interaction of PTX with Sq-Gem can be further supported by the higher drug encapsulation efficiency that could be achieved (i.e. 20%) compared to the singly loaded formulations (10%); it should be noted that Sq-Gem is colloidally stable due to its own amphiphilic character and hence it could possibly contribute to the further stabilisation of the formulation.

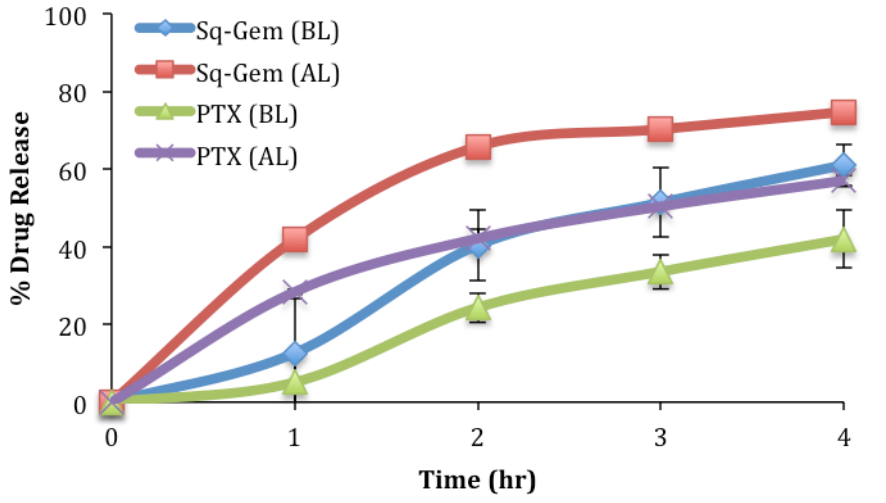

Figure 53. Combinational Sq-Gem and PTX drug release from polymeric micelles below and at LCST.

1.6.11 In vitro cytotoxicity assay

Human pancreatic tumor lines

The MiaPaCa-2 cell line has been derived from biopsy specimen of adenocarcinoma of the pancreas tumor tissue obtained from a 65 years old Caucasian male (ATCC Company website https://www.lgcstandards-atcc.org). Figures 54 and 55 the characteristics of MiaPaCa-2 cells in low and high density.

A.

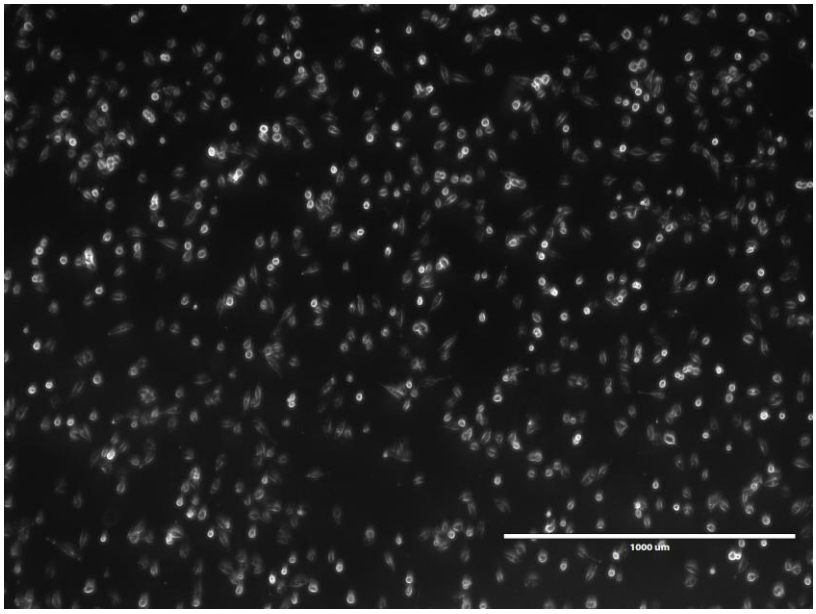

B.

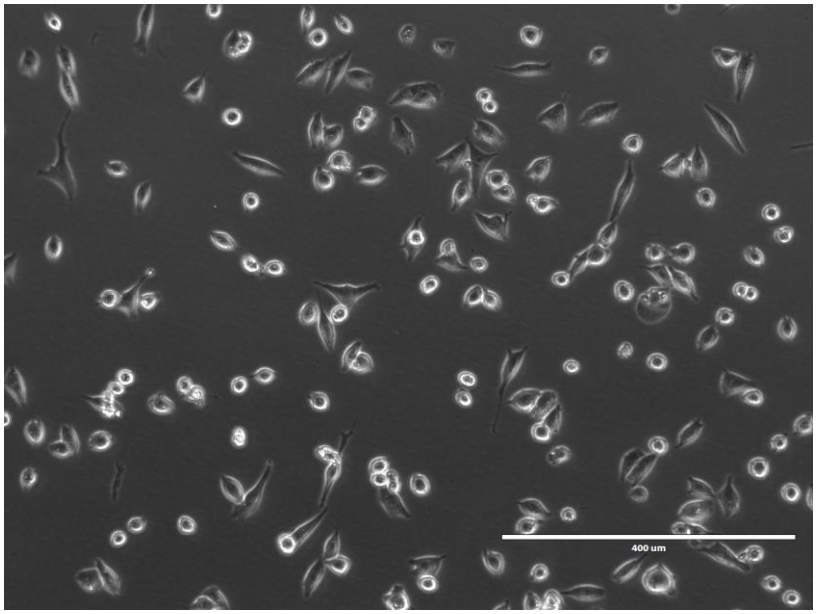

Figure 54. Show the characteristics of MiaPaCa-2 cells in low density. A. The microscope was adjusted on 4x lens. The scale bar is 1000μm. B. The microscope was adjusted on 10x lens. The scale bar is 400μm.

A.

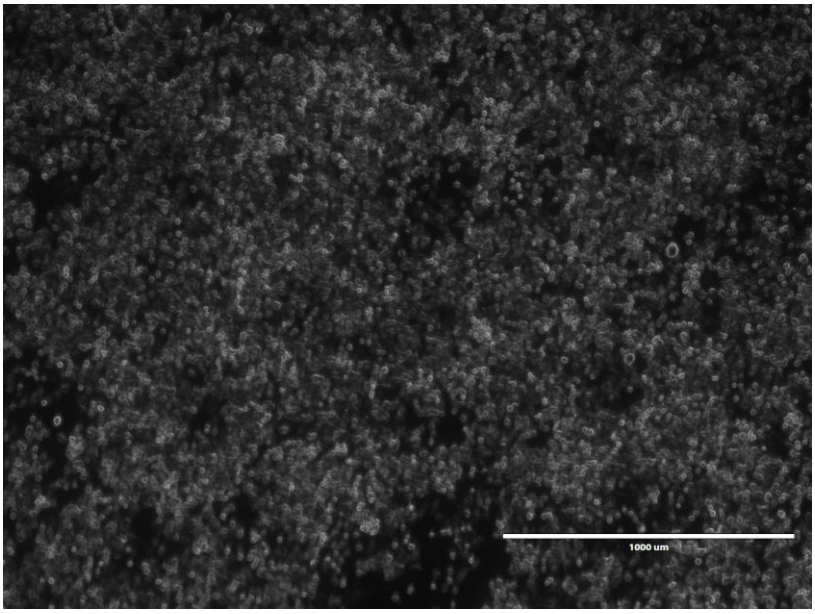

B.

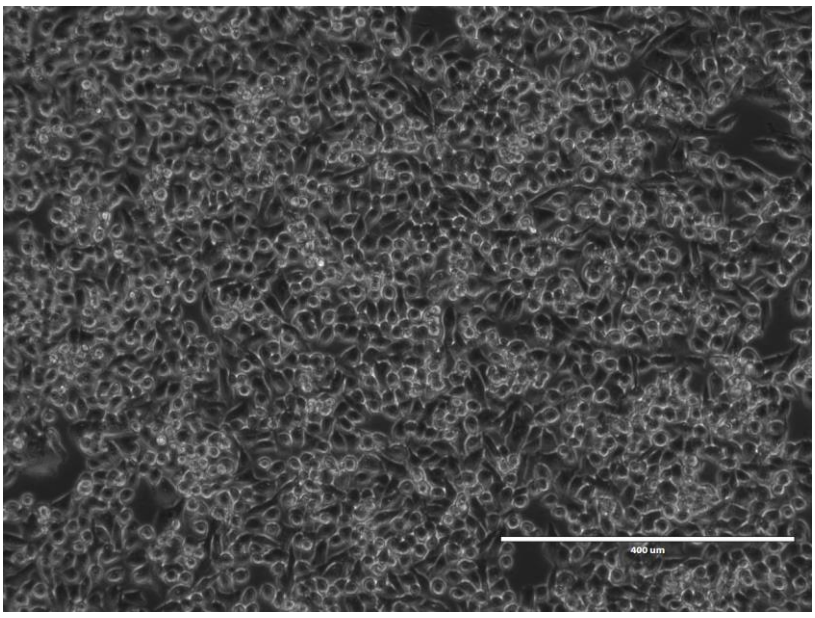

Figure 55. Show the characteristics of MiaPaCa-2 cells in high density. A. The microscope was adjusted on 4x lens. The scale bar is 1000µm. B. The microscope was adjusted on 10x lens. The scale bar is 400µm.

The percentage MiaPaCa-2 cell viability was measured over a wide range of concentrations (0.0001 to 10 µM) of Sq-Gem loaded micelles, PTX loaded micelles and combinational loaded Sq-Gem and PTX micelles (Figure 56). The cell viability of the formulations was evaluated at 37°C and 40°C, which are the temperature below and at the LCST of the TR polymer. The cells viability was almost 100% at 0.0001 and 0.001 µM for all formulations BL and AL. Decrease in cell viability started at 0.01 µM of drug concentration. Below LCST, only co-encapsulated Sq-Gem and PTX micelles reduced the cell

viability to 50% cell population. However the cell viability further reduced to 30% when the same formulation was heated AL at 40°C. By increasing the drug concentration the cell viability AL reduced to less than 25% and remained the same as the drug concentration increased to 10 µM. Overall, the percentage cell viability was less in the formulations AL compared to BL.

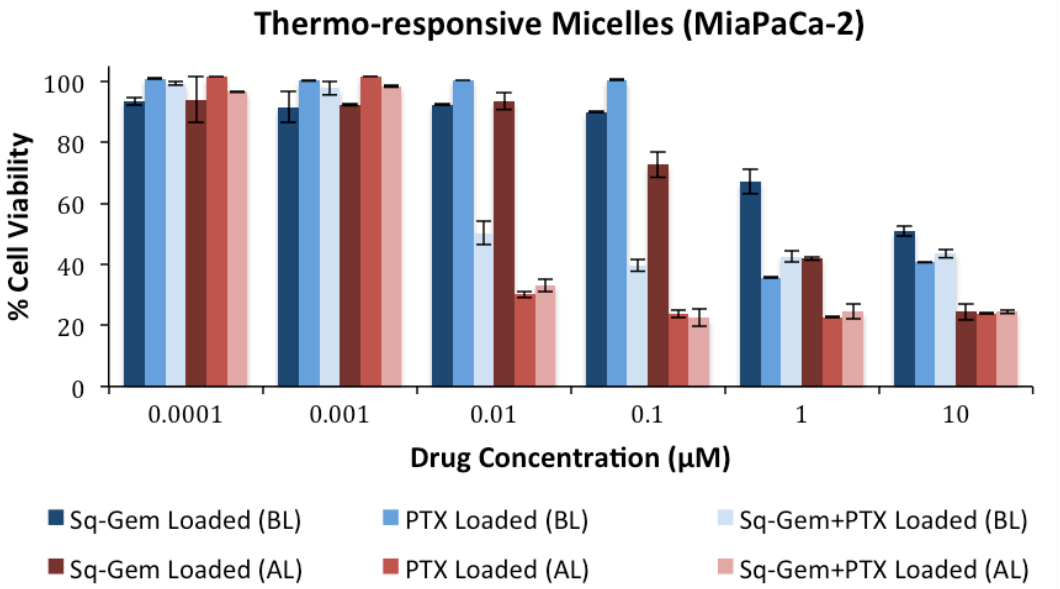

Figure 56. MiaPaCa-2 cells' viability was measured at a range of concentrations of 0.0001 to 10 µM of drug loaded micelles after 72 hr.

The cytotoxicity of the formulations was tested against model pancreatic cancer cell line MiaPaCa-2, using the MTT assay. Initially, we tested the possible toxicity of temperature increase (to 40°C)(Figure 57), DMSO (which was used as a co-solvent to dissolve free drugs), and the polymer without drugs loaded above and below its LCST; it was found that these parameters did not induce any detectable cytotoxicity. Having established that the experimental conditions were not toxic to the cells, we determined the half maximal inhibitory concentration (IC_{50}) of the drugs, the formulations and their combinations under various conditions.

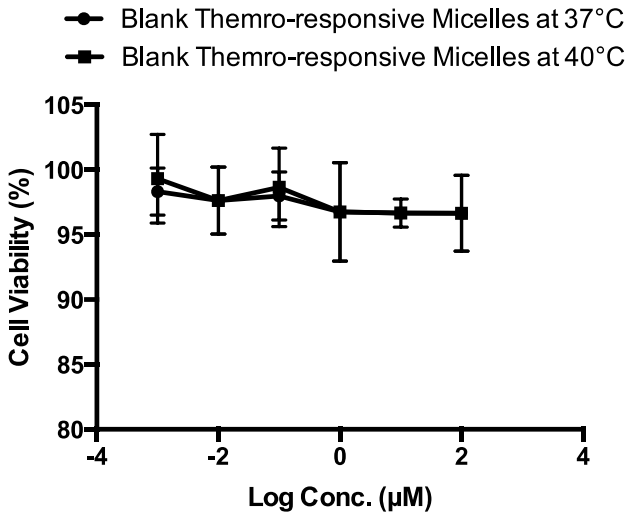

Figure 57. Cytotoxicity effect of blank TR micelles BL and AL after 72 hr.

Figure 58 shows the cytotoxicity of Sq-Gem on MiaPaCa-2 pancreatic cells. Sq-Gem was found to have an IC_{50} of 1122 nM which is significantly higher than the parent drug (Table 7) (Couvreur, P. et al. 2006; Réjiba, S. et al. 2011). Also, the obtained IC_{50} value is considerably higher than the IC_{50} of Sq-Gem in its nano-assembled form (i.e. 40 nM on MiaPaCa-2 cells (Caron, J. et al 2014)), which signifies the marked variances in the cytotoxicity profile of the same molecule under different formulations. Remarkably, Sq-Gem that was loaded in the micelles did not show any cytotoxicity under the conditions tested and it was not possible to extract an IC_{50} value. Conversely, above the polymers' LCST, the Sq-Gem-loaded formulation had an IC_{50} of 310.5 nM which is a 3.6 fold improvement compared to the non-encapsulated sample.

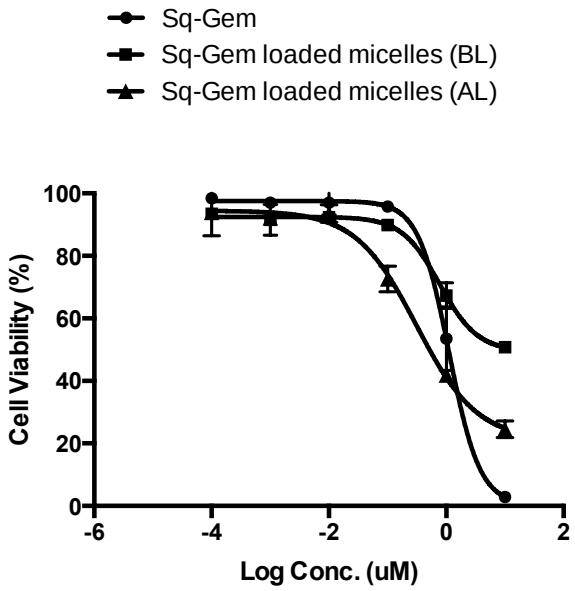

Figure 58. Cytotoxicity of Sq-Gem alone, Sq-Gem loaded micelles below LCST and Sq-Gem loaded micelles at LCST after 72 hr.

Figure 59 shows cytotoxicity of PTX on MiaPaCa-2 cells. PTX was found to have an IC_{50} of 9.44 nM, which is in accord with previous reports (Lin, Y. et al. 2012). The micelles could reduce the cytoxicity of the parent drug by almost 3-fold as the formulation had an IC_{50} of 29.22 nM which could be fully restored (and marginally improved) at the LCST (IC_{50}=7.25 nM) (Table 7).

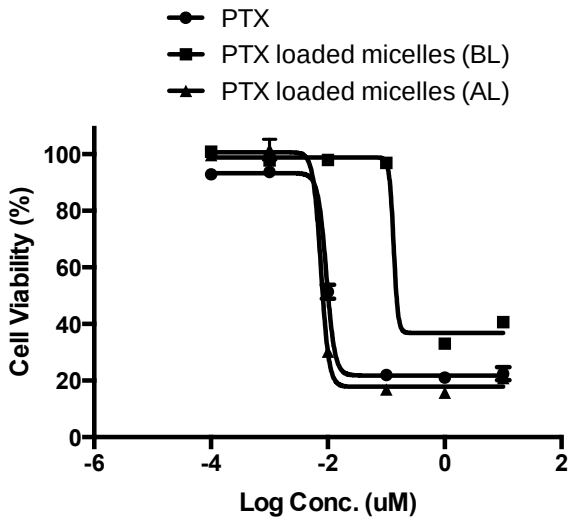

Figure 59. Cytotoxicity of PTX alone, PTX loaded micelles below LCST and PTX loaded micelles at LCST after 72 hr.

Sq-Gem and PTX co-loaded micelles (Figure 60) showed significant decrease in IC_{50} (Table 7) revealing the fact that the co-delivery of these two chemotherapeutic drugs increased cell apoptosis in a synergistic way. The combinational chemotherapy of free Sq-Gem and PTX caused cell death in very low IC_{50} (3.033 nM) when compared to free Sq-Gem (1122 nM) and free PTX (9.443 nM) separately. The encapsulation of both drugs in the micelles followed by incubation below the LCST showed an increase in IC_{50} due to the retention of the drugs in the micelle's core. Moreover, the toxicity further increased by application of heat at LCST of polymeric micelles which in turn reduced the IC_{50} of combinational delivery further down to 1.928 nM.

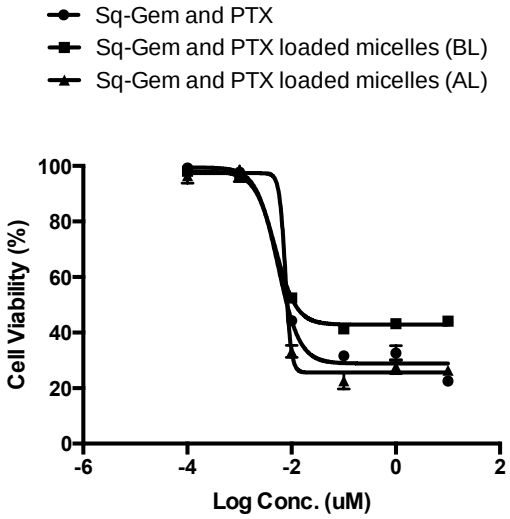

Figure 60. Cytotoxicity of Sq-Gem and PTX, Sq-Gem and PTX loaded micelles below LCST and Sq-Gem and PTX loaded micelles at LCST after 72 hr.

The IC_{50} of the native drugs was considerably increased when encapsulated in TR polymeric micelles and incubated below LCST demonstrating the reduced cytotoxicity of the nano-carrier below the LCST (Table 7). Strikingly, a drastic reduction of the IC_{50} of the encapsulated drugs at the LCST compared to the native drugs was observed due to the increased cellular uptake of the micelles at the LCST, as shown by fluorescence microscopy studies (Section 1.6.13). In addition, combinational Sq-Gem and PTX loaded micelles significantly enhanced the cytotoxicity, proving the synergistic effect of these anti-cancer drugs against pancreatic cancer cells, in concert with the stimulus responsive properties of the micelles.

Table 7. The IC_{50} values of native and encapsulated drugs measured by the MTT cytotoxicity assay.

Anti-cancer Drug	*LCST*	*IC_{50} (nM)*	*SD*
Sq-Gem	Not encapsulated (in DMSO)	1122	± 258.59
	Nanoassembled form	40	-
	Below	-	-
	At	310.4	± 55.44
PTX	Not encapsulated	9.44	± 0.17
	Below	29.22	± 1.75
	At	7.25	± 0.16
Sq-Gem and PTX	Not encapsulated	3.03	± 0.30
	Below	4.24	± 0.16
	At	1.93	± 0.10

1.6.12 The combination index calculation

The synergistic activity of the two drugs on MiaPaCa-2 cells was verified by the Chou-Talalay combination index (CI)(Table 8); it was found that the CI of the non-loaded drugs was 0.32 which verifies the synergism of the two drug molecules (CI<1 is indicative of synergistic activity). It was not possible to calculate a CI value for the micelles below the LCST as Sq-Gem loaded micelles were virtually non-toxic under the experimental conditions. At LCST, the CI was 0.27 indicating a further enhancement of the synergistic activity of Sq-Gem and PTX in the formulated form.

Table 8. CI values of Sq-Gem and PTX loaded micelles on MiaPaCa-2.

	CI
Drug only	0.32
Below LCST	---
At LCST	0.27

- CI could not be calculated due to the absence of IC_{50} in some micelles.

Overall, these results indicate that in all cases, the encapsulation of the drugs, individually or in combination, resulted in retention or significant enhancement of the cytotoxicity at the LCST and in a reduction of the cytotoxicity below the LCST. However, a careful interpretation of the data based merely on the drug release patterns cannot justify the large differences observed. Therefore, the hypothesis was that the polymer itself might be actively interacting with cellular organelles (i.e. the cell membrane) in a temperature dependent manner which could further augment the drug uptake rates at the LCST.

1.6.13 Thermo-dependent cellular uptake of fluorescent thermo-responsive polymer

Hiruta and co-workers synthesised three different thermo-responsive fluorescence polymer probes and investigated the effect of temperature on cellular uptake. The results indicated (Figure 61) that the temperature could precisely control the cellular uptakes of thermoresponsive polymers. The cellular uptakes of the fluorescent polymer probes were suppressed below the LCST and increased at the LCST which was explained as a result of two factors. The first one was due to the changes in the hydrophilicity/hydrophobicity properties of the thermo-responsive polymer chains. Below the LCST, the polymer chain was hydrophilic and had a hydration layer around the polymer chain which inhibited the interactions between the polymer chain and cell membranes, and as a result, the cellular uptake of the fluorescence polymer probe could not be observed. In contrast, at the LCST, the polymer chains turned hydrophobic and enhanced the hydrophobic interactions between the polymer chain and the cell membranes therefore the cellular uptake of the fluorescent polymer probe was enhanced.

The second factor was explained as the changes in the hydrodynamic size of the polymer. The hydrodynamic size of the polymer increased at the LCST which enhanced the interactions between aggregates of the fluorescence polymer probe and the cell membranes and ultimately improved the cellular uptake (Hiruta, Y. et al. 2014).

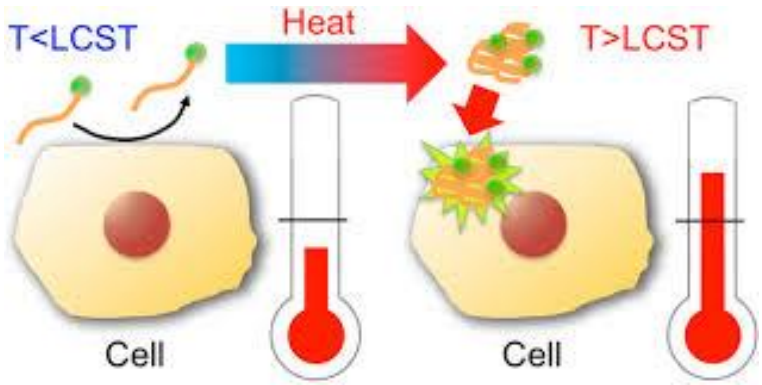

Figure 61. The cellular uptake of thermoresponsive polymers could be accurately controlled by temperature (Hiruta, Y. et al. 2014).

Furthermore, Akimoto et al. investigated the temperature-induced intracellular uptake mechanism of thermo-responsive polymeric micelles (Figure 62). They also observed an increase in the hydrodynamic sizes of the micelles from 20 nm below the LCST to ca. 600 nm at the LCST due to the aggregation of micelles. The thermo-responsive phase transition of the micellar coronas enhanced the interactions between cells and the micelles. However the intracellular micelle uptake mechanism and the micelle distributions were unclear. In addition, they investigated the internalisation of the micelles using various organelle specific stain agents. They detected the micelles localisation at the Golgi apparatus/ endoplasmic reticulum and not inside the lysosome. Interestingly, they found out that the temperature modulation across the micellar LCST could promote selective drug delivery by lysosome-bypassing intracellular uptake only at the heated targeting sites. (Akimoto, J. et al 2010).

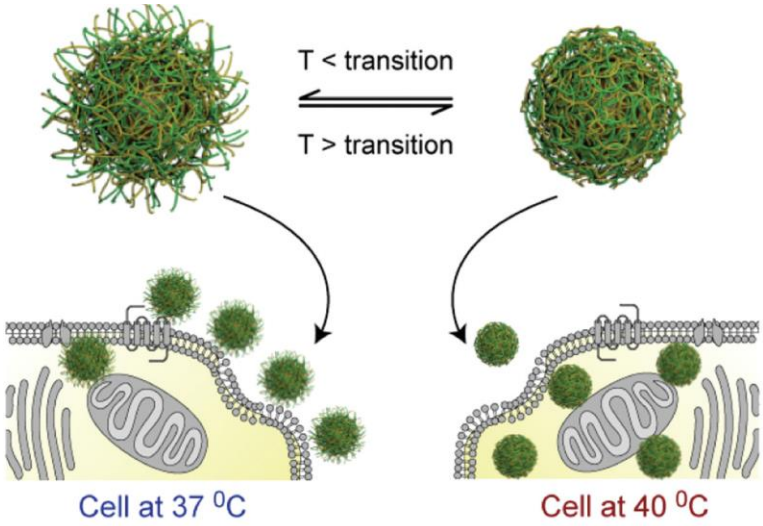

Figure 62. Thermo-responsive micelles enhance cellular uptake due to changes on the surface corona with thermal response (Abulateefeh, S. R. et al. 2013).

In another study, the Alexander research group synthesised thermo-responsive polymeric micelles and encapsulated the dye rhodamine 6G and the PTX. PTX-loaded micelles reduced the cytotoxicity of the encapsulated PTX below the LCST. In contrast, enhanced cytotoxicity at the LCST was reported due to an increase in the cellular uptake by the endo-lysosomal pathway which is a standard route for micellar uptake (Abulateefeh, S. R. et al. 2013).

In this research, a block copolymer was synthesised with a fluorescent tag that could be tractable with fluorescence spectrometry/microscopy. The polymer was incubated with MiaPaCa-2 cells for 30 min below or at the LCST, and then the cells were visualised by fluorescence microscopy. Interestingly, it was found that the polymer only adsorbed onto the cellular membrane and did not permeate inside cells when incubated below LCST (at 37°C) (Figure 63A) as the fluorescence signal was persistently tracked at the periphery of the cells. On the other hand, when the cells were incubated with the fluorescent polymer at the LCST (at 40°C), the cells displayed stronger fluorescent signal inside the cell cytosol (Figure 63B). These results indicated that increasing the temperature effectively increases the cell internalisation of the fluorescent polymer first by eliciting a direct interaction of the lipophilic pEHMA block of the polymer with the cell membrane followed by enhanced internalisation,

likely driven by the thermal collapsing of the PEGMA block.

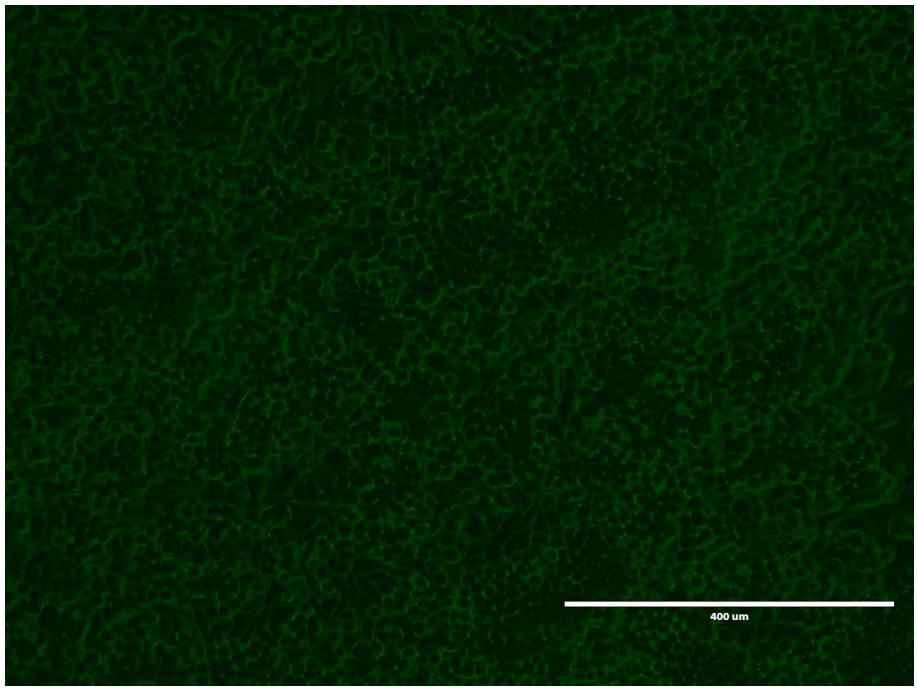

A.

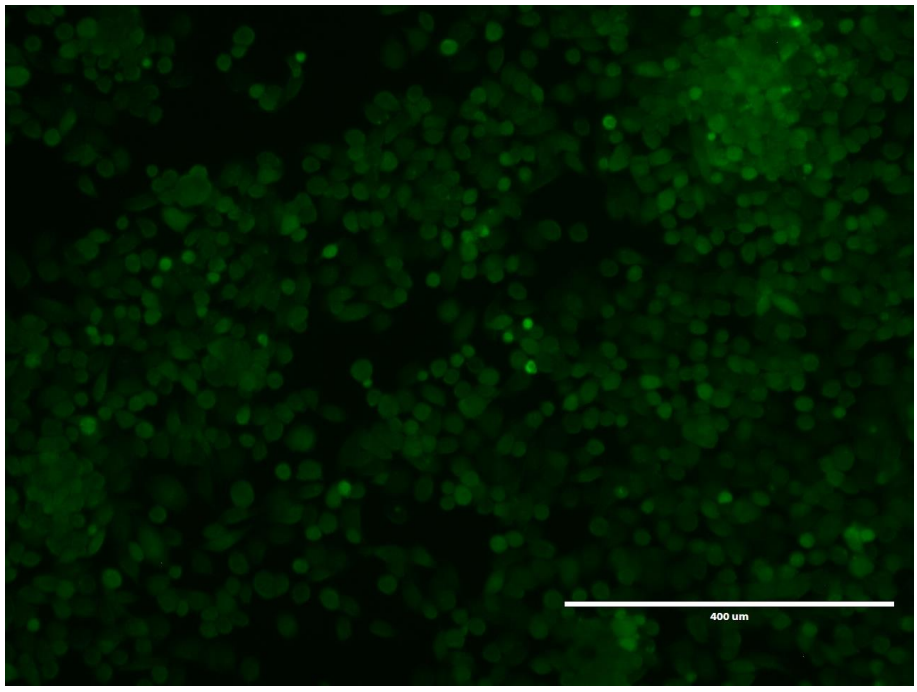

B.

Figure 63. Cellular uptake of fluorescent TR polymer **A.** below and **B.** at LCST. The scale bars show the size of 400 μm.

1.6.14 Flow Cytometry

Figure 64 shows a standard curve divided into two curves, one with lower intensity and the other one shifting towards higher intensity. The first band was attributed to the fluorescence signal from the polymer adsorbed on the cell membrane while the second band corresponded to the signal resulting from the cell internalised polymer. The flow cytometry profile above the polymers' LCST showed more cells with more fluorescent polymer adsorbed on the cell membrane when compared to the curve below LCST. Moreover, the fluorescent signal corresponding to internalised polymer increased significantly at the LCST as evidenced by the pronounced right-shifting of the fluorescent band. These results corroborate with the hypothesis that the polymer was initially adsorbed on the cell membrane via hydrophobic interactions primarily due to the pEHMA followed by enhanced cellular uptake driven by the collapsing of the thermoresponsive profiles and point to a more complex and collective cytotoxic mechanism pattern which is justified by: 1. The enhanced drug release controlled by the temperature stimulus which effectively leads to increased drug translocation across the cell membrane, 2. The direct interaction of the polymer with the cell membrane which potentially results in an increased permeability of the cell membrane at the polymers LCST which could further augment the translocation rates of both lipophilic drugs and 3. The enhanced cellular uptake of the micelles at the LCST via endocytosis mechanism (Abulateefeh, S.R. et al. 2013; Akimoto, J. et al.2010; Hiruta, Y. et al. 2014)

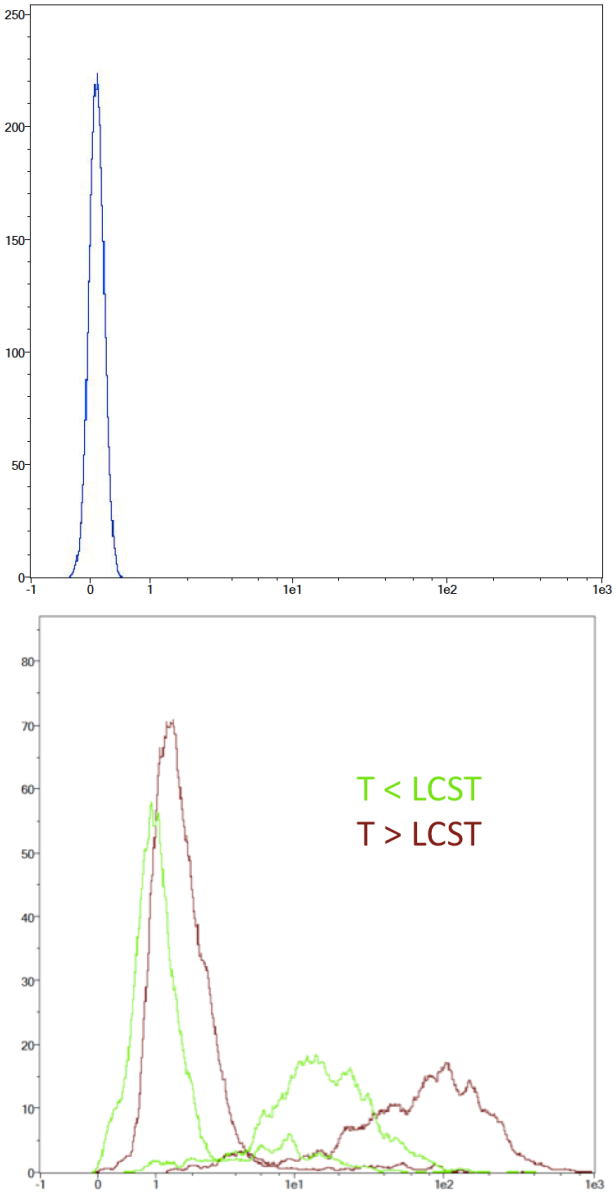

Figure 64. The flow cytometry graph is plotted between number of cells along Y -axis and cell fluorescence intensity (in arbitrary units) along the X-axis. A. The graph shows standard curve of MiaPaCa-2 cells without fluorescent probing. B. The graph shows results obtained from below LCST (green curves) and at LCST (red curves).

1.6.15 Clonogenic cell survival assay

A clonogenic cell survival assay was conducted to investigate the proliferative ability of the survived cells post treatment (Table 9). The clonogenic cell survival assay measures the long-term cytotoxic effects of the drugs by measuring their ability to propagate from a single cell to a clone and produce a viable colony (Figure 65) (Roper, P.R. et al., 1976). According to the results obtained for each concentration of drugs, some single cells formed colonies (100-200 cells), some remained single and few stopped dividing after formation of small colonies (5-20 cells). The number of colonies produced after treatment is inversely proportional to the drugs concentration (µM).

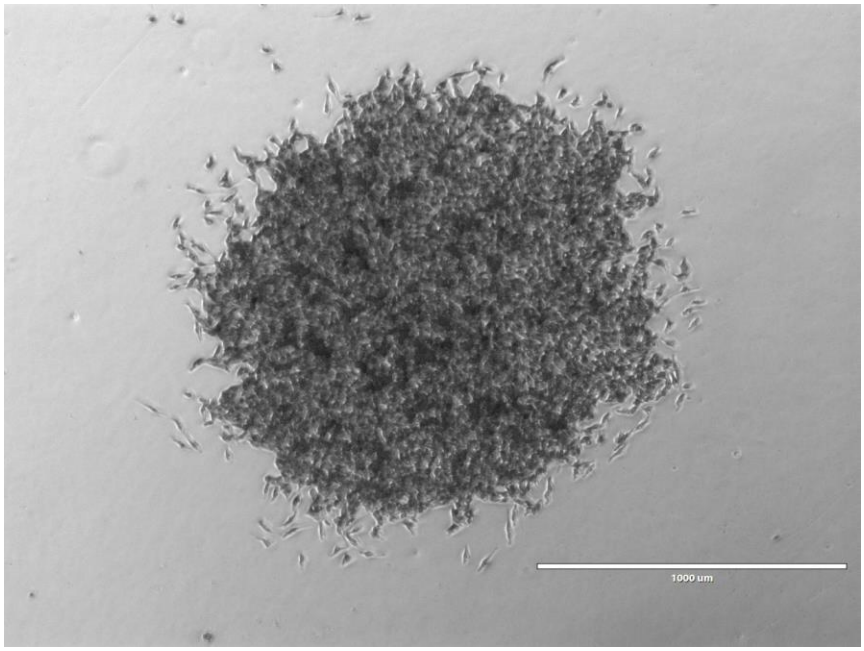

Figure 65. Shows the standard colonies formed from MiaPaCa-2 cells without application of formulations after 14 days. The scale bar shows the size of 1000 µm.

Table 9. Plates showing colonies of MiaPaCa-2 cells post treatment with Sq-Gem +PTX loaded micelles at 37°C and 40°C after 14 days.

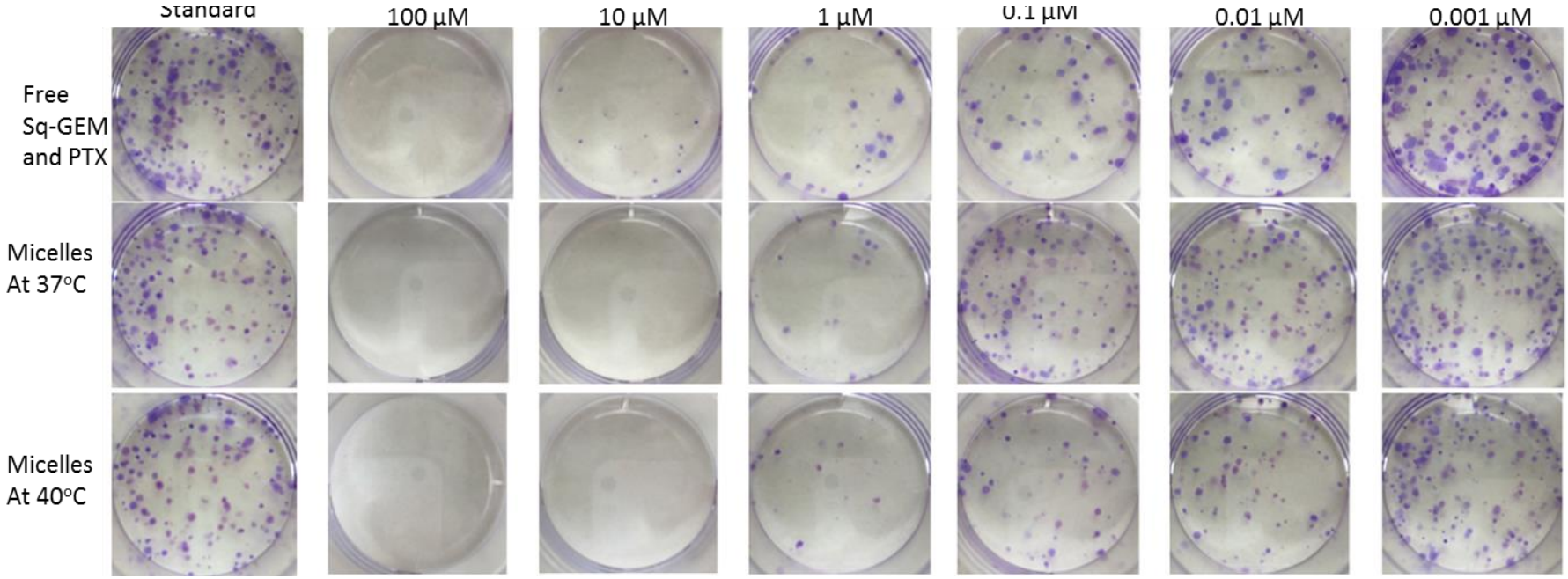

The survival fraction was calculated 14 days post treatment in order to probe the cytotoxic properties of the micelles in the longer term. As expected, it was found that the survival fraction decreased as the concentration of the drugs increased. Interestingly, the micelles below the LCST, were found to decrease the survival fraction induced by the drugs at concentrations from 0.001 μM to 0.1 μM. However, at the LCST, the survival fraction was still more diminished and was very close to the values for the free drugs (note that for 0.001 μM Sq-GEM/PTX it was statistically improved)(Figure 66). This longer term effect of the polymer micelles further supports our proposed mechanism of action as previously discussed, especially given the fact that the release of the drugs is controlled only for a few hours by temperature; therefore, a longer term mechanism as evidenced by the cell membrane interaction studies could indeed explain the longer term effects of temperature on the cytotoxicity profiles of the drugs.

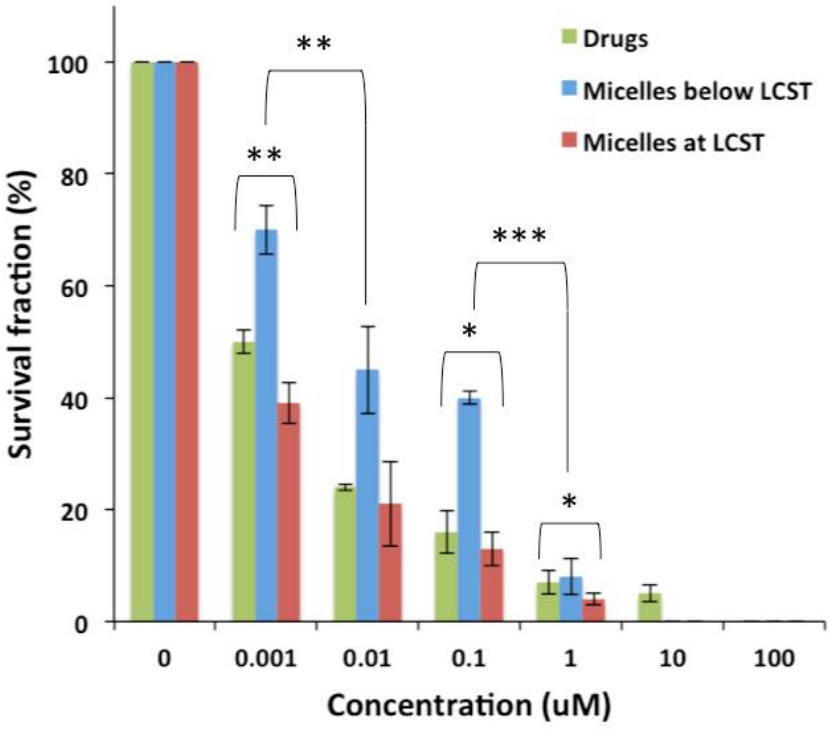

Figure 66. The survival fraction of MiaPaCa-2 cells decreased as the concentration of drug increased. P value 0.0001 to 0.001 indicated with *** meaning extremely significant; P value 0.001 to 0.01 indicated with ** meaning very significant; P value 0.01 to 0.05 indicated with * meaning significant.

1. 7 Conclusion

This study introduces a new thermoresponsive block copolymer that self assembles in sub-50 nm micelles and can be co-loaded with two potent anticancer drugs, namely, PTX, and Sq-GEM. We demonstrated that the polymer micelles could modulate the release profiles of two drugs simultaneously and elicit synergistic cytotoxicity against a model pancreatic cell line. More importantly, it was experimentally demonstrated that the polymer actively interacted with the cell membrane which in turn thermally modulated and augmented the synergistic activity of the drugs in the longer term. Although, there are many studies in thermoresponsive block copolymer micelles, the potential role of the actual carrier, that is the polymer, is almost systematically neglected and hence we anticipate that our study will be insightful for the design of polymer based nanomedicinal formulations for cancer, especially for formulations aimed for drug combinations where the therapeutic window is far more challenging to exploit.

Chapter 2

Dual Controlled Delivery of Gemcitabine and Cisplatin using Polymer Modified Thermo-sensitive Liposome for Pancreatic Cancer

2.1 Abstract

Cisplatin is an anticancer drug used to treat several types of cancers. The drug is administered through a vein (intravenously or IV) as an infusion. However, after administration the drug does not undergo hydrolysis due to high concentration of Cl^- ion in blood stream. As the deactivated drug excretes in the urine within 24 hr, there would be no drug left to enter the cell and stop DNA replication. Moreover, gemcitabine is the most potent anti-cancer drug for the treatment of pancreatic cancer but it undergoes deamination in the bloodstream and becomes biologically inactive. Hence both drugs should be protected in the bloodstream and delivered to the site of action. Clinically it has been proven that gemcitabine and cisplatin combinational therapy increase the survival rate of patients. For this reason, a polymeric modified thermo-responsive liposome (PMTL) was developed to encapsulate these hydrophilic chemotherapeutic drugs inside its hydrophilic core. PMTL is new generation of liposomes in which the exterior shell is covered with thermo-responsive (TR) polymers. By application of hyperthermia, these TR polymers on the surface of the liposomes undergo coil to globule transition which leads to disruption of the lipid membrane which in turn leads to triggered drug release. As a result, PMTL would protect the encapsulated drug from premature inactivation by the physiological medium and release (activate) the drug only at the site of action. In this research, poly [(di(ethylene glycol) methyl ether methacrylate –co- poly(ethylene glycol) methyl ether methacrylate$_{300}$) –b- (2-Ethylhexyl methacrylate)] [Poly (DiEGMA-co-OEGMA$_{300}$)-b-EHMA] block copolymer was synthesised by reversible addition fragmentation chain transfer (RAFT) polymerisation and was incorporated into the membrane of a traditional thermosensitive liposome (TTL). After application of hyperthermia at 40°C, the PMTL showed improvement in drug release compared to TTL. In vitro cytotoxicity assays on two pancreatic cancer cell lines, MiaPaCa-2 and BxPC-3 cells, revealed that combinational co-delivery of gemcitabine plus cisplatin (GemCis) with PMTL showed synergistic effect and considerably decreased cancer cells viability compared to each drug separately. In addition, the PMTL reduced the IC_{50} (half maximal

inhibitory concentration) of the native drugs compared to TTL. Furthermore, investigation of the proliferative ability of the survived cells after treatment showed that co-loaded PMTL at 40°C reduced the cell survival fraction percentage compared to free drugs. Lastly, fluorescent cellular uptake studies demonstrated that enhanced cytotoxicity is due to induced liposome cell-binding interaction and cellular uptake resulting from the transition of hydrophilic the TR polymer to hydrophobic at 40°C.

2.2 Introduction

Liposomes are the first nanomedicine used clinically and ever since it been established as the gold standard in drug delivery research. To date, over seventeen lipid-based nano-carriers or liposomes have been successful in the delivery of chemotherapeutic agents and clinically approved (Ta, T. et al. 2013).

Liposomes (Figure 67) are spherical nano-carrier that consists of phospholipids, the major component of cell membrane. A phospholipid consists of two fatty acid tail (non-polar) and a phosphate head (polar). They self assemble to form a lipid bilayer surrounded by polar head groups on the interior vesicle and exterior shell. They are capable of encapsulating hydrophilic drugs within their vesicle and hydrophobic drugs inside their lipid bilayer (Akbarzadeh, A. et al. 2013; Torchilin, V. P. 2005).

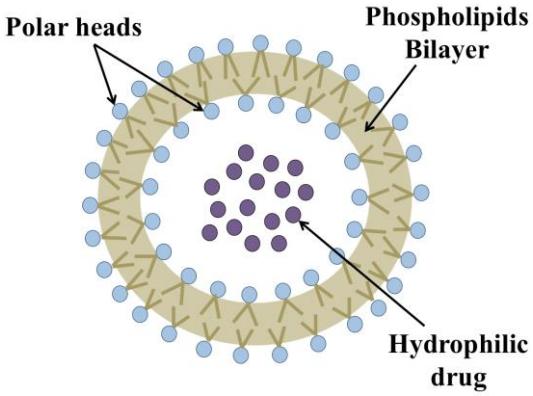

Figure 67. Liposome structure

Moreover, they are biocompatible, biodegradable, have no toxic effects, protect the patient from side effects of the encapsulated drug and protect the encapsulated drug from premature inactivation by the physiological medium. Yatvin and coworkers first introduced thermosensitive liposomes over 30 years ago and used mild local hyperthermia to control the release of entrapped drugs from these liposomes (Yatvin M. B. et al. 1978; Weinstein, J.

N. et al. 1979). Mild hyperthermia comprises the heating of tumors to temperature up to 43°C and it is usually in combination with chemotherapy or radiation to improve the therapeutic outcome (Figure 68). Hyperthermia is applied locally at the tumor by using radiofrequency electrodes implanted in the tumor or microwave antennas or ultrasound transducers that apply their energy to the tumor non-invasively. Mild hyperthermia increases the perforation of tumor blood vessels, microconvection in the interstitium, and perforation of the cell membrane which in turn render tumor cells temporarily more sensitive to chemotherapy or radiation (Koning, G. A. et al. 2010; Landon, C. D. et al. 2011; Gaber, M. H. et al. 1996).

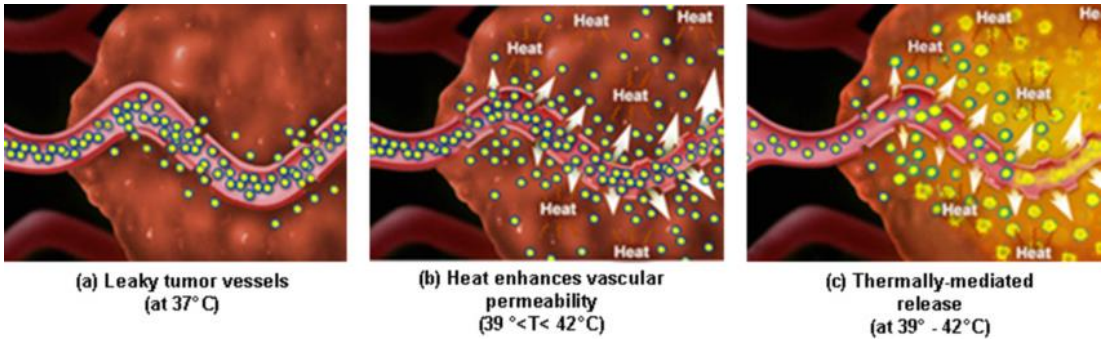

Figure 68. Possible mechanisms involved in combination with hyperthermia and thermosensitive liposome therapy. (a) Non-thermosensitive liposomes extravasate inside the tumor by the EPR effect, (b) Mild hyperthermia further increases tumor vasculature pore size and enhances non-thermosensitive liposome extravasation, and (c) Combination of TTL and hyperthermia increases extravasation of TTL in the tumor interstitium. Adapted from (Landon, C. D. et al. 2011).

Currently there are three types of thermosensitive liposomes (i) Traditional thermosensitive liposomes (TTL), (ii) Lysolipid-containing thermosensitive liposomes (LTL), and (iii) Polymer modified thermosensitive liposomes (PMTL).

2.2.1 Traditional thermosensitive liposomes (TTL)

In 1978 Yatvin et al. introduced the first class of thermorsensitive liposomes. Thermorsensitive liposomes consist of a lipid membrane that undergoes a phase transition from solid (ordered) phase to liquid (disordered) phase when heated above their transition temperature (T_m) (Figure 69). Below the T_m, the

lipid chains are ordered and packed due to the extension of C-C single bond and an immobile head group at the water interface. However, at the temperature greater than T_m the lipid bilayer fluidises due to changes in the orientation of C-C single bond from trans to gauche state. Furthermore, there is increase in the headgroup mobility and therefore the permeability is further enhanced.

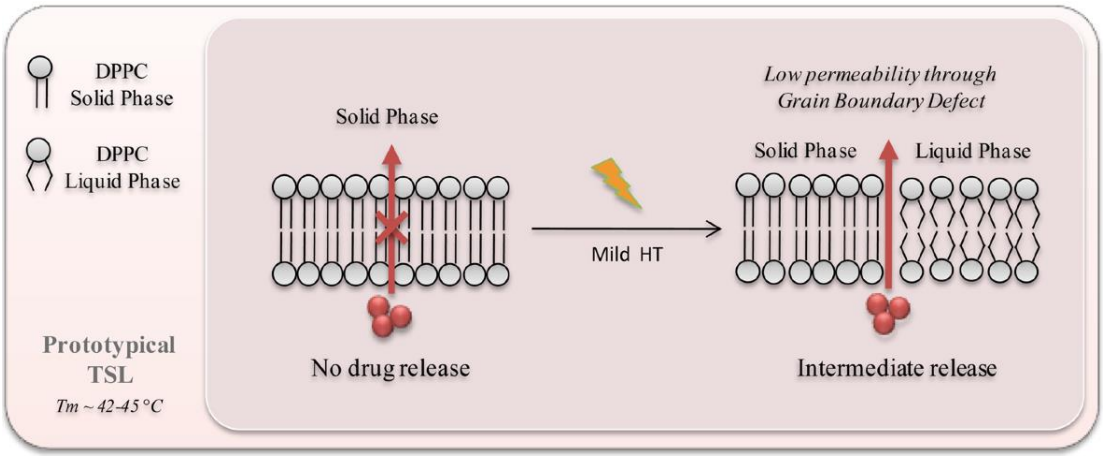

Figure 69. Presents the behavior of TTL around T_m (42-45 °C). DPPC (1,2-dipalmitoyl-*sn*-glycero-3-phosphocholine) is a lipid bilayer component. Below T_m, the lipid bilayer is solid and closely packed which ceases the drug permeability. However above T_m, there is formation of grain boundaries which appear due to the presence of both solid and liquid phases. The grain boundaries are able to increase the permeation to some extent. Adapted from (Al-Ahmady, Z.et al. 2016).

During the liposome preparation when the lipid bilayer is cooled close to T_m, the lipids do not solidify uniformly and produce nucleated solid domains within the melted domain. The solid domain, or 'grains', with crystalline structure increase in number as the lipids cool down and the entire lipid droplet is transformed to solid. As a result, the grain boundaries appear among the solidified domain with imperfect crystalline structure leading to planar defects at the boundaries (Figure 70).

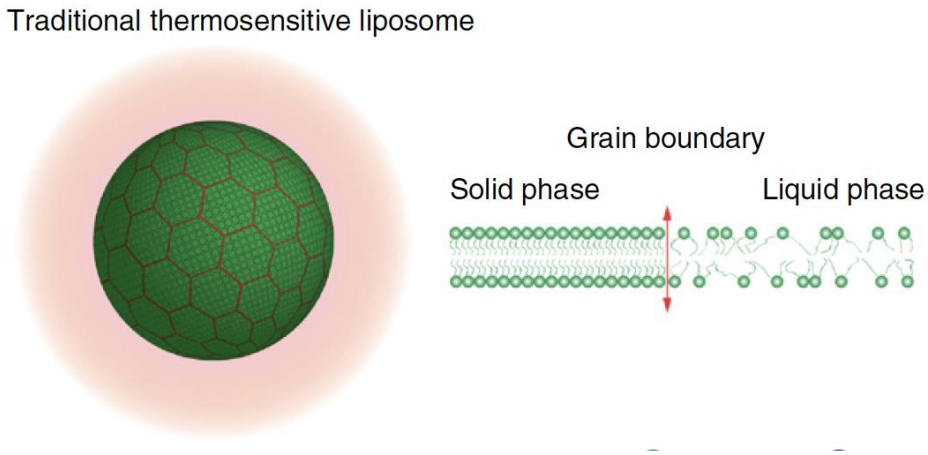

Figure 70. Shows the formation of grain boundaries between the solid and the liquid interface in TTL. Adapted from (Ta, T. et al. 2013).

1,2-dipalmitoyl-*sn*-glycero-3-phosphocholine (DPPC) (Figure 71) acts as solid phase lipid capable of producing grain boundaries. The phospholipid with two long acyl chains (C15) is the main lipid bilayer component of TTL. The T_m of DPPC is 42 ° C.

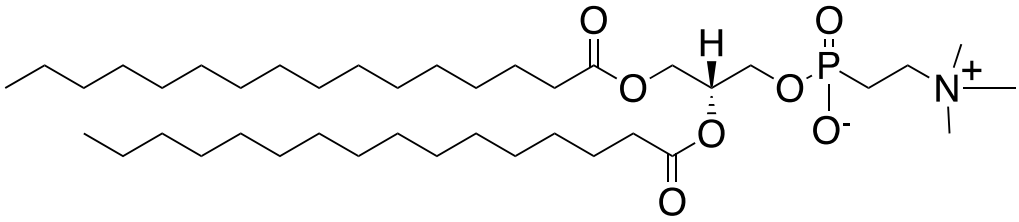

Figure 71. DPPC structure.

L-α-phosphatidylcholine, hydrogenated (Soy) (HSPC) (Figure 72) is another phospholipid with longer acyl chains (C17) which increase the T_m to 55° C. Using DPPC:HSPC lipid mix with 7:3 molar ratio results in a T_m range between 41 and 43 ° C.

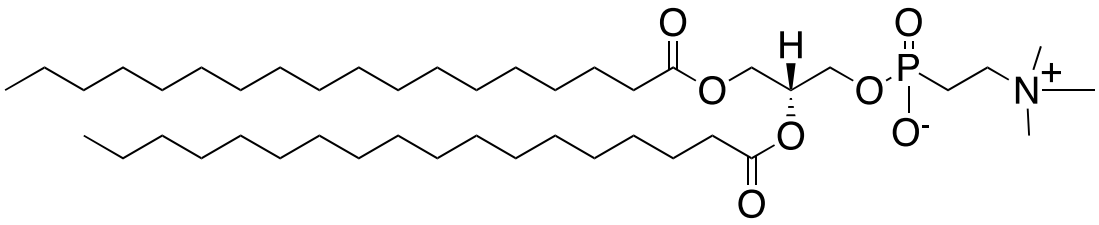

Figure 72. HSPC structure.

The integration of PEGylated lipid such as 1,2-distearoyl-*sn*-glycero-3-phosphoethanolamine-N-[amino(polyethylene glycol)-2000] (ammonium salt) (DSPE-PEG2000) (Figure 73) into liposomes increases the serum stability and acts as an steric stabilising component. PEGylation sterically hinders the surface of the liposome, resulting in reduced opsonisation of the liposome by the plasma proteins which in turn reduces the recognition of the liposomes by the Mononuclear phagocyte system (MPS) involved in their removal from the blood circulation by phagocytosis (Figure 74) (Allen, T. M. 1993; Immordino, M. et al. 2006).

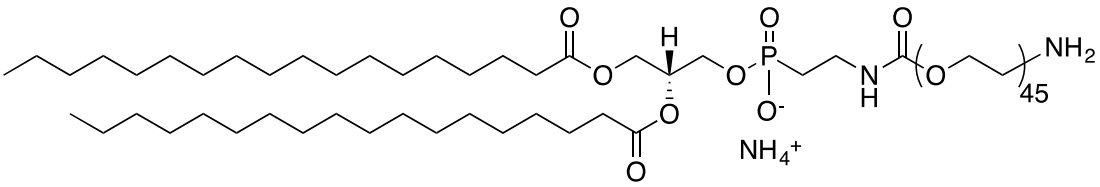

Figure 73. DSPE-PEG2000 structure.

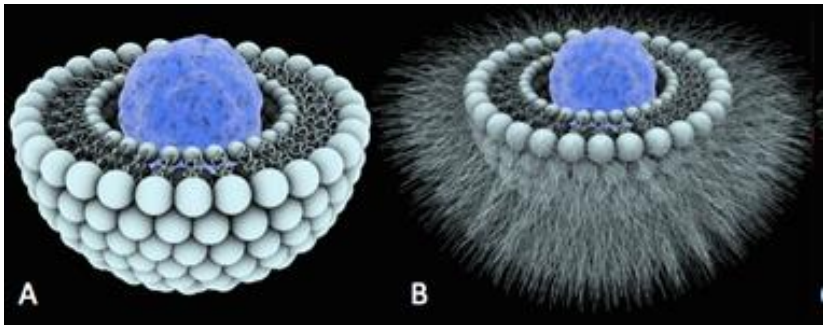

Figure 74. Shows **A.** unilamellar liposomes and **B.** PEGylated unilamellar liposomes. The liposomes coated by PEG in order to avoid opsonisation in the bloodstream. The blue sphere represents the encapsulated hydrophilic drug. Adapted from http://reflexions.ulg.ac.be (Last accessed: January 2017).

Cholesterol (Figure 75) is incorporated inside phospholipids in order to improve the characteristics of the membrane below and above T_m. Below T_m cholesterol increases fluidity of lipid membrane by disrupting the close packing of acyl chains whereas above T_m it decreases the fluidity by constraining their motion. Cholesterol has T_m of 148 °C which results in a broadening of the lipid bilayer's T_m.

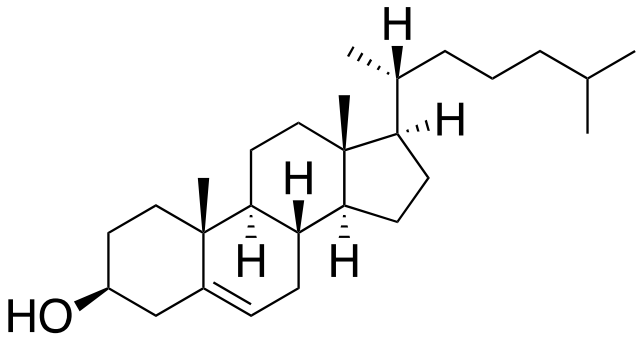

Figure 75. Cholesterol structure.

TTL formulations require high heating in order to reach their transition temperature and become permeable. The high temperature can result in hemorrhage and trigger necrosis to neighboring healthy tissue. Hence, new approaches have been developed to reduce the transition temperature of thermosensitive liposomes to the range of mild hyperthermia (39-42° C). The new approaches comprise the (i) integration of lysolipids directly into the lipid membrane (ii) formulation of polymer-modified thermosensitive liposomes (Al-Ahmady, Z.et al. 2016; Ta, T. et al. 2013)

2.2.2 Lysolipid-containing thermosensitive liposomes (LTL)

In 1999 Anyarambhatla and Needham introduced the incorporation of lysolipids into the lipid membrane in order to reduce the transition temperature and enhance the drug release (Anyarambhatla, G. et al. 1999). Lysolipids are lipids that contain only one acyl chain. They have a large polar head compared to their single acyl chain which results in a positive intrinsic curvature and ultimately form micelles. 1-palmitoyl-2-hydroxy-sn-glycero-3-phosphatidylcholine (MPPC) (Figure 76) and 1-stearoyl-2-hydroxy-sn-glycero-3-phosphocholine (MSPC) (Figure 77) are two examples of lysolipids having critical micelle concentration (CMC) of 4 - 8.3 μM and 0.4 μM respectively.

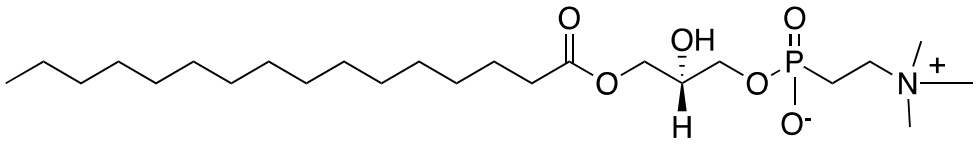

Figure 76. 1-palmitoyl-2-hydroxy-sn-glycero-3-phosphatidylcholine (MPPC) structure.

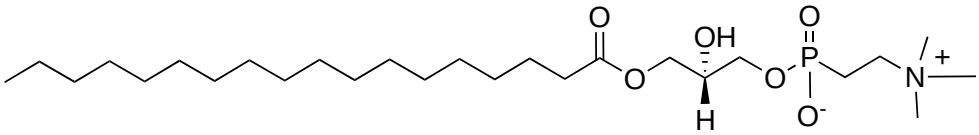

Figure 77. 1-stearoyl-2-hydroxy-sn-glycero-3-phosphocholine (MSPC) structure.

By increasing the temperature close to T_m the grain boundaries melt and initiate free lateral diffusion of the phospholipids. This mobility allows the lysolipids to gather at the boundaries and due to their micelle formation's tendency produce defects in grain boundaries (Figure 78).

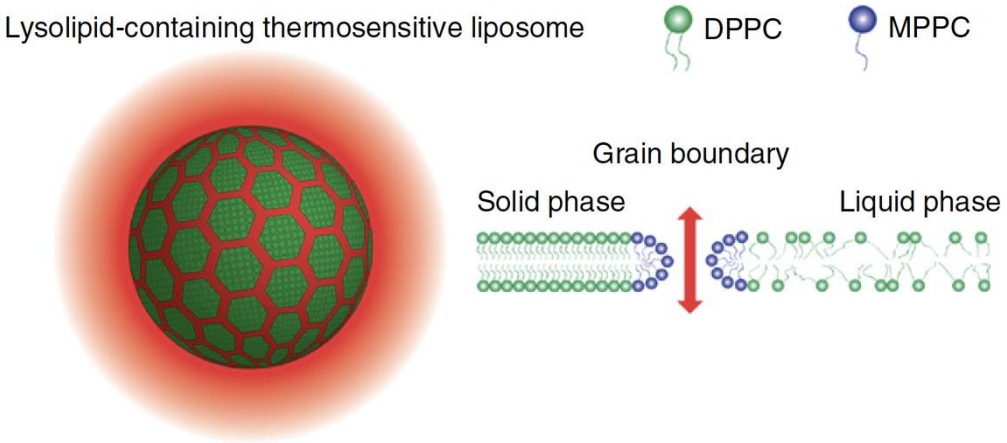

Figure 78. Shows accumulation of lysolipids at the grain boundaries and formation of stable defects which lead to increase of the content release. Adapted from (Ta, T. et al. 2013).

Incorporation of lysolipids reduces the T_m of TTL formulations and provides rapid release upon heating (Figure 79). Banno et al. showed that nearly 70% of lysolipids are extracted from the LTL within 1 hr in vivo administration due

to the adsorption of serum proteins which destabilise the LTL. They showed significant Doxorubicin leakage from LTL at 37°C ~1 h after in vivo administration (Banno, B. et al. 2010). In conclusion, the desorption of lysolipids from LTL in blood stream leaves a defect in the liposome membrane leading to premature drug leakage under physiological conditions. To overcome these drawbacks the new generation of thermosensitive liposomes was proposed.

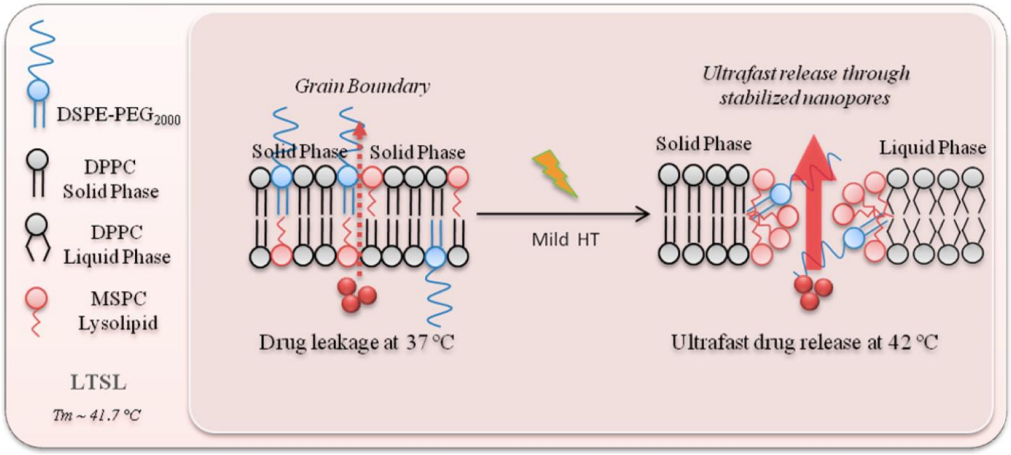

Figure 79. Presents the structure of LTL where the incorporation of lysolipids in the lipid membrane reduces the T_m. Below T_m, there is drug leakage through the grain boundaries produced by the lysolipids. Above T_m, there is ultrafast drug release due to formation of larger nanopores by the lysolipids. Adapted from (Al-Ahmady, Z. et al. 2016).

2.2.3 Polymer modified thermosensitive liposomes (PMTL)

A new strategy was proposed by Kono et al. to design thermosensitive liposomes which comprised the incorporation of synthetic polymers into the lipid membrane (Figure 80)(Kono, K. et al. 1994). These synthetic polymers consisted of block copolymers with TR hydrophilic block and hydrophobic blocks. The hydrophobic block acts as an anchor which is fixes the polymer inside the lipid bilayer whereas the TR hydrophobic block moves freely on the surface of the liposome. At the temperature at the LCST, the TR block undergoes coil to globule transition and this change in conformation in response to environmental temperature leads to disruption of the lipid membrane and promoting the content release (Kono, K. 2001, Landon, C. D. et al. 2011).

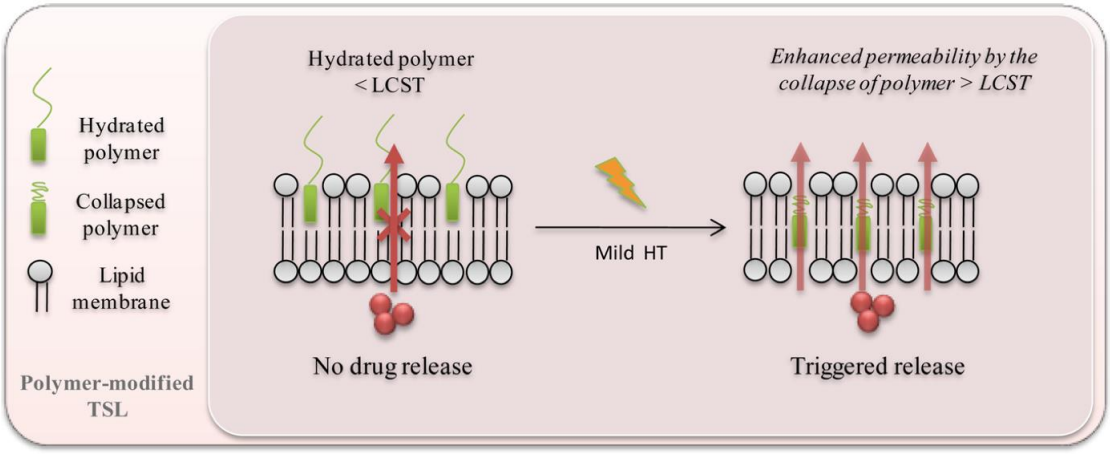

Figure 80. Shows the mechanism of drug release from PMTL. Below the LCST, the polymer chains are hydrophilic and soluble in the surrounding aqueous medium. However, at the LCST the polymer turns hydrophobic and undergoes coil to globule transition which destabilises the lipid bilayer and releases the drug. Adapted from (Al-Ahmady, Z. et al. 2016).

For the first time, Kono and coworkers fixed a thermosensitive N-isopropylacrylamide (NIPAAM) onto the liposome lipid membrane by copolymerising it with 1% molar octadecyl acrylate (ODA) using free radical polymerisation. The long alkyl chain of ODA acted as an anchor to incorporate the hydrated part of the polymer (NIPAAM) into the liposome surface. The LCST of NIPAAM was 32 °C and co-polymersation with 1% ODA reduced the LCST to 27 °C. The authors prepared non-thermosensitive egg yolk phosphatidylcholine (EYPC) liposome and thermosensitive dipalmitoylphosphatidylcholine (DPPC) liposome and modified their surface by poly(NIPAAM-co-ODA). Furthermore, fluorescent dyes (Calcein / Carboxyfluorescein (CF)) were used to load the liposomes. The formulations revealed increased dye release at the LCST but minimal release below the LCST in both formulations. However, the release was higher in DPPC liposomes showing the synergism between thermosensitivity of the DPPC membrane and the temperature-dependent membrane disruption properties of the polymer (Kono, K. et al. 1994).

In another study (Figure 81), Kono et al. prepared PMTL using a synthetic block copolymer poly(EOEOVE)-OD_4. The block copolymer consisted of poly[2-(2-ethoxy) ethoxyethyl vinyl ether (EOEOVE)] as the thermosensitive

block and Octadecyl vinyl ether (ODVE) as the hydrophobic block. The LCST of poly(EOEOVE)-OD_4 was determined to be 40 °C. The formulation was prepared for tumor-specific chemotherapy with Doxorubicin (DOX). It was shown that the cellular internalisation of the PMTL was largely temperature dependent. The PMTL formulations did not reduce the HeLa cell viability below LCST whereas the cytotoxicity significantly increased at the LCST (Kono, K. et al. 2010).

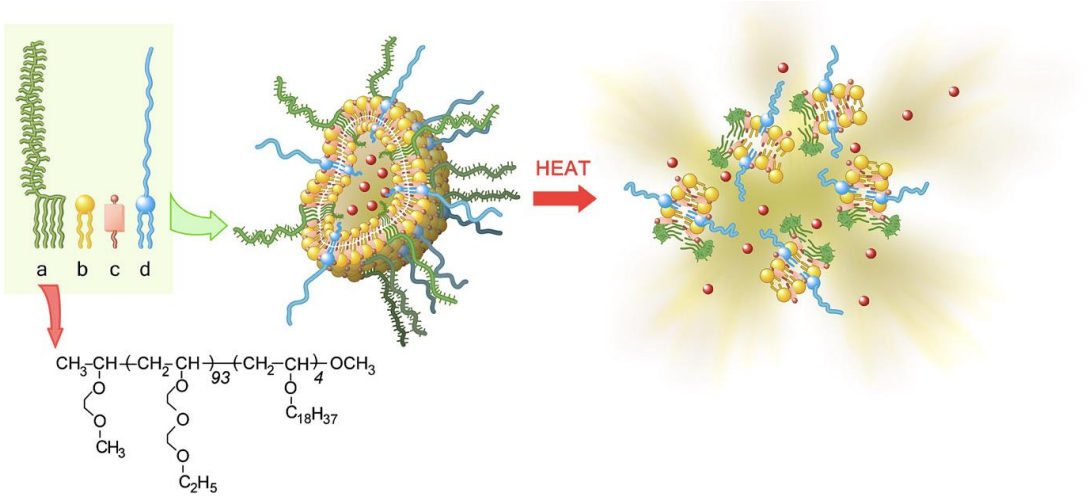

Figure 81. Schematic demonstration of the PMTL made by Kono et al. **a.** Its thermosensitive block copolymer consists of the hydrophilic block [poly(EOEOVE)] and a hydrophobic anchor for its fixation onto the liposome **b.** Membrane forming egg yolk phosphatidylcholine (EYPC) **c.** Membrane stabilising cholesterol **d.** Highly hydrophilic and non-toxic N-[methoxy (polyethylene glycol) 5000]-distearoyl phosphatidylethanolamine (PEG-PE). The red dots represent DOX. Adapted from (Kono, K. et al. 2010).

Table 10. A brief summary of PMTLs with different thermoresponsive block copolymers. Some of these PMTLs progressed to preclinical investigation. Adapted from (Al-Ahmady, Z. et al. 2016).

liposomal composition	temperature-sensitive polymer	LCST (°C)	dye/ drug	experimental design
EPC and DPPC	p-(NIPAM-ODA)	27	CF calcein	in vitro release study
DOPE	p-(NIPAM-ODA)	32	calcein	in vitro release study
EPC, DMPC:DPPC DPPC and DSPC	p-(NIPAM-AA-ODA)	30–43	calcein	in vitro release study
DLPC DPPC DSPC	p-(NIPAM-ODA)	32	calcein	in vitro release study
EPC and EPC:DOPE	p-(NIPAM-NDDAM)	28	calcein	in vitro release study
EPC	p-(APr-NIPAM)-$2C_{12}$	40	MTX	in vitro release study and cellular cytotoxicity
DOPE	p-(APr-NIPAM)-$2C_{12}$ p-(APr-NIPAM-NDDAM)	33–34	calcein	in vitro release study
DOPE:EPC	p-(NIPAM-NDDAM-AAM) p-(NIPAM-AAM)	39–46	calcein	in vitro release study (increasing LCST)
DOPE	p-(APr-NIPAM)-$2C_{12}$ PEG_{550}-$2C_{12}$	38	calcein	in vitro release study and serum stability (effect of PEG)
EPC	p-(APr-NIPAM)-$2C_{12}$ p-(DMAM-NIPAM)-$2C_{12}$ p-(NIPAMAM-NIPAM)-$2C_{12}$	40	calcein	in vitro release study (effect of ΔH)
DOPE:EPC	p-(EOEOVE-ODVE)	36	calcein	in vitro release study
DPPC:HSPC:CHOL:DSPE-PEG-2000	p(NIPAM-AAM)	40 and 47	DOX	in vitro release and stability study
DPPC:HSPC:CHOL:DSPE-PEG_{2000}[a]	p(NIPAM-AAM)	40	DOX	in vitro and in vivo study
DPPC:CHOL and DOPE-EPC	p(HPMA mono/dilactate)-CHOL	42	calcein DOX	in vitro release study/HIFU
DPPC:HSPC:CHOL:DSPE-PEG_{2000}	p(NIPAM-PAA)-DMP	42 °C at pH 6.5	DOX	in vitro pH and temperature sensitivity
EPC:CHOL-DSPE-PEG_{2000}[a] EPC:CHOL-DSPE-PEG_{2000}-Gd[a]	p(EOEOVE-ODVE)	40	DOX	in vitro and in vivo study
EPC:DSPE-PEG_{5000}-Fe 3O4	p(EOEOVE-ODVE)	40	pyrene	magnetic imaging and heat triggered release

[a]These studies represent polymer-modified liposomes that progressed to preclinical investigation.

In this research, a liposome formulation was synthesised using **a** DPPC/HSPC/Chol/DSPE-PEG2000 composition, coated with a thermo-sensitive block copolymer Poly (DiEGMA-co-$OEGMA_{300}$)-b-EHMA to simultaneously encapsulate two hydrophilic chemotherapeutic drugs, namely, cisplatin and gemcitabine.

2.2.4 Cisplatin

Cisplatin (cis-diamminedichloridoplatinum(II) (Figure 82) abbreviated in literature as cis-DDP, cisplatin, cis-platinium, CDDP, DDP, CP and PDD is the first member in the class of platinum-containing anti-cancer drugs which supress the cell cycle in G2/M phase (Siddik, Z. H. 2003).

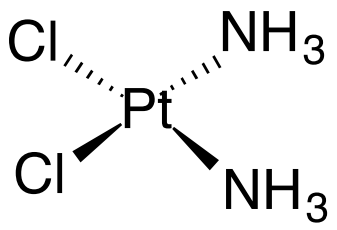

Figure 82. Cisplatin structure.

After administration of Cisplatin (CP), high concentration of Cl^- ion in the blood protects the drug from hydrolysis and hinders fast reaction with blood proteins, RNA and DNA. Around 50-70% of the administered drug is excreted within 24 hr and the remaining drug diffuses through the cell walls. Due to the very low concentration of Cl^- ions inside the cells the drug undergoes hydrolysis. The hydrolysis product, cis-$[Pt(NH_3)_2(H_2O)Cl]^+$, undergoes reaction with the DNA inside the cell **(**Reedijk, J. et al. 1984).

CP exerts its cytotoxic effect through formation of a DNA adduct (Figure 83). Once it enters cells, it forms a transient monoadduct followed by a stable diadduct via covalent binding to the N(7) site of guanine residues. In the majority of cases these are DNA intra-strand adducts (crosslinks) rather than DNA interstrand or DNA–protein adducts. These adducts or crosslinks are capable of blocking both DNA replication and transcription and induce cell apoptosis (programmed cell death) (Eastman, A. 1987).

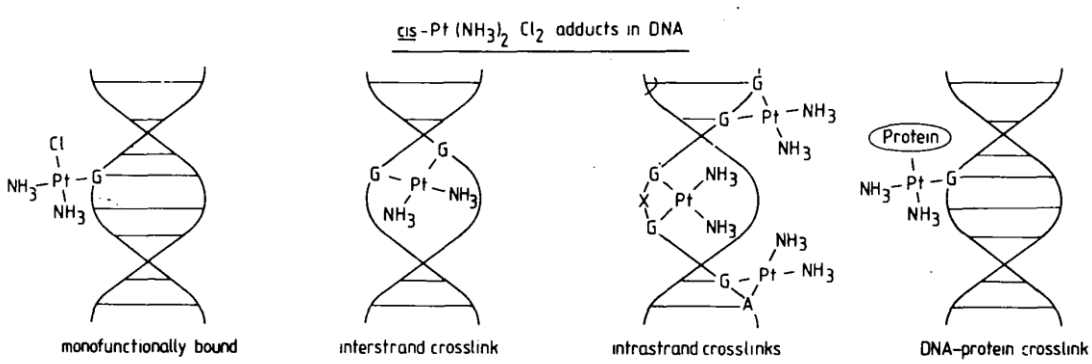

Figure 83. Mechanism of action of cisplatin. 'G' represents Guanine nucleobase. Adapted from **(**Reedijk, J. et al. 1984).

CP has several drawbacks which include drug resistance due to reduced intracellular drug accumulation (Siddik, Z. H. 2003), poor oral bioavailability (Olszewski, U. et al 2010) and severe toxicity leading to renal cell death (Miller, R. P et al 2010). Although the drug is widely used as antineoplastic agent, its non-specific targeting results in nephrotoxicity even when administered at standard doses (Tsang, R. Y. et al. 2009). Therefore a new nano-carrier is required to deliver this platinum-based anticancer drug intravenously.

2.2.5 Optimisation of chemotherapy by combination drug therapy

The synergistic mechanism of Gemcitabine plus Cisplatin (GemCis) is not fully understood. Some evidence suggest that the incorporation of 2'2'-difluoro-2'–deoxycytidine triphosphate (dFdCTP) into DNA results in conformational changes and affect the binding of CP to the guanine nucleotide opposite to the cytosine analog (substituted by GEM) which in turn enhance the formation of CP adducts (van Moorsel, C.J. et al. 1999).

Symon et al. investigated whether GEM and CP exert synergistic effect in BxPC3 and Panc-1 human pancreatic cancer cell lines. The cells were treated with three different schedules before radiation: (A) Expose the cells to gemcitabine for 2 h followed by cisplatin for 2 h, (B) Incubation of gemcitabine for 2 h, followed by washout of the drug, replenishment of media for a 24-h incubation, followed by cisplatin for 2 h, and (C) gemcitabine for 24 h with a concurrent incubation of cisplatin for the last 2 h. Schedule A showed the strongest cytotoxic synergism while schedules B and C exerted moderate synergistic cytotoxicity effect (Symon, Z. et al. 2002).

Heinemann et al. conducted a phase II study for the tolerability and safety of GemCis in 41 patients with locally advanced or metastatic pancreatic cancer. They administered GEM 1000 mg/m^2 on days 1, 8, and 15 of a 28-day schedule, and CP 50 mg/m^2 on days 1 and 15. The untreated unresectable

pancreatic cancer has a median survival of 3 to 6 months. The results of combinational GemCis therapy showed that median survival improved to 8.2 months. In addition, the GEM plus CP combination was well tolerated and enhanced the quality of life (Heinemann, V. et al. 2000).

In another study, Heinemann and coworkers performed a randomised phase III trial to compare the effectiveness and tolerability of GemCis versus GEM alone. The trial was assigned to 195 patients with advanced adenocarcinoma of the pancreas. Patients received either 1,000 mg/m^2 of GEM plus 50 mg/m^2 of CP on days 1 and 15 of a 4-week cycle or a dose of 1,000 mg/m^2 of GEM alone on days 1, 8, and 15 of a 4-week. The primary end point of study was overall survival. The results showed the efficacy and tolerability of GemCis treatment (every-2-weeks). Combinational GemCis treatment showed prolonged median progression-free survival (5.3 months) versus GEM alone (3.1 months). In addition, median overall survival was longer for patients treated in the GemCis as compared with the GEM alone (7.5 Vs. 6.0 months)(Heinemann, V. et al. 2006).

To the best of my knowledge, this is one of the very first reports on co-encapsulation and co-delivery of two potent chemotherapeutic drugs by polymer modified thermo-sensitive liposomes. Also it is one of the very first reports on drug synergism augmentation by polymer modified thermo-sensitive liposome accompanied by simultaneous cell membrane interaction.

2.3 Aim

The objective of this research is to synthesise a PMTL which could be used as a nano-carrier to co-encapsulate two hydrophilic chemotherapeutic drugs, Gemcitabine and Cisplatin, to improve their delivery and exert their synergistic cytotoxic effect (Figure 84).

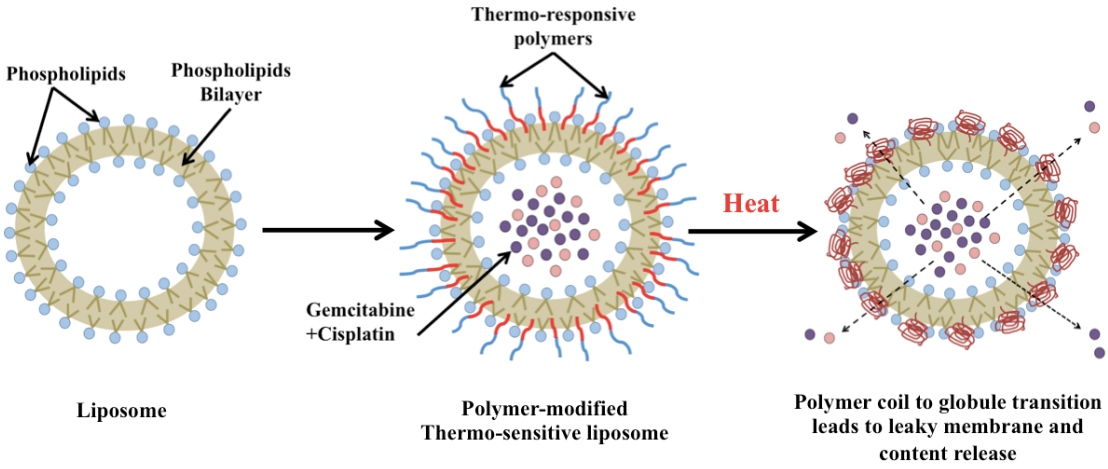

Figure 84. Schematic demonstration of proposed polymer modified thermo-sensitive liposome. After application of heat, the TR block undergoes coil to globule transition and leads to disruption of lipid membrane and content release.

2.4 Materials

1,2-dipalmitoyl-*sn*-glycero-3-phosphocholine (DPPC), 1,2-distearoyl-*sn*-glycero-3-phosphoethanolamine-N-[amino(polyethyleneglycol)-2000] (ammonium salt) (DSPE-PEG2000), 2,2′-azobis(2-methylpropionitrile) (AIBN), 2-butanone, 2-cyano-2-propyl benzodithioate (CTA/RAFT agent), 2-ethylhexyl methacrylate (EHMA), cisplatin, cholesterol (Chol), chloroform, deuterated chloroform ($CDCl_3$), diethyl ether, di(ethylene glycol) methyl ether methacrylate (DiEGMA), dimethyl sulfoxide (DMSO), dulbecco's modified eagle's medium- high glucose (DMEM), dulbecco's phosphate buffered saline (DPBS), fetal bovine serum (FBS), fluorescein *O*-methacrylate, hexane, lauryl methacrylate, l-glutamine, l-α-phosphatidylcholine, hydrogenated (Soy) (HSPC), methanol, NaCl, oligo(ethylene glycol) methyl ether methacrylate ($OEGMA_{300}$), phosphate buffered saline (PBS) tablets, penicillin-streptomycin, pyrene, tetrahydrofuran (THF), thiazolyl blue tetrazolium bromide (MTT) were purchased from Sigma-Aldrich. Gemcitabine.HCl was purchased from Sequoia Research Products Ltd. MiaPaCa-2 and BxPC3 cell line were purchased from ATTC company.

2.5 Methods

2.5.1 One pot synthesis of Poly (DiEGMA-co-$OEGMA_{300}$)-b-EHMA by RAFT polymerisation

Refer to section 1.5.1.

2.5.2 Nuclear magnetic resonance spectroscopy

Refer to section 1.5.2.

2.5.3 Gel permeation chromatography

Refer to section 1.5.3.

2.5.4 Determination of the polymers' LCST

Refer to section 1.5.4.

2.5.5 Preparation of polymer modified thermo-sensitive liposomes (PMTL)

Liposome formulations consisted of DPPC/HSPC/Chol/DSPE-PEG2000 (100/50/30/6 molar ratio). The lipids colloidal suspensions were prepared by dissolving the lipid mixture in a Chloroform:Methanol (3:1 v/v) solvent mixture. The solvents were evaporated with a rotatory evaporator to form a thin layer of lipid film on the inner wall of the round bottom flask. GEM or CIS (3 mg) were dissolved in 0.9% NaCl and the solution was used to rehydrate the lipid film (for co-encapsulation of GemCis 1.5 mg of each drug was used). The temperature of the solution was kept above the transition temperature (T_m) of the lipid mixture (50 °C) to ensure high permeability through the liposome membrane and to enhance the drug entrapment efficiency. After stirring the lipid film in 1 mL of 0.9% NaCl solution at 50 °C for 1 hr, the obtained multilamellar vesicles were submitted to ten cycles of freezing (with dry ice) and thawing (with oil bath at 50 °C). The resulting colloidal suspension of multilamellar vesicles were extruded (Avanti polar lipids, Inc.) through 800 µm and 100 µm pore size polycarbonate membrane filters to transform them to unilamellar vesicles. The untrappted 0.9% NaCl solution was removed by centrifugation at 13300 rpm (Thermo Scientific Heraeus Fresco 17) for 1 hr at 4 °C. Subsequently the loaded liposomes were incubated with the TR polymer at ratio polymer : lipid (1:1) for 1 hr at 30°C. The unattached TR polymers were removed by centrifugation at 13300 rpm for 1 hr at 4 °C.

2.5.6 Synthesis of a fluorescent polymer for cellular uptake assessment

Refer to section 1.5.15.

2.5.7 Amount of polymer bound on the surface of PMTL

Poly (DiEGMA-co-OEGMA$_{300}$)-b-(EHMA-co-FOMA), fluorescent thermo-responsive polymer, was used to modify surface of TTL and prepare PMTL. The amount of polymer attached on the surface was determined by fluorescence spectrophotometry (SpectraMax multi-mode microplate reader, Molecular device). The emission and excitation wavelength were 525 and 490 nm, respectively. Briefly, the loaded liposomes were incubated with poly (DiEGMA-co-OEGMA$_{300}$)-b-(EHMA-co-FOMA), at ratio polymer : lipid (1:1) for 1 hr at 30 °C. The unattached fluorescent thermo-responsive polymer was removed by centrifugation at 13300 rpm for 1 hr at 4 °C. The amount of fluorescent polymer on the surface of liposome was determined from the calibration curve of the fluorescent polymer.

2.5.8 Dynamic light scattering

Refer to section 1.5.7.

2.5.9 Transmission electron microscopy

Refer to section 1.5.9.

2.5.10 HPLC analysis for drug encapsulation and release determination

The HPLC assay for the quantification of both gemcitabine and cisplatin was developed using an Agilent Technologies 1200 Series HPLC system. The data was acquired and analysed using ChemStation for LC software, also by Agilent Technologies, UK. The chromatographic separation was achieved

using a Discovery® HS F5-5 15cmx 4.6 mm, 5 µm (SUPELCO Analytical). Buffer and DMF (95:5) were introduced to the column as mobile phase under gradient conditions (Table 11). The aqueous buffer was prepared by dissolving 3.86 g of ammonium acetate (0.05M) and 1 g of sodium-1-octane-sulphate in 1 liter of HPLC grade water and adjusted to pH 4 with glacial acetic acid. The mobile phase was pumped through the column at a flow rate of 1 mL/min. The UV detector was set at 300 nm and the injection volume was 20 µL. The GEM and CIS standard solutions used for quantification were prepared by suitably diluting a 100 µg/mL working standard of each drug in the buffer solution.

Table 11. HPLC gradient method

Time (min)	Buffer (%)	DMF (%)
0	95	5
15	95	5
20	70	30
30	20	80
31	95	5
35	95	5

2.5.11 Drug encapsulation efficiency

The drug encapsulation efficacy of PMTL was analysed by HPLC analysis in order to measure the amount of drug entrapped within the liposome's core. The encapsulation efficiency (EE) was measured using the formula:

$$EE(\%)=\frac{\text{Amount of entrapped drug}}{\text{Amount of drug added initialy}}x100$$

2.5.12 Determination of in vitro drug release

The drug release profile from the PMTL was evaluated using a Slide-A-Lyzer dialysis cassette (MWCO=7 kDa, Spectrum laboratories). Drug loaded

liposomes dispersed in 1 mL of 0.9% NaCl solution were transferred in the dialysis cassette by using a syringe which was immersed in 0.9% NaCl solution. The drug release experiments were performed under mild stirring below and at the LCST, 37°C and 40°C respectively, in order to compare the drug release profiles at different temperatures. At predetermined time intervals, aliquots (0.1 mL) were withdrawn from the cassette which was replenished with fresh NaCl solution. The collected samples were centrifuged (Thermo Scientific Heraeus Fresco 17) at 13300 rpm for 10 min and analysed by HPLC to measure the released drug.

2.5.13 In vitro cytotoxicity assay

The cytotoxicity of the PMTL was evaluated by the MTT (3-(4,5-Dimethyl-2-thiazolyl)-2,5-diphenyl-2H-tetrazolium bromide) assay. Liposomes displaying LCST behavior at 40°C, were prepared and investigated for cytotoxicity, stability in serum-containing media and cellular uptake using MiaPaCa-2 and BxPC-3 cell lines. Both cells were seeded in a 96-well plate at a density of 1×10^4 cells per well. MiaPaCa-2 cells consumed Dulbecco's modified eagle's medium- high glucose containing supplemented with 10% fetal bovine serum, 1% penicillin-streptomycin and 1% l-glutamine. BxPC-3 cells consumed RPMI-1640 medium supplemented with 10% fetal bovine serum and 1% Penicillin-Streptomycin. Both cells were incubated either at 37°C or 40°C in humidified atmosphere with 5% CO_2 for 24 h before the assay. The cells were incubated with medium of PMTL with different concentration of drug ranging from 0.0001 to 100 µM. After incubation for 72 h, the medium was replaced by 100 µL of fresh medium and 25 µL of MTT stock solution (5 mg/mL in PBS) and incubated for an additional 4 h. Subsequently, the medium was removed and the formazan crystals were dissolved in 200 µL of DMSO. The plates were shaken for 2 min at room temperature before measuring the optical density (OD) at 570 nm on a SpectraMax® M2/M2e Multimode Microplate Reader, with SoftMax® Pro Software.

2.5.14 The combination index calculation

Refer to section 1.5.14.

2.5.15 Thermo-dependent cellular uptake of fluorescent liposome

The effect of temperature on cellular uptake of thermo-responsive liposomes below and above their thermal transition temperatures was studied using fluorescence microscopy. MiaPaCa-2 and BxPC-3 cells were seeded in 6-well plates at a concentration of $1x10^5$ cells/well and incubated at 37 °C and 5% CO_2 to allow the cells to attach and reach confluency. The media in each well was replaced with medium containing 1 mg of fluorescent liposomes which were covered with Poly (DiEGMA-co-$OEGMA_{300}$)-b-(EHMA-co-FOMA) (1:1 ratio) and dissolved in 2 mL of culture medium. After 30 min, the media were removed and the cells were rinsed with Dulbecco's phosphate buffered saline (DPBS) once at room temperature. The washed cells were fixed using 4% paraformaldehyde phosphate buffer solution for 20 min and rinsed twice with DPBS. The cells were observed in 6-well plates using the EVOS® FL Imaging System.

2.5.16 Flow Cytometry analysis

MiaPaCa-2 and BxPC-3 cells were plated in 6 well plate at a seeded density of $1x10^5$. After the cells reached confluency, they were treated with 1 mg of fluorescent liposomes which were covered with Poly (DiEGMA-co-$OEGMA_{300}$)-b-(EHMA-co-FOMA) (1:1 ratio) and dissolved in 2 mL of culture medium. After 30 min, cells were washed with cold PBS (4°C) several times to stop the intake. 1 mL of cold PBS (4°C) was added, the cells were scraped and transferred into Nalgene® centrifuge tubes to be analysed by MACSQuant Analyzer 10 Flow Cytometer.

2.5.17 Clonogenic cell survival assay

$2x10^5$ MiaPaCa-2 or BxPC-3 cells were seeded in a 25 cm^2 T-flask (using 5 mL of culture medium). Once the cells reached confluency, each flask was treated with different concentration of drugs in combination. One flask remained untreated as a control. After 24 hours, the treated and untreated cells were trypsinised, counted and subsequently 250 cells from each flask were seeded in the 6 well plate. After 14 days, the colonies were washed with PBS and then fixed using methanol and acetic acid in ratio 3:1. The colonies were stained with 0.5% crystal violet solution (diluted with methanol) for 5 min. The stained plates were rinsed in the tray full of distilled water and left in the fume hood over night to dry. Colonies appeared as clusters of violet stained cells visualised with the naked eye. The number of air-dried colonies for the average of three colony counts for each plate was recorded. A cluster of 50 or more cells were counted as one colony.

The plating efficiency (PE) was calculated by dividing the number of colonies counted by the number of cells plated and then multiplying by 100:

$$\%\ \text{Plating efficiency} = \frac{\text{No. of colonies counted}}{\text{No. of cells plated}} \text{x}100$$

PE was determined to investigate the percentage of single cells seeded in the plates that form a colony. PE of the control was considered as 100%. By determining PE, Survival fraction of the single cells seeded in the plates also calculated by dividing the PE of the treated cells by the PE of the control and then multiplying by 100:

$$\%\ \text{Survival fraction} = \frac{\text{PE of the treated cells}}{\text{PE of the control}} \text{x}100$$

The survival fraction was calculated to find out the fraction of surviving after exposure to the different concentrations of drugs (Munshi et al. 2005).

All experiments were performed in triplicate.

2.6 Results and discussion

The traditional thermo-sensitive liposome was synthesised and the thermo-responsive polymer Poly (DiEGMA-co-$OEGMA_{300}$)-b-EHMA was attached on the shell. For polymer characterisation refer to section 1.5.1 (structure), section 1.5.2 (^{1}H NMR), section 1.5.3 (GPC), section 1.5.4 (LCST).

2.6.1 Amount of polymer bound on the surface of PMTL

The amount of attached polymer on the liposomal surface was determined by measuring fluorescence intensity after labeling fluorescein *O*-methacrylate on the polymer poly(DiEGMA-co-$OEGMA_{300}$)-b-EHMA. The amount of fluorescent polymer, poly(DiEGMA-co-$OEGMA_{300}$)-b-(EHMA-co-FOMA) on the surface of liposomes was measured to be 0.43 ± 0.07 mg/mg lipid. This result indicated that the TR polymer was adequately attached on the surface of the liposomes.

2.6.2 Dynamic light scattering

DLS was used to determine the size and size distribution of the liposomes (Table 12 and figure 85). In this research, the TR polymer attached on the surface of the blank PMTL, having M_n of 39,500 Da, increased the hydrodynamic diameter of the liposomes to 137.0 ± 2.11 nm which is in almost perfect agreement with similar studies (Ta, T. et al. 2010). Ta and coworkers synthesised similar TTL for the triggered release of doxorubicin. They also used lipid film hydration and extrusion method with the same ratio of lipids. The diameter and polydispersity index (PDI) of blank TTL liposomes were measured by DLS and found to be 131.7 ± 13.3 nm (PDI = 0.063 ± 0.068).

Furthermore, the average particle size was measured for Gem and Cis loaded PMTL and also for co-loaded GemCis PMTL. The average diameter of PMTL was increased after drug encapsulation. However, all the formulations maintained narrow PDI.

Table 12. Size and distribution of blank and loaded PMTL liposomes obtained by DLS.

PMTL loaded liposome	*Diameter (nm)*	*PDI*	*Zeta potential (mV)*
Blank	137.0 ± 2.1	0.104 ± 0.02	-1.97
Gem	149.4 ± 3.1	0.147 ± 0.02	-1.27
Cis	145 ± 4.1	0.192 ± 0.02	-1.31
GemCis	146.8 ± 3.1	0.233 ± 0.03	-1.83

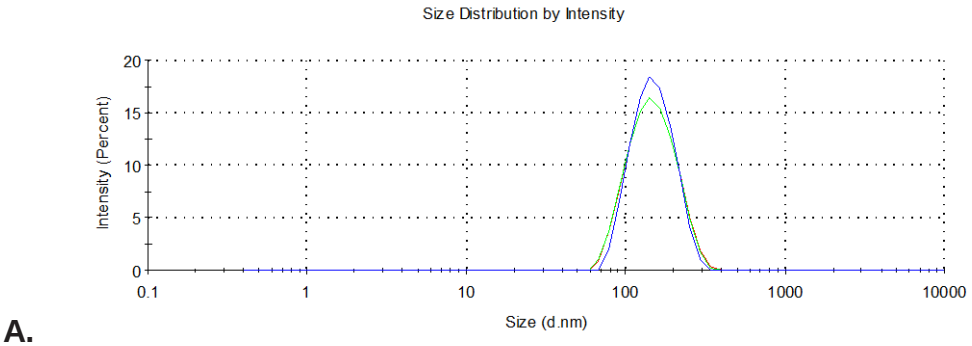

A.

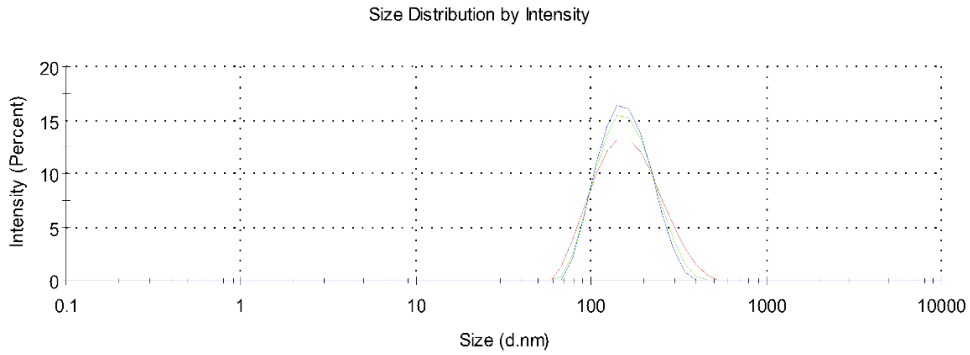

B.

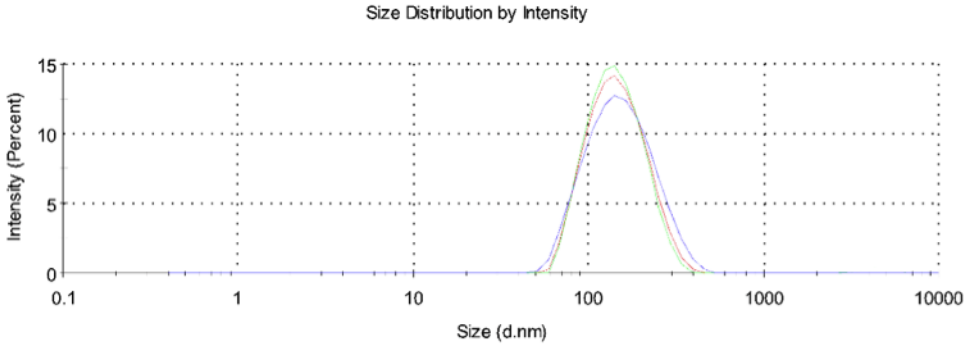

C.

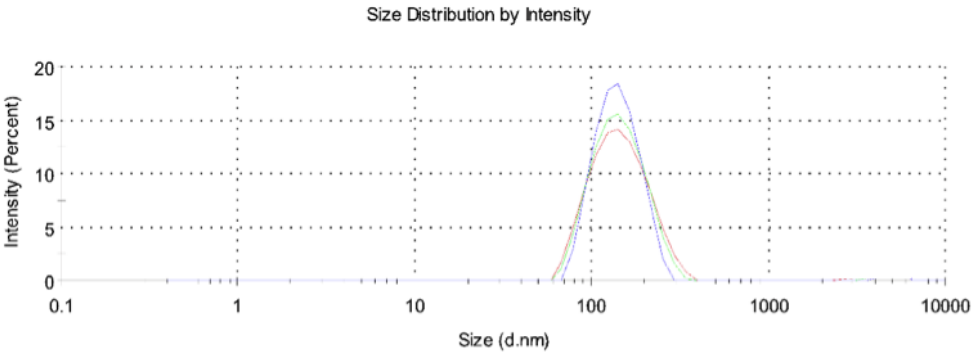

D.

Figure 85. The graphs show the size distribution of **A.** Blank PMTL and **B,** Gemcitabine **C.** Cisplatin **D.** GemCis loaded PMTL liposomes measured by DLS in triplicate

2.6.3 Transmission electron microscopy

TEM was used to determine the morphology, and the size distribution of PMTL as a complementary method to DLS. Figure 86 shows the TEM images of PMTL loaded with the drugs. The loaded PMTLs had a well-defined spherical shape with an average diameter in accord with DLS results. In addition, the images showed almost complete absence of multilamellar liposomes. The synthesised PMTL were unilamellar with a clear lipid bilayer shell.

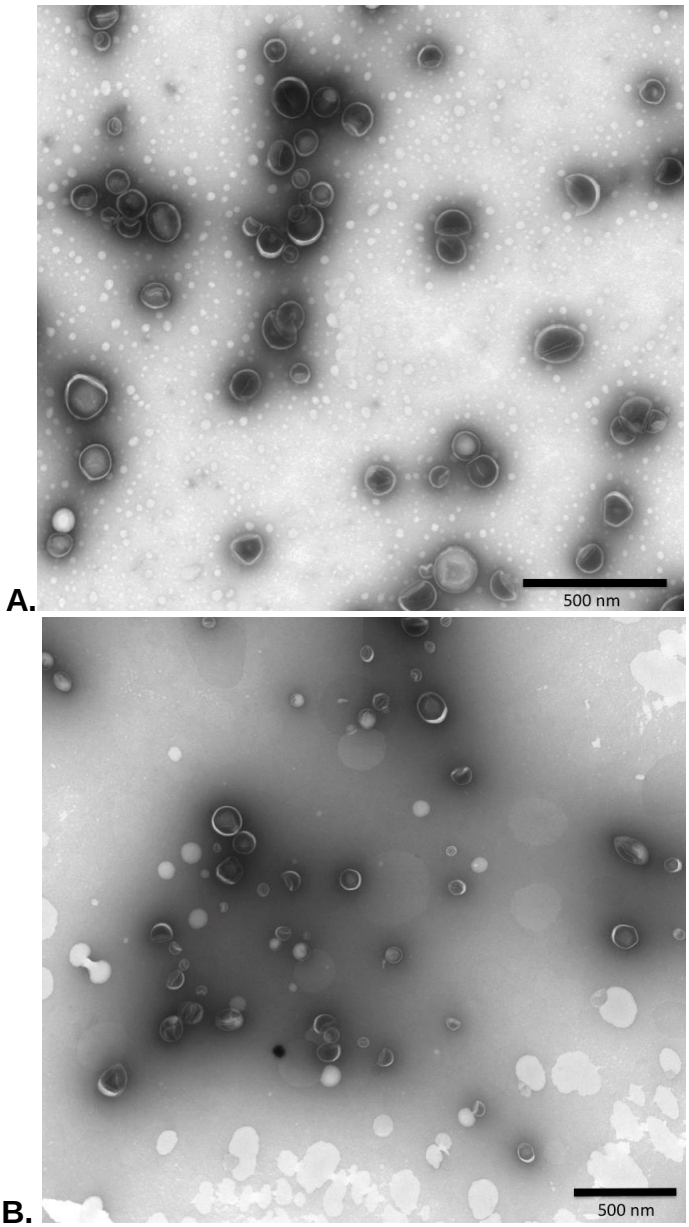

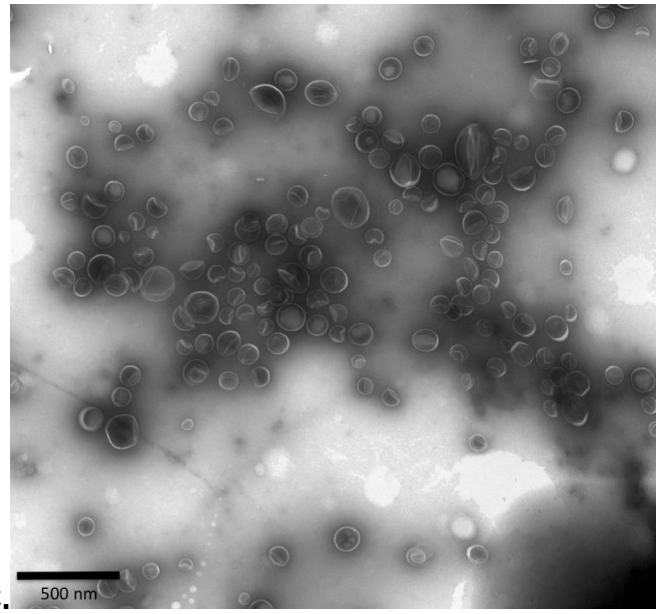

Figure 86. TEM images of PMTL encapsulated **A.** Gemcitabine only **B.** Cisplatin only **C.** GemCis in combination. The scale bars show the size of 500 nm.

Distribution frequency

The size distribution of PMTL liposomes was measured quantitatively from the TEM images using ImageJ software (Figure 87). The size of 150 liposomes was measured to plot the histogram of diameter range distribution for each drug-loaded PMTL. The frequency distribution curve of the liposomes showed Gaussian size distribution. Mode represents the liposome size that appeared most frequently in the data set of 150 and mean shows the average liposome diameter size. The values are in agreement with the size and size distribution obtained by DLS.

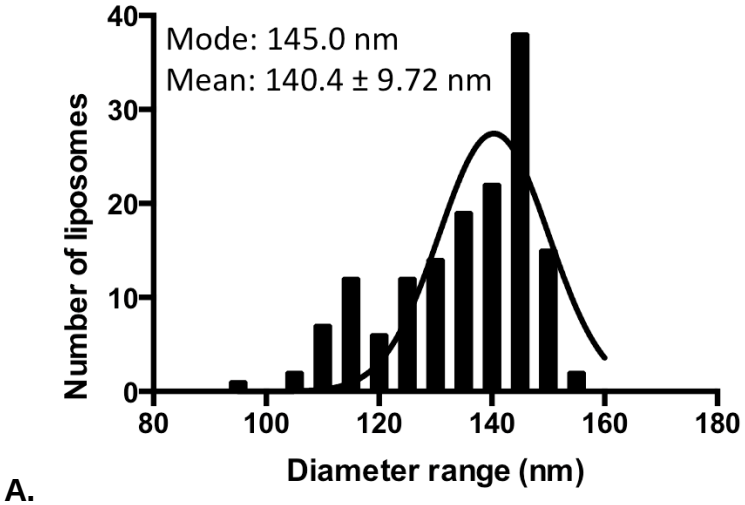

A.

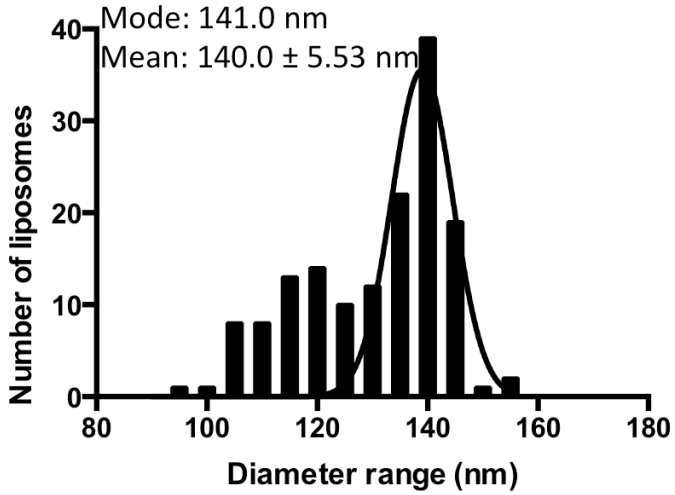

B.

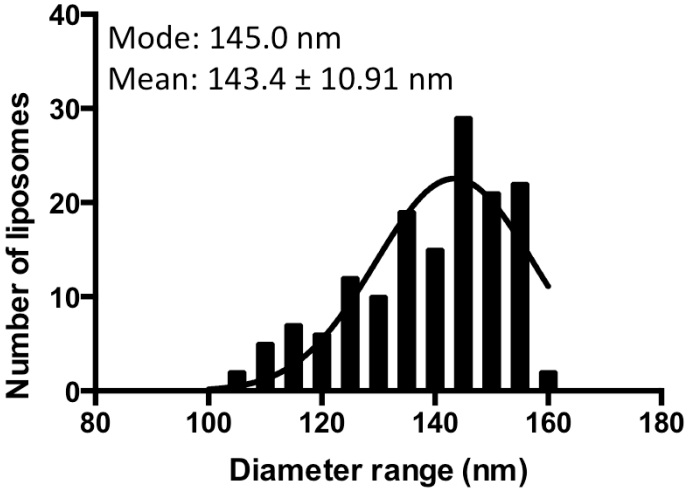

C.

Figure 87. The histograms show the size distribution of liposomes loaded with **A.** Gemcitabine only **B.** Cisplatin only **C.** GemCis in combination.

2.6.4 HPLC analysis for drug encapsulation and release determination

Gem and Cis loaded PMTL were analysed by HPLC in order to measure the amount of drug that was encapsulated within their vesicle. The separations were achieved using buffer and DMF as the mobile phase. The gradient method was used to separate Cis and Gem around 2 min and 10 min respectively (Figure 88). The percentage of DMF flow through the column was increased gradually within 30 min to remove all the lipids from the column and clear it for the next measurement. Initially, the pressure inside the column was 99 bar, after 15 min the pressure increased to 243 bar up to 28 min and back to 99 in 34 min. The area under the curve was measured and the concentration of each drug was determined by using known concentrations of a previously prepared standard calibration curve.

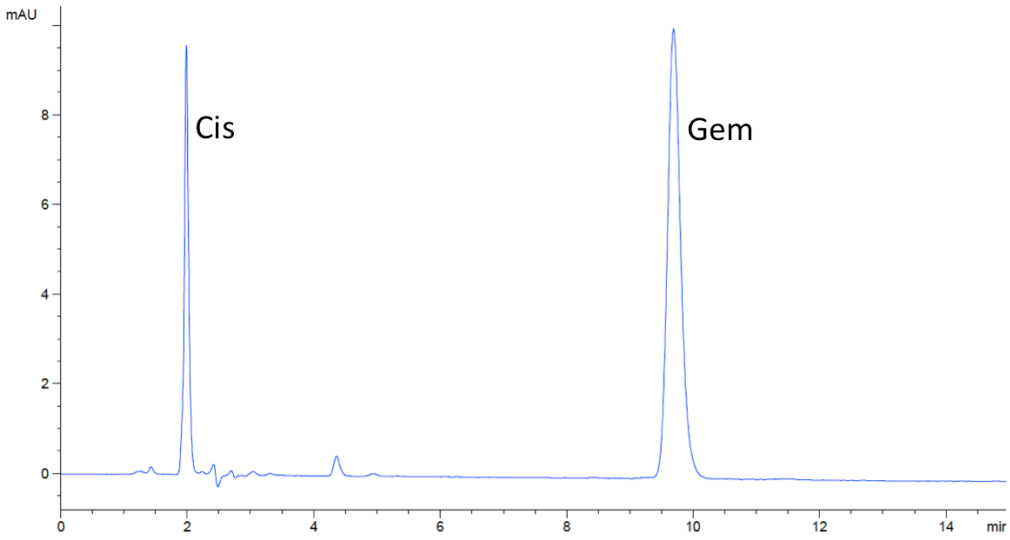

Figure 88. HPLC chromatogram showing the separation of Cis and Gem around 2 min and 10 min respectively.

Table 13 shows the encapsulation efficiency of TTL and PMTL loaded liposomes measured by HPLC.

Table 13. The average encapsulation efficiency of liposomes.

	Average (%)	*SD*
Gem loaded TTL	16.37	± 3.66
Cis loaded TTL	18.52	± 2.09
GemCis loaded TTL		
Gem	10.99	± 1.80
Cis	11.06	± 1.05
Gem loaded PMTL	11.06	± 2.46
Cis loaded PMTL	17.90	± 1.66
GemCis loaded PMTL		
Gem	8.11	± 1.21
Cis	9.08	± 0.94

2.6.5 Determination of in vitro drug release

Initially, the drug release from combinational loaded TTL was measured in order to evaluate the effect of the thermosensitive polymer on the modification of the PMTL surface (Figure 89). The release studies of the formulations were conducted at 37°C and 40°C, which are the temperatures below and at the LCST of the TR polymer attached on PMTL surface. Figure 89 shows a combinational GemCis release pattern from TTL as a function of time. The TTL formulation demonstrated temperature sensitivity at both 37°C and 40°C. In general, the drug release was increased gradually in an almost linear pattern in the first 4 hours. At 37°C, TTL released about 40% Cis and 47% Gem of its content in 2 hours, while, the release reached ca. 58% and 65% within 4 hours for Cis and Gem, respectively. At 40°C, the release increased to about 63% and 74% for Cis and Gem respectively during 4 hours. The drug release was virtually constant after 4 hours at both temperatures.

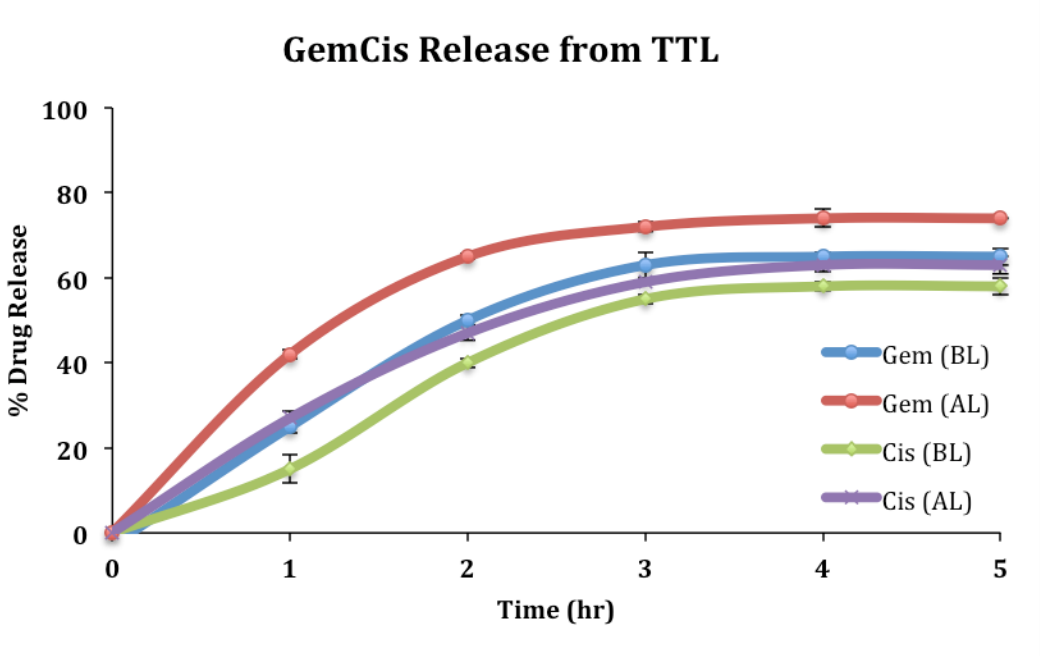

Figure 89. Combinational loaded TTL liposomes revealed controlled release profile below (BL) and at LCST (AL).

Figure 90 shows the release behaviour of combinational loaded PMTL at 37°C and 40°C, which are the temperature below and at LCST of copolymers attached on the liposomes' surface. In comparison with the combinational loaded TTL liposomes the release profile of combinational loaded PMTL liposomes exhibited significantly increased drug release. The incorporation of the copolymer on the surface of the PMTL, improved the thermosensitivity of the liposomes and resulted in an increase in drug leakage. The increase in drug release was due to the transformation of the TR polymers AL from being hydrophilic to hydrophobic which consequently undergo coil to globule transition on the surface of PMTL and in turn destabilise the lipid bilayer to release the drug more effectively.

Below LCST (BL) of the copolymer, the release percentage of Cis and Gem was about 53% and 65% respectively, after 2 hours. Both drugs continued to release up to 71% and 86% after 4 hours, respectively. At LCST (AL) of copolymer, the drug content of PMTL was almost fully released and reached plateau in 4 hours, where PMTL released over 77% and 93% of Cis and Gem respectively. In conclusion, the release from the liposomes was significantly modified by the change of the liposomal surface and was strongly dependent

on the temperature. The PMTL liposomes controlled and increased the rate of release of the co-loaded drugs by a thermal stimulus and an improvement in the drug release profile was observed AL compared to BL for both drugs.

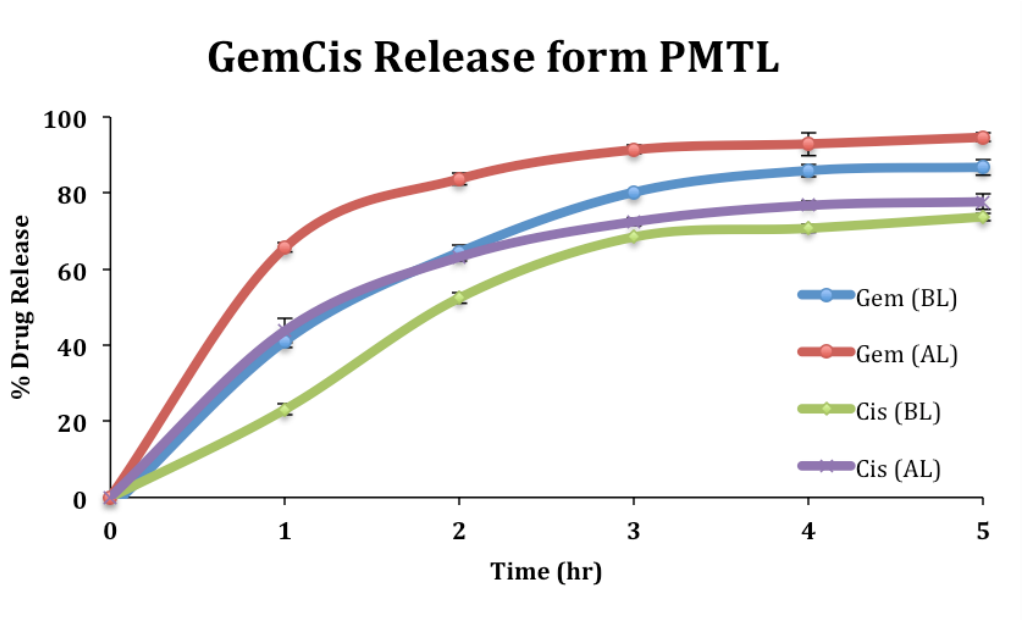

Figure 90. Combinational loaded PMTL liposomes drug release profile below (BL) and at LCST (AL).

2.6.6 In vitro cytotoxicity assay

To further explain the observed results from release studies and evaluate the formulations, the In vitro cytotoxicity assay was performed. The MTT assay was carried out on MiaPaCa-2 and BxPC-3 cell lines in order to measure the cytotoxic effect of the formulations.

Two human pancreatic cancer cell lines were used to confirm the effect of the formulations on pancreatic adenocarcinoma. For general information and characteristics of MiaPaCa-2 cell line refer to section 1.6.11.

BxPC-3 cell line (Figure 91 and 92) has been obtained from a biopsy specimen of adenocarcinoma of the body of the pancreas of a 61 year old female (ATCC Company website https://www.lgcstandards-atcc.org). Figures show the characteristics of BxPC-3 cells in low and high density.

A.

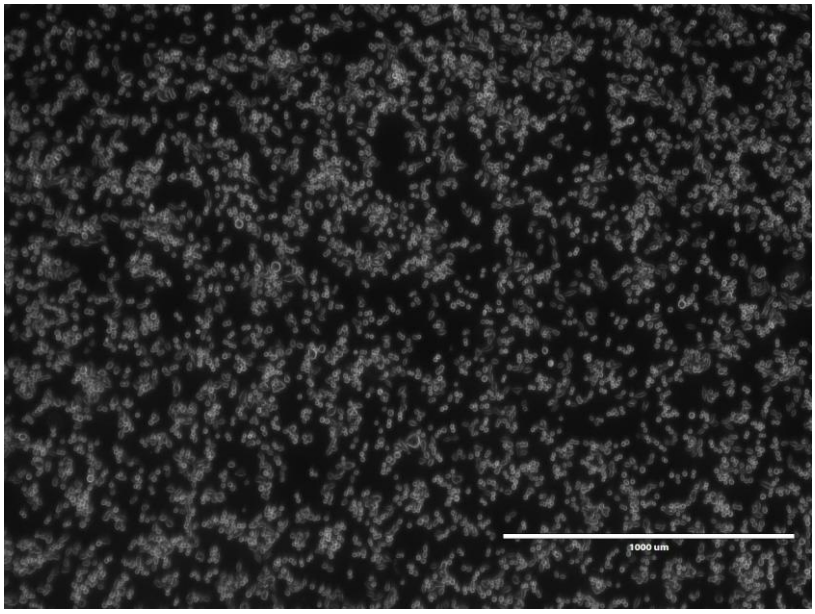

B.

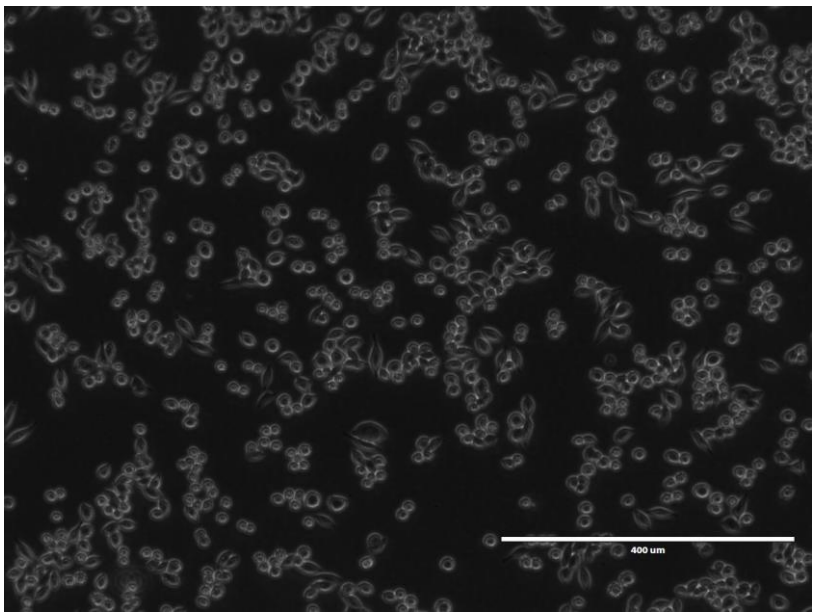

Figure 91. The characteristics of BxPC-3 cells in low density. **A.** The microscope was adjusted on 4x lens. The scale bar is 1000 μm. **B.** The microscope was adjusted on 10x lens. The scale bar is 400 μm**.**

A.

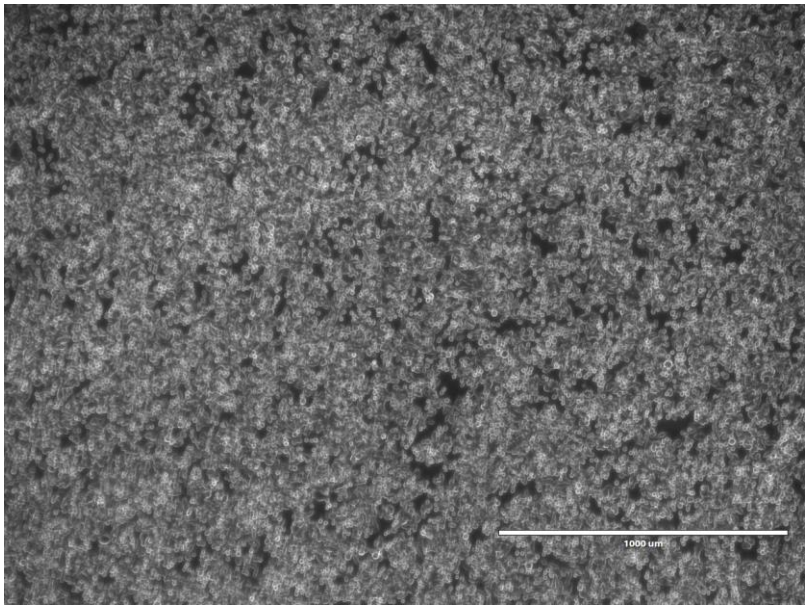

B.

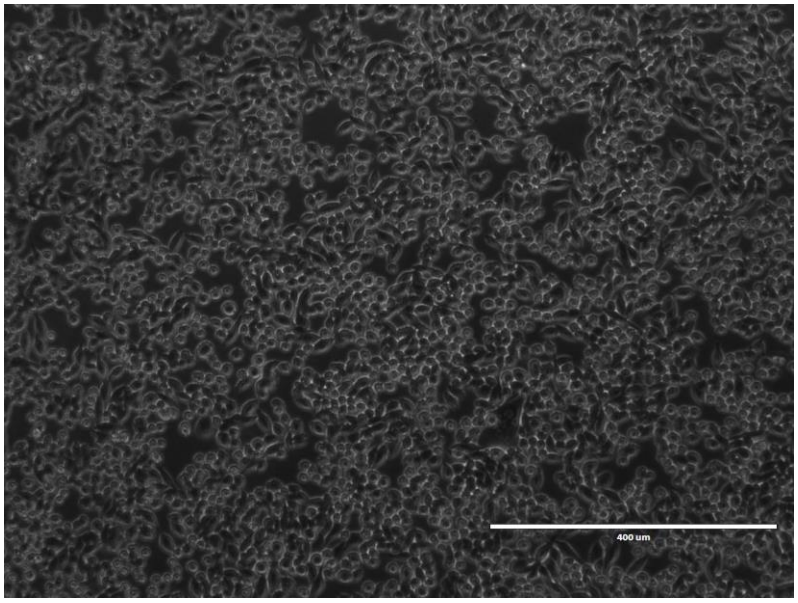

Figure 92. The characteristics of BxPC-3 cells in high density. **A.** The microscope was adjusted on 4x lens. The scale bar is 1000 μm. **B.** The microscope was adjusted on 10x lens. The scale bar is 400 μm.

Initially, the MTT assay was performed by incubating drug-free TTL and PMTL to determine the liposomes' cytotoxicity. The liposomes showed no obvious toxicities on MiaPaCa-2 and BxPC-3 cells with concentrations up to 1mg/mL. The same procedure was repeated by incubating untreated cells to high temperature of 40°C to determine possible cytotoxicity of hyperthermia. No measurable cytotoxicity effect of hyperthermia alone was observed on the viability of both cell lines. Therefore the experimental conditions were not toxic to the cells.

The percentage of MiaPaCa-2 cell viability was measured with wide range of concentrations (0.0001 to 100 µM) of Gem loaded TTL, Cis loaded TTL and combinational GemCis loaded TTL (Figure 93). The cell viability of the formulations were evaluated at 37°C and 40°C, which are the temperature below and at LCST of the TR polymer attached on the PMTL surface. The cells viability was almost 100% at 0.001, 0.001 and 0.01 µM for all formulations BL and AL. Decrease in cell viability started at 1 µM of drug concentration. However, only GemCis loaded TTL (AL) brought the cell viability down to 50% of the cell population. As the concentration of drugs increased to 100 µM the cell viability reduced in the Gem loaded TTL and Cis loaded TTL, while it reached 0% by combinational GemCis loaded TTL in both BL and AL.

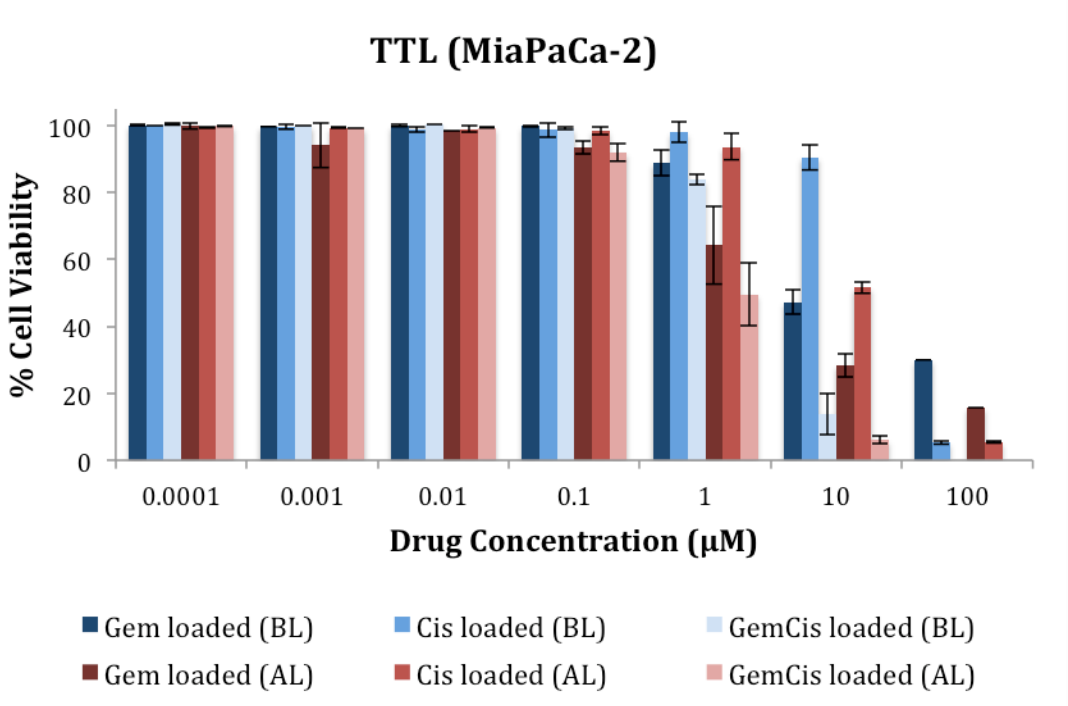

Figure 93. MiaPaCa-2 cells viability of loaded TTL (drug concentrations from 0.0001 to 100 µM) after 72hr.

In comparison to TTL, in PMTL the effect of drugs was observed even at the lowest concentration tested (Figure 94). The MiaPaCa-2 cell viability decreased gradually as the concentration of drugs increased at both BL and AL. Considerable cell growth inhibition was observed at 1 µM where it reached less than 40% in GemCis loaded (AL) and less than 80% in other

formulations. As the drug concentrations increased to 10 µM, the cell viability of the formulations with hyperthermia above AL were significantly reduced compared to the formulations without hyperthermia. At the maximum concentration tested (100 µM), the survival rate declined sharply to 0% by GemCis loaded PMTL. The combination of the PMTL with hyperthermia shows higher cytotoxicity effect on the cells compared to the separately loaded formulations. This might be due to the fact that without hyperthermia when the temperature is below LCST of polymers, the encapsulation impeded the release of the drugs while application of heat AL, the drug diffuses at higher rates to kill the cells, as shown in the drug release studies.

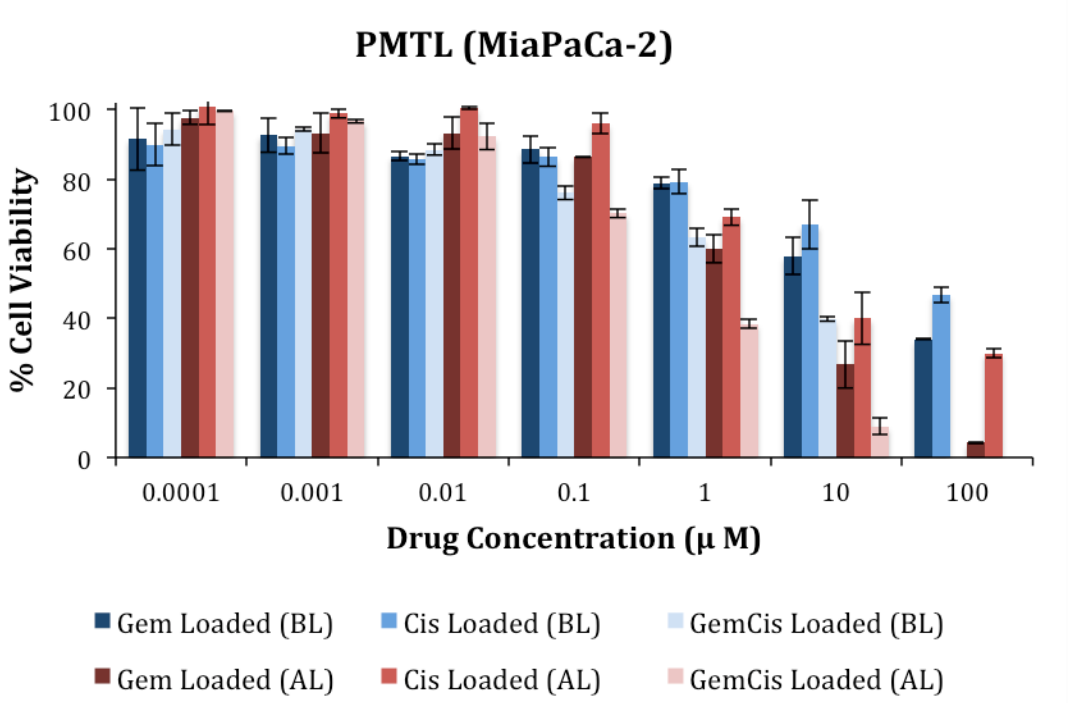

Figure 94. MiaPaCa-2 cells' viability of loaded PMTL (drug concentrations from 0.0001 to 100 µM) after 72hr.

The same formulations where applied on the BxPC-3 cell line which was found to be even more sensitive to the formulations (Figure 95). As expected, the TTL reduced the cell viability steadily in dose dependent manner. Cis loaded formulations in concentration range from 1 µM to 100 µM, could not inhibit the cell growth on their own compared to Gem loaded formulations, for both BL and AL. However, when Cis was encapsulated with Gem and applied in combination, the cell survival rate reduced sharply to 0% by exerting a

synergistic effect. In general, the cytotoxicity was considerably enhanced in the formulations applied with hyperthermia compared to formulations without.

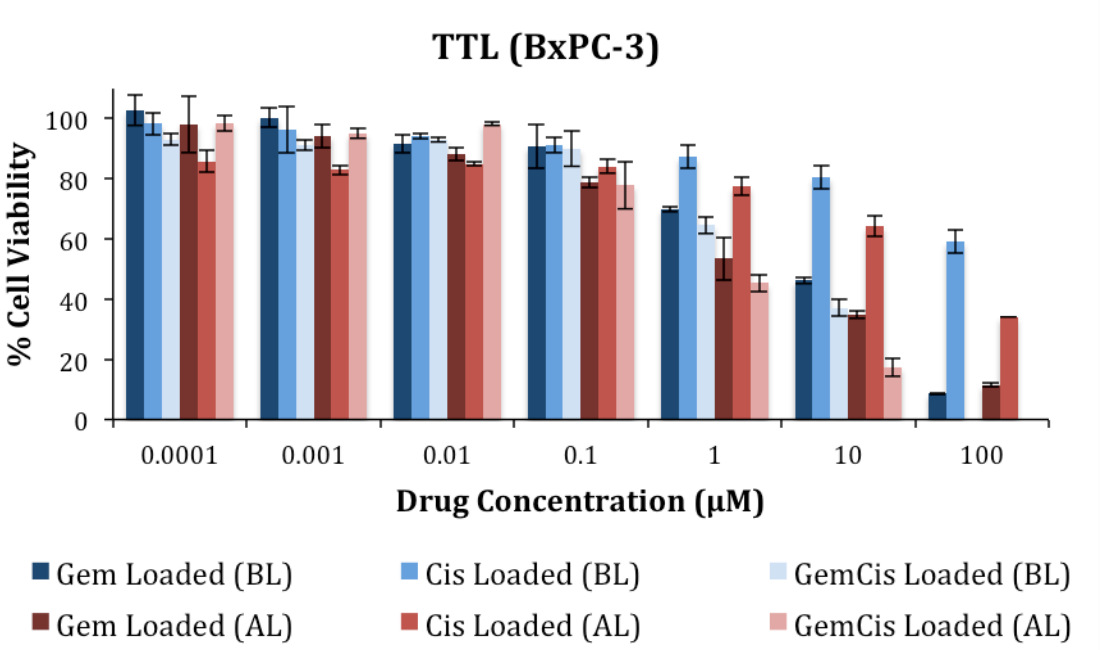

Figure 95. BxPC-3 cells viability was measured with wide range of concentrations (0.0001 to 100 µM) of loaded TTL after 72 hr.

PMTL showed higher cytotoxic on BxPC-3 cells compared to TTL (Figure 96). The toxicity started from a concentration as low as 0.1 µM where the cell growth inhibition reached less than 70% in all formulations except the Cis loaded PMTL. As the drug concentration increased to 1 µM, the BxPC-3 cell survival rate droped to less than 40% in all formulations except the Cis loaded PMTL. The combinational GemCis loaded PMTL, AL, reduced the cell viability down to 20% at 1 µM drugs concentration only. At 10 µM, the PMTL (AL) could further reduce the cell population to 25%, 20% and 7% for Gem, Cis and GemCis loaded PMTL, respectively. The formulation could considerably reduce the cell viability when only Cis only applied. As the concentration increased to 100 µM, the survival rate diminished to 3% in both Gem and Cis loaded PMTL whereas 0% cell survival was observed in the GemCis loaded PMTL at both BL and AL. PMTL enhanced the cytotoxicity of the encapsulated drugs significantly once the temperature was increased above the polymers' LCST, at 40°C. In general, PMTL treated cell lines showed greater cell growth inhibition than TTL treated cells. These results suggested

that PMTL could achieve admirable cytotoxic effects compared to TTL due to the presence of TR polymer modified surface, which in turn could improve the release of encapsulated drugs and enhance the cell death.

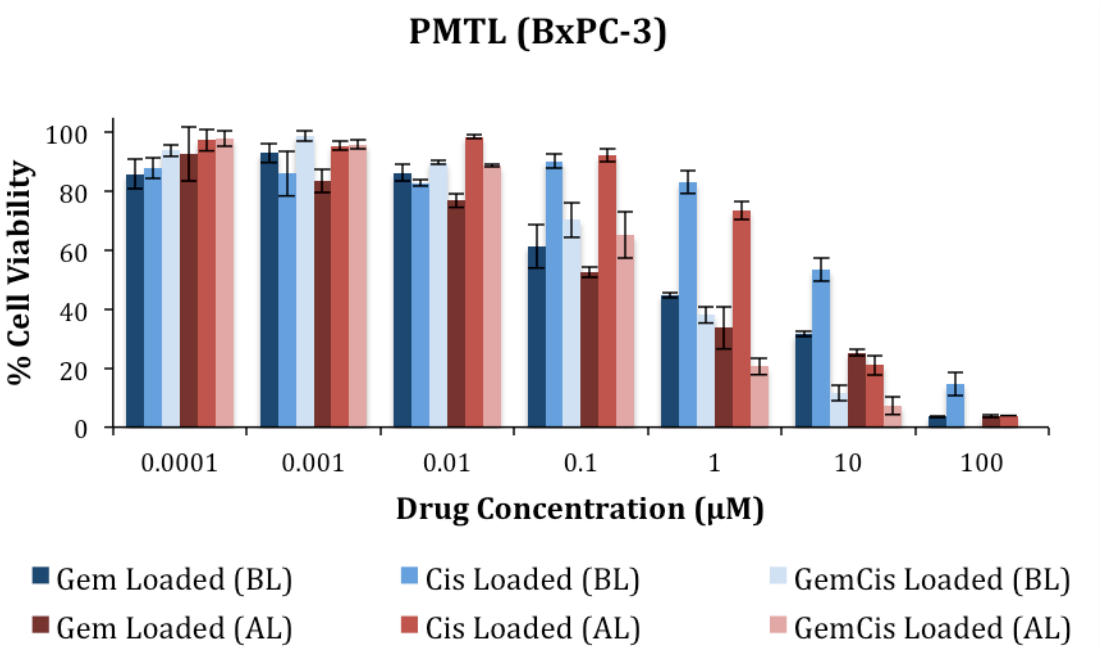

Figure 96. BxPC-3 cells viability was measured with wide range of concentrations (0.0001 to 100 µM) of loaded PMTL after 72hr.

In addition to cell viability, the IC_{50} was calculated by the MTT assay to investigate the concentration at which the formulations could inhibit 50% of the cell growth. The effectiveness of formulations was determined by correlating the formulation efficacy to its IC_{50}. Table 14 show the cytotoxicity of Gem loaded, Cis loaded and GemCis loaded TTL and PMTL on MiaPaCa-2 cells. The graphs plotted cell viability (%) versus logarithmic concentration (µM) of encapsulated drugs, BL and AL. Initially, free Gem was found to have an IC_{50} of 3.0 ± 0.78 µM (Table 16). After encapsulation of Gem in TTL and PMTL the IC_{50} increased to 7.3 ± 1.5 µM and 5.4 ± 0.47 µM, respectively. However, by application of hyperthermia at 40°C the IC_{50} was further reduced to 1.7 ± 0.39 µM in TTL which is significantly lower than the parent drug. PMTL liposomes reduced the IC_{50} further down to 1.6 ± 0.3 µM, which signifies the marked variances in the cytotoxicity profile of the same molecule under different formulations. The sigmoidal curves in table 14 also showed

reduction in cell viability once Gem was loaded in the liposomes AL compared to the free drug. Cis is not a first line drug for the treatment of pancreatic cancer therefore it showed a high IC_{50} of 13.0 ± 3.79 µM when used as free drug (Table 16). IC_{50} was not achieved in the Cis loaded TTL because the cell viability was only obtained at very high concentrations (Table 14). The IC_{50} of the Cis loaded PMTL was also not achieved because the formulation did not inhibit the cell growth up to 50% of the cell population. However, when Cis was loaded and heated at 40°C, the IC_{50} was reduced to 11.0 ± 3.47 µM in TTL and drastically reduced to 2.0 ± 0.36 µM in PMTL (Table 16). Also, the PMTL reduced the cytotoxicity of Cis by almost 6 fold. Finally, the simultaneous addition of the two parent drugs (GemCis) resulted in a reduction of the IC_{50} to 1.5 ± 0.07 µM. Encapsulation of GemCis followed by incubation at 37°C increased the IC_{50} to 3.0 ± 0.80 µM and 7.5 ± 1.61 µM in TTL and PMTL, respectively. Whereas, The IC_{50} was significantly enhanced at 40°C and the concentration required to inhibit 50% of cell growth reached down to 1.0 ± 0.27 µM and 0.5 ± 0.08 µM in TTL and PMTL, respectively. The GemCis co-loaded liposomes (Table 14) had their curves slightly shifted to the left which showed significant decrease in terms of drug concentrations required to halt cell viability, revealing the fact that the co-delivery of these two chemotherapeutic drugs increased the cell death, possibly, in a synergistic way. To sum up, in all formulations once the drug was encapsulated in the liposomes and incubated BL (at 37°C), the formulation reduced the toxicity compared to free drugs resulting from the ability of the liposomes to encapsulate and retain the drug inside the core so that it is not up taken by cells BL. On the other hand, encapsulation of the drugs in the liposomes followed by incubation AL (at 40°C), improved the chemotherapeutic effect and supressed the cancer cells growth.

Table 14. Cytotoxicity profiles of native and encapsulated drugs in TTL and PMTL, on MiaPaCa-2 cells measured by MTT cytotoxicity assay after 72hr.

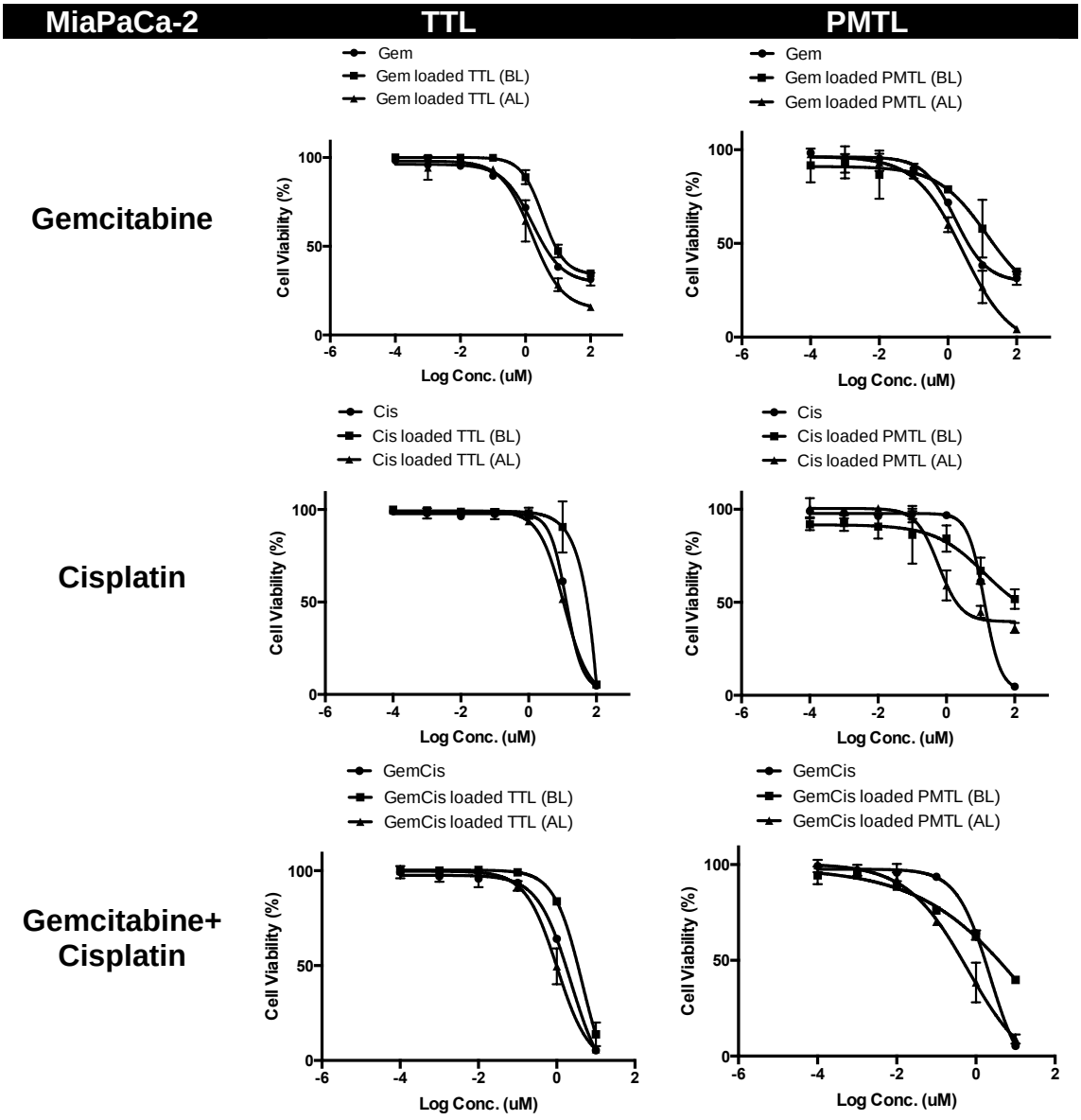

Table 15 shows the cytotoxicity of Gem, Cis and GemCis loaded TTL and PMTL on BxPC-3 cells. The same trend was observed as in the case of MiaPaCa-2 cells. When the drug was encapsulated and incubated BL, the toxicity was reduced compared to free drugs due to retention of the drug inside the liposomes' vesicle. However, an increase in toxicity and cell viability reduction occurred due to the encapsulation of the drugs in the liposomes and incubation AL showed the effectiveness of the nano-carrier in, possibly, increasing the cellular uptake of the drugs in combination with heat. By

application of free Gem on BxPC-3 cells, no sigmoidal curve was obtained and the IC_{50} could not be calculated (Table 15). The IC_{50} of Gem loaded TTL and PMTL at 37°C was found to be 6.4 ± 0.82 µM and 1.9 ± 0.46 µM, respectively (Table 16). The Gem loaded TTL and PMTL at 40°C decreased the IC_{50} significantly to 3.8 ± 0.20 µM and 0.4 ± 0.05 µM, respectively. Free Cis had an IC_{50} = 8.1 ± 1.30 µM whereas Cis loaded TTL could not inhibit 50% of cell growth. However, Cis loaded PMTL increased the IC_{50} up to 12.4 ± 3.27 µM. Cis loaded TTL at 40°C, showed an IC_{50} of 14.6 ± 3.32 µM, which was an improvement compared to Cis loaded TTL at 37°C but higher than the parent drug. Nevertheless, Cis loaded PMTL at 40°C reduced the IC_{50} (2.8 ± 0.29 µM) significantly by almost 3 fold compared to the free drug. As expected, the combinational co-delivery of two chemotherapeutic drugs, GemCis loaded TTL and PMTL, showed a slight shift of curves to the left (Table 15). As a result less concentration of drugs required to supress the cell viability when compared to free drugs separately. By application of free GemCis, again no sigmoidal curve was obtained and an IC_{50} was not calculated. However, encapsulation of the drugs in TTL and PMTL improved the fidelity of the data to better fit a sigmoidal curve. The combinational application of GemCis reduced the IC_{50} compared to each drug separately (Table 15). The IC_{50} of GemCis co-loaded liposomes at 37°C was 2.1 ± 0.56 µM and 0.5 ± 0.23 µM for TTL and PMTL, respectively. At 40°C, the IC_{50} was further reduced to 0.6 ± 0.12 µM and 0.2 ± 0.09 µM for TTL and PMTL, respectively (Table 16). The IC_{50} achieved from the PMTL was less than that of TTL, showing the augmentation of the drugs cytotoxicity by the PMTL.

To conclude, the cytotoxicity of the drugs was enhanced once the liposomes where subjected to hyperthermia at 40°C. In addition, TR polymers on the surface of PMTL improved the cytotoxic effect of the chemotherapeutic drugs considerably.

Table 15. The cytotoxicity curves of native and encapsulated drugs in TTL and PMTL, on BxPC-3 cells measured by MTT cytotoxicity assay after 72hr.

BxPC-3	TTL	PMTL
Gemcitabine	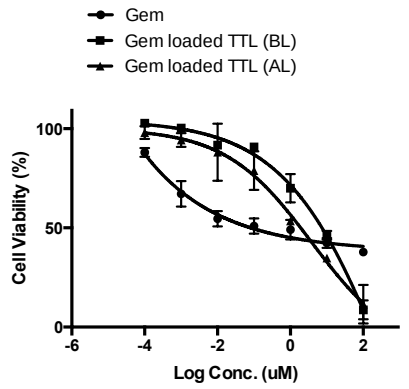	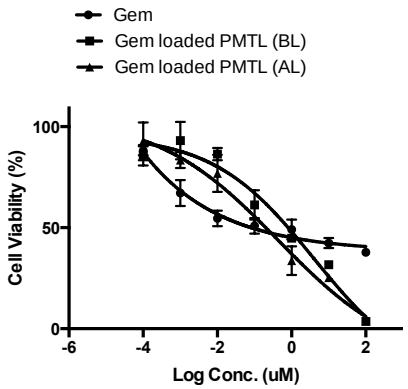
Cisplatin	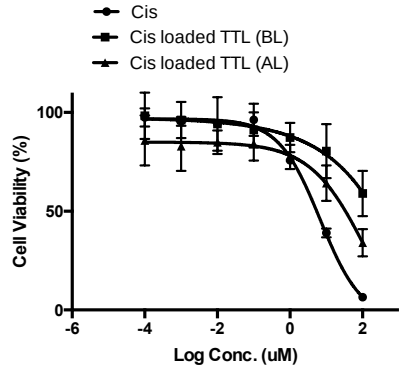	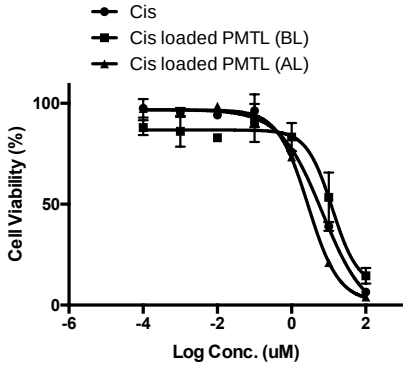
Gemcitabine+ Cisplatin	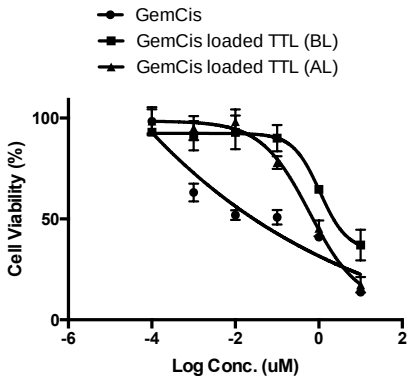	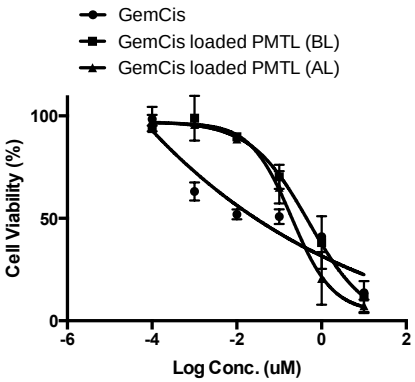

As regard to table 16, the IC_{50} of the native drugs was considerably increased when encapsulated in liposomes and incubated at 37°C; demonstrating reduced cytotoxicity of the liposomes below transition temperature (T_m) in TTL and below the LCST in PMTL. However, the IC_{50} further reduced or reached the IC_{50} of native drugs when the TTL and PMTL heated at 40°C. The TTL liposomes still showed improvement in toxicity and reduction of the IC_{50} at 40°C, in spite of having T_m of 43°C (Ta, T. et al. 2010).

Table 16. The IC_{50} values of native and encapsulated drugs in TTL and PMTL, on two different pancreatic cancer cell lines MiaPaCa-2 and BxPC-3 incubated for 72hr.

Anti-cancer Drug	Type of liposome	Temp. (°C)	IC_{50} (μM) MiaPaCa-2	IC_{50} (μM) BxPC-3
Gemcitabine	Not encapsulated	-	3.0 ± 0.78	Very wide
	TTL	37	7.3 ± 1.5	6.4 ± 0.82
		40	1.7 ± 0.39	3.8 ± 0.20
	PMTL	37	5.4 ± 0.47	1.9 ± 0.46
		40	1.6 ± 0.3	0.4 ± 0.05
Cisplatin	Not encapsulated	-	13.0 ± 3.79	8.1 ± 1.30
	TTL	37	Very wide	*
		40	11.0 ± 3.47	14.6 ± 3.32
	PMTL	37	*	12.4 ± 3.27
		40	2.0 ± 0.36	2.8 ± 0. 29
GemCis	Not encapsulated	-	1.5 ± 0.07	Very wide
	TTL	37	3.0 ± 0.80	2.1 ± 0.56
		40	1.0 ± 0.27	0.6 ± 0.12
	PMTL	37	7.5 ± 1.61	0.5 ± 0.23
		40	0.5 ± 0.08	0.2 ± 0.09

*: Did not kill 50% cell population.

2.6.7 The combination index analysis

The IC_{50} obtained from the MTT assay (Table 16) showed an improvement in drug cytotoxicity when they were loaded in liposomes and hyperthermia at 40°C was applied. In addition, the combinational application of GemCis

further improved cytotoxicity. To investigate whether the cytotoxic improvement was an additive or synergistic effect, the combination index (CI) was calculated. Table 17 shows the CI calculated from the IC_{50} of liposomes on MiaPaCa-2 cells. It was found that the CI of the non-loaded GemCis was 0.62 which verifies the synergism of the two drug molecules (CI<1 is indicative of synergistic activity). The CI value was not obtained for the TTL and PMTL at 37°C (below the LCST) as no IC_{50} was obtained for the encapsulated drugs at 37°C due to the drug retention inside the liposome vesicle. The CI of the TTL at 40°C was found to be 0.68, representing synergistic effect too. The CI value achieved by the PMTL at LCST at 40°C, was considerably lower compared to the CI value of free drugs and the loaded TTL sample. The CI of 0.56 indicated a further enhancement of the synergistic activity of GemCis in the formulated form. As a result, the in vitro studies showed that combinational therapy of the two drugs, Gem and Cis, has synergistic effect on pancreatic cancer cells. Moreover, this synergism was further significantly enhanced by encapsulating the drugs in PMTL at 40°C.

Table 17. CI values of GemCis loaded liposomes on MiaPaCa-2 cells incubated for 72hr.

	Temp. (°C)	**CI**
Free drugs	**-**	0.62
TTL	37	-
	40	0.68
PMTL	37	-
	40	0.56

- CI was not achieved due to the absence of IC_{50}.

In vitro CI analysis on BxPC-3 cells was also conducted (Table 18). Application of the free drugs did not exert any effect due to the wide range of toxicity and the CI could not be calculated. The CI of the loaded TTL at 37°C also was not possible to calculate due to the absence of IC_{50} value in one of the formulations. On the other hand, encapsulation of drugs in TTL at 40°C had very low CI = 0.20 representing very strong synergism. In drug loaded PMTL synergism was observed with CI values less than 1.0. The CI was 0.30 and 0.57 for PMTL at 37°C and at 40°C, respectively. The CI values obtained from PMTL at 40 °C were similar on both MiaPaCa-2 and BxPC-3 cells. To conclude, the free drugs did not exert any effect when applied directly to

BxPC-3 cells; but once encapsulated in liposomes, their delivery improved and significant synergism was observed.

Table 18. CI values of GemCis loaded liposomes on BxPC-3 cells incubated for 72hr.

	Temp. (°C)	CI
Free drugs	-	-
TTL	37	-
	40	0.20
PMTL	37	0.30
	40	0.57

- CI was not achieved due to the absence of IC_{50}.

By far, a careful interpretation of the data showed that the PMTL formulations exert more pronounced cytotoxic effect than their TTL counterparts which, however, could not be justified based only on the drug release patterns. Therefore, the hypothesis was that the polymer itself might be actively interacting with the cell membrane in a temperature dependent manner which could further augment the drug uptake rates at the LCST. For this reason, fluorescence study was conducted to observe the early mechanism of the liposomal uptake.

2.6.8 Thermo-dependent cellular uptake of fluorescent liposome

Previous studies showed that the liposome–cell interaction is affected by the surface properties of liposomes. For example, the attachment of hydrophilic poly(ethylene glycol) (PEG) polymer to a liposome surface reduces the cellular uptake of the liposome due to the low affinity of the cell membrane with the steric barrier of PEG. (Miller, C.R. et al. 1998; Vertut-Doi, A. et al. 1996; Zeisig, R. et al.1996). On the other hand, as the surface properties of the thermosensitive polymer modified liposomes changes with temperature, their interaction with the cells can be controlled by temperature. Kono et al. prepared egg yolk phosphatidylcholine (EYPC) liposomes modified with the thermosensitive copolymer of N-acryloylpyrrolidine (APr) and poly(N-isopropylacrylamide) (NIPAM) having two dodecyl groups at the terminal

(poly(Apr-co-NIPAM)-2C_{12}) (Figure 97).

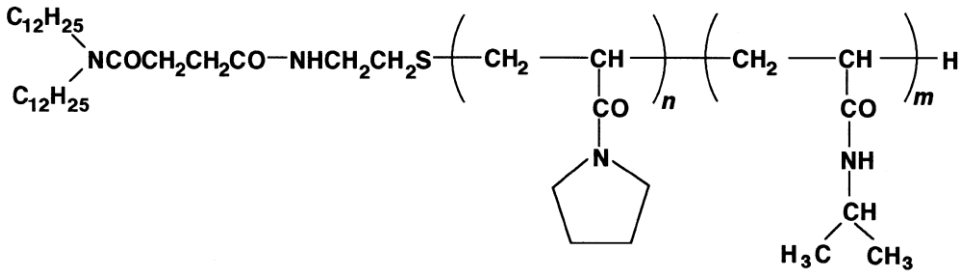

Figure 97. the structure of poly(APr-co-NIPAM)-2C_{12} (Kono, K. et al. 1999).

They investigated the effect of temperature on the interaction between EYPC liposomes modified with the copolymer of poly(APr-co-NIPAM)-2C_{12} having LCST of ca. 40°C with CV1 cells, an African green monkey kidney cell line. The result showed that when unmodified, the EYPC liposomes were uptaken by the at almost the same extent at 37°C and 42°C. In contrast, when polymer modified EYPC liposomes was applied, the cellular uptake was slightly reduced at 37°C, but improved by twofold at 42°C compared to the unmodified EYPC liposomes. As a result, the affinity of the modified liposomes to the cell was increased by temperature. The copolymer changed the hydrophobicity of the liposome surface and inhibited the CV1 cell proliferation strongly (Kono, K. et al. 1999).

Recently, Wang et al. synthesised temperature-responsive polymer poly(N -isopropylacrylamide)-co-N,N′-dimethylaminopropylacrylamide (P(NIPAAm-co-DMAPAAm)) to investigate the intracellular delivery of liposomes. (Wang, J. et al. 2017). They examined the cellular uptake of rhodamine-labeled PEGylated liposomes and rhodamine-labeled temperature-responsive liposomes on RAW264.7 and HeLa cell lines using fluorescence microscopy and flow cytometry. The results revealed that the tunable surface of the temperature-responsive polymer modified liposomes increased the fluorescence intensity at 40 °C compared to 30 °C (Figure 98). The faster cellular uptake of the modified liposomes compared to the non-modified liposomes at the LCST was due to the heat-induced transformation of the thermo-responsive polymer from hydrophilic to hydrophobic which in turn

reduced the fixed aqueous layer thickness and enhanced the interaction of the liposomes with the cell membrane.

The cellular uptake mechanism of the liposomes was also investigated. It was shown that the internalisation of the liposomes into cells occurred by endocytosis in an energy-dependent manner since approximately 65% of the cellular uptake was significantly blocked at 4 °C. They also suggested that the uptake of the modified liposomes into HeLa cells was mediated by microtubule-dependent transport and clathrin-mediated endocytosis rather than caveolin-mediated endocytosis (Wang, J. et al. 2017). However, the nature and the size of the nano-carrier along with the cell type were suggested to be involved to the route of the cellular entry (Rejman, J. et al. 2004; Yatvin, M. B. et al. 1978).

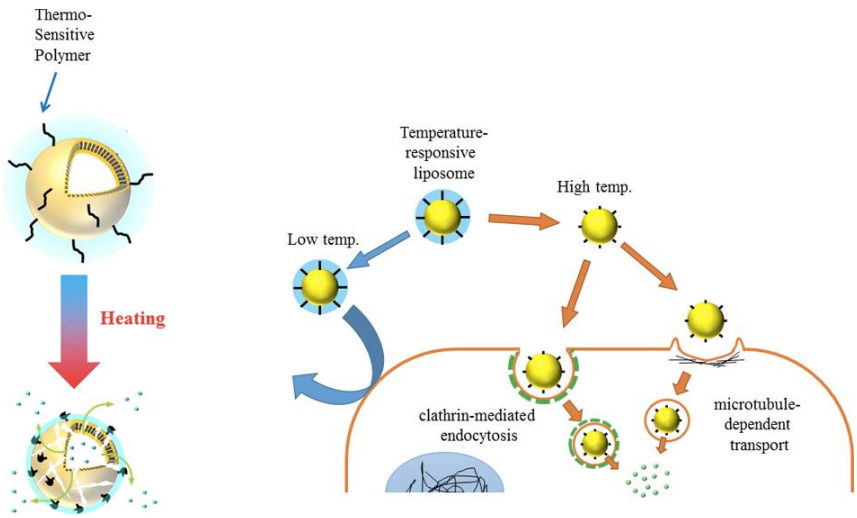

Figure 98. Liposome–cell interaction is affected by hydrophilicity and hydrophobicity properties of liposomes surface (Wang, J. et al. 2017).

In this research, a fluorescent thermo-responsive polymer was synthesised in order to determine the cellular uptake of PMTL below and at LCST. As demonstrated earlier in section 2.6.1, the fluorescent polymers were attached on the surface of PMTL (PMTL-fl) successfully. Both MiaPaCa-2 and BxPC-3 cancer cells were incubated with the PMTL-fl at 37°C and 40°C. Once PMTL-fl internalised into the cells, the fluorescent cells were visualised by fluorescence microscopy. The results showed that the PMTL-fl was only

adsorbed on the cell membrane and did not permeate inside cells when incubated below LCST (at 37°C)(Figure 99-A and Figure 100-A). On the other hand, the cells which were incubated with the PMTL-fl at the LCST (at 40°C) showed stronger fluorescent signal inside their cytosol (Figure 99-B and Figure 100-B). The images illustrated that the cell internalisation of PMTL-fl was temperature dependent. By increasing the temperature, the PEGMA block of fluorescent polymers turned hydrophobic and improved its cell binding and eventually the intracellular uptake.

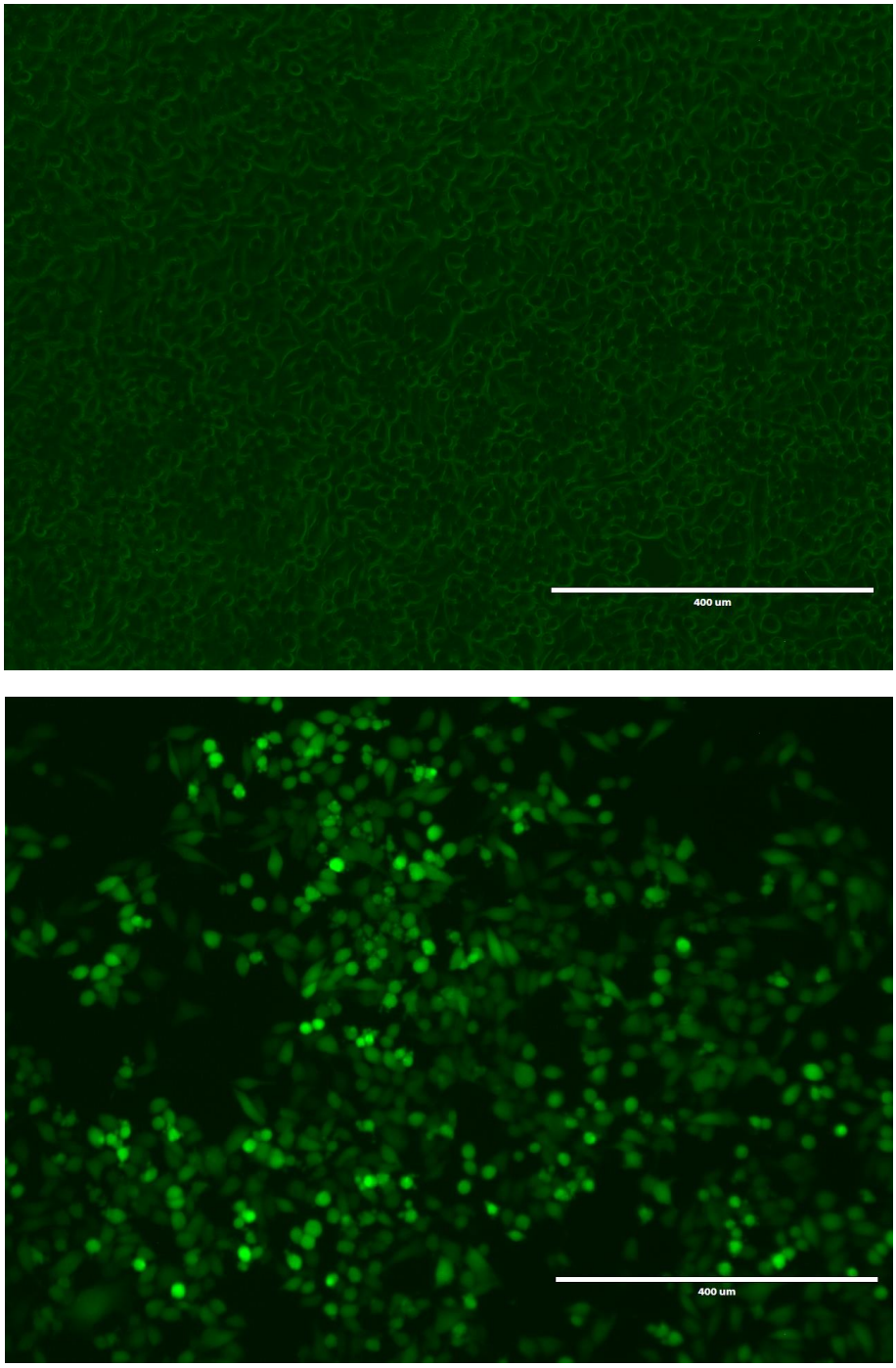

Figure 99. Cellular uptake of PMTL-fl by MiaPaCa-2 cells(A) below and (B) at the LCST, the scale bar shows the size of 400 μm.

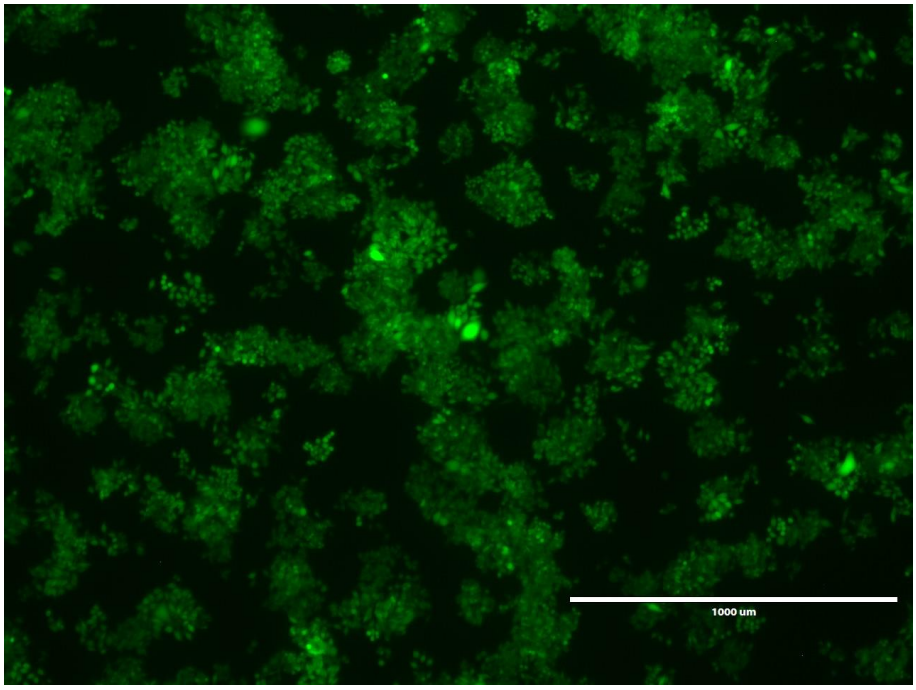

A

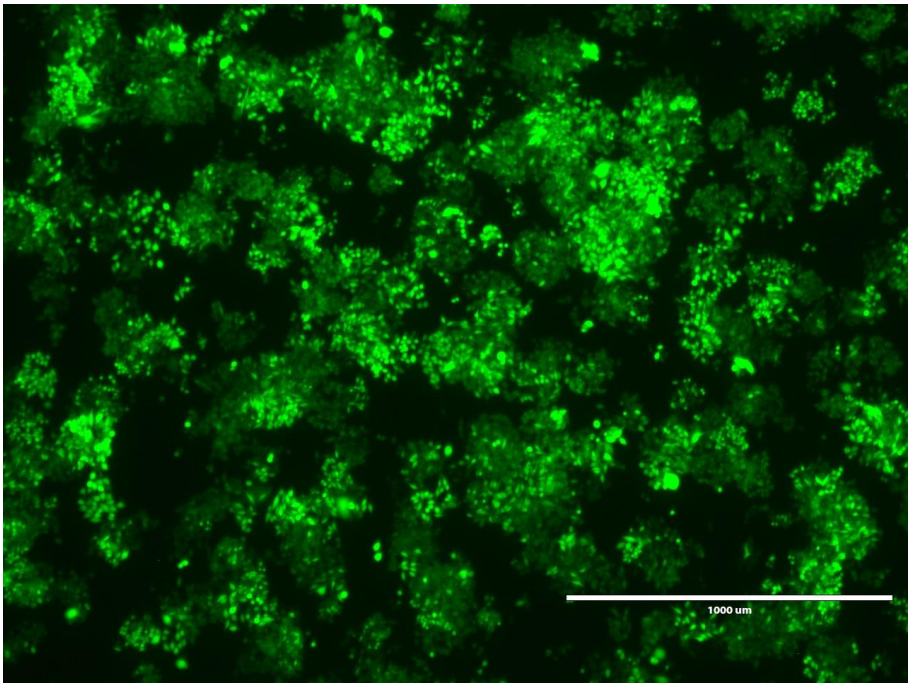

B

Figure 100. Cellular uptake of PMTL-fl by BxPC-3 cells (A) below and (B) at the LCST, the scale bar shows the size of 1000 µm.

2.6.9 Flow Cytometry

Flow cytometry was used to further confirm the cellular uptake of the PMTL-fl on both MiaPaCa-2 and BxPC-3 cancer cells at 37°C and 40°C. The PMTL-fl block copolymer attached on the shell was incubated with cells for 30 min prior to analysis.

Figure 101-A shows the graph of a standard curve obtained from MiaPaCa-2 cells incubated without PMTL-fl. As expected, the instrument detected cells without any fluorescent intensity. On the other hand, when MiaPaCa-2 cells incubated with PMTL-fl (figure 101-B), the standard curve was divided into two curves, one with lower intensity (closer to zero) and another one shifting right towards higher intensity. The first bell shaped curve represents the cells which have PMTL-fl adsorbed only on the cell membrane, and hence these cells have weaker fluorescent intensity. The second bell shaped curve represents the cells which have uptaken more PMTL-fl in addition to cellular membrane adsorption. The two overlaid curves in figure 101-B shows the cell count below LCST (green curves) and at LCST (red curves). The curve at LCST showed more number of cells having PMTL-fl adsorbed on the cell membrane when compared to the curve below the LCST. Moreover, the fluorescent intensity of the cells increased and the curve shifted towards right showing higher uptake by the cells at the LCST.

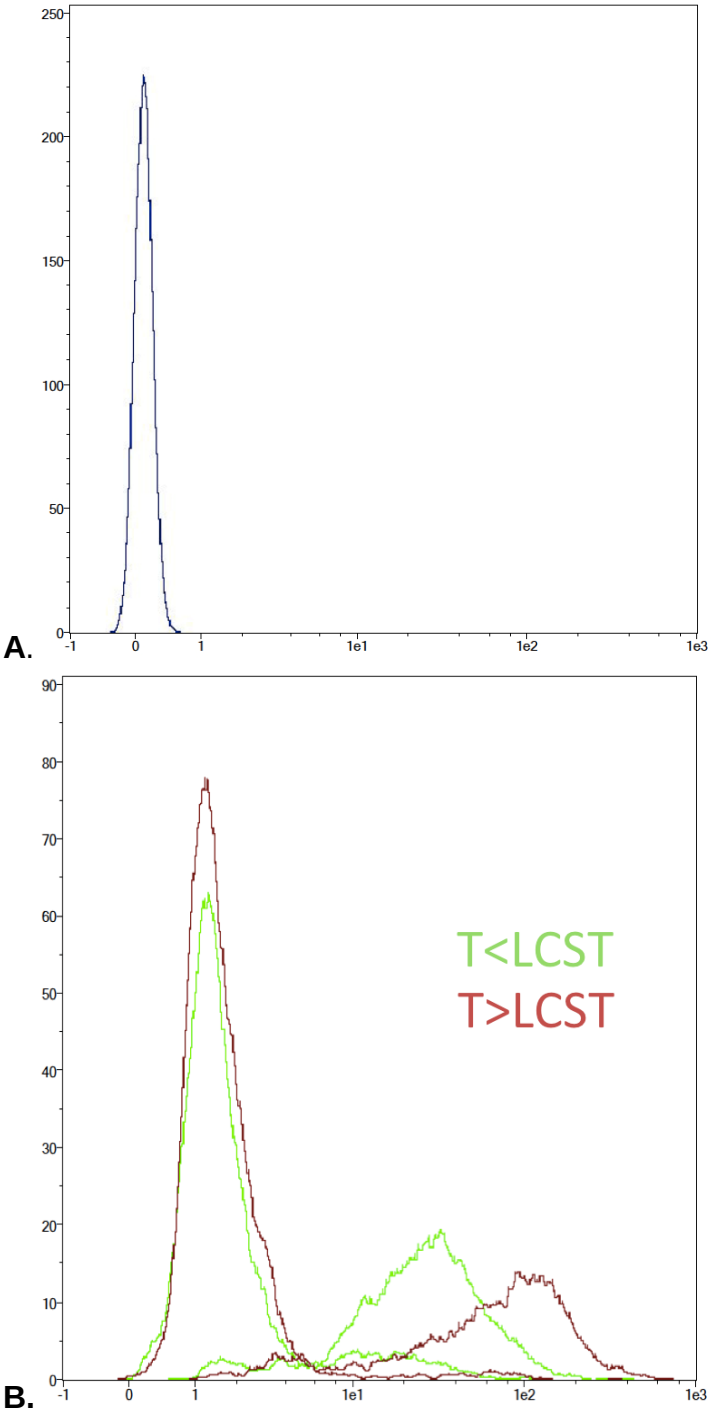

Figure 101. A. The graph shows standard curve of MiaPaCa-2 cells without any fluorescent tag. **B.** MiaPaCa-2 cells were incubated for 30 min in the presence of O-fluorescein-tagged block co-polymer. The graph shows results obtained from below LCST (green curves) and at LCST (red lines).

Figure 102-A shows the graph of standard curve obtained from BxPC-3 cells incubated without PMTL-fl. The two overlaid curves in figure 102-B shows the cell count below LCST (green curves) and at LCST (red curves). Here, the number of cells that have uptaken the fluorescent tag liposome increased significantly compared to MiaPaca-2 cells. This result complied with the cell viability studies, where BxPC-3 cells were more sensitive to formulations and the liposomes resulted in higher cell growth inhibition. Furthermore, the curve at the LCST showed substantial shift to higher fluorescent intensity showing faster cellular association of the liposome at 40°C. The results showed that the PMTL-fl was internalised in a temperature dependent manner. As the temperature increased from 37°C to 40°C, the liposome-cell interaction improved effectively. The flow cytometry findings corroborated well with microscopy findings that were demonstrated in section 2.6.8.

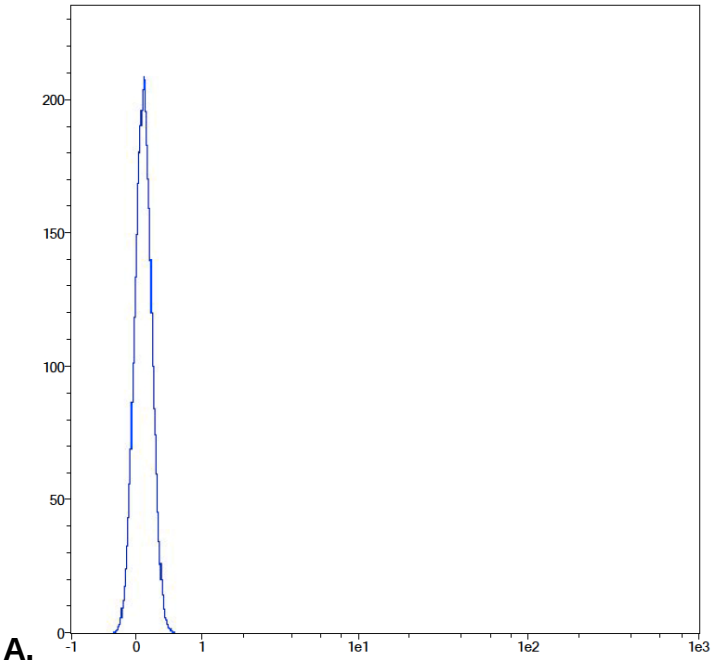

A.

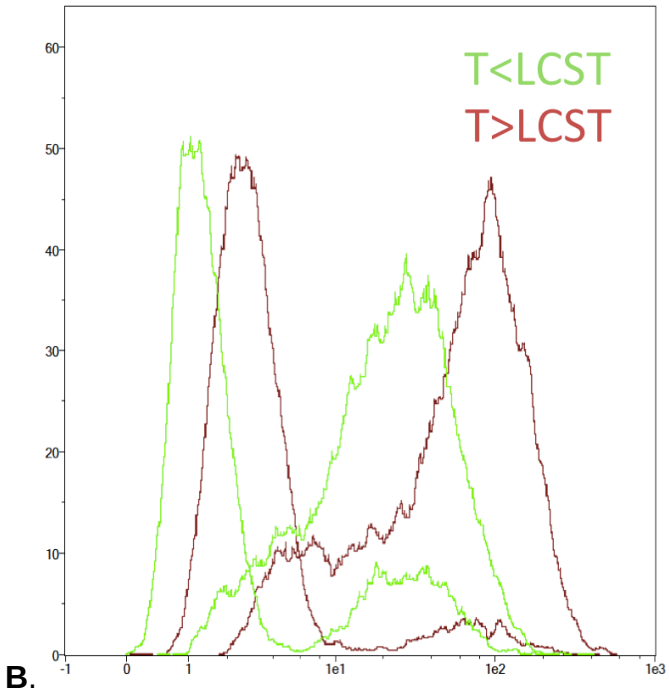

B.

Figure 102. The flow cytometry graph is plotted between number of cells along Y - axis and cell fluorescence, a.u. along X-axis. **A.** The graph shows standard curve of MiaPaCa-2 cells without a fluorescent tag. **B.** The graph shows fluorescent intensity obtained from below LCST (green curves) and at the LCST (red curves).

2.6.10 Clonogenic cell survival assay

The clonogenic cell survival assay was conducted to investigate the proliferative ability of survived cells post treatment (Table 19 and 20). According to the results obtained for each concentration of drugs, some single cells formed colonies (100-200 cells), some remained single and few stopped dividing after formation of small colonies (5-20 cells). The number of colonies produced after treatment is inversely proportional to the drugs concentration.

Table 19. Digital photographs of the clonogenic assay of MiaPaCa-2 cells performed with the combination of free GemCis or loaded in TTL and PMTL below and at the LCST for 14 consecutive days in 6-well plates (the diameter of each well is approx. 34.8 mm).

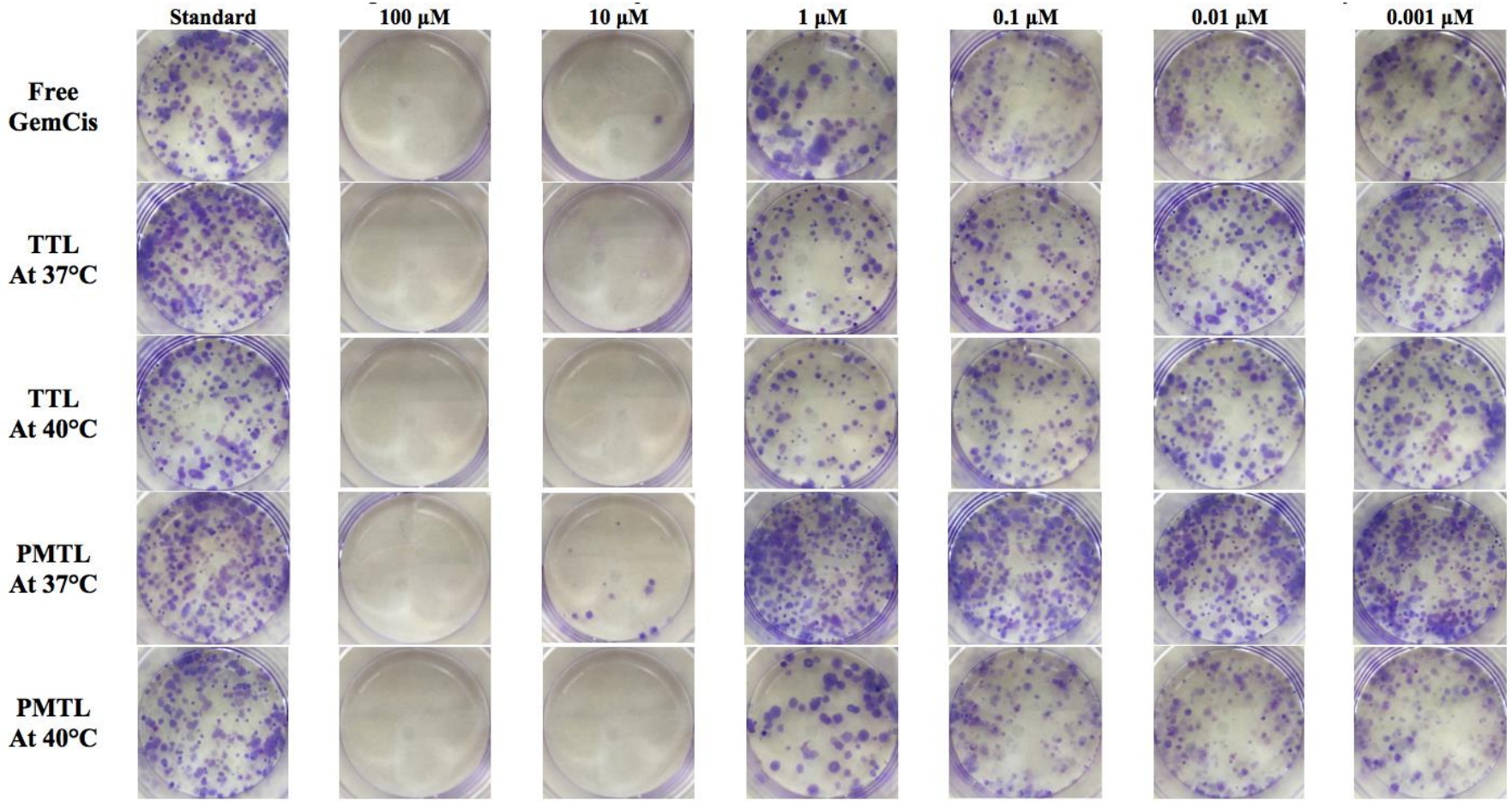

Table 20. Digital photographs of the clonogenic assay of BxPC-3 cells performed with the combination of free GemCis or loaded in TTL and PMTL below and at the LCST for 14 consecutive days in 6-well plates (the diameter of each well is approx. 34.8 mm).

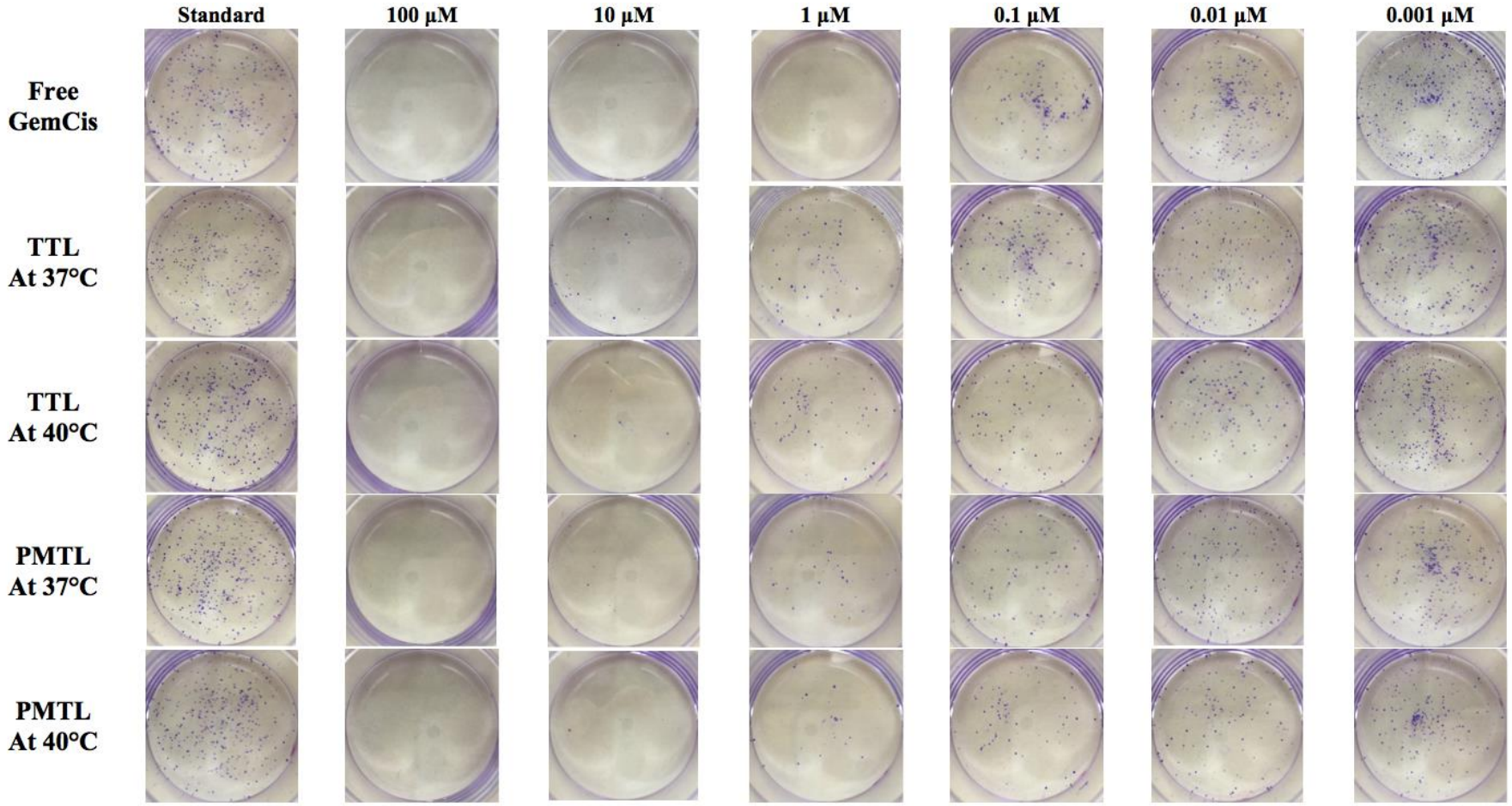

Figure 103 shows the standard colonies formed by MiaPaCa-2 and BxPC-3 cells. MiaPaCa-2 colonies were larger in size compared to BxPC-3 colonies. In addition the BxPC-3 cells formed colonies smaller than 50 cells which were excluded from the calculations.

A.

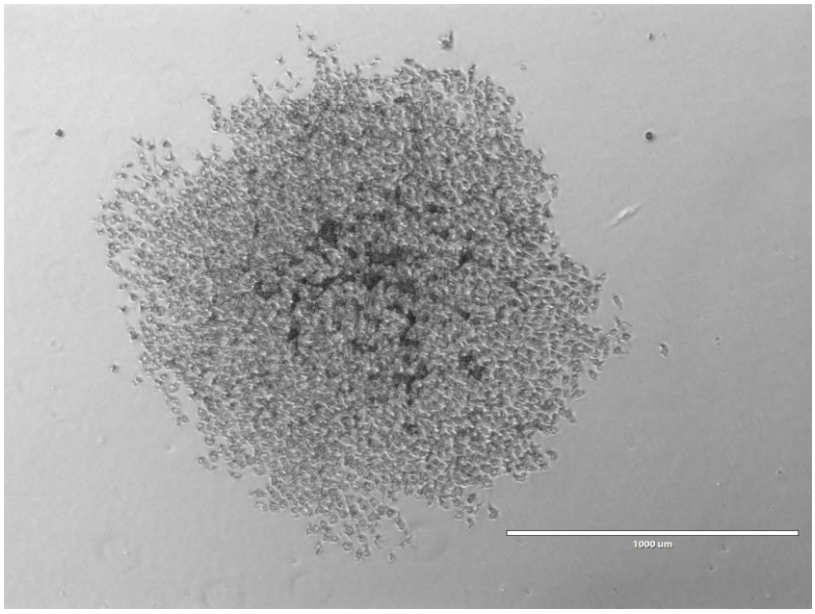

B.

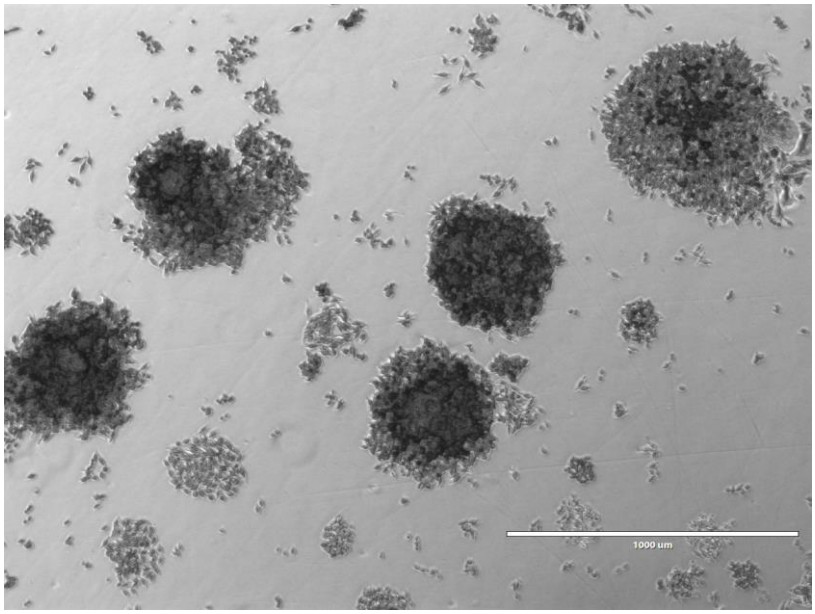

Figure 103. Standard colonies formed by **A.** MiaPaCa-2 cells **B.** BxPC3 cells without application of formulations after 14 days. The scale bar shows the size of 1000 µm.

In-vitro cell survival after treatment

The SF of MiaPaCa-2 cells was calculated after the exposure to the different concentration of drug (from 0.001 to 100 µM)(Figure 104). The SF of cells

after treatment was inversely proportional to the drugs concentration (μM) i.e as the concentration of drugs decreased the SF of cells increased and more colonies were formed. Almost all the formulations showed significant reduction in the number of colonies and cell survival as GemCis concentration increased from 10 μM and 100 μM. At 0.001 to 0.1 μM concentrations, a striking difference was observed between the SF (%) of cells treated with PMTL at 37°C (BL) and at 40°C (AL). The SF of MiaPaCa-2 cells exposed to PMTL (BL) were almost 100%, indicating that the cells fully retained their ability to reproduce. Conversely PMTL (AL) considerably reduced the SF of cells compared to GemCis as free drugs. There was no significant difference between the cell survival of TTL (BL) and TTL (AL) at lower concentrations (0.001 to 0.1 μM). The SF of cells exposed to TTL (AL) was reduced as the drug concentration increased to 1 μM but the overall SF obtained from TTL formulations were higher than free GemCis and no improvement in cytotoxicity was observed. On the other hand, PMTL (AL) was the only formulation which could reduce the SF % to less than 50% in all the concentrations tested and showed statistically significant reduction in SF% compared to free GemCis.

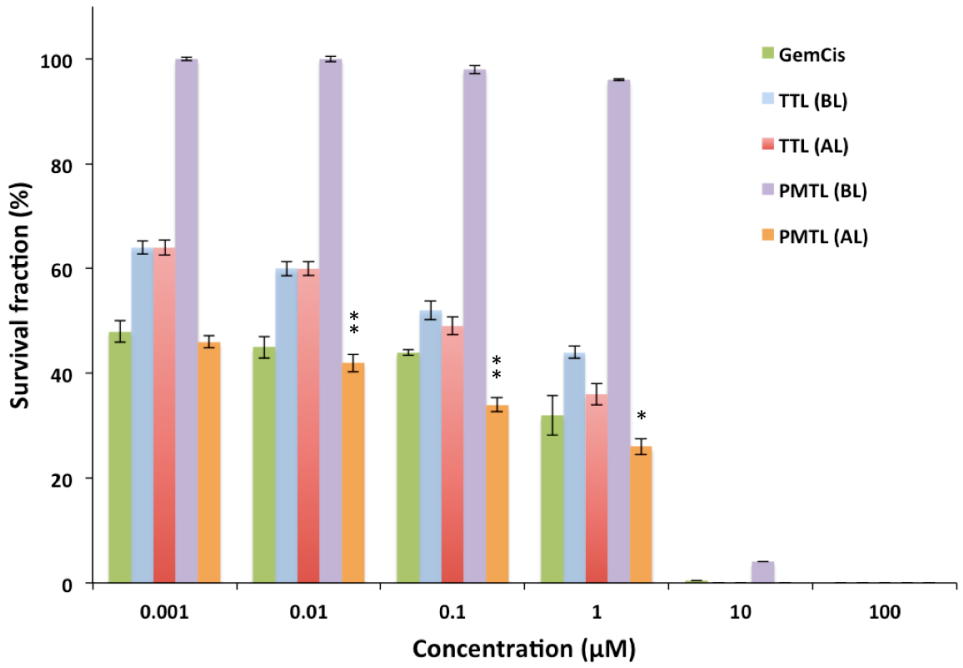

Figure 104. The percentage survival fraction of MiaPaCa-2 cells post treatment with GemCis loaded TTL and PMTL after 14 days. P value 0.001 to 0.01 indicated with ** means very significant; P value 0.01 to 0.05 indicated with * means significant. The P values were calculated from comparison of the percentage survival fraction of the nano-formulations with the free GemCis.

Exposing BxPC-3 cells to different concentrations of drug also showed a dose dependent SF (Figure 105). The gradual and steady decrease in cell survival was observed with an increase in drug concentration, as expected. However, as demonstrated earlier, BxPC-3 cells showed more sensitivity to the formulations. At lower concentrations (0.001 to 0.1 µM) almost all the formulations reduced the SF % significantly compared to free GemCis. Moreover, PMTL (AL) significantly decreased the SF % compared to free GemCis. Free GemCis combinational therapy inhibited the colony formation from 1 µM to 100 µM. In contrast to SF obtained from MiaPaCa-2 cells, the SF of TTL (BL and AL) and PMTL (BL) was significantly lower than the SF of free GemCis in BxPC-3 cells. As the concentration increased to 10 µM and 100 µM, the SF reduced to 0% by free GemCis and PMTL (AL) only. In all the concentrations, the PMTL (AL) was the only formulation which could inhibit the colonies growth to less than 50%. Additionally, the SF remained the least when the PMTL was applied in combination with heat at 40°C (AL).

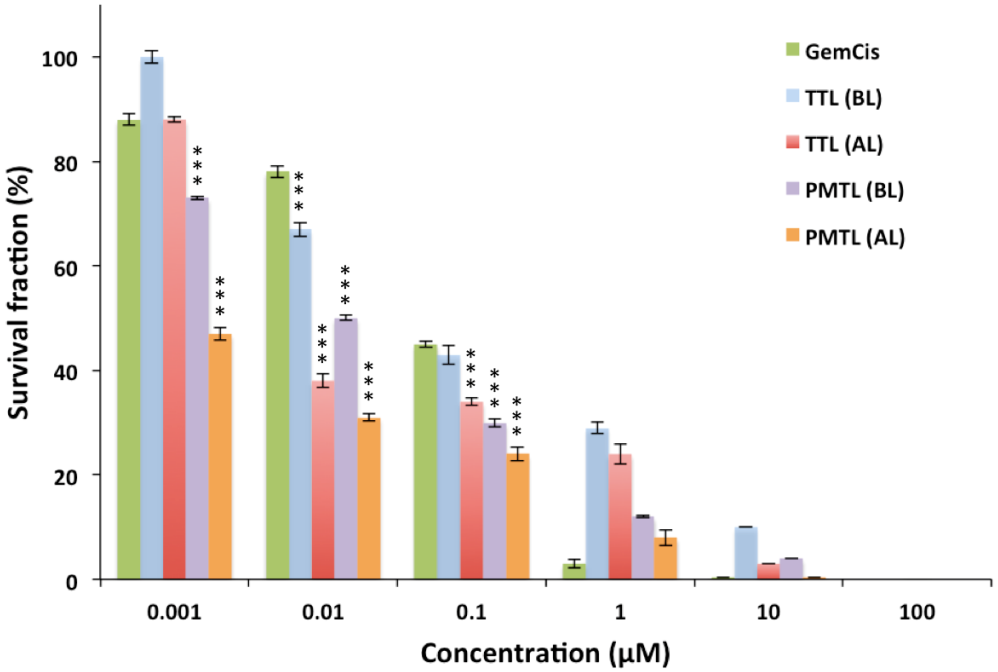

Figure 105. The percentage survival fraction of BxPC-3 cells post treatment with GemCis loaded TTL and PMTL after 14 days. P value 0.0001 to 0.001 indicated with *** means extremely significant; P value 0.001 to 0.01 indicated with ** means very significant; P value 0.01 to 0.05 indicated with * means significant. P value was calculated from comparison of the percentage survival fraction of the nano-formulations with the free GemCis.

Overviewing the performance of TTL and PMTL, PMTL formulations in combination with heat at 40°C (AL) could reduce the cell viability (%), decrease the IC_{50} of chemotherapeutic drugs, enhance the cellular uptake of the drugs and inhibit the proliferation ability of cells after treatment compared to the parent drugs. The presence of thermosensitive polymers on the surface of liposomes rendered the formulations to a effective nano-carriers for the to delivery of chemotherapeutic drugs to cancer cells.

2.7 Conclusion

To improve the controlled release of the liposome content, a Poly (DiEGMA-co-$OEGMA_{300}$)-b-EHMA modified thermo-sensitive liposome was synthesised. Furthermore, the physicochemical properties of the copolymer and the liposomes were investigated. The results showed that, at the LCST of the copolymer, the PMTL showed an increased drug release compared to the TTL formulation. Furthermore, MTT cytotoxicity studies on MiaPaCa-2 and BxPC-3 pancreatic cancer cell lines showed that the PMTL is highly capable of reducing the IC_{50} of chemotherapeutic drugs and improved their cytotoxic effect at the LCST of the copolymer. In addition, the combinational application of gemcitabine and cisplatin exerted synergistic effect and enhanced the cytotoxic effect compared to each drug separately. This result was further investigated and the survival fraction rate was measured to determine the long-term cytotoxic effect after treatment. The survival fraction and the number of colonies formed were both reduced by application of combinational loaded PMTL at the LCST of the copolymer. Therefore, we hypothesised that the dehydration of the copolymers in the PMTL formulation at the LCST induced faster cellular uptake than the parent drugs. For this reason, fluorescence microscopy and cytometry studies were performed and the results showed that the TR copolymers increased the cellular uptake of a fluorescently tagged liposome into the cytosol at the LCST by enhancing the cell membrane interaction and cellular uptake. In conclusion, the PMTL could be a highly efficient nano-carrier which could control the drug release content and improve the intracellular delivery in a temperature dependent manner.

3. Thesis conclusion

Two thermo-responsive nano-formulations, polymeric micelles and polymer modified liposomes, were synthesised. Chemotherapeutic drugs with low and high water solubility were successfully co-encapsulated into the micelles and the liposomes, respectively. In TR polymeric micelles, the polymers were soluble in surrounding medium at body temperature and could successfully co-loaded Sq-Gem and PTX. However, at the transition temperature the polymers turn hydrophobic and form a cross-linked globule which enhanced the drug release in a controlled manner. In addition, experiments further showed that the transition of the polymer at LCST eliminated the hydration layer around the micelle and improved the cell binding interaction of the micelles in vitro. The co-delivery of the Sq-Gem and PTX showed synergistic cytotoxic effect on MiaPaCa-2 pancreatic cancer cells compared to each drug separately. In addition, fluorescence spectroscopy experiments showed significantly higher uptake of TR micelles at the LCST compared to body temperature. The result of long term cytotoxicity assay showed that the proliferative ability of pancreatic cancer cells after treatment was significantly reduced by the combinational therapy of co-loaded micelles and temperature at the LCST.

In polymer modified liposomes, the studies showed that attachment of the polymer on the surface of the liposomes not only improved the temperature sensitivity from 42°C (T_m of lipids) to 40°C (LCST of TR polymer), but also enhanced the drug release and significantly increased the liposome - cell binding interaction which in turn augmented the cytotoxicity of the drugs at the LCST. Co-loading of GemCis showed synergistic effects on MiaPaCa-2 and BxPC-3 pancreatic cancer cells in vitro and enhanced the cytotoxic effect compared to each drug separately. Furthermore, the proliferative ability of pancreatic cancer cells was reduced and less number of colonies grew by combinational therapy of co-loaded liposomes and temperature at the LCST.

Based on the obtained results, the TR nano-formulations could co-encapsulate two potent chemotherapeutic drugs which potentially could act as protective nanocarriers in the blood stream and reduce the systemic toxicity. Furthermore, once these TR nano-formulations accumulate at the tumor, application of heat could facilitate the drug release, augment the cell membrane binding affinity and enhance the cellular internalisation of the drugs.

Ultimately, the proposed formulations exhibit certain design features that render them appealing in the design of “smart” nanomedicines; namely, the TR-polymers are relatively easy to synthesise with precise molecular control on the molecular weight and molecular weight distribution and more importantly, they can be readily integrated in diverse nano-vehicles of different mode of action. This was demonstrated by formulating the TR- polymers with micelles or liposomes, which in principle constitute conceptually different drug delivery platforms for formulations aimed for precision medicine.

4. Future work

Further experiments have been left for the future especially for in vivo studies. There are some ideas that I would have liked to point out. This thesis has been mainly focused on the preparation of nano-formulations and their characterisation, leaving the detailed molecular uptake mechanism and further in vivo studies outside the scope of the thesis. This research would arise deeper cellular biology analysis. I suggest the following future extensions to my work:

The detailed In vitro cellular uptake mechanism can be investigated for the temperature-responsive nano-formulations using various endocytic inhibitors. Pretreating pancreatic cancer cells with cytochalasin D, nocodazole, sucrose, and filipin III, inhibits actin-based transport, microtubular transport, clathrin-mediated endocytosis, and caveolin-mediated endocytosis pathways, respectively. Consequently, subsequent application of the fluorescent-labeled nano-formulations followed by fluorescent detection using flow cytometry will help determining the mechanism of the cellular uptake (Wang, J. et al. 2017). The assay can also be used:

- To investigate the cellular uptake mechanism of the thermoresponsive nanoparticles (both micelle and liposome) with and without hyperthermia. And further investigate if the uptake mechanism changes in a temperature dependent manner.

- To determine if the route of cellular entry is different in micelles and liposomes. And further, to investigate if the size of nanoparticles is involved in the cellular uptake mechanism.

In vivo studies:

Further work is needed to generate more robust understanding of the role of temperature and its interplay with thermo-sensitive nano-formulations in

vivo. Orthotopic tumor mouse models has been widely used in preclinical studies because they offer tissue site-specific pathology, metastasis studies, and are generally considered more clinically relevant in compared to heterotopic mouse model. The cancer cell lines can be implanting to mouse by surgical procedure to generate orthotopic mouse models for pancreatic cancer (Qiu, W. et al. 2013). To minimise the surgical wound to the recipient animals, Huynh and co-workers used an ultrasound-guided method of injection of tumor cells into pancreas for the development of orthotopic pancreatic cancer mouse model (Huynh, A. S. et. al. 2011). Fluorescent-labeled nano-formulations can be injected via the tail vein into tumor bearing mouse and monitor using fluorescent imaging. HIFU can be used to deposit heat and trigger tumor site locally (Kono, K. et al. 2015; Ta, T. et al. 2014). The in vivo assay can also be used:

- To investigate the benefits of controlled release and hyperthermia as targeted therapy. Furthermore, to confirm the presence of the nano-formulations at the tumor site rather preferably than in healthy tissue.

- To investigate the ideal time to apply hyperthermia, if the heat should be applied to the tumor before, during or after the administration of the nano-formulations.

- To investigate the optimum duration of heat application in order to achieve the best result in a non-invasive way.

- To investigate if application of heat could improve the penetration of the nano-formulations in vivo.

- Finally, to examine if the drug loaded thermo-sensitive nano-formulations reduce the systemic cytotoxicity and tumor size compared to the parent drugs.

5. References

Abulateefeh, S. R.; Spain, S. G.; Aylott J. W.; Chan, W. C.; Garnett, M. C.; Alexander C. (2011). Thermoresponsive polymer colloids for drug delivery and cancer therapy. Macromol. Biosci. 11, 1722–1734.

Abulateefeh, S. R.; Spain, S. G.; Thurecht, K. J.; Aylott, J. W.; Chan, W. C.; Garnett, M. C.; Alexander, C. (2013). Enhanced uptake of nanoparticle drug carriers via a thermo-responsive shell enhances cytotoxicity in a cancer cell line. Biomater. Sci., 1, 434-442.

Adams J. D.; Flora K. P.; Goldspiel B. R. (1993). Taxol: a history of pharmaceutical development and current pharmaceutical concerns. Monogr Natl Cancer Inst 15:141-7.

Aguiar, J.; Carpena, P.; Molina-Bolívar, J.A. ; Carnero Ruiz C. (2003). On the determination of the critical micelle concentration by the pyrene 1:3 ratio method. Journal of Colloid and Interface Science 258,116–122.

Akbarzadeh, A.; Rezaei-Sadabady, R.; Davaran, S.; Woo Joo, S.; Zarghami, N.; Hanifehpour, Y.; Samiei, M.; Kouhi, M.; Nejati-Koshki, K. (2013). Liposome: classification, preparation, and applications Nanoscale Research Letters, 8:102.

Akimoto, J.; Nakayama, M.; Sakai, K.; Okano, T. (2010). Thermally controlled intracellular uptake system of polymeric micelles possessing Poly(N-isopropylacrylamide)-based outer coronas. Molecular pharmaceutics Vol. 7, NO. 4, 926–935.

Al-Ahmady, Z.; Kostarelos, K.(2016). Chemical Components for the Design of Temperature-Responsive Vesicles as Cancer Therapeutics. Chem. Rev. 116, 3883−3918.

Alberts, S. R.; Townley, P. M.; Goldberg, R. M.; Cha, S. S.; Sargent, D. J.;

Moore Jr, D. F.; Krook, J. E.; Pitot, H. C.; Fitch, T. R.; Wiesenfeld, M.; Mailliard, J. A. (2003). Gemcitabine and oxaliplatin for metastatic pancreatic adenocarcinoma: a North Central Cancer Treatment Group phase II study. Annals of Oncology 14: 580–585.

Alcindor, T.; Beauger, N. (2011). Oxaliplatin: a review in the era of molecularly targeted therapy. Curr Oncol. 2011 Feb; 18(1): 18–25.

Allen, T. M. (1994). The use of glycolipids and hydrophilic polymers in avoiding rapid uptake of liposomes by the mononuclear phagocyte system. Advanced Drug Delivery Reviews, 13, 285-309.

Amundadottir, L.; Kraft, P.; Stolzenberg-Solomon, R. Z. (2009). Genome-wide association study identifies variants in the ABO locus associated with susceptibility to pancreatic cancer. Nat Genet. 41:986–90.

Anyarambhatla, G. R.; Needham, D. (1999). Enhancement of the phase pransition permeability of DPPC liposomes by incorporation of MPPC: A new temperature-sensitive liposome for use with mild hyperthermia. J. liposome Res. 9, 491-506.

Ataman, M. (1987). Properties of aqueous salt solutions of poly(ethylene oxide) cloud point, theta temperature. Colloid Polm. Sci. 265, 19–25.

Bae, Y. H. (2009). Drug targeting and tumor heterogeneity. Journal of Controlled Release 133, 2–3.

Bakke, A. (2001). The Principles of flow cytometry. Laboratory medicine. 4:32, 207-211.

Banno, B.; Ickenstein, L. M.; Chiu, G. N. C.; Bally, M. B.; Thewalt, J.; Brief, E.; Wasan, E. K. (2010). The Functional Roles of Poly(Ethylene Glycol)-Lipid and Lysolipid in the Drug Retention and Release from Lysolipid-Containing Thermosensitive Liposomes in Vitro and in Vivo. J. Pharm. Sci., 99, 2295−2308.

Becer, C. R.; Hahn, S.; Fijten, M. W. M.; Thijs, H. M. L.; Hoogenboom, R.; Schubert, U. S. (2008). Libraries of methacrylic acid and oligo(ethylene glycol) methacrylate copolymers with LCST behavior. Journal of Polymer Science: Part A: Polymer Chemistry, Vol. 46, 7138–7147.

Becker, E. D. (1999). High resolution NMR: Theory and chemical applications, Academic Press, US.

Bender, D. M.; Bao, J.; Dantzig, A. H.; Diseroad, W. D.; Law, K. L.; Magnus, N. A.; Peterson, J. A.; Perkins, E. J.; Pu, Y. J.; Reutzel-Edens, S. M.; Remick, D. M.; Starling, J. J.; Stephenson, G. A.; Vaid, R. K.; Zhang, D. and McCarthy J. R. (2009). Synthesis, crystallization, and biological evaluation of an orally active prodrug of gemcitabine. J. Med. Chem., 52, 6958–6961.

Berne, B. J.; Pecora, R. (1976). Dynamic Light Scattering: With Applications to Chemistry, Biology, and Physics. New York. Dover publications. INC.

Blanco, E.; Shen, H.; Ferrari, M. (2015). Principles of nanoparticle design for overcoming biological barriers to drug delivery. Nature biotechnology, 33,9,941-951.

Braganza, J. M.; Hunt, L. P.; Warwick, F. (1982). Relationship between pancreatic exocrine function and ductal morphology in chronic pancreatitis. Gastroenterology. 82:1341.

Bekkara-Aounallah, F.; Gref, R.; Othman, M.; Reddy, L.H.; Pili, B.; Allain, V.; Bourgaux, C.; Hillaireau, H.; Lepêtre-Mouelhi, S.; Desmaële, D.; Nicolas, J.; Chafi, N.; Couvreur, P. (2008) Novel PEGylated nanoassemblies made of self-assembled squalenoyl nucleoside analogues, Adv. Funct. Mater. 18, 3715–3725.

Bernstein, R. E.; Cruz, C. A.; Paul, D. R.; Barlow, J. W. (1977). LCST Behavior in Polymer Blends. Macromolecules. 10 (3) : 681-686.

Berridge, M.V.; Herst, P.M. ; Tan, A. S. (2005). Tetrazolium dyes as tools in cell biology: new insights into their cellular reduction. Biotechnol Annu Rev. 2005;11:127-52.

Bildstein, L.; Marsaud, V.; Chacun, H.; Lepêtre-Mouelhi, S.; Desmaële, D.; Couvreur, P.; Dubernet, C. (2010). Extracellular-protein-enhanced cellular uptake of squalenoyl gemcitabine from nanoassemblies, Soft Matter 6, 5570–5580.

Brown, M. ; Wittwer, C. (2000). Flow cytometry: Principles and clinical Applications in hematology. Clinical Chemistry 46:8 (B) 1221–1229.

Bui, D. T.; D. Julien Nicolas, J.; Maksimenko, A.; Desmaele, D.; Couvreur, P. (2014). Multifunctional squalene-based prodrug nanoparticles for targeted cancer therapy. Chem. Commun. 50, 5336.

Cabral, H.; Matsumoto, Y.; Mizuno, K.; Chen, Q.; Murakami, M.; Kimura, M.; Terada, Y.; Kano, M. R.; Miyazono, K.; Uesaka, M.; Nishiyama, N.; Kataoka, K. (2011). Accumulation of sub-100 nm polymeric micelles in poorly permeable tumours depends on size. Nature Nanotechnology 6, 815–823.

Caron, J.; Maksimenko, A.; Mougin, J.; Couvreur, P.; Desmaele, D. (2014). Combined antitumoral therapy with nanoassemblies of bolaform polyisoprenoyl paclitaxel/gemcitabine prodrugs. Polym. Chem., 5, 1662.

Cattel, L.; Airoldi, M.; Delprino, L.; Passera, R.; Milla, P.; Pedani, F. (2006). Pharmacokinetic evaluation of gemcitabine and 2',2'-difluorodeoxycytidine-5'-triphosphate after prolonged infusion in patients affected by different solid tumors. Annals of Oncology 17 (Supplement 5): v142–v147.

Chen, Y.; Zhang, W.; Huang, Y.; Gao, F.; Sha, X.; Fang, X. (2015). Pluronic-based functional polymeric mixed micelles for co-delivery of doxorubicin and paclitaxel to multidrug resistant tumor. Int. J. Pharm, 488, 1-2, 44-58.

Chitkara, D.; Mittal, A.; Behrman, S. W.; Kumar, N.; Mahato, R. I. (2013). Self-assembling, amphiphilic polymer−gemcitabine conjugate shows enhanced antitumor efficacy against human pancreatic adenocarcinoma. Bioconjugate Chem. 24, 1161−1173.

Chou, T.C. ; Talalay, P. (1984) Quantitative analysis of dose-effect relationships: the combined effects of multiple drugs or enzyme inhibitors. Adv Enzyme Regul., 22: 27-55.

Chou, T.C. (2010). Drug combination studies and their synergy quantification using the Chou-Talalay Method. Cancer Res; 70(2).

Chuang, K.-H.; Wang, H.-E.; Chen, F.-M.; Tzou, S.-C.; Cheng, C.-M.; Chang, Y.- C.; Tseng, W.-L.; Shiea, J.; Lin, S.-R.; Wang, J.-Y.; Chen, B.-M.; Roffler, S. R.; Cheng, T.-L. (2010). Endocytosis of PEGylated agents enhances cancer imaging and anticancer efficacy. Mol. Cancer Ther., 9, 1903–1912.

Chung, J.E.; Yokoyama, M.; Yamato, M.; Aoyagi, T.; Sakurai, Y.; Okano, T. (1999) Thermo-responsive drug delivery from polymeric micelles constructed using block copolymers of poly(N-isopropylacrylamide) and poly(butylmethacrylate). Journal of Controlled Release 62, 115–127.

Chung, W-G.; Sandoval, M. A.; Sloat, B. R.; Lansakara-P., D. S. P.; Cui, Z. (2012). Stearoyl gemcitabine nanoparticles overcome resistance related to the over-expression of ribonucleotide reductase subunit M1. J Control Release, 157(1): 132–140.

Colombani, D. (1997). Chain-growth control in free radical polymerization. Prog. Polym. Sci.,Vol. 22, 1649-1720.

Conroy, T.; Desseigne, F.; Ychou, M.; Bouché, O.; Guimbaud, R.; Bécouarn, Y.; Adenis, A.; Raoul, J.-L.; Gourgou-Bourgade, S.; de la Fouchardière, C.;

Bennouna, J.; Bachet, J. B.; Khemissa-Akouz, F.; Péré-Vergé, D.; Delbaldo, C.; Assenat, E.; Chauffert, B.; Michel, P.; Montoto-Grillot, C.; Ducreux, M. (2011). FOLFIRINOX versus gemcitabine for metastatic pancreatic cancer. et al. N Engl J Med 2011;364:1817–25.

Couvreur, P.; Stella, B.; Reddy, L.H.; Hillaireau, H.; Dubernet, C.; Desmaële, D.; Lepêtre-Mouelhi, S.; Rocco, F.; Dereuddre-Bosquet, Clayette, N. P.; Rosilio, V.; Marsaud, V.; Renoir, J.M.; and Cattel, L. (2006). Squalenoyl nanomedicines as potential therapeutics. Nano Lett., *6* (11), 2544–2548.

Croy, S. R. ; Kwon, G. S. (2006). Polymeric micelles for drug delivery. Curr Pharm Des. 12(36):4669-84.

Daman, Z.; Ostad, S.; Amini, M. ; Gilani, K. (2014). Preparation, optimization and in vitro characterization of stearoyl-gemcitabine polymeric micelles: A comparison with its self-assembled nanoparticles. Int J Pharm. 468(1-2):142-51.

Dand, N.; Patel, P.; Ayre, A.; Kadam, V. (2013). Polymeric micelles as a drug carrier for tumor targeting. Chronicles of Young Scientists, 4, 2, 94-101.

Danhier, F.; Feron, O.; Préat, V. (2010). To exploit the tumor microenvironment: Passive and active tumor targeting of nanocarriers for anti-cancer drug delivery. Journal of Controlled Release 148, 135–146.

Debele, T. A.; Lee, K.-Y.; Hsu, N.-Y.; Chiang, Y.-T.; Yu, L.-Y.; Shena Y.-A.; Lo, C.-L. (2017). A pH sensitive polymeric micelle for co-delivery of doxorubicin and α-TOS for colon cancer therapy. J. Mater. Chem. *B*, 2017,5, 5870-5880.

Dehghan Kelishady, P.; Saadat, E.; Ravar, F.; Akbari, H.; Dorkoosh, F. (2015). Pluronic F127 polymeric micelles for co-delivery of paclitaxel and lapatinib against metastatic breast cancer: preparation, optimization and in vitro evaluation. Pharm. Dev. Technol, 20, 8, 1009-1017.

De las Heras Alarcon, C.; Pennadam, S.; Alexander, C. (2005). Stimuli responsive polymers for biomedical applications. Chem. Soc. Rev., 34, 276–285.

Desmaële, D.; Gref, R.; Couvreur, P. (2012). Squalenoylation: A generic platform for nanoparticular drug delivery. J.Control. Release, 161, 609–618.

Dimou, A.; Syrigos, K. N.; Saif, M. W. (2012). Overcoming the stromal barrier: technologies to optimize drug delivery in pancreatic cancer. Ther Adv Med Oncol, 4, 5, 271–279.

Du, H.; Wickramasinghe, R.; Qian, X. (2010) Effects of Salt on the Lower Critical Solution Temperature of Poly (N-Isopropylacrylamide). J. Phys. Chem. B, 114, 16594–16604.

Duncan, R. (2006). Polymer conjugates as anticancer nanomedicines, Nat. Rev. Cancer 6, 688–701.

Eastman, A. (1987). The formation, isolation and characterization of DNA adducts produced by anticancer platinum complexes. Pharmacol Ther. 34, 2, 155-66.

Eeckman, F.; Amighi, K.; Moes, A. J. (2001). Effect of some physiological and non-physiological compounds on the phase transition temperature of thermoresponsive polymers intended for oral controlled-drug delivery. International Journal of Pharmaceutics 222, 259–270.

Emami, J.; Rezazadeh, M.; Mashayekhi, M.; Rostami, M.; Jahanian-Najafabadi, A. (2017). A novel mixed polymeric micelle for co-delivery of paclitaxel and retinoic acid and overcoming multidrug resistance: synthesis, characterization, cytotoxicity, and pharmacokinetic evaluation. Drug Dev Ind Pharm.

Fleige, E.; Quadir, M. A.; Haag, R. (2012). Stimuli-responsive polymeric nanocarriers for the controlled transport of active compounds: Concepts and applications. Advanced Drug Delivery Reviews 64, 866–884.

Freeman, C.; Halperin, E.C.; Brady, L.W.; Wazer, D.E. (2008). Perez and Brady's principles and practice of radiation oncology, Lippincott Williams and Wilkins, Philadelphia.

Frese, K. K.; Neesse, A.; Cook, N.; Bapiro, T. E.; Lolkema, M. P.; Jodrell, D. I.; Tuveson, D. A. (2012). nab-Paclitaxel potentiates gemcitabine activity by reducing cytidine deaminase levels in a mouse model of pancreatic cancer. American Association for Cancer research.

Gaber, M. H.; Wu, N. Z.; Hong, K.; Huang, S. K.; Dewhirst, M. W. (1996). Thermoresponsive liposomes: Extravasation and release of contents in tumor microvascular networks. Int. J. Radiation Oncology Biol. Phys., Vol. 36, No. 5, pp. 1177-l 187.

Gao, G. H.; Li, Y.; Lee, D. S. (2013). Environmental pH-sensitive polymeric micelles for cancer diagnosis and targeted therapy. Journal of Controlled Release 169, 180–184.

Gasselhuber, A.; Dreher, M. R.; Partanen, A.; Yarmolenko, P. S.; Woods, D.; Wood, B. J.; Haemmerich D. (2012). Targeted drug delivery by high intensity focused ultrasound mediated hyperthermia combined with temperature-sensitive liposomes: Computational modelling and preliminary in vivo validation. Int. J. Hyperthermia, 28(4): 337–348.

Gelderblom, H.; Verweij, J.; Nooter, K.; Sparreboom, A. (2001). Cremophor EL: the drawbacks and advantages of vehicle selection for drug formulation. Eur J Cancer. 37(13):1590-8.

Gil, E. S.; Hudson, S. M. (2004). Stimuli-reponsive polymers and their bioconjugates. Prog. Polym. Sci. 29 , 1173–1222.

Graeser, R.; Bornmann, C.; Esser, N.; Ziroli, V.; Jantscheff, P.; Unger, C.; Hopt, U. T.; Schaechtele, C.; Dobschuetz, E.; Massing, U. (2009). Antimetastatic Effects of Liposomal Gemcitabine and Empty Liposomes in an Orthotopic Mouse Model of Pancreatic Cancer. Pancreas 38 (3): 330-337.

Gregory, A.; Stenzel, M. H. (2012). Complex polymer architectures via RAFT polymerization: From fundamental process to extending the scope using click chemistry and nature's building blocks, Progress in Polymer Science 37, 38–105.

Grippo, P. J.; Munshi, H. G. (2012). Pancreatic Cancer and Tumor Microenvironment. Trivandrum (India): Transworld Research Network; 2012. ISBN-13: 978-81-7895-548-3.

Hamel, E.; Del campo, A. A.; Lowe, M. C.; Lin, C. (1981). Interactions of taxol, microtubule associated proteins, and guanine nucleotide in tubulin polymerization. J. Biol. Chem. 256 (22): 11887–11894.

Hare, J. I.; Lammers, T.; Ashford, M. B.; Puri, G.; Storm, G.; Barry, S. T. (2017). Challenges and strategies in anti-cancer nanomedicine development: An industry perspective. Advanced Drug Delivery Reviews 108, 25–38.

Heinemann, V.; Wilke, H.; Mergenthaler, H.-G.; Clemens, M.; Konig, H.; Illiger, H. J.; Arning, M.; Schalhorn, A.; Possinger, K.; Fink, U. (2000). Gemcitabine and cisplatin in the treatment of advanced or metastatic pancreatic cancer. Annals of Oncology 11: 1399-1403.

Heinemann, V.; Quietzsch, D.; Gieseler, F.; Gonnermann, M.; Schönekas, H.; Rost, A.; Neuhaus, H.; Haag, C.; Clemens, M.; Heinrich, B.; Vehling-Kaiser, U.; Fuchs, M.; Fleckenstein, D.; Gesierich, W.; Uthgenannt, D.; Einsele, H.; Holstege, A.; Hinke, A.; Schalhorn, A.; Wilkowski, R. (2006). Randomized phase III trial of gemcitabine plus cisplatin compared with gemcitabine alone in advanced pancreatic cancer. J Clin Oncol 24:3946-3952.

Heldin, C. H.; Rubin, K.; Pietras, K.; Östman|, A. (2004). High interstitial fluid

pressure – an abstacle in cancer therapy. *Nature Reviews Cancer* 4, 806-813.

Henderson, E.; Lee, B. H.; Cui, Z.; McLemore, R.; Brandon, T. A.; Vernon, B. L. (2009). In vivo evaluation of injectable thermo-sensitive polymer with time-dependent LCST. J Biomed Mater Res A. 90 (4) : 1186–1197.

Hildebrandt, B.; Wust, P.; Ahlers, O.; Dieing, A.; Sreenivasa, G.; Kerner, T.; Felix, R.; Riess, H. (2002). The cellular and molecular basis of hyperthermia. Critical Reviews in Oncology/Hematology 43: 33–56.

Hiruta, Y.; Shimamura, M.; Matsuura, M.; Maekawa, Y.; Funatsu, T.; Suzuki, Y.; Ayano, E.; Okano, T.; Kanazawa, H. (2014). Temperature-responsive fluorescence polymer probes with accurate thermally controlled cellular uptakes. *ACS Macro Lett.*, *3* (3), pp 281–285.

Horne, R.A.; Almeida, J.P.; Day, A.F.; Yu, N.-T. (1971). Macromolecule hydration and the effect of solutes on the cloud point of aqueous solutions of polyvinyl–methyl-ether: a possible model for protein denaturation and temperature control in homeothermic animals. J. Colloid Surfaces Sci. 35.

Howard, B.; Gao, A.; Lee, S.-W.; Seo, M.-H.; Rapoport, N. (2006) Ultrasound enhanced chemotherapy of drug-resistant breast cancer tumors by micellar-encapsulated paclitaxel, Am. J. Drug Deliv. 4, 97–104.

Hung, S. W.; Mody, H. R.; Rajgopal Govindarajan, R. (2012). Overcoming nucleoside analog chemoresistance of pancreatic cancer: A therapeutic challenge. Cancer Lett . 320(2): 138–149.

Husseini, G. A.; Pitt, W. G. (2008). Micelles and nanoparticles for ultrasonic drug and gene delivery. Advanced Drug Delivery Reviews 60, 1137–1152.

Husseini, G. A.; Pitt, W. G.; Martins, A. M. (2014). Ultrasonically triggered drug delivery: Breaking the barrier. Colloids and surfaces B: Biointerfaces 123, 364-386.

Huynh, A. S.; Abrahams, D. F.; Torres, M. S.; Baldwin, M. K.; Gillies, R. J.; Morse, D. L. (2011). Development of an orthotopic human pancreatic cancer xenograft model using ultrasound guided injection of cells. PLoS One, 6(5): e20330.

Immordino, M. L.; Brusa, P.; Rocco, F.; Arpicco, S.; Ceruti, M.; Cattel, L. (2004). Preparation, characterization, cytotoxicity and pharmacokinetics of liposomes containing lipophilic gemcitabine prodrugs. Journal of Controlled Release 100, 331–346.

Immordino, M. L.; Dosio, F. D.; Cattel, L. (2006). Stealth liposomes: review of the basic science, rationale, and clinical applications, existing and potential. International Journal of Nanomedicine 1, 3, 297–315.

Iyer, A. K.; Khaled, G.; Fang, J.; Maeda, H. (2006). Exploiting the enhanced permeability and retention effect for tumor targeting, Drug Discov. Today 11, 812–818.

Jones, M.C. ; Leroux, J.C. (1999). Polymeric micelles - a new generation of colloidal drug carriers. European Journal of Pharmaceutics and Biopharmaceutics 48, 101-111.

Kalyanasundaram, K. ; Thomas, J. K. (1997). Environmental effects on vibronic band intensities in pyrene monomer fluorescence and their application in studies of micellar systems. J. Am. Chem. Soc., 99 (7), 2039–2044.

Kataoka, K.; Harada, A.; Nagasaki, Y. (2001). Block polymer micelles for drug delivery, design, characterization and biological significance. Adv Drug Deliv Rev, 47:113-31.

Kataoka, K.; Harada, A.; Nagasaki, Y. (2012). Block copolymer micelles for drug delivery: Design, characterization and biological significance. Advanced

Drug Delivery Reviews 64, 37–48.

Ke, X.-Y.; Lin, N. G. V. W.; Gao, S. J.; Tong, Y. W; Hedrick, J. L.; Yang, Y. Y. (2014). Co-delivery of thioridazine and doxorubicin using polymeric micelles for targeting both cancer cells and cancer stem cells. Biomaterials, 35, 3, 1096-1108.

Kim, V. M.; Ahuja, N. (2015). Early detection of pancreatic cancer. Chin J Cancer Res. 27(4): 321–331.

Kirui, D. K.; Celia, C.; Molinaro, R.; Bansal, S. S.; Cosco, D.; Fresta, M.; Shen, H.; Ferrari, M. (2015). Mild hyperthermia enhances transport of liposomal gemcitabine and improves in vivo therapeutic response. Adv. Healthcare Mater.

Klein, A. P.; Brune, K. A.; Petersen, G. M. (2004). Prospective risk of pancreatic cancer in familial pancreatic cancer kindreds. Cancer Res. 2004; 64:2634–38.

Komar, G.; Kauhanen, S.; Liukko, K.; Seppanen, M.; Kajander, S.; Ovaska, J.; Nuutila, P.; Minn, H. (2009). Decreased blood flow with increased metabolic activity: a novel sign of pancreatic tumor aggressiveness. Clin Cancer Res. 15:5511–5517.

Kong, G.; Braun, R. D.; Dewhirst, M. W. (2000) Hyperthermia enables tumor-specific nanoparticle delivery: effect of particle size. Cancer research 60, 4440–4445.

Koning, G. A.; Eggermont, A. M. M.; Lindner, L. H.; Hagen, T. L. M. T. (2010). Hyperthermia and thermosensitive liposomes for improved delivery of chemotherapeutic drugs to solid tumors. Pharm Res, 27:1750–1754.

Kono, K. (2001). Thermosensitive polymer-modified liposomes. Advanced Drug Delivery Reviews 53, 307–319.

Kono, K.; Hayashi, H.; Takagishi, T. (1994). Temperature-Sensitive Liposomes: Liposomes Bearing Poly (N-Isopropylacrylamide). J. Controlled Release, 30, 69−75.

Konno, T.; Maeda, H.; Iwai, K.; Maki, S.; Tashiro, S.; Uchida, M.; Miyauchi, Y. (1984). Selective targeting of anti-cancer drug and simultaneous image enhancement in solid tumors by arterially administered lipid contrast medium, Cancer 54 (11) 2367–2374.

Kono, K.; Nakaia, R.; Morimotoa, K.; Takagishi, T. (1999). Temperature-dependent interaction of thermo-sensitive polymer-modified liposomes with CV1 cells. FEBS Letters 456, 306-310.

Kono, K.; Ozawa, T.; Yoshida, T.; Ozaki, F.; Ishizaka, Y.; Maruyama, K.; Kojima, C.; Harada, A.; Aoshima, S. (2010). Highly Temperature-Sensitive Liposomes Based on a Thermosensitive Block Copolymer for Tumor-Specific Chemotherapy. Biomaterials, 31, 7096−7105.

Kono, K.; Takashima, M.; Yuba, E.; Harada, A.; Hiramatsu, Y.; Kitagawa, H.; Otani, T.; Maruyama, K.; Aoshima, S. (2015). Multifunctional liposomes having target specificity, temperature-triggered release, and near-infrared fluorescence imaging for tumor-specific chemotherapy. Journal of Controlled Release 216, 69–77.

Kornmann M, Fakler H, Butzer U et al. Oxaliplatin exerts potent in vitro cytotoxicity in colorectal and pancreatic cancer cell lines and liver metastases. Anticancer Res 2000; 20: 3259–3264.

Landon, C. D.; Park,J.-Y.; Needham, D.; Dewhirst, M. W. (2011). Nanoscale drug delivery and hyperthermia: The materials design and preclinical and clinical testing of low temperature-sensitive liposomes used in combination with mild hyperthermia in the treatment of local cancer. Open Nanomed J , 3,

38–64.

Lee, E. S.; Lee, J. Y.; Kim, H.; Choi, Y.; Park, J.; Han, J. K.; Choi, B. I. (2013). Pulsed high-intensity focused ultrasound enhances apoptosis of pancreatic cancer xenograft with gemcitabine. Ultrasound in Med. & Biol., Vol. 39, No. 11, pp. 1991–2000.

Lee, J. Y.; Choi, B.I.; Ryu, J.K.; Kim, Y.; Hwang, J. H.; Kim, S. H.; Han, J. K. (2011). Concurrent chemotherapy and pulsed high-intensity focused ultrasound therapy for the treatment of unresectable pancreatic cancer: Initial Experiences. Korean J Radiol, 12(2):176-186.

Lee, S.C; Huh, K.M.; Lee, J.; Cho, Y.W.; Galinsky, R.E.; Park, K. (2007). Hydrotropic Polymeric Micelles for Enhanced Paclitaxel Solubility: In Vitro and In Vivo Characterization. Biomacromolecules, 8, 202-208.

Lepock, J. R. (2003) Cellular effects of hyperthermia: relevance to the minimum dose for thermal damage. INT. J. Hyperthermia. 19, 3: 252–266.

Lepock, J. R.; Frey, H. E.; Ritchie, K. P. (1993). Protein denaturation in intact hepatocytes and isolated cellular organelles during heat shock. The Journal of Cell Biology, 122, 6: 1267-1276.

Li, H.; Yu, H.; Zhu, C.; Hu, J.; Du, M.; Zhang, F.; Yang, D. (2016). Cisplatin and doxorubicin dual-loaded mesoporous silica nanoparticles for controlled drug delivery. RSC Adv., 6, 94160-94169.

Li, J.; Wang, B.; Liu, P. (2008). Possibility of active targeting to tumor by local hyperthermia with temperature-sensitive nanoparticles. Medical Hypotheses, 71, 249–251.

Li, R.; Xie, L.; Zhu, Z.; Liu, Q.; Hu, Y.; Jiang, X.; Yu, L.; Qian, X.; Guo, W.; Ding, Y.; Liu, B. (2011). Reversion of pH-Induced physiological drug

resistance: A novel function of copolymeric nanoparticles. PLoS One. , 6(9):e24172.

Liggins, R. T.; Burt, H. M. (2002). Polyether–polyester diblock copolymers for the preparation of paclitaxel loaded polymeric micelle formulations. Advanced Drug Delivery Reviews 54:191–202.

Lin, Y.; Richards, F. M.; Krippendorff, B. F.; Bramhall, J. L.; Harrington, J. A.; Bapiro, T. E.; Robertson, A.; Zheleva, D.; Jodrell, D. I. (2012). Paclitaxel and CYC3, an aurora kinase A inhibitor, synergise in pancreatic cancer cells but not bone marrow precursor cells. *Br J Cancer*, 107, 1692-1701.

Liu, X.; Cheng, F.; Liu, H.; Chen, Y. (2008). Unusual salt effect on the lower critical solution temperature of hyperbranched thermoresponsive polymers. Soft Matter, 4, 1991–1994.

Liu, Y.; Wang, W.; Yang, J.; Zhou, C.; Sun, J. (2013). pH-sensitive polymeric micelles triggered drug release for extracellular and intracellular drug targeting delivery. Asian journal of pharmaceutical sciences 8, 159-167.

Lough, W. J. ; Wainer, I. W. (1995). High performance liquid chromatography-fundamental principles and practice. London: Blaclue Academic and Professional, 276 pp.

Louvet, C.; Labianca, R.; Hammel, P.; Lledo, G.; Zampino, M.G.; André, T.; Zaniboni, A.; Ducreux, M.; Aitini, E.; Taı¨eb, J.; Faroux, R.; Lepere, C.; de Gramont, A. (2005). Gemcitabine in Combination With Oxaliplatin Compared With Gemcitabine Alone in Locally Advanced or Metastatic Pancreatic Cancer: Results of a GERCOR and GISCAD Phase III Trial. J Clin Oncol 23:3509-3516.

Lutz. J.F. (2008). Polymerization of Oligo (Ethylene Glycol) (Meth) Acrylates: Toward New Generations of Smart Biocompatible Materials. Journal of

Polymer Science: Part A: Polymer Chemistry, Vol. 46, 3459–3470.

Lv, S.; Tang, Z.; Li, J.; Lin, J.; Song, W.; Liu, H.; Huang, Y.; Zhang, Y.; Chen, X. (2014). Co-delivery of doxorubicin and paclitaxel by PEG-polypeptide nanovehicle for the treatment of non-small cell lung cancer. Biomaterials, 35, 23, 6118-6129.

Maeda, H. (2001). The enhanced permeability and retention (EPR) effect in tumor vasculature: the key role of tumor-selective macromolecular drug targeting. Advan. Enzyme Regul., 41,189–207.

Maeda, H. (2015). Toward a full understanding of the EPR effect in primary and metastatic tumors as well as issues related to its heterogeneity, Adv. Drug Deliv. Rev. 91, 3–6.

Maeda, H. ; Matsumura, Y. (1989). Tumoritropic and lymphotropic principles of macromolecular drugs, Crit. Rev. Ther. Drug Carrier Sys. 6, 193–210.

Matsumura, Y.; Maeda, H. (1986). A new concept for macromolecular therapeutics in cancer chemotherapy: mechanism of tumoritropic accumulation of proteins and the antitumor agent Smancs, Cancer Res. 46, 6387–6392.

Matyjaszewski, K.; Spanswick, J. (2005). Controlled/living radical polymerization. Materials today, Review features 26-33.

May, J. P.; Ernsting, M. J.; Undzys, E.; Li S.D. (2013). Thermosensitive Liposomes for the Delivery of Gemcitabine and Oxaliplatin to Tumors. Mol. Pharmaceutics, 10, 4499−4508.

Michalski, C. W.; Erkan, M.; Friess, H.; Kleeff, J. (2010). Tumor metabolism to blood flow ratio in pancreatic cancer: helpful in patient stratification? Future Oncol. 6(1), 13-15.

Miller, C.R.; Bondurant, B.; McLean, S.D.; McGovern, K.A.; O'Brien, D.F. (1998). Liposome–cell interactions in vitro: effect of liposome surface charge on the binding and endocytosis of conventional and sterically stabilized liposomes, Biochemistry 37, 12875–12883.

Miller, R. P.; Tadagavadi, R. K.; Ramesh, G.; Reeves, W. B. (2010). Mechanisms of Cisplatin Nephrotoxicity. *Toxins*, *2*, 2490-2518.

Milosevic, M. F.; Fyles, A. W.; Wong, R.; Pintilie, M.; Kavanagh, M. C.; Levin, W. (1998). Interstitial fl uid pressure in cervical carcinoma: within tumor heterogeneity, and relation to oxygen tension. Cancer 82 : 2418 – 26.

Mishra, V.; Kumar, R. (2012). Living radical polymerization: A review. Journal of Scientific Research, Vol. 56, 2012 : 141-176.

Moad, G.; Rizzardo, E.; Thang, S. H. (2005). Living Radical Polymerization by the RAFT Process. Aust. J. Chem., 58, 379-410.

Moad, G.; Rizzardo, E.; Thang, S. H. (2005). RAFT choosing the right agent. Aust. J. Chem. 58: 379-410.

Moad, G.; Rizzardo, E.; Thang, S. H. (2006). Living Radical Polymerization by the RAFT Process—A First Update. Aust. J. Chem. 2006, 59, 669–692.

Moad, G.; Rizzardo, E.; Thang, S. H. (2009). Living Radical Polymerization by the RAFT Process – A Second Update. Aust. J. Chem. 2009, 62, 1402–1472.

Moad, G.; Rizzardo, E.; Thang, S. H. (2012). Living Radical Polymerization by the RAFT Process – A Third Update. Australian Journal of Chemistry 65(8) 985-1076.

Mondal, G.; Almawash, S.; Kumar Chaudhary, A.; Mahato, R. I. (2017). EGFR-Targeted Cationic Polymeric Mixed Micelles for Co-delivery of

Gemcitabine and miR-205 for Treating Advanced Pancreatic Cancer. Mol. Pharmaceutics, 14 (9), 3121–3133.

Moore, J.C. (1964). Gel permeation chromatography. I. A new method for molecular weight distribution of high polymers. J. Polym. Sci. 2, pp. 835-843.

Mosmann, T. (1983). Rapid Colorimetric Assay for Cellular Growth and Survival: Application to Proliferation and Cytotoxicity Assays. Journal of lmmunological Methods, 65 , 55-63

Nanjwade, B. K.; Bechra, H.M.; Derkar, G.K.; Manvi, F. V.; Nanjwade, V. K. (2009). Dendrimers: emerging polymers for drug-delivery systems, Eur. J. Pharm. Sci. 38, 185–196.

Natfji, A. A.; Ravishankar, D.; Osborn, H. M. I.; Greco, F. (2017). Parameters Affecting the Enhanced Permeability and Retention Effect: The Need for Patient Selection. Journal of Pharmaceutical Sciences 106, 3179-3187.

Nishio, R.; Tsuchiya, H.; Yasui, T.; Matsuura, S.; Kanki, K.; Kurimasa, A.; Hisatome, I.; Shiota, G. (2011). Disrupted plasma membrane localization of equilibrative nucleoside transporter 2 in the chemoresistance to gemcitabine (dFdCyd) of human pancreatic cancer cells. Cancer Science.102:622–629.

Noghuchi, Y.; Wu, J.; Duncan, R.; Strohalm, J.; Ulbrich, K.; Akaike, T.; Maeda, H. (1998). Early phase tumor accumulation of macromolecules: a great difference in clearance rate between tumor and normal tissues. Jpn. J. Cancer Res. 89, 307–314.

Olive, K. P.; Jacobetz, M. A.; Davidson, C. J.; Gopinathan, A.; McIntyre, D.; Honess, D.; Madhu, B.; Goldgraben, M. A.; Caldwell, M. E.; Allard, D.; Frese, K. K.; Denicola, G.; Feig, C.; Combs, C.; Winter, S. P.; Ireland-Zecchini, H.; Reichelt, S.; Howat, W. J.; Chang, A.; Dhara, M.; Wang, L.; Ruckert, F.; Grutzmann, R.; Pilarsky, C.; Izeradjene, K.; Hingorani, S. R.; Huang, P.; Davies, S. E.; Plunkett, W.; Egorin, M.; Hruban, R. H.; Whitebread, N.;

McGovern, K.; Adams, J.; Iacobuzio-Donahue, C.; Griffiths, J.; Tuveson, D. A. (2009). Inhibition of Hedgehog signaling enhances delivery of chemotherapy in a mouse model of pancreatic cancer. Science. 324:1457–1461.

Olszewski, U.; Hamilton, G. (2010). A better platinum-based anticancer drug yet to come? Anticancer Agents Med Chem.10, 4, 293-301.

Ougizawa, T.; Inoue, T. (1986). UCST and LCST behaviour in polymer blends and its thermodynamic interpretation. Polymer Journal. 18 (7) : 521-527.

Owens, D. E. III, Peppas, N.A. (2006). Opsonization, biodistribution, and pharmacokinetics of polymeric nanoparticles, Int. J. Pharm. 307, 93–102.

Owen, S. C.; Chan, D. P.Y. ; Shoichet, M. S. (2012) Polymeric micelle stability. Nano Today 7, 53-65.

Paolino, D.; Cosco, D.; Racanicchi, L.; Trapasso, E.; Celia, C.; Iannone, M.; Puxeddu, E.; Costante, G.; Filetti, S.; Russo, D.; Fresta, M. (2010). Gemcitabine-loaded PEGylated unilamellar liposomes vs GEMZAR®: Biodistribution, pharmacokinetic features and in vivo antitumor activity. Journal of Controlled Release 144. 144–150.

Parness, J.; Horwitz, S.B. (1981). Taxol binds to polymerized tubulin in _vitro. J. Cell Biol. 91, 479–487.

Pili, B.; Bourgaux, C.; Amenitsch, H.; Keller, G.; Lepêtre-Mouelhi, S.; Desmaële, D.; Couvreur, P.; Ollivon, M. (2010). Interaction of a new anticancer prodrug, gemcitabinesqualene, with a model membrane: coupled DSC and XRD study, Biochim. Biophys. Acta, Biomembr. 1798, 1522–1532.

Pitto-Barry, A.; Barry, N. P. E. (2014). Pluronic® block-copolymers in medicine: from chemical and biological versatility to rationalization and clinical advances. Polym. Chem., 5, 3291.

Plate, N. A.; Lebedeva, T. L.; Valuev L. I. (1999). Lower critical solution temperature in aqueous solutions of N-Alkyl-Substituted polyacrylamides. Polymer Journal. 31 (1): 21-27.

Qiu, W.; Su, G. H. (2013). Development of orthotopic pancreatic tumor mouse models. Methods Mol Biol.; 980: 215–223.

Raimondi, S.; Maisonneuve, P.; Lowenfels, A. B. (2009). Epidemiology of pancreatic cancer: an overview Nat. Rev. Gastroenterol. Hepatol. 6, 699–708.

Rapoport, N.Y.; Herron, J.N.; Pitt,W.G.; Pitina, L. (1999) Micellar delivery of doxorubicin and its paramagnetic analog, ruboxyl, to hl-60 cells: effect of micelle structure and ultrasound on the intracellular drug uptake, J. Control. Release 58, 153–162.

Reddy, H.; Dubernet, C.; Mouelhi, S. L.; Marque, P. E.; Desmaele, D.; Patrick Couvreur, P. (2007). A new nanomedicine of gemcitabine displays enhanced anticancer activity in sensitive and resistant leukemia types. Journal of Controlled Release 124, 20–27 L.

Reedijk, J.; Lohman, P.H.M. (1984). Cisplatin: synthesis, antitumour activity and mechanism of action. Pharm Weekbl [Sci] 7,173-80.

Réjiba, S.; Reddy, L.H.; Bigand, C.; Parmentier, C.; Couvreur, P.; Hajri, A. (2011). Squalenoyl gemcitabine nanomedicine overcomes the low efficacy of gemcitabine therapy in pancreatic cancer. Nanomedicine: Nanotechnology, Biology, and Medicine 7, 841–849.

Rejman, J.; Oberle, V.; Zuhorn, I. S.; Hoekstra, D. (2004). Size dependent internalization of particles via the pathways of clathrin- and caveolae-mediated endocytosis. Biochem. J., 377, 159−169.

Roper, P.R.; Drewinko, B. (1976). Comparison of in vitro methods to determine drug-induced cell lethality. *Cancer Res.*; 36 : 2182–2188.

Rowinsky, E.K.; Cazenave, L.A,; Donehower, R.C. (1990). Taxol: a novel investigational antimicrotubule agent. J Natl Cancer Inst. 82:1247-59.

Schiff, P.B.; Fant, J.; Horwitz, S.B. (1979). Promotion of microtubule assembly in _vitro by taxol. Nature 277, 665–667.

Schiff, P.B.; Horwitz, S.B. (1981). Taxol stabilize microtubules in mouse fibroblast cells. Biochemistry 20, 3247–3252.

Schroedera, A.; Kostb, J.; Barenholza, Y. (2009). Ultrasound, liposomes, and drug delivery: principles for using ultrasound to control the release of drugs from liposomes. Chemistry and Physics of Lipids 162, 1–16.

Seetharam, R. N. ; Sood, A. ; Goel, S. (2009). Oxaliplatin: pre-clinical perspectives on the mechanisms of action, response and resistance. ecancer, 3:153.

Siddik, Z. H. (2003). Cisplatin: mode of cytotoxic action and molecular basis of resistance. Oncogene, 22, 7265–7279.

Singla, A. K.; Garg, A.; Aggarwal, D. (2002). Paclitaxel and its formulations. International Journal of Pharmaceutics 235:1–2, 179–192.

Skoog, D.A. (2006). Principles of Instrumental Analysis. 6th ed. Belmont, CA. Thompson Brooks/Cole, Chapter 28.

Smith, A. E.; Xua, X.; McCormick C. L. (2010). Stimuli-responsive amphiphilic (co)polymers via RAFT polymerization . Progress in Polymer Science 35 (2010) 45–93.

Song, C. W.; Griffin, R.; Park, H. J. (2006). Influence of tumor pH on therapeutic response, Cancer Drug Discovery and Development : Cancer Drug Resistance, pp 21-42.

Staruchi, R. M.; Ganguly, M.; Tannock I. F.; Hynynen, K.; Chopra R. (2012). Enhanced drug delivery in rabbit VX2 tumours using thermosensitive liposomes and MRI-controlled focused ultrasound hyperthermia. Int. J. Hyperthermia, December 2012; 28(8): 776–787.

Stohrer, M.; Boucher, Y.; Stangassinger, M.; Jain, R. K. (2000). Oncotic pressure in solid tumors is elevated . Cancer Res. 60 : 4251 – 5.

Suffness, M. (1995) Taxol® science and applications, Boca Raton, FL. CRC Press.

Sylvester, P. W. (2011). Optimization of the Tetrazolium Dye (MTT) Colorimetric Assay for Cellular Growth and Viability. Drug Design and Discovery, 716 of the series Methods in Molecular Biology pp 157-168.

Symon, Z.; Davis, M.; McGinn, C. J.; Zalupski, M.M.; Lawrence, T.S. (2002). Concurrent chemoradiotherapy with gemcitabine and cisplatin for pancreatic cancer: from the laboratory to the clinic. Int. J. Radiation Oncology Biol. Phys., 53, 1, 140–145.

Ta, T.; Bartolak-Suki, E.; Park, E.-J..; Karrobi, K.; McDannold, N. J.; Porter, T. M. (2014). Localized delivery of doxorubicin in vivo from polymer-modified thermosensitive liposomes with MR-guided focused ultrasound-mediated heating. Journal of Controlled Release 194, 71–81.

Ta, T.; Convertine, A. J.; Reyes, C. R.; Stayton, P. S.; Porter, T. M. (2010). Thermosensitive Liposomes Modified with Poly(N-isopropylacrylamide-co-propylacrylic acid) Copolymers for Triggered Release of Doxorubicin. Biomacromolecules 11, 1915–1920.

Ta, T.; Porter, T. M. (2013). Thermosensitive liposomes for localized delivery and triggered release of chemotherapy. Journal of Controlled Release 169, 112–125

Torchillin, V. P. (2001). Polymeric micelles as targeted pharmaceutical carriers.J Control Release, 73:137-45.

Torchilin, V. P. (2005). Recent advances with liposomes as pharmaceutical carriers. Nature Reviews Drug Discovery 4, 145-160.

Trédan, O.; Galmarini, C.M.; Patel, K.; Tannock, I.F. (2007). Drug resistance and the solid tumor microenvironment. J Natl Cancer Inst., 99(19):1441-54.
Van Meerloo, J. ; Kaspers, G.J. ; Cloos, J. (2011). Cell sensitivity assays: the MTT assay. Methods Mol Biol. 731:237-45. doi: 10.1007/978-1-61779-080-5-20.

Tsang, R. Y.; Al-Fayea, T.; Au, H. J. (2009). Cisplatin Overdose Toxicities and Management. Drug Saf, 32, 12, 1109-1122.

Uludag, H.; Sefton, M. V. (1990). Calorimetric assay for cellular activiy in microcapsules. Biomaterials, 11, 9, 708-712.

Van Moorsel, C.J.; Kroep, J.R.; Pinedo, H.M.; Veerman, G.; Voorn, D. A.; Postmus, P. E.; Vermorken, J. B.; van Groeningen, C. J.; Van der Vijgh, W. J. F.; Peters, G. J. (1999). Pharmacokinetic schedule finding study of the combination of gemcitabine and cisplatin in patients with solid tumors. Ann Oncol;10:441–448.

Vana, P. (2007). Kinetic aspects of RAFT polymerization. Macromol. Symp. 248, 71-81.

Vandana, M.; Sahoo, S. K. (2010). Long circulation and cytotoxicity of PEGylated gemcitabine and its potential for the treatment of pancreatic cancer. Biomaterials, 31, 9340–9356.

Velichko, A. K.; Markova, E. K.; Petrova, N. V.; Razin, S. V.; Kantidze, O. L. (2013). Mechanisms of heat shock response in mammals. Cell. Mol. Life Sci. 70, 22: 4229-41.

Vertut-Doi, A.; Ishikawa, H.; Miyajima, K. (1996). Binding and uptake of liposomes containing a poly(ethylene glycol) derivative of cholesterol (stealth liposomes) by the macrophage cell line J774: influence of PEG content and its molecular weight, Biochim. Biophys. Acta 1278, 19–28.

Vogel, S. M.; Minshall, R. D.; Pilipovic, M.; Tiruppathi, C.; Malik, A.B. (2001). Albumin uptake and transcytosis in endothelial cells in vivo induced by albumin-binding protein. Am J Physiol Lung Cell Mol Physiol ; 281:L1512–22.

Von Hoff, D. D.; Ervin, T.; Arena, F. P.; Chiorean, E. G.; Infante, J.; Moore, M.; Seay, T.; Tjulandin, S. A.; Ma, W. W.; Saleh, M. N.; Harris, M.; Reni, M.; Dowden, S.; Laheru, D.; Bahary, N.; Ramanathan, R. K.; Tabernero, J.; Hidalgo, M.; Goldstein, D.; Van Cutsem, E.; Wei, X.; Iglesias, J.; Renschler, M. F. (2013). Increased Survival in Pancreatic Cancer with nab-Paclitaxel plus Gemcitabine. N Engl J Med 2013; 369:1691-1703.

Von Hoff D.D.; Ramanathan, R.K.; Borad, M.J.; Laheru, D.A.; Smith, L.S.; Wood, T.E.; Korn, R. L.; Desai, N.; Trieu, V.; Iglesias, J. L.; Zhang, H.; Soon-Shiong, P.; Shi, T.; Rajeshkumar, N.V.; Maitra, A.; Hidalgo, M. (2011). Gemcitabine plus nab-paclitaxel is an active regimen in patients with advanced pancreatic cancer: a phase I/II trial. J Clin Oncol;29:4548–54.

Wang, J.; Ayano, E.; Maitani, Y.; Kanazawa, H. (2017). Tunable surface properties of temperature-responsive Polymer-Modified liposomes induce faster cellular uptake. ACS Omega, 2, 316−325.

Ward, M. A.; Georgiou, T. K. (2011). Thermoresponsive Polymers for Biomedical Applications Polymers, 3, 1215-1242.

Weinstein, J. N.; Magin, R. L.; Yatvin, M. B.; Zaharko, D. S. (1979). Liposomes and local hyperthermia: selective delivery of methotrexate to heated tumors. Science 1979, 204, 188−191.

Weiss, J. T.; Dawson, J. C. ; Fraser, C.; Rybski, W.; Torres-Sánchez, C.; Bradley, M.; Patton E. E.; Carragher, N. O. and Unciti-Broceta A. (2014). Development and bioorthogonal activation of Palladium-Labile prodrugs of gemcitabine. J. Med. Chem., 57, 5395−5404.

Wilhelm, S.; Tavares, A.J.; Dai, Q.; Ohta, S.; Audet, J.; Dvorak, H.F.; Chan, W. C. W. (2016). Analysis of nanoparticle delivery to tumours. Nat Rev Mater. 1:16014.

Williams, D. B. ; Carter, C. B. (2009). Transmission Electron Microscopy:A Textbook for Materials Science, Springer, New York.

Wu, W.; Sigmond, J.; Peters, G. J; Borch, R. F. (2007). Synthesis and biological activity of a gemcitabine phosphoramidate prodrug. J. Med. Chem., 50, 3743-3746.

Wolpin, B. M.; Chan, A.T.; Hartge, P. (2009). ABO blood group and the risk of pancreatic cancer. J. Natl. Cancer Inst. 101:424–31.

Yatvin, M.B.; Weinstein, J.N.; Dennis, W.H.; Blumenthal, R. (1978). Design of liposomes for enhanced local release of drugs by hyperthermia. Science, 22; 202 (4374): 1290-93.

York, A. W.; Kirkland, S. E.; McCormick, C. L. (2008). Advances in the synthesis of amphiphilic block copolymers via RAFT polymerization: Stimuli-responsive drug and gene delivery. Advanced Drug Delivery Reviews 60, 1018–1036.

Zeisig, R.; Shimada, K.; Hirota, S.; Arndt, D. (1996). Effect of sterical stabilization on macrophage uptake in vitro and on thickness of the fixed

aqueous layer of liposomes made from alkylin phosphocholines, Biochim. Biophys. Acta 1285, 237–245.

Zhang, C-G.; Zhu, W.-J.; Liu, Y.; Yuan, Z.-Q.; Yang, S.-D.; Chen, W.-L.; Li, J.-Z.; Zhou, X.-F.; Liu, C.; Zhang, X.-N. (2016). Novel polymer micelle mediated co-delivery of doxorubicin and P-glycoprotein siRNA for reversal of multidrug resistance and synergistic tumor therapy. Scientific 6, 23859.

Zhang, Y. and Cremer, P. S. (2006). Interactions between macromolecules and ions: the Hofmeister series. Current Opinion in Chemical Biology, 10:1–6.

Zhang, Y.; Furyk, S.; Sagle, L. B.; Cho, Y.; Bergbreiter, D. E.; Paul S. Cremer P. S. (2007). Effects of hofmeister anions on the LCST of PNIPAM as a function of molecular weight. J Phys Chem C Nanomater Interfaces. 111(25): 8916–8924.

Zhao, J.; Pispas, S.; Zhang, G. (2009). Effect of Sonication on Polymeric Aggregates Formed by Poly(ethylene oxide)-Based Amphiphilic Block Copolymers . Macromol. Chem. Phys., 210, 1026–1032.

Zhao, X.; Poon, Z.; Engler, A. C.; Bonner, D. K.; Hammond, P. T. (2012) Enhanced Stability of Polymeric Micelles Based on Postfunctionalized Poly(ethylene glycol)-b-poly(γ-propargyl Lglutamate): The Substituent Effect. Biomacromolecules, 13, 1315−1322.

Zhou, Q.; Liu, L.; Zhang, D.; Fan, X. (2012). Preparation and characterization of gemcitabine liposome injections. Pharmazie.67(10):844-7.

Zhu, S.; Lansakara-P., D. S. P.; Li, X.; Cui, Z. (2012). Lysosomal Delivery of a Lipophilic Gemcitabine Prodrug Using Novel Acid-Sensitive Micelles Improved Its Antitumor Activity. Bioconjugate Chem., 23, 966−980.